Spring 5-2021

Microplankton Dynamics in the River-Dominated Mississippi Bight

Adam D. Boyette

MICROPLANKTON DYNAMICS IN THE RIVER-DOMINATED MISSISSIPPI BIGHT

by

Adam Boyette

A Dissertation
Submitted to the Graduate School,
the College of Arts and Sciences
and the School of Ocean Science and Engineering
at The University of Southern Mississippi
in Partial Fulfillment of the Requirements
for the Degree of Doctor of Philosophy

Approved by:

William ‘Monty’ Graham, Committee Chair
Donald Redalje
Jerry Wiggert
Stephen Howden
Jeffrey Krause

May 2021

ABSTRACT

The Mississippi Bight (MSB) is a river-dominated continental margin influenced by multiple large river systems, including the Mississippi River, Alabama and Tombigbee rivers via Mobile Bay, and numerous smaller rivers, creeks, and bayous. This is part of a biologically-rich ecosystem that supports the second largest fishery industry by volume in the United States. Despite our understanding of the linkages between primary production with higher trophic levels, there remains limited studies quantifying these trophic interactions in this system. Microplankton (<200 µm) community dynamics and trophic connectivity between primary producers and heterotrophic protists represent a critical nexus influencing overall biological productivity in this region. These processes were examined using a combination of a novel morphological-based (MBFG) classification system derived from in-flow plankton imaging (*i.e.* FlowCAM), a suite of in situ biogeochemical and biological measurements, and multivariate statistics to describe patterns of microplankton community composition, biomass, primary productivity, and microzooplankton grazing relative to prevailing physicochemical conditions. Results indicated that the MSB is a highly productive ecosystem, oscillating from a mesotrophic state under reduced river discharge and nutrients to eutrophic conditions during high discharge and elevated nutrient concentrations. Microplankton communities shifted under differing environmental conditions, though diatoms and nanoplankton were predominant throughout the study. Both size fractions (0.6-5 µm and > 5 µm) contributed nearly equivalent proportions to biomass and productivity during low discharge, whereas >5 µm size fraction contributed more biomass and productivity during the spring freshet. Microzooplankton grazing (i.e. ciliates) exerted a significant

top-down control on phytoplankton biomass (30-60%) and productivity (> 60%), despite enhanced phytoplankton growth in spring. The effects of environmental variability on biological productivity and ecological resilience in the MSB are best understood within the context of microplankton community dynamics among primary producers and their trophic intermediaries. Results from this research highlight these key ecological relationships that are fundamental to ecosystem function, productivity, and resilience in this system.

ACKNOWLEDGMENTS

I am incredibly humbled and grateful to all who contributed to the success of this dissertation. I am thankful for their patience, advice, and guidance throughout this process. First, this dissertation would not have been possible without the tragedy of the Deep Water Horizon oil spill and the subsequent development of the Gulf of Mexico Research Initiative (GOMRI). I would like to thank my advisor, William 'Monty' Graham, for providing me the opportunity and intellectual freedom to pursue a dissertation in his lab. I am grateful for his guidance in encouraging me to ask the important questions to help me see the "big picture." I would especially like to thank my other committee members, Don Redalje and Jeffrey Krause for their unending support and invaluable guidance in navigating the difficult waters of the dissertation process. Additionally, they provided extensive knowledge in protist ecology, phytoplankton dynamics, and biogeochemistry, and were instrumental in helping me with materials and sampling. Dr. Redalje always had time to lend an ear, not only to my pressing questions and complaints, but also in his appreciation of fine music. I am grateful for his mentorship, humor, and candor. Dr. Krause was central in providing me the essential materials for my dilution experiments, data from the primary productivity and biomass incubations, and phytoplankton image data. Most importantly, he welcomed me in as one of his own lab members (i.e. Krausling) and provided me the essential guidance in steering me towards the fundamental questions about plankton ecology. I would also like to thank my other committee members, Jerry Wiggert and Stephan Howden, for their valuable insight on biophysical interactions and expertise in coastal oceanographic processes.

I would also like to thank Captain Nic and the crew of the *R/V Point Sur* for all of their hard work and commitment to ensure the safety and success of our research. I would like to thank Kevin Martin for making sure we had plenty of water samples. I also would like to thank Laura Linn (DISL) and Allie Mojzis for their exceptional laboratory skills for nutrient and biomass analyses. Thanks also to Gunnar Olson (MSU) for his assistance with ArcGIS. Funding for my graduate education and field work came from the GOMRI-funded CONsortium for COastal River-Dominated Ecosystems (CONCORDE). Special thanks to Drs. Alan Shiller, Frank Hernandez, Jeff Book (NRL), and Alan "Blackcloud" Weidemann (NRL) for their mentorship during the CONCORDE campaign. Also, thanks to Liz Hamm and Jamie Davis form being an integral component to the success of CONCORDE. I am thankful to Mrs. Linda Downs for ensuring that all of my administrative paperwork and courses were done properly and in a timely manner.

I am especially grateful to my CONCORDE post-doctoral mentors, peers and lab mates for their assistance in sampling, data analysis, proof-reading, and professional development. Valerie Cruz and Sydney Acton were essential with post processing of the FlowCAM images. Particular reverence goes to Drs. Adam Greer, Luciano (Lucho) Chiaverano, and Egan Rowe for their valuable help with writing and statistical interpretation, and for indulging me in exuberant scientific dialogue. Additionally, Drs. Inia Soto, Mustafa Kemal Cambazoglu, and Sabrina Parra helped with writing and professional development. Without their mentoring and friendship, I would not be the scientist I am today. I would like to thank my peers and lab mates Courage Klutse, Naoimi Yoder, Antonio Piru, Kandice Gunning, Dr. Stephan O'Brien, Dr. Katrina

Aleska, Ryan Vandermeulen, Dr. Peng Ho, Dr. Laura Whitmore, and Liesl Cole for their support and encouragement throughout my dissertation.

Lastly, but most importantly, I would like to thank my family. My parents, Doug and Kathy, encouraged me to explore nature and fed my natural curiosity with books, trips to the beach, and unwavering support for me to pursue my dream of studying the ocean. Thanks also to my siblings, Meredith and Jonathan, my nephew Zayd and brother-in-law Aziz, for their love and support while I toiled away in the lab. I am especially grateful to my Grandpa and Grandma Coker for taking me fishing and for allowing me to spend coutless hours exploring the mountains and streams in the Ouachita National Forest. These are the experiences that awaken the senses and inspire a life passion for natural exploration and scientific discovery. I would also like to thank the Brents: Howard, Carole, Jessica, Eden, and Lincoln, and Taylor Haxton and Giles Kelly for their love, support, and encouragement while I endeavored to persevere through my graduate studies. I am a better scientist and individual today because of them. Finally, I would like to thank my life long partner and best friend, Bronwynne, who has been so patient and supportive throughout my graduate career. I am incredibly lucky to have such a wonderful, compassionate, and loving person in my life.

DEDICATION

This work is dedicated to the eleven souls who perished on April 20, 2010 from the Deep Water Horizon drilling rig explosion. May their memory be eternal.

TABLE OF CONTENTS

ABSTRACT ii

ACKNOWLEDGMENTS iv

DEDICATION vii

LIST OF TABLES xii

LIST OF EQUATIONS xvi

LIST OF ABBREVIATIONS xvii

CHAPTER I – INTRODUCTION 1

1.1 BACKGROUND 2

1.2 OBJECTIVES AND HYPOTHESES 9

CHAPTER II – MICROPLANKTON COMMUNITY STRUCTURE ALONG THE RIVER-DOMINATED MISSISSIPPI-ALABAMA SHELF 12

2.1 INTRODUCTION 12

2.1.1 Description of the study area 15

2.2 METHODS 16

2.2.1 Cruise and sampling strategy 17

2.2.2 Microplankton image analysis and classification 17

2.2.3 Diatom chain cell count estimates 22

2.2.4 Microplankton biomass 24

2.2.5 Ancillary measurements 25

2.2.6 Statistical analysis 26
2.3 RESULTS 27
2.3.1 Hydrographic and environmental conditions 27
2.3.2 Seasonal and spatial patterns in microplankton communities and biomass 37
2.3.2.2 Estuarine and inner-shelf communities 41
2.3.2.3 Mid-shelf communities 44
2.3.2.4 Outer-shelf communities 47
2.3.3 Canonical correspondence analysis 49
2.4 DISCUSSION 61
2.4.1 Environmental drivers structuring microplankton communities 62
2.4.2 Microplankton community structure 63
2.5 CONCLUSION 70
CHAPTER III – PRIMARY PRODUCTIVITY ALONG THE CONTINENTAL SHELF IN THE MISSISSIPPI BIGHT 72
3.1 INTRODUCTION 72
3.2 METHODS 77
3.2.1 Sampling 77
3.2.2 Statistical Analysis 79
3.3 RESULTS 81
3.3.1 Size-fractionated particulate organic matter and biomass 81

3.3.2 Primary productivity 87

3.3.3 Principal component analysis 96

3.4 DISCUSSION 104

3.4.1 Primary productivity in the Mississippi Bight 105

3.4.2 Influence of river plumes on microplankton shelf communities 107

3.4.3 Phytoplankton biomass dynamics 109

3.5 CONCLUSION 114

CHAPTER IV – MICROZOOPLANKTON GRAZING IN THE MISSISSIPPI BIGHT 117

4.1 INTRODUCTION 117

4.2 METHODS 119

4.2.1 Sampling 120

4.2.2 Seawater dilution experiments 122

4.2.3 Ciliate potential grazing 126

4.2.3.1 Microzooplankton herbivory trophic strategy definitions 126

4.2.3.2 Prey definitions 127

4.2.3.3 Potential grazing rates 127

4.2.4 Data analysis 129

4.3 RESULTS 129

4.3.1 Microzooplankton grazing rates 129

4.3.2 Nanoplankton biomass, primary productivity, and ciliate community biomass 137

4.3.3 Potential grazing rates by ciliates 138

4.4 DISCUSSION 144

4.4.1 Microzooplankton herbivory on phytoplankton in the Mississippi Bight 144

4.4.2 Grazing potential of ciliates on phytoplankton productivity 150

4.5 CONCLUSION 154

CHAPTER V – GENERAL SUMMARY AND CONCLUSIONS 155

APPENDIX A– ENVIRONMENTAL DATA 161

APPENDIX B–SIZE-FRACTIONATED BIOMASS AND PRIMARY PRODUCTIVITY 169

APPENDIX C–PARTICLE IMAGING USING FLOWCAM 177

APPENDIX D–MICROPLANKTON CLASSIFICATION AND PARTICLE PROPERTIES 181

APPENDIX E–SERIAL DILUTION EXPERIMENTS 219

APPENDIX F-SPEARMAN'S RANK CORRELATION ANALYSIS 228

REFERENCES 238

LIST OF TABLES

Table 2.1 Morphological-Based Functional Groups (MBFG) Classification..... 21

Table 2.2 Morphological-Based Functional Groups for Chain-Forming Diatoms..... 23

Table 2.3 Diatom Chain Cell Count Estimates..... 24

Table 2.4 Biovolume to Carbon Allometry (C_{BV}) 25

Table 2.5 Median + MAD values of physico-chemical constituents..... 34

Table 2.6 Kruskal-Wallis analysis of spatial variability for environmental variables..... 36

Table 2.7 Mann-Whitney test for differences between seasons for environmental variables 36

Table 2.8 Summary of CCA for the biological and environmental data in autumn 53

Table 2.9 Inter-set correlations of environmental variables with CCA axes for autumn. 53

Table 2.10 Summary of CCA for the biological and environmental data in spring. 54

Table 2.11 Inter-set correlations of environmental variables with CCA axes for autumn. 54

Table 3.1 Median + MAD values for microplankton biovolume-carbon, and size-fractionated POC, and PON..... 83

Table 3.2 Median + MAD values for size-fractionated Chl a, primary productivity, and Chl a-normalized productivity 86

Table 3.3 Median + MAD values for ratios of POC/PON and POC/Chl a 87

Table 3.4 Mann-Whitney test for seasonal differences for biotic variables 90

Table 3.5 Kruskal-Wallis analysis of spatial variability for biological variables..... 91

Table 3.6 Wilcoxon rank sum for seasonal comparison between size-fractions 92

Table 3.7 Wilcoxon rank sum for each water type across seasons..... 93

Table 3.8 PCA of environmental variables for autumn and spring 99
Table 3.9 PCA of environmental variables for the different water types 103
Table 4.1 Microzooplankton grazing and phytoplankton growth in the Mississippi Bight 132
Table 4.2 Potential grazing rates, biovolume-derived carbon for microplankton community, and primary productivity 141
Table 4.3 Summary of microplankton biomass compared Chl a concentrations 142
Table 4.4 Microzooplankton grazing in sub-tropical river dominated ecosystems 143
Table A.1 Environmental Data for Autumn 2015 161
Table A.2 Environmental Data for Spring 2016 165
Table B.2 Size-fractionated biomass and primary productivity for Spring 2016 173
Table C.1 FlowCAM Imaging Particle Counts for Autumn 2015 177
Table C.2 FlowCAM Imaging Particle Counts for Spring 2016 179
Table D.1 Microplankton Morphological-Based Functional Groups (MBFGs) Reference 181
Table D.2 Microplankton MBFGs Particle Counts for Autumn 2015 183
Table D.3 Microplankton MBFGs Particle Counts for Spring 2016 189
Table D.4 Microplankton MBFGs Biovolume for Autumn 2015 195
Table D.5 Microplankton MBFGs Biovolume for Spring 2016 201
Table D.6 Microplankton MBFGs Area Based Diameter (ABD) for Autumn 2015 207
Table D.7 Microplankton MBFGs Area Based Diameter (ABD) for Spring 2016 213
Table E.1 Serial dilution experiment chlorophyll a and net growth rate for Autumn 2015 219

LIST OF ILLUSTRATIONS

Figure 2.1 Map of study area. 18

Figure 2.2 Morphological-based functional group (MBFG) classification scheme. 20

Figure 2.3 River Discharge 29

Figure 2.4 Vertical profiles of temperature, salinity, and chlorophyll fluorescence 31

Figure 2.5 Photosynthetically active radiation (PAR, mol m^{-2} d^{-1}) 31

Figure 2.6 Hierarchical Cluster Analysis for Autumn 32

Figure 2.7 Hierarchical Cluster Analysis for Spring 33

Figure 2.8 Absolute concentrations for inorganic nutrients for the different water types. 35

Figure 2.9 Seasonal median + MAD classified particle variables for Nanoplankton, Flagellates, Non-Flagellates, and Microzooplankton. 40

Figure 2.10 Community composition for the different morphological based functional groups for Flagellates 50

Figure 2.11 Community composition for the different morphological based functional groups for Non-Flagellates 51

Figure 2.12 Community composition for the different morphological based functional groups for Microzooplankton 52

Figure 2.13 Seasonal CCA biplots for environmental vectors and station data 57

Figure 2.14 Seasonal ordination diagrams of constrained species scores for Flagellates 58

Figure 2.15 Seasonal ordination diagrams of constrained species scores for Non-flagellates 59

Figure 2.16 Seasonal ordination diagrams of constrained species scores for Microzooplankton 60

..... 60

Figure 3.1 Relationship between POC and PON in the Mississippi Bight..... 84

Figure 3.2 Seasonal distributions of size-fractionated POC, PON, and Chl a across different water types 85

Figure 3.3 Seasonal size-fractionated primary productivity across in the Mississippi Bight across different water types 89

Figure 3.4 Vertical profiles of primary productivity 95

Figure 3.5 Principal component analysis for autumn and spring..... 98

Figure 3.6 Principal component analysis for estuarine and inner-shelf waters 100

Figure 3.7 Principal component analysis for mid-shelf waters..... 101

Figure 3.8 Principal component analysis for outer-shelf waters..... 102

Figure 4.1 Station map of surface sampling stations for microplankton imaging and seawater dilution experiments (SWDE) for autumn and spring 122

Figure 4.2 Idealized seawater dilution model 125

Figure 4.3 Seawater dilution experiments for autumn..... 133

Figure 4.4 Seawater dilution experiments for spring estuarine and inner-shelf waters.. 134

Figure 4.5 Seawater dilution experiments for spring mid-shelf and outer-shelf waters. 135

Figure 4.6 Phytoplankton apparent growth rate versus grazing rate 136

Figure 4.7 Seasonal ciliate potential grazing rates between water types..... 140

LIST OF EQUATIONS

Equation

2.1 $MBFG_{DC} = \sum_{n=1}^{7}(b_n \times L_n)$ ……15

2.2 $C = \sum_{n=1}^{19}\left(BV_{shape} \times BV{:}C\right)$……..…..17

4.1 $\left({}^{1}/_{t}\right)ln\left({}^{P_t}/_{P_0}\right) = k - g$……..……136

4.2 $\%PBG = (1 - e^{-g}) * 100\%.$ ……..….136

4.3 $\%PPG = ((e^{\mu} - e^{(\mu - g)})/e^{\mu - 1}) * 100\%$……..…….136

4.4 $I_{max} = 50.1 \cdot V_{cil}^{-0.225}$……..……..…….139

4.5 $C_{max} = 70.6 \cdot 10^{-6} \cdot V_{cil}^{-0.225}$……..……139

4.6 $K_m = \frac{I_{max}}{C_{max}}$…..……..……..……..……..……..……..……..……..……..……140

4.7 $I(d, T, V_{cil}) = \frac{1}{V_{sample}} \cdot \left(\frac{I_{max} \cdot d}{(K_m + d)} \cdot Q_{10}^{\frac{(T-20)}{10}}\right)$……..……..……..…….140

LIST OF ABBREVIATIONS

ABD	area based diameter
BCS	Bonnet Carré Spillway
C_{BV}	biovolume-derived carbon
Chl a	chlorophyll *a*
CONCORDE	CONsortium for COastal River-Dominated Ecosystems
FlowCAM	Flow Cytometry and Microcsopy
MBFG	morphological-based functional group
MSB	Mississippi Bight
MSR	Mississppi River
MSS	Mississippi Sound
nGOM	northern Gulf of Mexico
POC	particulate organic carbon
PON	particulate organic nitrogen
VSS	Visual Spreadsheet® software

CHAPTER I – INTRODUCTION

Plankton communities are essential components of aquatic ecosystems. Collectively, microplankton (20-200 μm) are a group of highly diverse photosynthetic, mixotrophic, and heterotrophic organisms occupying an essential niche in planktonic food webs. Phytoplankton (e.g. diatoms, dinoflagellates) are the major primary producers in the global ocean, accounting for more than half of Earth's photosynthetically-fixed carbon (Falkowski and Raven, 2013). They respond quickly (< 1 day) to changes in environmental conditions (e.g. light or nutrients) and to top-down pressures from grazing by zooplankton. Consequently, the phytoplankton community reflects not only changes in environment, but shifts in the community structure can also impact biogeochemical processes and food web structure (Falkowski and Raven, 2013). Microzooplankton are the main grazers of phytoplankton biomass and production in marine systems, often consuming more than 65% of the daily primary production (Calbet *et al.*, 2008). This group broadly includes protists, such as ciliates and tintinnids, as well as rotifers, appendicularians, and larval crustaceans. In addition to fueling microbial remineralization, microzooplankton are important trophic intermediaries for larger mesozooplankton and larval fishes (McManus and Santoferrara, 2013).

River-dominated continental margins are among the world's most productive ecosystems. Rivers introduce large quantities of freshwater laden with terrestrially-derived organic and inorganic matter to continental shelf waters, which greatly impacts regional physical and biogeochemical conditions. These ecosystems are characteristically high in biological productivity, often exhibiting sharp gradients in biological communities and biogeochemical processing of resources (Dagg *et al.*, 2004). Coastal

river-dominated food webs tend to support productive fisheries (Grimes, 2001), which is a function of the elevated rates of primary and secondary production within these systems (Lohrenz *et al.*, 1994; Dagg *et al.*, 2004). Thus, microplankton community dynamics and trophic connectivity between primary producers and microzooplankton grazers represent a critical nexus influencing overall biological productivity in coastal river-dominated shelf food webs. Describing the ecological relationships within these communities will provide a more robust measure of trophic transfer available to higher order organisms, as well as advancing an improved mechanistic understanding of ecosystem function, productivity, and resilience in aquatic ecosystems.

1.1 BACKGROUND

The northern Gulf of Mexico (nGOM) is a hydrographically dynamic and complex river-dominated continental margin influenced by multiple large river systems, including the Mississippi River, Atchafalaya River, and the Alabama and Tombigbee rivers via Mobile Bay, as well as numerous smaller rivers, creeks, and bayous. This is a biologically-rich ecosystem that supports the second largest fishery industry by volume in the United States (National Marine Fisheries Service, 2017), and is often referred to as the "fertile fisheries crescent" (Gunter, 1969, Grimes, 2000). The National Oceanic and Atmospheric Administration (NOAA) reported that of the $11.5 billion dollars in revenue that was generated from United States domestic commercial landings in 2018, over 16% came from the nGOM (NMFS, 2020). The region supports the country's largest shrimp and oyster harvests, accounting for 74% and 50% of the national total, respectively, as well as a substantial menhaden reduction industry, with annual harvests over one billion pounds and valued at more than $160 million (NMFS, 2020). The nGOM also supports a

vibrant recreational fisheries industry, accounting for 37% of the 194 million fishing trips logged by anglers in U.S. coastal waters in 2018 (NMFS, 2020). Collectively, these industries provide significant economic resources to local and state communities throughout the central nGOM.

The river-influenced shelf waters along the nGOM are also prone to serious water quality problems, including bottom-water hypoxia and noxious, often toxic, harmful algal blooms (HABs). Seasonal hypoxia, defined as dissolved oxygen (DO) concentrations $\leq$ 2 mg L^{-1}, occurs each summer in the bottom waters along the Louisiana shelf. Many fish and shellfish cannot thrive in these low oxygen waters and are often displaced to areas with higher DO concentrations (Rabalais and Turner, 2019). This "dead zone" is the largest area of human-induced ecological degradation along the U.S. coast, and often reaches a maximal areal coverage of more than 23,000 km^2 (Rabalais and Turner, 2019). Shelf hypoxia in this region is directly linked to the nutrient-rich Mississippi River (MSR) waters, which stimulates extensive phytoplankton blooms that eventually sinks and is respired by bacteria, and the physical stratification resulting from the immense volume of buoyant freshwater overlying the bottom waters (Dzwonkowski *et al*., 2018). While the MSR is the primary driver of shelf hypoxia along the Louisiana shelf, local rivers east of the bird-foot Delta have the potential to induce hypoxia in the Mississippi Bight (MSB) coastal ecosystem. Collectively, local rivers discharging into the MSB contribute to less than half of the MSR discharge, but the stratifying effects of buoyant freshwater, coupled with limited physical mechanisms to vertically mix the water column, increase the potential for hypoxia in this system (Dzwonkowski *et al*., 2018). The areal extent of hypoxia in the MSB is approximately one-tenth of that along

the Louisiana shelf, but far less is known about its duration and frequency in this ecosystem (Dzwonkowski *et al*., 2018). Moreover, the MSB and Louisiana Shelf are biogeochemically distinct, with river-borne nutrient concentrations being much lower in these local river systems relative to the MSR (Dzwonkowski *et al*., 2018). However, additional nutrient sources (e.g. submarine groundwater discharge) may represent an alternative route for ammonium and nitrate delivery to the MSB during low discharge conditions (Dzwonkowski *et al.*, 2018). Additionally, shifts in offshore circulation patterns (e.g. Loop Current and associated eddies) can alter MSR discharge flow, so that up to 47% of this nutrient-rich river water can be diverted east of the bird-foot Delta and influence the physics biogeochemistry in the MSB (Dzwonkowski *et al.*, 2018).

Flood control structures, such as the Bonnet Carré Spillway (BCS) and Caernarvan freshwater diversion, can introduce significant amounts of nutrient-rich Mississisippi River waters periodically into the MSB. These alternative pathways for nutrient-rich MSR waters, though infrequent, can alter the biogeochemistry and food web dynamics significantly within the MSB. Recent openings of the BCS in 2016 and 2019 demonstrated contrasting ecological influences these openings have on the MSB coastal ecosystem. Parra *et al.* (2020) demonstrated that the timing and magnitude of the BCS openings greatly influences where the nutrient-laden MSR freshwaters are advected in the MSB. Thus, while the 2016 wintertime opening had minimal influences on the biogeochemistry in the MSB, the record long 2019 BCS opening resulted in multiple, severe ecosystem consequences (Parra *et al.*, 2020). Most notable were the widespread low salinities (< 5), which caused mass mortality of oysters, marine turtles, and dolphins, and it triggered a persistent, coast-wide toxic cyanobacteria bloom (Parra *et al.*, 2020).

The ecosystem response to nutrient enrichment is a continuous process and the resident phytoplankton communities respond differently to eutrophication processes in coastal waters (Gilbert and Burkholder, 2006). However, the causative elements that underlie the initiation and dispersal of HABs usually point to anthropogenic eutrophication of coastal waters (Anderson *et al.*, 2008). HABs are defined as the proliferation of algal (*i.e.* phytoplankton) biomass, which causes deleterious effects to marine life and/or humans (NOAA). Such algal densities can replace vital food sources for marine organisms, clog gills of fish and shellfish, and contribute to hypoxia (NOAA). Some HAB species also produce potent neurotoxins that can bioaccumulate in local food webs, causing mass mortality of many marine species, including fish, shellfish, birds, and marine mammals. In addition to public health concerns, the loss of many economically important fish and shellfish severely impacts local economies (NOAA).

Studies have documented a strong, positive correlation between nitrogen loading by the MSR and the proliferation of the toxic diatom species *Pseudo-nitzschia pseudodelicatissima* over the last several decades in coastal Louisiana (Parsons *et al.*, 2002, Bargu *et al.*, 2016). Similar findings by Dortch *et al.* (1999) identified twenty-four toxic species representing five taxonomic groups in the coastal waters of Louisiana, including Lake Pontchartrain and Lake Borgne. *Pseudo-nitszchia* is a pennate diatom that produces domoic acid (DA), which is a powerful neurotoxin that bioaccumulates in finfish and shellfish. It is the causative agent for amnesic shellfish poisoning and is responsible for mass mortality of marine mammals, particularly along the West Coast of the U.S. (Anderson et al. 1990). Similarly, the dinoflagellate, *Karenia brevis*, is of particular concern to Mississippi coastal communities due to recently documented

blooms throughout the Mississippi Sound (MSS) in 2015 (Soto *et al.,* 2018). Toxicosis from brevetoxin, the neurotoxin produced by *K. brevis*, is caused by consumption of contaminated shellfish (e.g. oysters) (NOAA). Symptoms of neurotoxic shellfish poisoning (NSP) include gastrointenstinal and neurological distress, including nausea and vomiting, ataxia, paraesthesias of the oropharynx and glossopharyngeal cavity, partial paralysis, and respiratory distress (Watkins *et al*. 2008). Additionally, brevetoxins that are released into the water when cells rupture may become aerosolized and carried onshore by the wind (Pierce *et al.* 2005). This can severely impact the air quality, causing respiratory irritation or distress in nearby communities.

Blooms of *K. brevis* are endemic to the Gulf of Mexico, and although much attention has focused on their occurrence in western Florida, enhanced nutrient loading, increased shipping traffic, and anthropogenic activities make Mississippi coastal waters a particularly high risk for persistent, toxic outbreaks as well (Holiday *et al.* 2007). While the ecological mechanisms for the initiation of *K. brevis* blooms are not fully understood, it is known that this HAB species exists offshore in a dormant state and blooms when environmental and hydrological conditions become conducive for growth (Steidinger *et al.,* 1998). Additionally, advection from areas with recurrent HABs may act as another bloom initiation mechanism. This may have been the case during the 2015 HAB event in the MSS, in which *K. brevis* blooms were advected westward from the Florida panhandle and persisted for several weeks (Soto *et al.*, 2018). The blooms caused widespread fish mortalities and prompted the closure of economically important oyster reefs. Unlike previous *K. brevis* blooms in the MSB, the 2015 event was preceded by post tropical cyclone Patricia, which pushed high salinity shelf waters into the inner shelf and estuaries

in the MSB and MSS (Camazoglu *et al.*, 2017). This was followed by elevated river discharge and nutrients after the passage of the storm that likely played a role in sustaining the advected bloom (Soto *et al.*, 2018). Shifts in phytoplankton composition and increased occurrences of hypoxia and HABs serve as indicators to the immediate pressures of a changing ecosystem (Anderson *et al.*, 2008). The nutrient-rich freshwater outflows, combined with intense anthropogenic development along the Mississippi Gulf Coast, enhance phytoplankton productivity, and greatly increase the potential for hypoxia and recurrent HAB events in the MSB.

River discharge is the most important driver of physical, chemical, and biological variability in the MSB. Therefore, describing the patterns of the lower trophic-level community dynamics and their relationship to biogeochemical and physical processes contributing to variability in time and space will provide insight to the region's biological productivity and susceptibility to eutrophication processes (e.g. hypoxia, HABs). Moreover, it will increase our understanding about ecosystem function and resilience in hydrographically complex environments. Despite our understanding about the linkages between environmentally-driven microplankton community dynamics, there are limited studies quantifying these trophic interactions in this system. Phytoplankton productivity and community structure have been characterized along the Mississippi River-influenced Louisiana Shelf (Lohrenz *et al.*, 1999, 2014; Chen *et al.*, 2000; Chakraborty and Lohrenz, 2015) and throughout other coastal (e.g. MacIntyre *et al.*, 2011; Qian *et al.*, 2003; Liefer *et al.*, 2013) and estuarine (e.g. Mortazavi *et al.*, 2000; Murrell *et al.*, 2004) systems along the central nGOM. Similarly, rates of microzooplankton herbivory have been determined along the Louisiana Shelf (e.g. Dagg, 1995; Strom and Strom, 1996) and

other coastal (e.g. Lehrter *et al.*, 1999; Ortell and Ortmann, 2014) and estuarine (McGehee and Redalje, 2016) systems in the nGOM. Despite multiple studies examining phytoplankton and microzooplankton dynamics throughout the nGOM, efforts to examine these trophic interactions within the MSB have been largely underrepresented.

It is widely recognized that microzooplankton grazing is a key process for structuring phytoplankton biomass and community composition (Strom 2002, Calbet and Landry 2004, Calbet 2008). The degree to which phytoplankton growth and mortality due to grazing pressures by microzooplankton are coupled in time provides insight on plankton community resilience and ultimately, ecosystem stability (Strom 2002). For instance, in coupled systems, rates of phytoplankton growth tend to be balanced by microzooplankton grazing, regardless of primary production, whereas these rates differ substantially in decoupled systems (Strom, 2002). While coupled systems (e.g. tropical oligotrophic waters) tend to be more stable and resistant to community-wide perturbations, decoupled systems (e.g. productive coastal waters) are less stable and often have abrupt shifts in phytoplankton community structure (e.g. HABs, eutrophication) (Strom, 2002). The nature and extent of coupling between protistan grazers and primary producers within various gradients in environmental conditions will help identify key processes structuring marine food webs in highly unstable environments like those characterized by coastal river-dominated shelf ecosystems.

This study provides a detailed description of the spatial and seasonal heterogeneity of the microplankton community structure, biomass, and rates of primary production, growth, and mortality due to grazing relative to the prevailing environmental conditions in the MSB waters. The work presented here attempts to resolve the

microplankton community structure and trophic connectivity through systematic analysis based on morphological-based functional group classification, size-fractionated biomass and productivity measurements, and estimates of microzooplankton grazing on phytoplankton. The study compared data under differing hydrographic conditions (low flow and high flow) across two seasons (autumn and spring), resulting in a unique dataset that will support further efforts to characterize this ecologically and economically important river-dominated ecosystem. This synoptic approach to characterizing the base trophic communities represents the first of its kind in the region.

1.2 OBJECTIVES AND HYPOTHESES

The overall research objective was to examine seasonal microplankton community dynamics under two contrasting hydrographic and biogeochemical regimes within the river-dominated shelf ecosystem of the MSB. This research was based on the biogeochemical, physical, and plankton imaging data collected during the CONsortium for oil exposure pathways in COastal River-Dominated Ecosystems (CONCORDE) autumn (October-November 2015) and spring (March-April 2016) campaigns aboard the *R/V Point Sur* along the continental shelf in the nGOM. This study utilized the freshwater influenced surface waters of the nGOM as a model study site to address how microplanktonic communities differ in terms of community structure and trophic interactions under a low discharge (autumn) scenario relative to high discharge (spring) hydrographic conditions. Specifically, this current body of work addressed two basic questions:

1. Does the microplankton community composition change seasonally with concomitant changes in the physical and biogeochemical structure of the shelf surface waters?
2. Are the shifts in the microplankton community reflected in the rates phytoplankton production and microzooplankton grazing?

The overarching research questions were addressed by 1) describing patterns of microplankton community composition, biomass distribution, and primary productivity across the study region using a combination of flow-imaging technology (*i.e.* Flow Cytometry And Microscopy, FlowCAM®), fluorometry, and ^{14}C-labeled productivity incubations, 2) quantifying phytoplankton growth and protist herbivory rates, and 3) relating variability in the microplankton community structure and trophic rates to prevailing physiochemical conditions.

The first objective was to describe the microplankton community composition and particle characteristics (*i.e.* particle size and frequency distributions, counts, and biovolume) using FlowCAM®. This objective used a novel trait-based classification approach to resolve the plankton community and multivariate statistics to highlight environmental parameters contributing to spatial and temporal variability in community composition in the nGOM. The following hypotheses were addressed:

1. The microplankton community will differ seasonally, with a flagellate-dominated community predominant in autumn, but transitioning to a diatom-dominated community in the spring.
2. The community will also differ along a salinity gradient across the shelf such that large-celled (> 50 μm area based diameter, ABD) microplankton will

predominate in nearshore waters, whereas smaller cells will be most abundant in offshore waters.

3. Seasonal variability in microplankton community abundance will be driven largely by physical conditions in autumn and nutrients in spring.

The second objective established size-fractionated phytoplankton biomass and production rates in surface waters and related these parameters to the microplantkon community structure and prevailing environmental conditions using principal component analysis and non-parametric statistics. The following hypothesis was addressed:

1. Phytoplankton biomass and primary productivity will vary spatially across horizontal salinity gradients and seasonally such that biomass and productivity will be greater in the spring under lower salinity and nutrient replete conditions.

The final objective examined phytoplankton community growth and mortality rates. This objective addressed questions pertaining to the degree to which phytoplankton and microzooplankton are coupled in the productive surface waters of the nGOM. This study component addressed the following hypotheses:

1. Phytoplankton growth will be tightly coupled to microzooplankton grazing in autumn, whereas phytoplankton growth will be greatly decoupled from herbivory in spring.
2. Microzooplankton grazing rates will be similar to other productive coastal systems.

CHAPTER II – MICROPLANKTON COMMUNITY STRUCTURE ALONG THE RIVER-DOMINATED MISSISSIPPI-ALABAMA SHELF

2.1 INTRODUCTION

Improved understanding of plankton community dynamics and trophic connectivity between primary producers and heterotrophic protists, and their relationship to the physical setting is a central tenet to plankton ecological studies. Temporal and spatial variability in physical and biogeochemical properties effectively shapes microplankton communities (Margalef, 1978; Smayda 1980).

Primary production is the process through which inorganic carbon and nutrients are converted to organic matter in marine ecosystems (Kemp et al. 1997; Gallegos and Neale 2015). The rate of primary production (*i.e.*. primary productivity) differs among groups of phytoplankton and the prevailing environmental conditions (e.g. light quality and intensity, nutrient concentrations, temperature) (Falkowski and Raven, 2013). Primary productivity has a profound impact on water quality (Malone et al. 1988; Gallegos and Neale 2015) and the movement of carbon through marine food webs to higher trophic levels (Lohrenz et al. 1994; Livingston 2001). Microzooplankton (< 200 µm) are a key component of marine food webs and the primary consumers of phytoplankton biomass in marine ecosystems. They often consume more than half of the daily phytoplankton production (Calbet and Landry 2004, Calbet 2008), serve as prey items for mesozooplankton and ichthyoplankton (Gifford 1991, Calbet & Saiz 2005, Calbet 2008), and occupy a key position in the marine microbial loop (Azam et al. 1983, Sherr & Sherr 2002, Calbet 2008).

Here, the spatial and temporal patterns of microplankton community composition and associated environmental parameters were investigated within different water types encountered along the continental shelf of the nGOM. This approach utilized an imaging system and a classification scheme based on morphologies and functional groups (*i.e.* morphological-based functional group, MBFG) to estimate microplankton abundance (as particle concentration, particles L^{-1}), particle size distribution (area based diameter, μm ABD; biovolume, μm^3 $cell^{-1}$), and biovolume-derived carbon (C_{BV}, μg C L^{-1}) contribution within each of the microplankton trophic groups for each of the water types studied.

Classification schemes using trait-based morphological-functional type groupings are extensive throughout freshwater systems (e.g. Reynolds, 1988; Kruk *et al.*, 2010), but are limited in marine systems (but see Smayda and Reynolds, 2001). Further, microplankton community structure and distribution in the nGOM are limited to phytoplankton pigment concentrations derived from high performance liquid chromatography (HPLC) with few microscopy studies (e.g. Strom and Strom, 1996; Quian *et al.*, 2003; Chakraborty and Lohrenz, 2015; Bargu *et al.*, 2016). HPLC analyses provide relative abundances of phytoplankton groups contributing to a total chlorophyll *a* (Chl *a*) biomass and uses a statistical approach (*i.e.* CHEMTAX, see Mackey *et al.*, 1996) to find the best fit of pigment data to infer phytoplankton community composition (Chakraborty and Lohrenz, 2015). Although HPLC pigment analysis provides robust estimates of phytoplankton biomass for multiple phytoplankton groups, this approach does not account for the different taxonomic assemblages or trait-based functionality within a pigment group. Thus, all pigment-containing particles are grouped together,

missing potentially important ecological patterns (e.g. toxic species). Another problem associated with a pigment-only approach is that it does not quantify microzooplankton, which are important components to the microplankton community.

The introduction of automated imaging systems to characterize the abundance and size spectra of planktonic organisms has transformed aquatic ecology by enhancing the ability to quantify plankton communities in near real-time (Alvarez *et al.*, 2012). Data provided by imaging systems provides both a quantitative estimate of the community, as well as providing size parameters (e.g. diameter, biovolume) for each imaged particle.

Observations were made as part of the CONCORDE project, which provided for the comparison of microplankton populations to physical and biogeochemical data collected simultaneously over the course of two research cruises in two seasons and under differing hydrographic regimes. This provided the setting to examine the spatial and temporal relationship of microplankton communities to their environment and potential carbon pools contained therein. The overall goal of the present study was to evaluate the microplankton community to determine what environmental conditions drive community variability, and to estimate the carbon contribution of each of microplankton MBFG groups. The importance of knowing the carbon estimates of each community will be useful for visualizing energy transfer potential to higher trophic levels, which ultimately defines ecosystem function and productivity. Three hypotheses were addressed to evaluate microplankton community dynamics in surface waters of the MSB

1. The microplankton community will differ seasonally, with a flagellate-dominated community predominant in autumn, but transitioning to a diatom-dominated community in the spring.

2. The community will differ along a salinity gradient across the shelf such that large-celled (> 50 μm area based diameter, ABD) microplankton will predominate in estuarine and inner-shelf waters, whereas smaller cells will be most abundant in offshore waters. Ancillary to this hypothesis is that > 50% of the total biovolume-derived carbon biomass will be found within the estuarine and inner-shelf communities in spring, concomitant with greatest chlorophyll *a* concentrations.
3. Seasonal variability in microplankton community abundance will be driven largely by physical conditions (*i.e.* temperature, salinity) in autumn and inorganic nutrients in spring.

2.1.1 Description of the study area

The MSB study region (Figure 2.1), located east of the MSR birdfoot delta in the central nGOM, is a biologically productive freshwater-dominated ecosystem receiving variable supplies of inorganic nutrients and particulate matter from multiple rivers, estuaries, and bayous (Dzwonkowski *et al.*, 2011, Greer *et al.*, 2018). Bounded to the north and west by barrier islands, a key geographic feature of this broad, relatively shallow shelf ecosystem is that the MSB is situated between the two largest river systems in terms of discharge into the Gulf of Mexico: the MSR to the west and the Alabama and Tombigbee Rivers via Mobile Bay to the east. The MSR system is the dominant source of freshwater input into the nGOM (mean discharge = ~17,000 $m^3 s^{-1}$) with a watershed draining nearly 41% of the continental United States, of which 70% passes through the MSR birdfoot delta (Walker *et al.*, 2005). While most of this freshwater discharge is deflected westward onto the Louisiana shelf, seasonal wind shifts to the north during

spring and summer can push the MSR freshwater plume eastward into the bight (Morey *et al.,* 2003, Schiller *et al.,* 2011). Additionally, intermittent openings of the BCS via Lake Pontchartrain represent an alternative source of MSR water impacting regional hydrography and biogeochemistry in the Mississippi Bight (Parra *et al.,* 2020).

The Alabama and Tombigbee rivers have a combined drainage basin of 115, 467 km^2 resulting in a discharge via Mobile Bay of approximately 1,700 $m^3\ s^{-1}$, which makes it the second largest river system discharging into the Gulf of Mexico and the fifth largest in the United States (Dzwonkowski *et al.,* 2011). Other local rivers flowing into the Mississippi Bight via the Mississippi Sound estuary include the Pascagoula, Pearl, Biloxi, Jourdan, and Wolf rivers. Collectively, these river systems contribute to ~44% of the Mississippi River discharge (Dzwonkowski *et al.*, 2018). However their combined input and subsequent physical interactions are important for generating wind- and buoyancy-driven flows that create strong horizontal and vertical gradients in physical, biogeochemical, and planktonic processes important for structuring local and regional food webs (Greer *et al.*, 2020).

2.2 METHODS

Microplankton community composition was determined using a combination of FlowCAM® plankton imaging and manual identification of imaged particles. Microplankton taxa were classified into morphological functional groups (MBFG) following methodologies similar to those outlined by Reynolds *et al*., (2002), Smayda and Reynolds (2003), Salmaso and Padisák (2007), Kruk *et al*., (2010) and Alvarez *et al*., (2012).

2.2.1 Cruise and sampling strategy

Two research cruises were conducted along three meridional transects to examine microplankton distributions and environmental variability in surface waters of the MSB in autumn 2015 (10/29/2015-11/05/2015) and spring 2016 (03/30/2016-04/07/2016) as part of the CONCORDE project (Figure 2.1). Stations included water types ranging from river-dominated, estuarine and inner shelf waters to mesotrophic slope-influenced outer shelf waters. Nighttime discrete water samples were obtained at surface depths ranging from < 0.5 to 2.0 m using a rosette sampler equipped with 12 L Niskin bottles, a SeaBird SBE911 plus conductivity-temperature-depth instrument profiler and a WET Labs ECO-AFL chlorophyll fluorometer. Subsamples from each Niskin bottle were taken to evaluate the microplankton community composition and biogeochemical properties (e.g. chlorophyll *a* (Chl *a*), inorganic nutrients). To evaluate the microplankton community structure, aliquots of 50 mL natural water samples were pre-filtered through a clean 202 μm nylon mesh into clean 150 mL dark polycarbonate bottles for immediate imaging.

2.2.2 Microplankton image analysis and classification

A total of 78 samples were taken at discrete surface stations in autumn 2015 (n = 38) and spring 2016 (n = 40) that generated 745 image files. Image files contained a number of individually segmented images ranging from < 20 at stations at offshore waters to more than ten million at stations at coastal, inner-shelf waters. Microplankton imaging was conducted using a FlowCAM® B3 Benchtop Series fitted with a 1.0 mL C70 Syringe pump, a 10X magnification objective, and a 100 μm flow cell. Unconcentrated water samples were analyzed in triplicate, duplicate, or single 5.0 mL aliquots in fluorescence-trigger mode, taking approximately 0.5 h to complete each run. These image

files were processed post cruise to manually remove image artifacts (e.g. bubbles, duplicate images) and to classify the microplankton community.

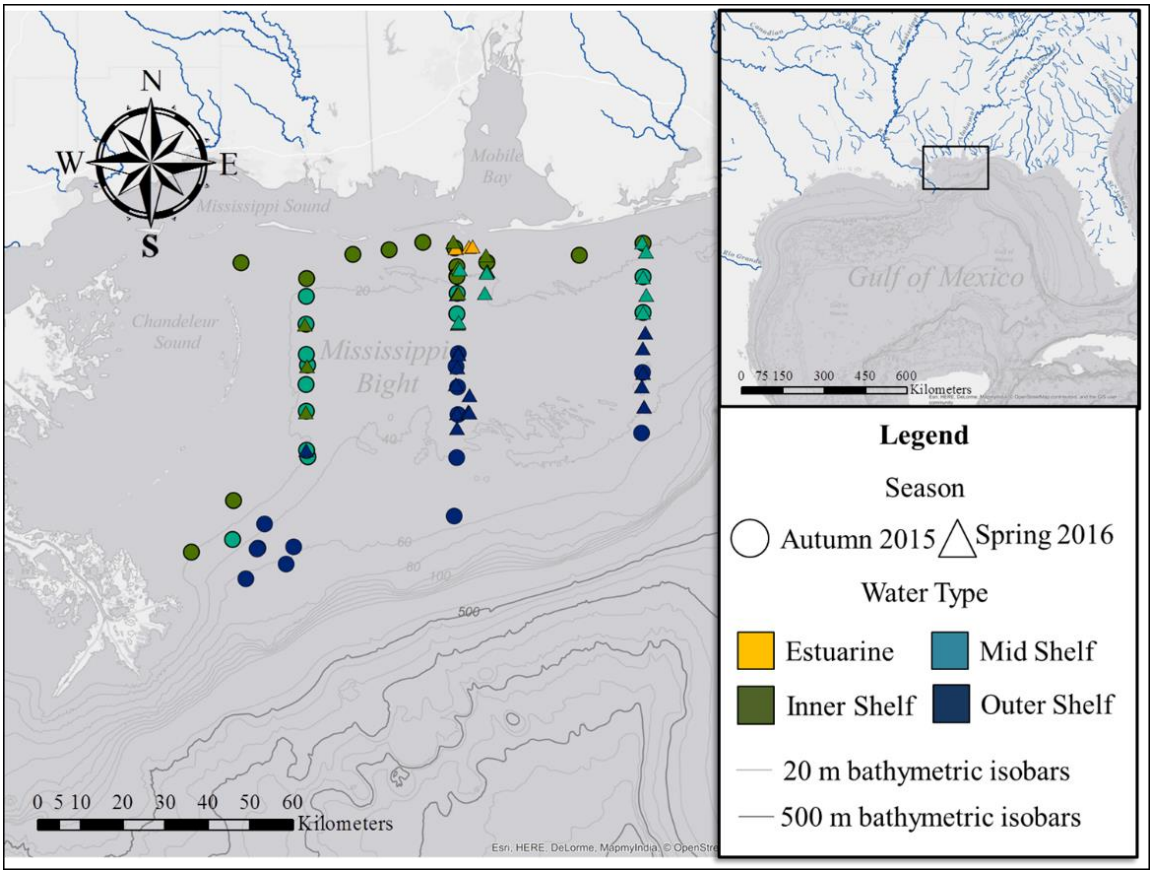

Figure 2.1 *Map of study area.*

Map of the Mississippi Bight showing the sampling stations where microplankton and environmental data were collected in autumn 2015 (circles) and spring (triangles). Colors indicate water types determined by hierarchical cluster analysis (HCA): estuarine (yellow), inner shelf (green), mid shelf (cyan), and outer shelf (blue).

Imaged particles were manually classified initially into two groups, classified microplankton and unclassified particulate matter. Particles that were not classified were placed into unclassified particulate matter bins and were not quantified or used in statistical analyses. The classified microplankton group was subsequently subdivided into four broad groups based on their size (*i.e.* < or > 20μm, area based diameter (ABD)),

motility (*i.e.* flagellum presence/absence), and trophic niche (e.g. microzooplankton), and included: nanoplankton (phytoplankton < 20μm), flagellates (phytoplankton > 20μm with flagellum), non-flagellates (phytoplankton > 20μm without a flagellum) and microzooplankton (any ciliate or naupliiar crustacean). Cell diameter (μm) and biovolume (μm^3 $cell^{-1}$) were determined by Visual Spreadsheet® (V4.11.12) software (VSS) using the area based diameter (ABD, μm) algorithm.

Microplankton taxa were manually classified into one of twenty-four morphological based functional groups (MBFG) using taxonomic guides by Tomas (1997), Dolan *et al*., (2004), and Louisiana Universities Marine CONsortium (LUMCON) online guide to phytoplankton (https://phytoplanktonguide.lumcon.edu/) (Figure 2.2, Table 2.1). The MBFG scheme was based on visual observations only, though it provided a framework to present a complex data set. This approach was used solely as a classification scheme and was based on methods similar to previous studies (e.g. Kruk *et al*. 2010, Alvarez *et al*. 2010). No further attempts were made to use the MBFGs in an environmental predictability capacity as some have argued (e.g. Reynolds *et al*. 2006; Salmaso and Padisák 2007; Kruk *et al*., 2010). Solid white lines divide three primary groups based on motility (*i.e.* flagellates or non-flagellates) and general trophic classification (*i.e.* microzooplankton) (Figure 2.2).

These groups were further subdivided based on a combination of shape (e.g. discoid, acerate cells) and taxonomic functional group (e.g. silicoflagellates, radiolarians). In some instances, the name to which the morphological-based functional group (MBFG) was given reflects the predominant genera for that shape. For example,

Prorocentroid MBFG 2 is comprised of the *Prorocentrum* Ehrenberg genus of dinoflagellates.

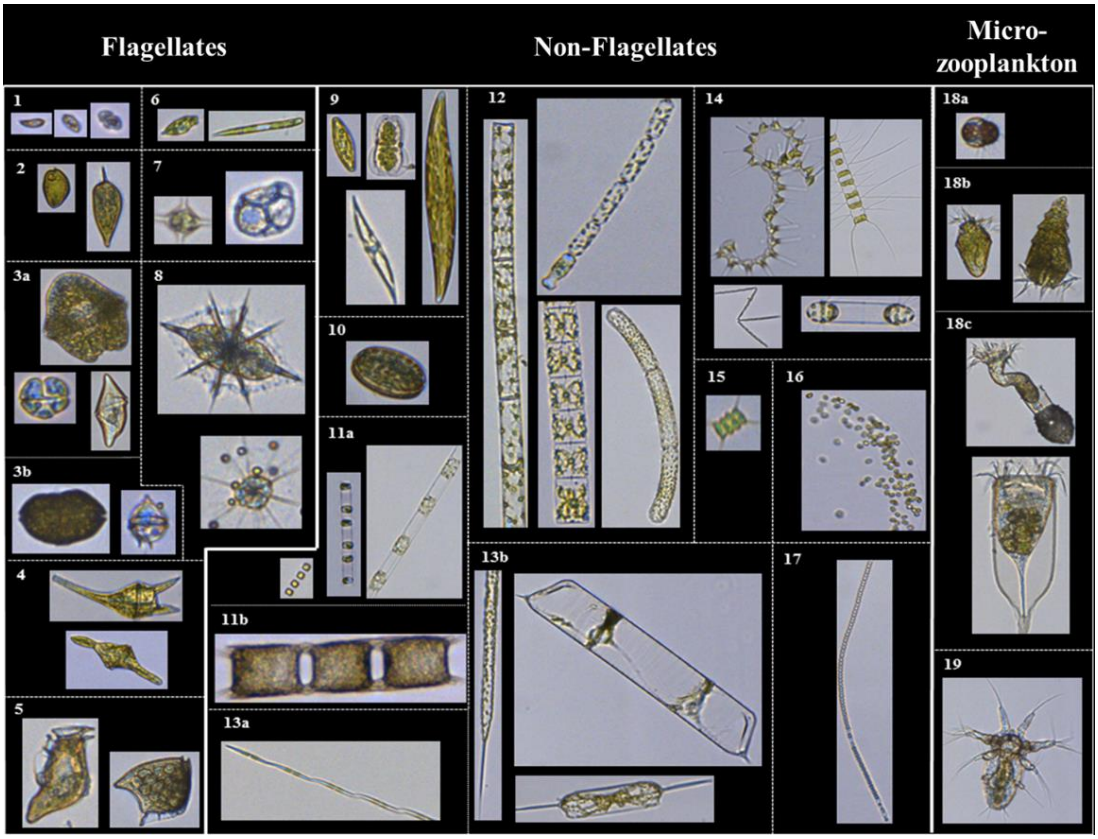

Figure 2.2 *Morphological-based functional group (MBFG) classification scheme.*

Three primary groups are subdivided into shared functional traits or life histories. *Nanoplankton, Flagellates, Non-flagellates, Microzooplankton*. Numbers correspond to the MBFG listed in table 1.

Although many of the representative examples of estuarine and marine taxa from each of the taxonomic functional groups are listed in Table 2.1, this is not an exhaustive list. The trophic status (e.g. autotrophic (a), mixotrophic (m), heterotrophic (h)) for each representative taxa is listed, as well as the presence of noxious or toxic species (*i.e.*. HAB species) (Table 2.1).

Table 2.1 *Morphological-Based Functional Groups (MBFG) Classification*

Primary microplankton groups (Flagellates, Nonflagellates, and Microzooplankton), the 24 morphological functional groups, the functional taxonomic group (*i.e.* Phylum, Class, Subclass, or generalized group such as the mesozooplankton), representative genera, and trophic level (TL) classification (a = autrophic, m = mixotrophic, h = heterotrophic, NA = not applicable). Nanoplankton were included as part of the Flagellates. Genera known to contribute harmful algal blooms are indicated by an asterisk (*).

MBFG					FunctionalGroup	Representative Taxa	TL
Nanoplankton	1	Nanoplankton			Chromophyte*/ Chlorophyte	*Heterocapsa, Scrippsiella, Chroomonas, Rhodomonas, , Actinomonas, Dictyocha, Dinobryon, Ochromonas, Ciliphyrs, Meringosphaera, Octactis, Isochrysis, Chrysochromulina, Prymnesium, Phaeocystis, Pavlova, Chlamydomonas, Choanoplankton, Skeletonema*	a, m, h
Flagellates	2	Prorocentroid			Dinophyceae	*Prorocentrum**	m
	3	Gymnodinoid	3a	athecate		*Gymnodinium, Karenia*, Akishiwo*, Gyrodinium*, Torodinium*	m, h
			3b	thecate		*Alexandrium*, Oxyphsis, Gamberidiscus*, Protoperidinium*	m, h
	4	Cerationoid				*Ceratium, Ceratoperidinium, Brachydinium*	a, m
	5	Dinophysoid				*Dinophysis*, Phalacroma, Oxyphysis, Oxytoxum**	a, m
	6	Euglenoid			Chlorophyceae	*Eutrepia, Euglena, Eutreptiella*	a
	7	Silicoflagellates			Chromophyta	*Dicyocha, Octactis, Mesocena, Ebria*	a
	8	Radiolarians			Radiolaria	*Acanthometra, Amphilonche*	a
Non-flagellates	9	Elliptic prism			Bacillariophyceae	*Navicula, Pleurosigma, Gyrosigma, Entomoneis*	a
	10	Discoid				*Coscinodiscus, Azpeitia, Hemidiscus, Actinocychus, Roperia*	a
	11	Skeletonemanoid	11a	small		*Skeletonema, Lauderia, Thalassiosira*	a
			11b	large		*Odontella, Hemiaulus*	a
	12	Cylindrical chains				*Dactyliosolen, Guinardia, Leptocylindrus, Corethron, Muneria*	a
	13	Acerate cells	13a	Nitzschioid		*Pseudo-nitzschia*, Nitzschia, Cylindrotheca*	a
			13b	Rhizosolenoid		*Rhizosolenia, Proboscia, Ditylum*	a
	14	Aserionellopsioid				*Asterionellopsis, Chaetoceros, Thalassionema, Lioloma*	a
	15	Desmids			Chlorophyceae	*Scendesmus, Pediastrum*	a
	16	Mucilagenous			Chlorophyceae	*Oocystis*	a
	17	Filamentous			Cyanophyta	*Dolichospermum*, Merismopedia*	a

Table 2.1 (continued).

MBFG					FunctionalGroup	Representative Taxa	TL
Microzooplankton	18	Ciliates	18a	*Mesodinium*	Ciliophora	*Mesodinium*	m
			18b	aloricate choreotrichids		*Laboea, Strombilidium, Strombidium, Euplotes, Diophrys*	m, h
			18c	tintinnids		*Favella, Tintinniopsis, Heliocostomella*	m, h
	19	mesozooplankton			mesozooplankton	copepod nauplii, rotifers, larvaceans	h
Other	20	particulate matter (PM)	20a	unidentified particles < 20 μm	PM	unidentified cells, dead fragments, appendages, fecal pellets, exuvia	NA
			20b	unidentified particles > 20 μm			NA

Because the FlowCAM® was not set up to image particles < 20 μm at a high resolution, nanoplankton were not classified to higher taxonomic resolution, but constituted a diverse group organisms that includes cryptophytes, dinoflagellates, prymnesiophytes, and chlorophytes, (Tomas, 1997). For simplicity, all ciliates were included in the microzooplankton, though it is recognized that multiple trophic strategies, including mixotropy and heterotrophy, exist within ciliated protist communities (Stoecker *et al*., 2017). It is also recognized that heterotrophic dinoflagellates are an important component to the microzooplankton community (Sherr and Sherr 2007).

2.2.3 Diatom chain cell count estimates

FlowCAM® image segmentation often does not identify the number of cells comprising a diatom chain and may grossly underestimate diatom cell counts in a sample. To address these discrepancies, VSS was used to create 7 filters based on particle length. Length (μm) is defined as the maximum value of the 36 feret measurements, which are the perpendicular distances between the parallel tangents touching opposite sides of the particle (FlowCAM® Manual). Length bins ranged from 15 μm to 1000 μm. A total of

906 library images were used to provide length and cell counts. Cell counts were manually counted for each diatom chain from the library images. Table 2.2 is a list of the genera and number of library images used to estimate cell counts for the representative chain forming diatom groups. Diatom chain cell count estimates for the respective MBFG were determined by multiplying the particle count from each bin by the respective MBFG cell count estimate, then sum for each MBFG (Equation 2.1, Table 2.2).

Equation 2.1

$$MBFG_{DC} = \sum_{n=1}^{7} (b_n \times L_n)$$

Where, $MBFG_{DC}$ is the diatom chain cell count estimate for the respective morphological based functional group, b_n is the length-based particle count in the respective bins, and L_n is the library-derived estimated cell counts.

Table 2.2 *Morphological-Based Functional Groups for Chain-Forming Diatoms*

MBFG			Representative Taxa	Number of library images used	R^2
11	Skeletonemanoid	small	*Skeletonema*	11	0.82
		large	*Thallassiosira*	112	
			Hemiaulus	4	
12	Cylindrical		*Leptocylindrus*	24	0.57
			Guinardia	19	
			Dactyliosolen	26	
			Meuneiera	3	
13	Acerate	Nitzschiod	*Pseudo-nitszchia*	127	0.78
			Cylindrotheca	53	
		Rhizosolenoid	*Rhizosolenia*	100	0.77
			Ditylum	7	
14	Asterionellopsioid		*Aserionellopsis*	127	0.28
			Chaetoceros	139	
			Thalassionema	15	

MBFGs for chain-forming diatoms used to estimate cell numbers. Representative Taxa is the representative genera from the image library, the number of library images used to estimate cell counts from each respective MBFG, and R^2 is the coefficient of determination of a best-fit line between the chain length and cell count.

Table 2.3 *Diatom Chain Cell Count Estimates*

Bin	**Length**	**Skeletonem-anoid**		**Cylindrical**	**Acerate**		**Asterionell-opsioid**
	(μm)	small (n = 127)	large (n = 139)	(n = 72)	Nitzschioid (n = 180)	Rhizosolenoid (n = 107)	(n = 281)
1	15-29	1.1	0.2	0.5	0.5	0.1	1.5
2	30-49	1.9	0.3	0.9	0.8	0.1	2.8
3	50-79	3.1	0.5	1.5	1.4	0.2	4.5
4	80-119	4.9	0.7	2.3	2.1	0.4	6.9
5	120-199	7.8	1.2	3.8	3.4	0.6	11.1
6	200-299	12.2	1.8	5.9	5.3	0.9	17.4
7	300-1000	31.7	4.8	15.3	13.9	2.4	45.3

Diatom chain cell count estimates based on length. Bin number, length (μm) is the maximum linear dimension of the 36 feret measurements, morphological based functional group (MBFG) cell count estimate, n is the number of library images used for analysis

2.2.4 Microplankton biomass

Biovolume (μm^3 $cell^{-1}$) for each microplankton group was estimated by FlowCAM's VSS using the area based diameter (ABD) volume following recommendations by Karnan *et al*. (2017). One of three shapes (sphere, prolate spheroid, or cylinder) was assigned to the different MBFGs (Table 2.4), and the shape used for the biovolume and the carbon conversion units using the allometric relationships between biovolume and cellular carbon (pg C $cell^{-1}$) content for protists (*i.e.* Menden-Deuer and Lessard 2000), ciliates (Putt and Stoecker 1989, Verity and Langdon, 1984), and microzooplankton crustaceans (e.g. copepod nauplii, Beers and Stewart 1970) (Table 2.4). Group carbon (C, μg C L^{-1}) was estimated for each MBFG by applying the carbon to biovolume relationship to each particle then summing for each group (Equation 2).

Equation 2.2

$$C = \sum_{n=1}^{19} \left(BV_{shape} \times C_{BV} \right)$$

Where, C (μg C L^{-1}) is the microplankton MBFG carbon normalized to sample volume, BV_{shape} is the assigned biovolume shape (*i.e.* spheroid, prolate spheroid, or cylinder) for the different groups, and C_{BV} is the allometric relationship for the different microplankton groups. Particulate matter was not quantified.

Table 2.4 *Biovolume to Carbon Allometry (C_{BV})*

Group	MBFG	Shape	C_{BV}	Reference
Flagellates	1	spheroid	$0.216 \times BV^{0.939}$	Menden-Deuer and Lessard (2000)
	2-8	prolate spheroid	$0.216 \times BV^{0.939}$	Menden-Deuer and Lessard (2000)
Non-flagellates	9-17	cylinder	$0.288 \times BV^{0.811}$	Menden-Deuer and Lessard (2000)
Microzooplankton	18-19	prolate spheroid		
aloricate ciliates*			$0.19 \times BV$	Putt and Stoecker (1989)
tintinnids			$0.053 \times BV + 444.5$	Verity and Langdon (1984)
nauplii, postnaupliar copepods			$0.08 \times BV$	Beers and Stewart (1970)

The biovolume ($_{BV}$) shape and $_{BV}$ to carbon allometry (C_{BV}) used for the difference microplankton groups and the corresponding morphological functional groups (MBFG). (*) includes *Mesodinium* spp.

2.2.5 Ancillary measurements

Samples for inorganic nutrient concentration and phytoplankton biomass, presented here as bulk chlorophyll *a* (Chl *a*), were taken at all surface stations. Samples for dissolved inorganic nutrients were obtained from the filtrate (~125 mL) obtained from Whatman GF/F filters, immediately frozen and stored until analyzed. Inorganic nutrients concentrations for nitrate + nitrite ($NO_3^- + NO_2^-$), ammonium (NH_4^+), orthophosphate (PO_4^{3-}), and silicic acid ($Si(OH)_4$) were determined colorimetrically using a Skalar auto analyzer (precision = $\pm$ 0.1 μM) (Leifer *et al.*, 2013, Dzwonkowksi *et al.*, 2017).

Dissolved inorganic nitrogen (DIN) was defined as $NO_3^- + NO_2^- + NH_4^+$. Potential nutrient stoichiometric limitations were determined using criteria by Dortch and Whitledge (1992) and Justić *et al.,* (1995). Triplicate samples for Chl *a* (μg L^{-1}) were determined fluorometrically using methanol extraction (Welschmeyer 1994) and analyzed on a Turner 10-AU fluorometer.

Total daily photosynthetically available radiation (PAR_0, mol photons m^{-2} d^{-1}) for the study time frame was obtained via a cosine PAR data sensor at the John C. Stennis Space Center, Mississippi (30.36^o N, 89.60^o W), which is approximately 75 kilometers (km) northwest from the study area. The monthly four-year average (2009-2013) was used on days in which PAR_0 data was unavailable.

2.2.6 Statistical analysis

Hierarchical cluster analysis (HCA, IBM SPSS Statistics 24.0) was used to classify water types based on temperature (T), salinity (S), bulk chlorophyll a (Chl *a*), bathymetry, and water column stability (N^2) following methods similar to Chakraborty and Lohrenz (2015). Ward's method and Block distance were used to cluster Z-score transformed data. Statistical differences between seasons, water types, environmental variables, and microplankton were analyzed using Kruskal-Wallis-H one-way analysis of variance on ranks and Mann-Whitney-U tests following a Shapiro-Wilk test to verify assumptions of normality using SPSS (IBM SPSS Statistics 24.0). All data are reported as median $\pm$ median absolute deviation (MAD) unless noted otherwise. The advantage to using the median absolute deviation as opposed to the standard deviation about the mean is that MAD provides a more robust measure of dispersion for non-parametric data with outliers (Leys *et al*., 2013). In terms of Chl *a*, the microplankton community biomass (μg

C L^{-1}), was binned into trophic states such that eutrophic (>5.0 μg Chl *a* L^{-1}), mesotrophic (0.5 to 5.0 μg Chl *a* L^{-1}), and oligotrophic (<0.5 μg Chl *a* L^{-1}) conditions were defined following criteria outlined by Sherr and Sherr (2009).

Canonical cluster analysis (CCA) was used to evaluate microplankton community composition to environmental variability and was applied using Canonical Community Ordination, CANOCO version 5.0. CCA is a multivariate technique that is applicable to plankton studies due to its capacity to handle nonlinearity caused by zeros in the dataset (ter Braak and Verdonschot, 1995). All community data were log transformed log10(x + a) following methods by Kruk *et al.* (2011). The importance of each variable was determined using an interactive forward selection procedure to identify parameters that best explained the variability. A Bonferroni correction was applied to the significance levels to correct for multiple sets of observations. Monte Carlo simulations with 499 unrestricted permutations were used to determine the statistical significance of each classification. A total of six environmental variables, which includes physical (*i.e.*. T, S, and N^2) and biogeochemical (*i.e.*. Chl *a*, $NO_2 + NO_3^-$, NH_4^+, PO_4^{3-}, and $Si(OH)_4$ constituents, were used in the analysis. Absolute values of the inter-set correlation coefficient, r >|0.4| were considered biologically significant following recommendations by Rakocinski *et al*. (1996).

2.3 RESULTS

2.3.1 Hydrographic and environmental conditions

Autumn hydrographic regime was vertically well-mixed and stratified in the spring sampling regimes (Greer *et al*., 2018). Post-tropical cyclone Patricia greatly influenced the vertical stratification and distribution of biogeochemical variables within

this region (see Dzwonkowski *et al.*, 2017). The autumn hydrography had lower freshwater discharge, but was warmer (24.4 $\pm$ 0.6 ^{o}C) and saltier (34.8 $\pm$ 0.6 PSU). A stratified water column with lower surface water temperature (20.3 $\pm$ 0.6 ^{o}C) and salinity (29.3 $\pm$ 3.6 PSU), and higher fluorescence characterized the springtime campaign (Figure 2.4). The mean $\pm$ standard deviation PAR for the 2009-2016 long term average was 31.8 $\pm$ 3.6 mol photon m^{-2} d^{-1} for the days 29 October- 05 November (autumn) and 35.8 $\pm$ 16.9 mol photon m^{-2} d^{-1} for the days 30 March-09 April (spring) (Figure 2.5). Though PAR was greater in spring than in autumn, it was not statistically different between seasons (Mann-Whitney U, $p \leq 0.05$).

Hydrographic regions were determined using HCA, where three water types were identified for autumn (inner-, mid-, and outer-shelf, Figure 2.6) and four water types (estuarine, inner-, mid-, and outer-shelf, Figure 2.7) were defined for spring.

Inorganic nutrient concentrations differed seasonally and spatially (Table 2.5, Figure 2.8). DIN was greater in spring (1.6 $\pm$ 1.4 μM) relative to autumn (0.3 $\pm$ 0.3 μM). DIN concentrations were greatest in estuarine waters in spring where (NO_2 + NO_3^-) was highest, and lowest in mid-shelf waters in autumn. NH_4^+ concentrations also were greater in spring relative to autumn, with highest concentrations found in the estuarine water type. Though seasonal median concentrations of PO_4^{3-} and $Si(OH)_4$ concentrations were higher in autumn than spring, springtime estuarine and inner shelf $Si(OH)_4$ concentrations were more than five times greater than autumn inner shelf waters. Nutrient ratios of both DIN:P < 10 and Si:DIN > 1 suggest that DIN likely was yield limiting in all water types in autumn and only in the outer shelf in spring, whereas PO_4^{3-} (Si:P and DIN: P > 22) may have been limiting in estuarine and inner shelf waters in spring.

The assessment of stoichiometric limitations does not indicate whether limitation is likely, but comparisons of ambient nutrient concentrations with those concentrations likely to limit nutrient uptake provide a better indication for nutrient limitations in aquatic ecosystems, thus, threshold values of 2.0 μM, 1.0 μM, and 0.1 μM were suggested for $Si(OH)_4$, DIN, and PO_4^{3-}, respectively, following criteria of Justić *et al.*(1995). Following these criteria, results suggest that only DIN was limiting and that was in autumn at all stations and PO_4^{3-} was limiting along the inner shelf waters in spring. Additionally, potential $Si(OH)_4$ limitation may have been approached for diatoms at mid and outer shelf stations in spring where median concentrations were 3.7 $\pm$ 3.7 μM and 2.0 $\pm$ 3.1 μM.

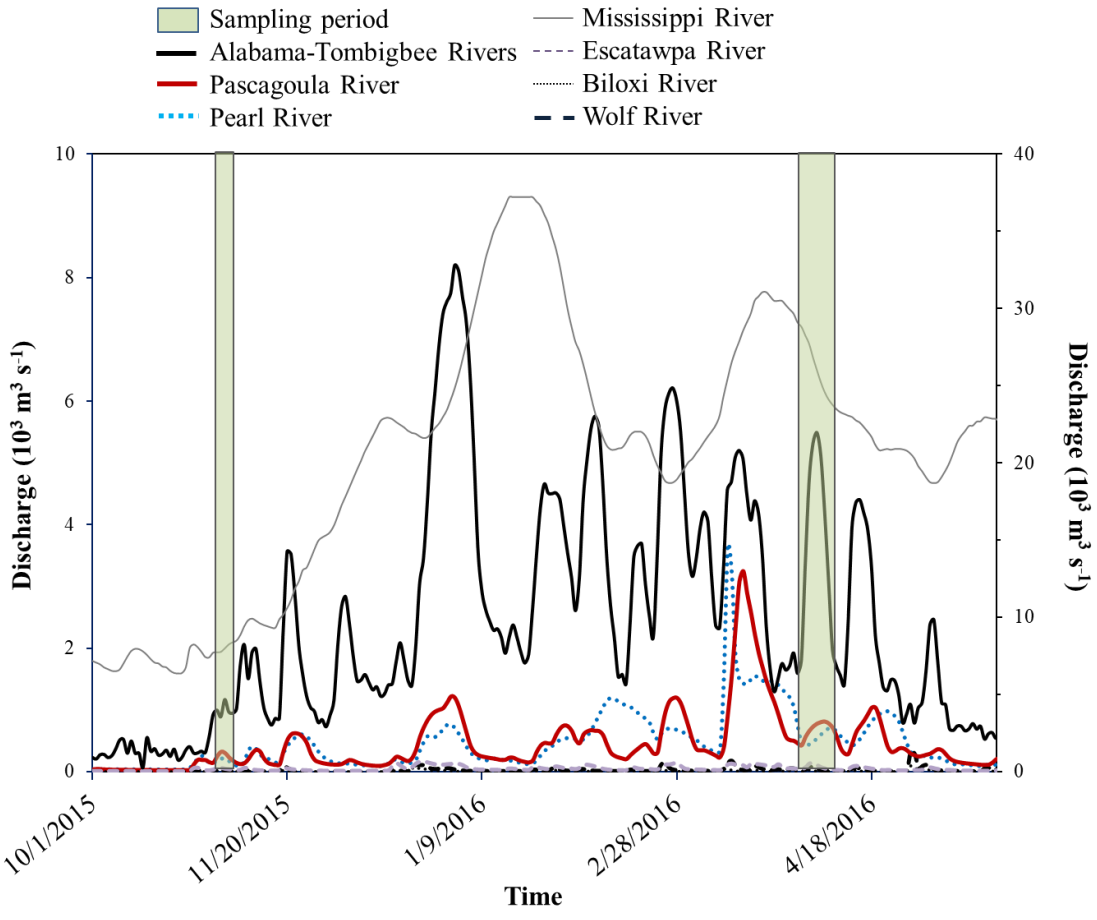

Figure 2.3 *River Discharge*

Mean daily discharge (10^3 m^3 s^{-1}) of the important rivers discharging into the Mississippi Bight and the Mississippi River (MSR) discharge is located on left and right y-axes, respectively. Discharge data was obtained from The United States Geological Survey (USGS) database (https://waterdata.usgs.gov/usa/nwis/sw). Discharge for the Alabama and Tombigbee rivers were combined to obtain the total discharge from the Mobile Bay. Shaded bars represent sampling periods for the two CONCORDE cruises (green) during the October-November 2015 and March-April 2016 field seasons.

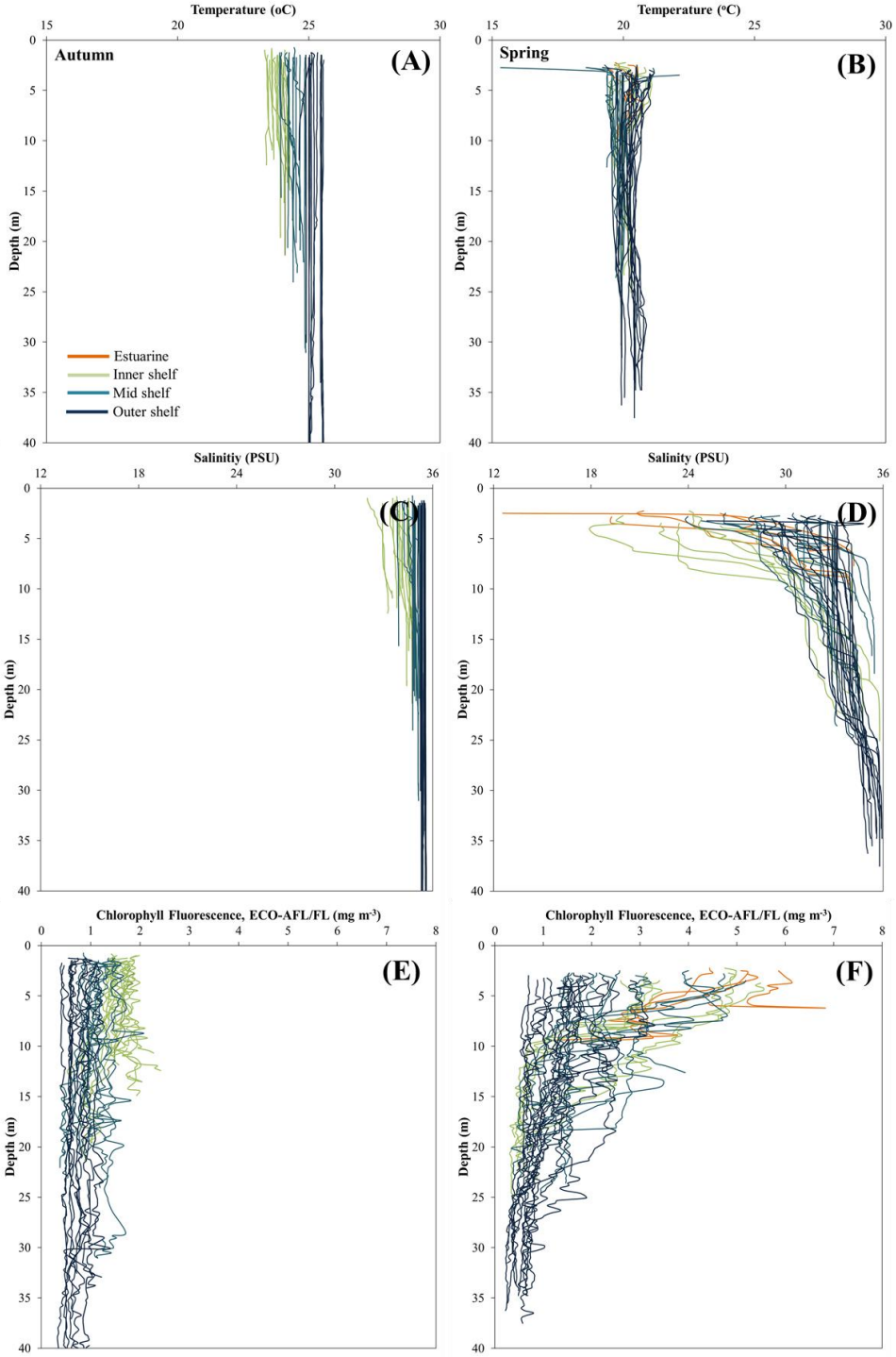

Figure 2.4 *Vertical profiles of temperature, salinity, and chlorophyll fluorescence*

Vertical profiles of temperature, salinity, and chlorophyll fluorescence in autumn (A, C, E) and spring (B, D, F). Water types are given for estuarine (yellow), inner-shelf (green), mid-shelf (malachite), and outer-shelf (blue).

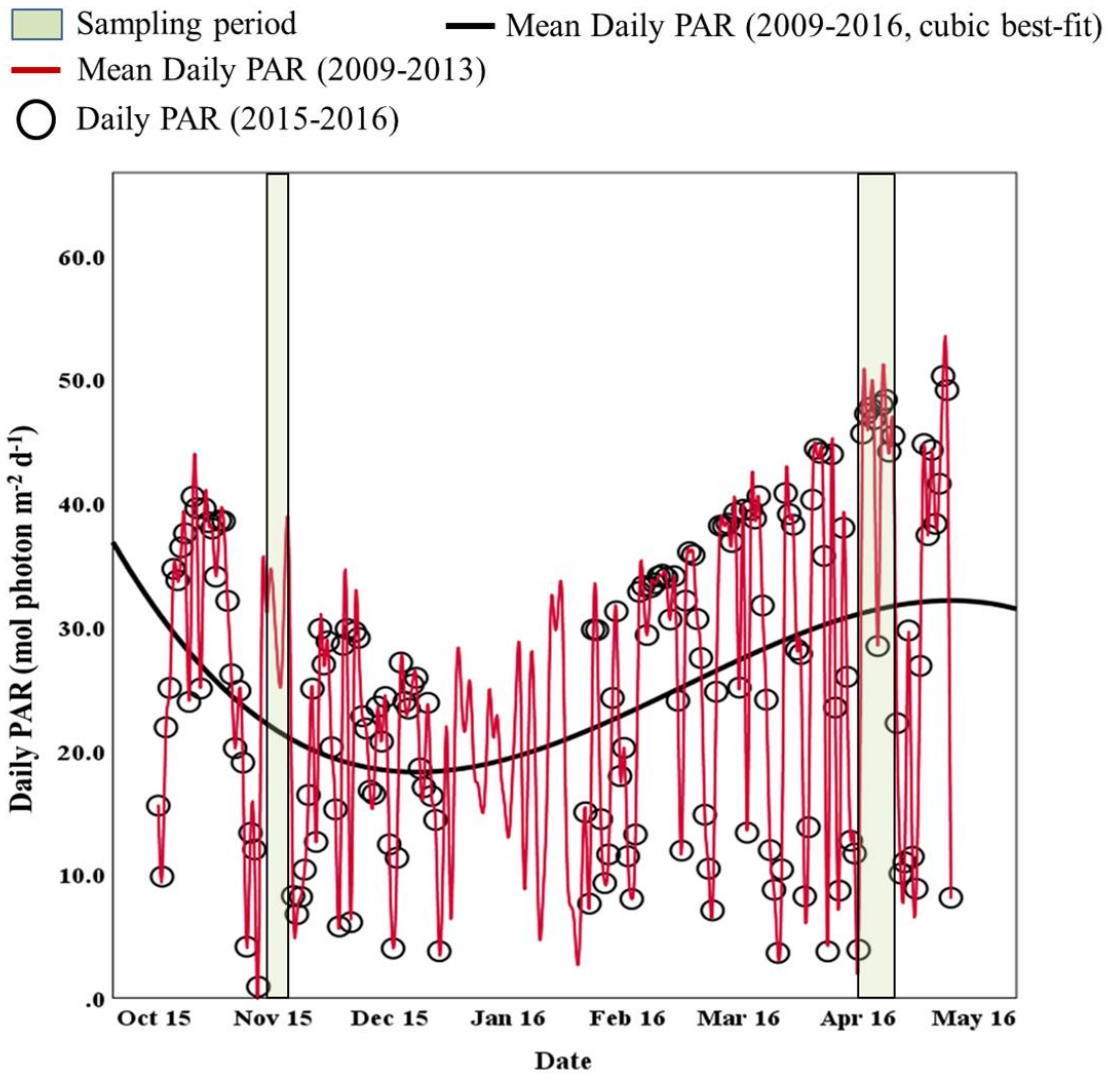

Figure 2.5 *Photosynthetically active radiation (PAR, mol m^{-2} d^{-1})*

PAR measured from Stennis Space Center, MS for October 2015-May 2016 (round circles), mean daily PAR from 2009-2013 (red line), and a best-fit 7-year average (solid black line). CONCORDE study periods indicated by vertical bars.

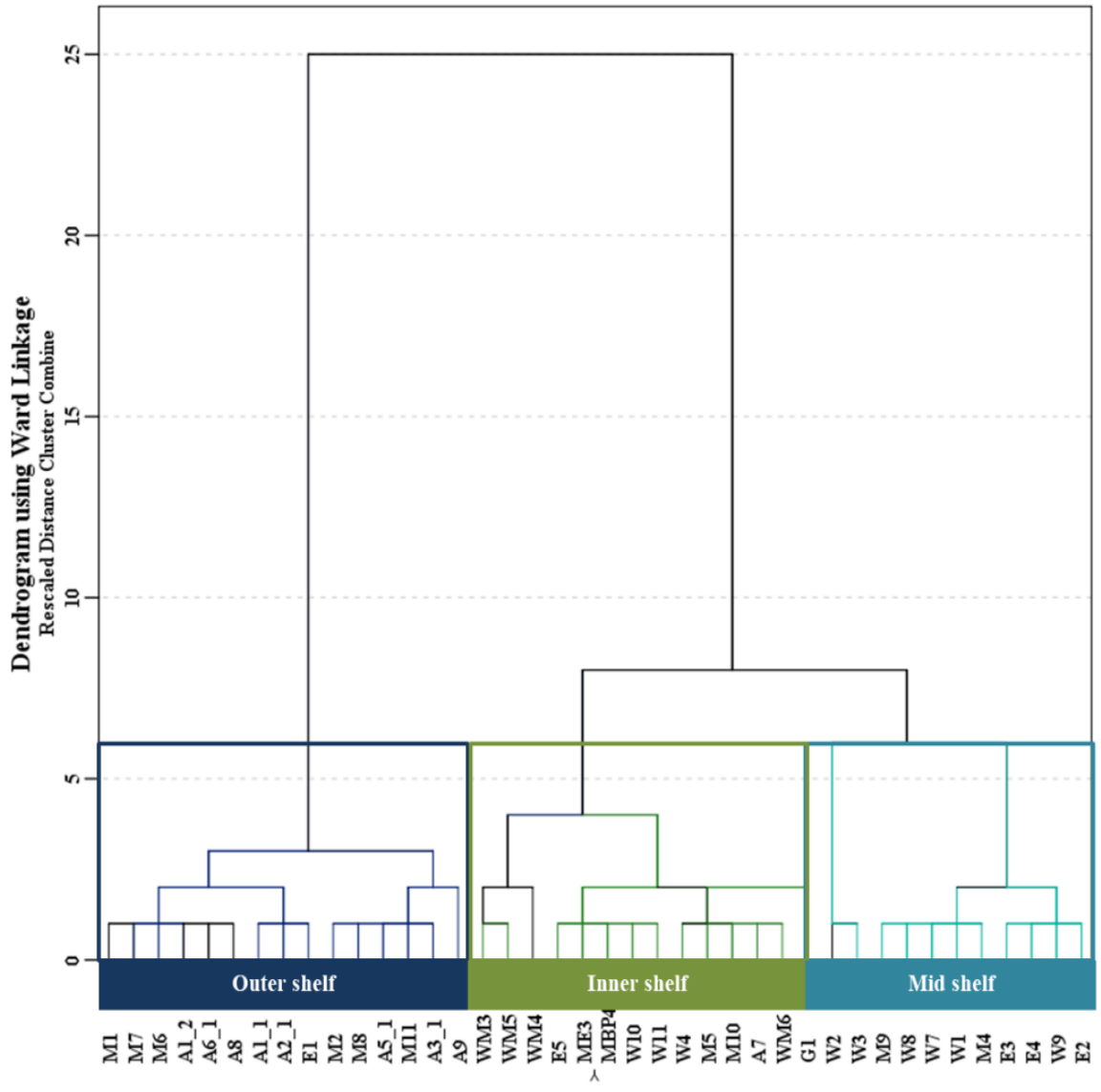

Figure 2.6 *Hierarchical Cluster Analysis for Autumn*

Hierarchical Cluster Analysis (HCA) dendrogram used to identify 3 water types (Inner, mid, outer shelf) in autumn. Clusters were chosen using 5 as the dissimilarity threshold. A Kruskal Wallis H test (one way ANOVA on ranks), (alpha < 0.05) indicated that two stations W2 and W3 were not statistically different from other stations within the mid shelf group.

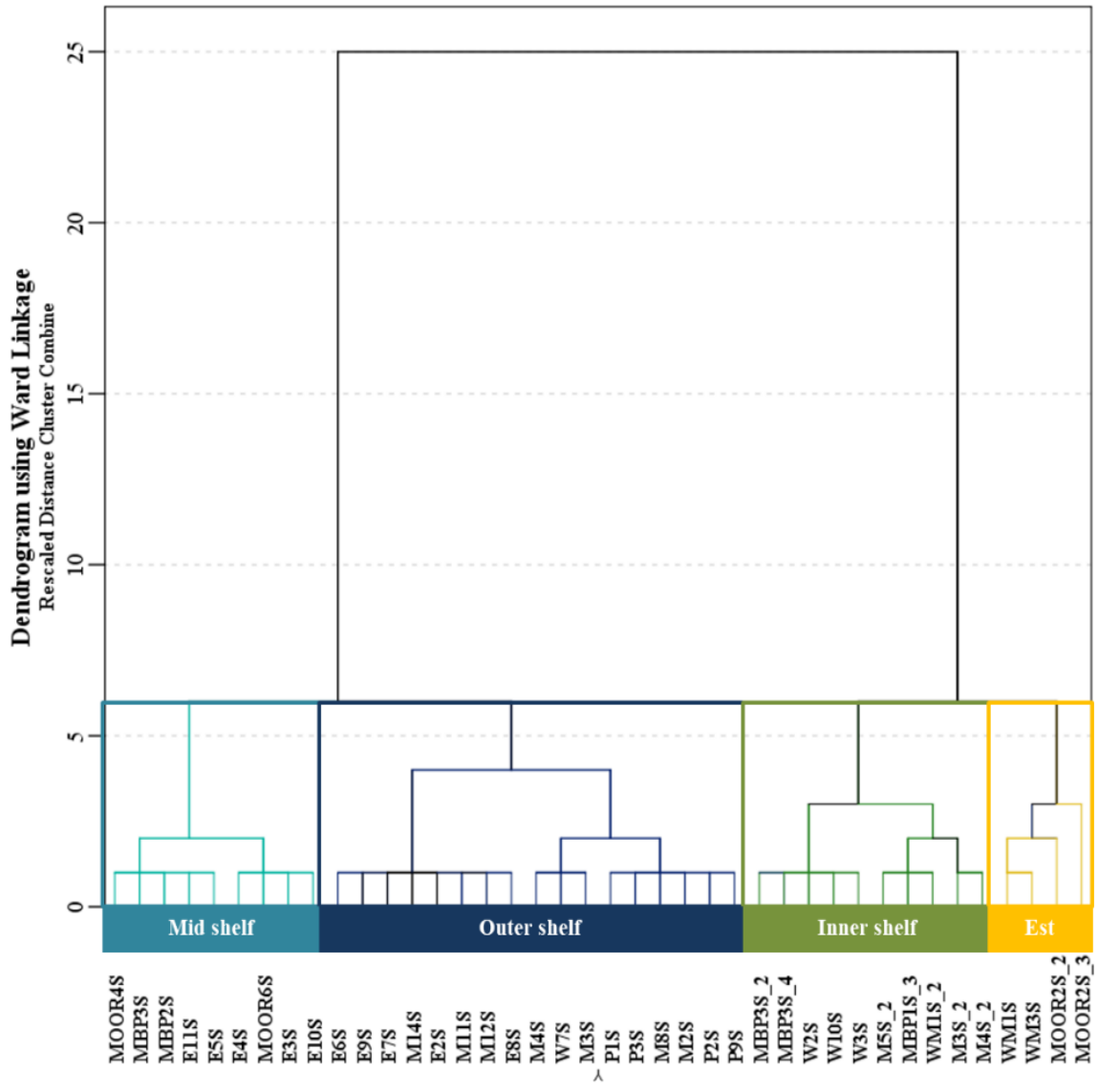

Figure 2.7 *Hierarchical Cluster Analysis for Spring*

HCA dendrogram used to identify 4 water types (estuarine, inner, mid, outer shelf) in spring. The parameters used to determine water types indicated that the stations were not statistically different from one another.

Table 2.5 *Median ± MAD values of physico-chemical constituents.*

Season	Water-Type	T (ºC)	S (PSU)	Chl *a* (μg L^{-1})	DIN (μM)	PO_4^{3-} (μM)	$Si(OH)_4$ (μM)	Si:DIN	Si:P	DIN:P
Autumn	IS	23.8 ± 0.2	33.9 ± 0.6	2.5 ± 0.7	0.6 ± 0.5	0.3 ± 0.1	5.7 ± 1.8	18.2 ± 11.7	17.9 ± 5.9	0.8 ± 0.4
	MS	24.3 ± 0.3	34.7 ± 0.4	1.7 ± 0.3	0.4 ± 0.5	0.3 ± 0.1	5.1 ± 1.1	29.5 ± 22.9	15.4 ± 4.1	0.4 ± 0.4
	OS	25.2 ± 0.2	35.4 ± 0.1	1.0 ± 0.2	0.6 ± 0.5	0.2 ± 0.1	2.4 ± 0.8	3.6 ± 14.2	9.2 ± 5.2	2.8 ± 2.1
Spring	ES	19.3 ± 1.3	20.6 ± 0.7	9.7 ± 3.3	3.3 ± 1.3	0.2 ± 0.0	33.4 ± 8.1	10.5 ± 9.7	167.1 ± 152.7	18.8 ± 18.1
	IS	20.6 ± 0.5	23.6 ± 2.2	7.1 ± 0.8	2.3 ± 3.0	0.1 ± 0.1	11.8 ± 10.6	5.1 ± 13.5	73.0 ± 58.6	16.0 ± 15.3
	MS	19.7 ± 0.2	30.9 ± 1.8	2.6 ± 0.5	3.0 ± 2.6	0.2 ± 0.1	3.7 ± 3.7	1.1 ± 17.6	7.5 ± 7.8	12.6 ± 12.0
	OS	20.5 ± 0.4	31.1 ± 1.9	1.9 ± 0.9	1.8 ± 2.0	0.2 ± 0.1	2.0 ± 3.1	0.8 ± 17.0	7.1 ± 8.2	5.4 ± 4.8

Median ± MAD values of temperature (T, ºC), salinity (S, practical salinity units, PSU), chlorophyll *a* (Chl *a*,μg L^{-1}), dissolved inorganic nitrogen (DIN = NO_2 + NO_3^- + NH_4^+, μM), orthophosphate (PO_4^{3-}, μM), silicic acid ($Si(OH)_4$, μM), and nutrient ratios within different water types (ES = estuarine, IS = inner-shelf, MS = mid-shelf, OS = outer-shelf). Nutrient ratios were determined as the medians of the ratios in each water type, where Si, DIN, P represent the silicic acid, dissolved inorganic nitrogen, and orthophosphate, respectively. Triplicate samples for Chl *a* were analyzed for autumn and spring. Nutrient samples were not replicated.

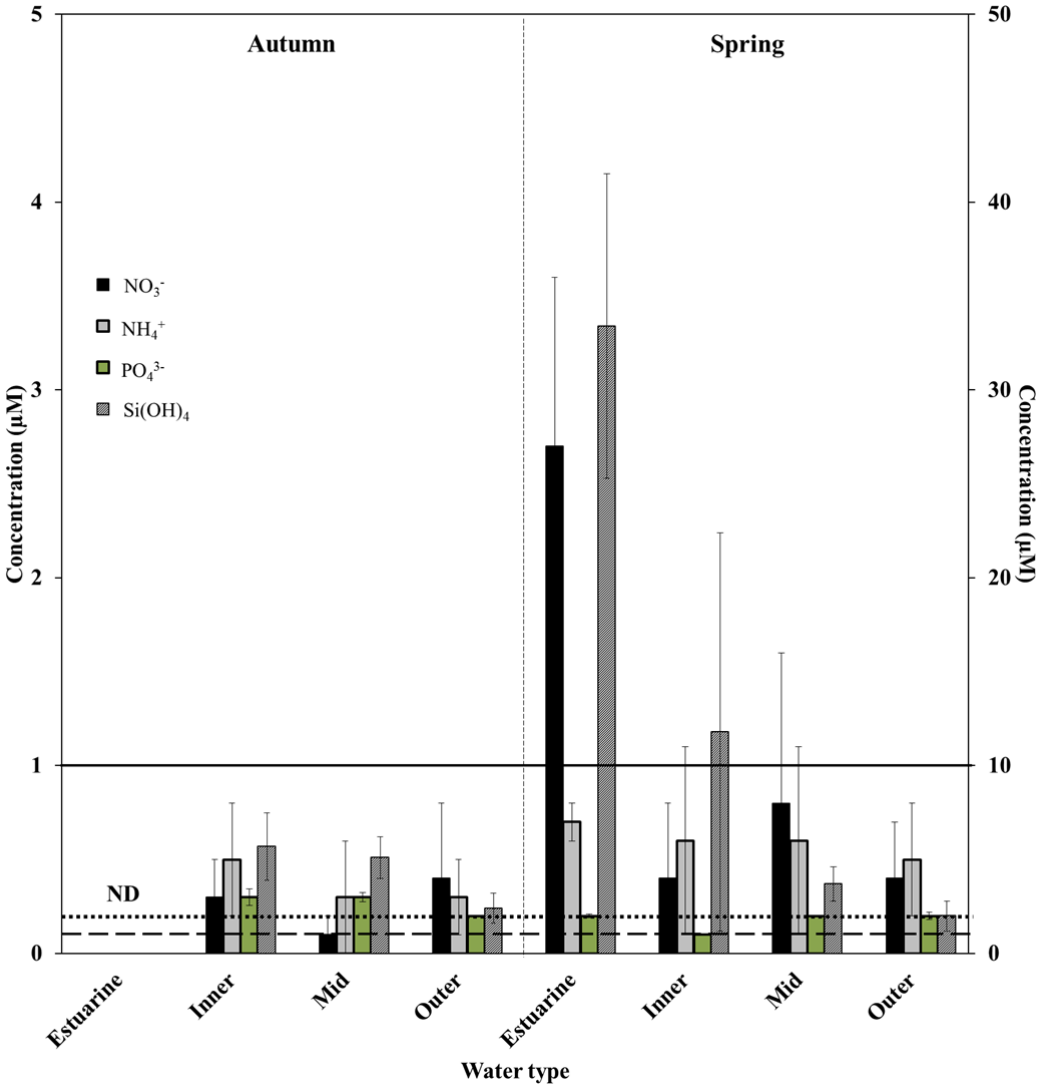

Figure 2.8 *Absolute concentrations for inorganic nutrients for the different water types.*

Absolute concentrations are presented in the bar plots, error bars represent the median absolute deviation (MAD). Silicic acid ($Si(OH)_4$) is plotted on the secondary y-axis. The solid horizontal line is the threshold for NO_3^- andNH_4^+ limitation (dissolved nitrogen, DN = 1 µM), the dashed line is the threshold for PO_4^{3-} limitation (0.1 µM), and the dotted line is the threshold for $Si(OH)_4$ limitation following the criteria of Justić *et al.* (1995).

Table 2.6 *Kruskal-Wallis analysis of spatial variability for environmental variables*

Kruskal-Wallis (KW) analysis of spatial variability for abiotic variables in autumn (df =1) and spring (df = 3). Significance between water types is given by χ^2 with a significance level $p \leq 0.01$ (**) and $p \leq 0.05$ (*). NO_x represents $NO_2 + NO_3^-$.

Parameter	Autumn		Spring	
	χ^2	p	χ^2	p
T (^oC)	12.055	0.001**	20.991	0.000**
Salinity (PSU)	11.624	0.001**	27.424	0.000**
Brunt Vaisala (s^{-1})	2.665	0.103	27.377	0.000**
PAR (mol photon m^{-2} d^{-1})	2.069	0.150	4.181	0.243
NO_x(µM)	1.702	0.192	6.147	0.105
NH_4^+ (µM)	0.560	0.454	1.283	0.733
PO_4^{3-} (µM)	0.241	0.623	4.344	0.227
$Si(OH)_4$ (µM)	0.500	0.480	20.945	0.000**
DIN:P	1.833	0.176	4.949	0.176

Table 2.7 *Mann-Whitney test for differences between seasons for environmental variables*

Mann-Whitney test for differences between autumn and spring. The MW statistic (U) with confidence intervals set at $p \leq 0.01$ (**) and $p \leq 0.05$ (*). NO_x represents $NO_2 + NO_3^-$.

Parameter	U	Significance	N
T (^oC)	0	0.000**	78
Salinity (PSU)	10	0.000**	78
Brunt Vaisala (s^{-1})	84	0.000**	78
PAR (mol photon m^{-2} d^{-1})	472	0.004**	78
NO_x(µM)	338	0.001**	70
NH_4^+ (µM)	126	0.001**	51
PO_4^{3-} (µM)	256	0.000**	72
$Si(OH)_4$ (µM)	572	0.395	72
DIN:P	116	0.000**	69

Chl *a*, (μg Chl *a* L^{-1}), ranged from (0.8 – 14.3 μg Chl *a* L^{-1}) and differed significantly (Kruskal-Wallis H, $p < 0.05$) between water types and seasons (Table 2.5). Median Chl *a* concentrations were greatest (9.7 $\pm$ 3.3 μg Chl a L^{-1}) in spring within estuarine waters, whereas the lowest median phytoplankton biomass (1.0 $\pm$ 0.2 μg Chl *a* L^{-1}) was found in autumn along the outer shelf stations. In terms of seasonality, mesotrophic conditions persisted in autumn (median range = 1.0 $\pm$ 0.2 to 2.5 μg Chl *a* L^{-1}), whereas eutrophic (7.1 $\pm$ 0.8 to 9.7 $\pm$ 3.3 μg Chl *a* L^{-1}) and mesotrophic (1.9 $\pm$ 0.9 to 2.6 $\pm$ 0.5 μg Chl *a* L^{-1}) conditions were identified in spring. Oligotrophic conditions were not observed in either season.

2.3.2 Seasonal and spatial patterns in microplankton communities and biomass

Classified microplankton and unclassified particulate matter were not statistically different (Mann-Whitney U, $p < 0.05$) among seasons. Classified microplankton (unclassified particulate matter) accounted for 52.1% (47.9%) and 51.3% (48.7%) of the imaged particles in autumn and spring, respectively (Figure 2.6). Median particle concentration was nearly an order of magnitude greater in spring relative to autumn, with $5.2 \times 10^5 \pm 1.8 \times 10^5$ particles L^{-1} and $8.5 \times 10^4 \pm 5.1 \times 10^4$ particles L^{-1} reported for classified microplankton in spring and autumn, respectively (Figure 2.6).

Microplankton community abundance was closely associated with water types for both seasons, where the highest particle concentrations were found within estuarine and inner shelf communities and reduced concentrations at stations within mid- to outer-shelf waters (Figure 2.9). Nanoplankton and non-flagellates were the most abundant groups in both seasons, though not statistically different from each other (Mann-Whitney U, $p < 0.05$), but they were significantly more abundant than flagellates and microzooplankton

groups (Figure 2.9). Nanoplankton were more abundant in spring than in autumn, accounting for 49.7% of the total classified particles in spring and only 42.0% in spring. Total nanoplankton particle concentration was significantly greater in spring ($1.9 \times 10^6 \pm 5.9 \times 10^5$ particles L^{-1}) than in autumn ($9.0 \times 10^4 \pm 6.0 \times 10^4$ particles L^{-1}). However, flagellates were relatively more abundant in autumn ($1.8 \times 10^4 \pm 1.3 \times 10^4$ particles L^{-1}) than spring ($5.3 \times 10^4 \pm 3.0 \times 10^4$ particles L^{-1}), yet accounted for only 8.5% and 1.4% for the total classified particles, respectively. Non-flagellates also were most abundant in terms of relative contribution to the classified images in spring (48.3%) than autumn (43.3%), with total median particle concentration for $1.8 \times 10^6 \pm 9.4 \times 10^5$ particles L^{-1} and $9.3 \times 10^4 \pm 3.8 \times 10^4$ particles L^{-1}, respectively. Microzooplankton concentrations were not significantly different between seasons (Mann-Whitney U, < 0.05), with median + MAD particle concentrations for autumn ($1.3 \times 10^4 \pm 5.0 \times 10^3$ particles L^{-1}) and spring ($2.0 \times 10^4 \pm 9.1 \times 10^3$ particles L^{-1}), yet their relative contribution to the classified images accounted for 6.2% in autumn, but only 0.5% in spring.

Microplankton cell diameter (μm, ABD) did not differ significantly between groups or seasonally (Mann-Whitney U, < 0.05), except estuarine springtime non-flagellates (15.4 ± 0.6 μm, ABD) whose cell diameters were significantly smaller than any other group in either season (Figure 2.9C). Nanoplankton median particle size distribution did not differ significantly between autumn (9.8 ± 0.7 μm, ABD) and spring (8.7 ± 0.2 μm, ABD). Median autumn (spring) particle size distributions across all water types for flagellates, non-flagellates, and microzooplankton were 21.8 ± 0.7 μm, ABD (23.0 ± 0.6 μm, ABD), 22.4 ± 0.3 μm, ABD (20.0 ± 0.3 μm, ABD), and 21.2 ± 0.3 μm, ABD (22.8 ± 2.2 μm, ABD), respectively. While the group median cell size did not differ

seasonally or between water types, the range of cell sizes increased in spring relative to autumn. flagellates, non-flagellates, and microzooplankton cell diameters ranged (minimum-maximum) from 10.9-68.2, 23.5-62.8, and 20.3-62.9 μm in autumn and 27.3-72.9, 28.0-61.3, and 37.8-78.3 μm in spring, respectively.

Total microplankton C_{BV} (μg C L^{-1}) was greater in spring (702.2 μg C L^{-1}) than autumn (214.4 μg C L^{-1}) (Figure 2.9D). Carbon biomass varied seasonally across all water types, with median values ranging 15.2 $\pm$ 10.7 μg C L^{-1} in autumn to 44.2 $\pm$ 34.2 μg C L^{-1} in spring. Biomass decreased across-shelf concomitant with particle abundance from the estuarine and inner shelf waters to outer-shelf waters. Nanoplankton, flagellates, and non-flagellates contributed more than 80% of the carbon biomass in spring, whereas Microzooplankton accounted for 55.1 % of the carbon biomass in autumn.

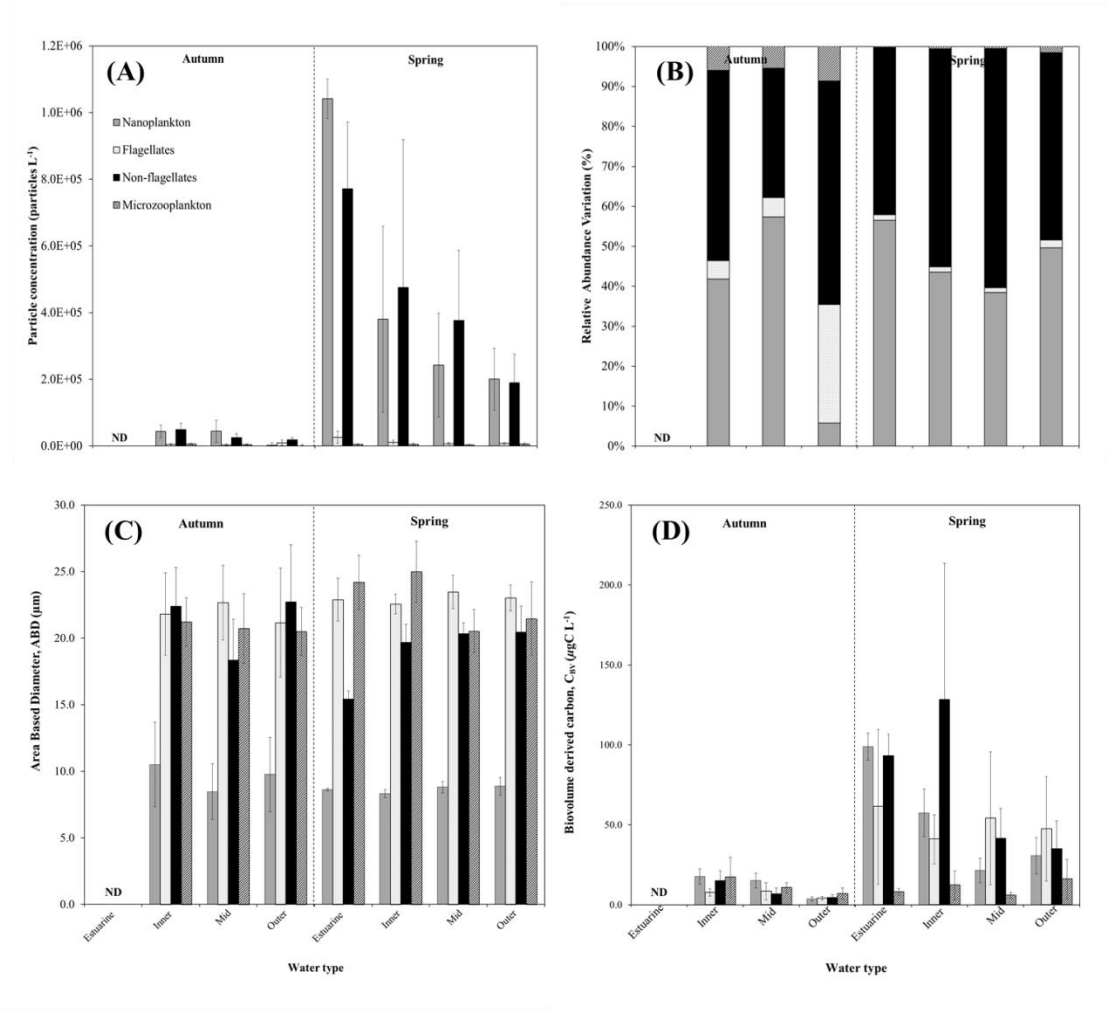

Figure 2.9 *Seasonal median ± MAD classified particle variables for Nanoplankton, Flagellates, Non-Flagellates, and Microzooplankton.*

Panels (A-D) represent the median ± MAD (error bars) particle concentration (particles L^{-1}) (A), relative abundance variation (%) for each group (B), area based diameter (μm, ABD) (C), and biovolume-derived carbon (μg C L^{-1}).

2.3.2.2 Estuarine and inner-shelf communities

Nanoplankton were the most abundant group in estuarine waters in spring (56.5%), whereas non-flagellates, mostly diatoms, were the most abundant microplankton group within inner shelf waters, contributing to 47.5% in autumn and 54.5% in spring (Figure 2.9). Flagellates and microzooplankton contributed < 10% of the classified particle concentration among the estuarine and inner shelf communities in both seasons (Figure 2.9).

Among the flagellate group, prorocentroids, gymnodinoids, and euglenoids were the most abundant groups in both autumn and spring (Figure 2.10A-C). Relatively low particle concentrations and percent contribution to classified images indicated that bloom levels were not reached for any flagellate group. Prorocentroids were the dominant flagellate group in spring, accounting for 67% in estuarine waters and more than 40% within inner shelf waters. Athecate gymnodinoids were represented by several dinoflagellate genera, including *Gyrodinium* Kofoid and Swezy spp. and *Karenia* (Davis) Gert Hansen and Moestrup spp. and were the dominant flagellate group along inner-shelf waters in autumn, contributing to more than 37% of the group community, whereas *Torodiniumn* (Pouchet) Kofoid and Swezy spp., *Akishiwo* (Hirasaka) Gert Hansen and Moestrup spp., and *Gyrodinium* Kofoid and Swezy spp. were predominant in spring. Thecate gymnodinoids consisted primarily of mixed assemblages of *Heterocapsa* (Ehrenberg) F.Stein spp. >20 μm ABD, with few *Alexandrium* Halim spp. and *Protoperidinium* Bergh spp. cells. Euglenoids increased in relative abundance from 14.6% in autumn to 19.3% in spring, with *Eutreptia* Perty spp. and *Euglena* Ehrenberg spp. the representative genera in both seasons.

Estuarine and inner-shelf nanoplankton carbon biomass was 17.7 $\pm$ 4.9 μg C L^{-1} in autumn, but increased nearly an order of magnitude to 156.4 $\pm$ 23.4 μg C L^{-1}spring. Flagellate carbon biomass increased from 7.7 $\pm$ 2.4 μg C L^{-1} in autumn to 102.3 $\pm$ 63.8 μg C L^{-1} in spring. Whereas gymnodinoids, prorocentroids, and cerationoids contributed significantly to flagellate biomass in autumn, a large (>50 μm, ABD) solitary *Acanthometra* Müller spp. radiolarian accounted for nearly 40% of the Flagellate carbon biomass in autumn. Prorocentroids and athecate-gymnodinoids each contributed 31.8 + 19.0 μg C L^{-1} and 14.2 $\pm$ 6.6 μg C L^{-1}, which accounted for a combined 42% of the total flagellate carbon biomass in spring (Figure 2.10C).

Diatoms were the most abundant non-motile group in both seasons (Figure 2.11A-C), with mixed assemblages of elliptic prism, skeletonemanoid, acerate_nitzschioid, and asterionellopsioid groups predominant in autumn, whereas skeletonemanoid and acerate_nitzschioid were predominant in spring. Relative contributions of acerate_nitzschioid increased significantly from autumn to spring, increasing from less than 17% in autumn to more than 71% of the total imaged microplankton biomass in springtime (Figure 2.10B). Taxonomic analysis of this group showed that springtime cells were elevated above 500,000 cells L^{-1} and consisted primarily of *Pseudo-nitzschia* Peragallo spp., though it is not certain whether these were DA-producing (*i.e.* HAB-forming) species. Small (< 20 μm, ABD), solitary cells and chains of *Skeletonema* Greville spp. and *Thalassiosira* (Cleve) Hasle spp. were the predominant skeletonemantoid cells, although their proportionate contribution did not differ significantly between seasons. Mixed assemblages of *Leptocylindrus* Lebour spp., *Guinardia* spp, Paralia Heiberg spp., and *Cymatosira* Grunow spp. contributed to the

cylindrical chains diatom biomass in autumn, whereas *Leptocylidrus* Lebour spp, *Guinardia* Peragallo spp., and *Dactyliosolen* Peragallo spp. were more abundant in spring for this group. Mixed assemblages of cyanobacteria and desmids were of lesser importance in these waters. Cyanobacteria consisted primarily of unidentifiable filaments and clumps of round cells, and were more abundant in autumn than in spring, whereas *Scenedesmus* Meyen spp. were present at inner shelf stations in spring.

Median non-flagellate biomass varied from 13.7 $\pm$ 10.9 μg C L^{-1} in autumn to 182.2 $\pm$ 80.4 μg C L^{-1} in spring. Diatoms contributed to more than 98% of this carbon biomass, with mixed assemblages of elliptic prism, cylindrical chains, and discoidal, mostly *Coscinodiscus* Ehrenberg spp., contributing 8.5 $\pm$ 4.7 μg C L^{-1} of the total biomass in autumn. However, springtime diatom biomass was dominated by Acerate_nitzschioid and Skeletonemanoid cells, which contributed a combined total of 162.3 $\pm$ 71.2 μg C L^{-1} (Figure 2.11C).

Microzooplankton groups consisted primarily of *Mesodinium* Lohman spp. and the aloricate choreotrichid ciliates (Figure 2.12A-C) *Strombidium* Claparède and Lachmann and *Strombilidium* spp. Autumn communities did not differ from one another in terms of relative particle concentration, although total concentration increased in spring (Figure 2.12 A). Aloricate choreotrichids was the dominant group in autumn, contributing to more than 54% of the classified microzooplankton community, whereas *Mesodinium* Lohman spp. contributed over 53% to the community in spring. Tintinnids and other microzooplankton were absent within estuarine waters and did not contribute significantly (<10%) to the overall microzooplankton community composition in inner shelf waters in either season.

Microzooplankton biomass varied seasonally ranging from 1.1 μg C L^{-1} to 40.5 μg C L^{-1} with median $\pm$ MAD significantly greater in autumn (44.2 $\pm$ 39.7 μg C L^{-1}) than spring (25.5 $\pm$ 17.6 μg C L^{-1}) (Figure 2.10C). The presence of rare, but large benthic foraminifera identified as *Ammodiscus* Reuss spp. contributed to 67% of the microzooplankton biomass in autumn, whereas aloricate choreotrichs accounted for a 59% of the springtime biomass.

2.3.2.3 Mid-shelf communities

Nanoplankton were the most abundant group in autumn, contributing 59.6% to the total community, yet only contributed 41.5% in spring. Although flagellate concentrations were significantly lower in autumn relative to spring, mid-shelf communities did not exhibit stark differences in community structure between either season or other water types (Figure 2.10). Mixed assemblages of athecate gymnodinoids, such as *Gymnodinium* Stein spp. and *Gyrodinium* Kofoid and Swezy spp., contributed to nearly 40% of the mid-shelf flagellate community in autumn, whereas thecate gymnodinoids, mainly >20 μm ABD *Heterocapsa* (Ehrenberg) F.Stein spp. and *Alexandrium* Halim spp., contributed to over 37% to the flagellate community in spring, increasing nearly three-fold from autumn.

Median nanoplankton carbon biomass ranged from 15.2 $\pm$ 4.5 μg C L^{-1} in autumn to 21.6 $\pm$ 7.7 μg C L^{-1} in spring across water types. Carbon biomass of flagellates was nearly three times greater in spring (35.7 μg C L^{-1}) than autumn (11.1 μg C L^{-1}). Although cerationoids were relatively rare throughout mid-shelf waters in both seasons, large (> 70 μm, ABD) *Ceratium* Schrank spp. cells contributed to 58.1% of the carbon biomass for flagellates in spring. Athecate gymnodinoid biomass accounted for 20.1% of

the total flagellate biomass in spring, doubling from 2.8 $\pm$ 1.7 μg C L^{-1} in autumn to 7.5 $\pm$ 3.6 μg C L^{-1}. Despite thecate gymnodinoid biomass nearly quadrupling in spring, (1.1 $\pm$ 0.6 μg C L^{-1} to 4.1 $\pm$ 2.3 μg C L^{-1}) their relative contribution to the total flagellate biomass remained relatively static between seasons, contributing 10.6% in autumn and 11.5% in spring.

Diatoms were the predominant non-flagellate group in both autumn and spring, and were the most abundant microplankton group in spring ($3.7 \times 10^5 \pm 2.0 \times 10^5$ particles L^{-1}). Autumn mid-shelf communities exhibited greater diversity in terms of the presence of multiple MBFGs, with mixed assemblages of acerate_nitzschioid cells (e.g. *Cylindrotheca* Rabenhorst spp., *Pseudo-nitzschia* Peragallo spp.) and asterionellopsioid chains, mainly *Chaetoceros* Ehrenberg spp. and *Thallasionema* (Grunow) Mereschkowsky spp., contributing to 35% and 23%, respectively (Figure 2.11B). Skeletonemanoid, elliptic prism, and cylindrical cells comprised less than 16% of the total non-flagellate community. This pattern was significantly different in spring, when the diatom community was dominated by acerate_nitzschioid cells, mostly *Pseudo-nitzschia* Peragallo spp. This group comprised over two-thirds of the diatom biomass and contributed nearly 60% of the total microplankton community in spring. *Chaetoceros* Ehrenberg spp. were the predominant genera within the asterionellopsioids, which contributed to nearly 30% of the total non-flagellate community. Although mixed assemblages of cyanobacteria, consisting of unidentifiable filaments and amorphous clumps of small (< 20 μm, ABD) cells, were present in autumn, these communities were mostly absent in spring.

Diatoms accounted for most of the non-flagellate biomass in both seasons, contributing 6.7 $\pm$ 4.7 μg C L^{-1} and 48.5 $\pm$ 23.4 μg C L^{-1} to the total microplankton biomass in autumn and spring, respectively. Springtime biomass was more than an order of magnitude greater than in autumn. Diatom biomass in autumn ranged from 0.4 $\pm$ 0.3 μg C L^{-1} to 1.8 $\pm$ 1.0 μg C L^{-1}, with all MBFGs contributing anywhere from 6.2% to 21.3% of the diatom biomass in autumn. This pattern differed in spring, concomitant with shifts in dominant taxa, with acerate_nitzschioid, asterionellopsioid, and cylindrical chains, contributing 47.3%, 30.8%, and 12.5%, respectively, of the total non-flagellate biomass in spring (Figure 2.11).

Mid-shelf microzooplankton communities were not significantly different in terms of abundance or structure between seasons. Aloricate choretrochids and *Mesodinium* Lohman spp. were the most abundant groups, collectively contributing over 95% and 86% of the microzooplankton community in autumn and spring, respectively. Tintinnids were rare in both seasons, although they were more abundant in spring than autumn (Figure 2.12).

Microzooplankton biomass increased in spring, with 31.0% of the biomass attributed to a single large tintinnid with an agglutinated lorica belonging to the *Tintinnopsis* Stein genus (Figure 2.12A-C). Aloricate choreotrichid biomass did not differ between seasonally, but was greater in autumn (8.0 $\pm$ 3.1 μg C L^{-1}) relative to spring (5.0 $\pm$ 1.3 μg C L^{-1}). Despite *Mesodinium* Lohman spp. being highly abundant in both seasons, they contributed only 12.0% of the autumn microzooplankton biomass, and only a fraction (<1.5%) of the biomass in spring mid-shelf waters.

2.3.2.4 Outer-shelf communities

Nanoplankton accounted for 28.7% and 53.1% of the community in autumn and spring, respectively (Figure 2.10A-B). Flagellates abundance was lowest in autumn, accounting for only 1.5% of the total community of microplankton. Athecate gymnodinoids were the most abundant flagellate accounting for 25.6% of the flagellate community and cerationoid 17.2%. Springtime abundances increased 94% to 9.2 x 10^3 $\pm$ 7.5 x 10^3 particles L^{-1}. Thecate and athecate gymnodinoids were the most abundant flagellates, accounting for 40.7% and 26.7%, respectively.

Nanoplankton biomass increased nearly an order of magnitude in spring (30.7 $\pm$ 11.3 μg C L^{-1}) from autumn (3.7 $\pm$ 1.3 μg C L^{-1}) (Figure 2.7). Flagellate biomass also was significantly greater in spring (24.6 $\pm$ 43.1 μg C L^{-1}) than autumn (10.1 $\pm$ 8.2 μg C L^{-1}), with cerationoids, athecate and thecate gymnodinoids accounting for 23.9%, 27.3% and 21.1%, respectively (Figure 2.10). Euglenoids comprised 10.2% of the biomass and were represented mainly by *Eutreptia* Perty spp.

Diatoms were the most abundant non-flagellate group and were significantly more abundant in spring (1.6 x 10^5 $\pm$ 8.1 x 10^4 particles L^{-1}) than in autumn (1.7 x 10^4 $\pm$ 1.0 x 10^4 particles L^{-1}) (Figure 2.11). Community structure was similar to other water types where the autumn community was comprised mainly of asterionellopsioid groups (45.1%), which was represented mainly by *Chaetoceros* Ehrenberg spp., as well as mixed assemblages of acerate_nitzschioid (21.2%) that was comprised mostly of *Cylindrotheca* Rabenhorst spp. and *Pseudo-nitzschia* Peragallo spp., and *Navicula* J.B.M. Bory de Saint-Vincent representing elliptic prisms (12.7%). While springtime diatoms consisted primarily of *Pseudo-nitzschia* Peragallo spp. of the acerate_nitzschioid groups (61.5%),

asterionellopsioids, represented by *Asterionellopsis* F.E. Round, R.M. Crawford, and D.G. Mann and *Chaetoceros* Ehrenberg spp., accounted for 25.8% of the non-flagellate community.

Carbon biomass mirrored particle abundance in outer-shelf waters, with diatoms contributing 4.7 $\pm$ 3.0 μg C L^{-1} in autumn and 32.0 $\pm$ 16.4 μg C L^{-1} in spring (Figure 2.9C). Large (>30 μm, ABD) *Coscinodsicus* Ehrenberg spp. and cylindrical chains of *Leptocylindrus* P.T. Cleve in C.G.J. Petersen spp. and *Guinardia* Peragallo spp., contributed 21.5% and 18.9 % to the autumn diatom biomass, respectively. Acerate_nitzschioid, asterionellopsioid, and cylindrical chain, mainly *Guinardia* Peragallo spp., communities each contributed 16.7 $\pm$ 6.5 μg C L^{-1}, 8.7 $\pm$ 5.7 μg C L^{-1}, 3.5 $\pm$ 1.9 μg C L^{-1}, respectively, which accounted for more than 97.2% of the non-flagellate community and 86.7% of the total microplankton community.

Microzooplankton abundance was greatest in outer-shelf stations in both seasons, with higher abundance in spring (7.6 x 10^3 $\pm$ 4.1 x 10^3 particles L^{-1}) relative to autumn (2.6 x 10^3 $\pm$ 1.7 x 10^3 particles L^{-1}) (Figure 2.12A-C). *Strombidium* Claparède and Lachmann spp. was the dominant aloricate choreotrichid ciliate, which comprised 49.9% and 67.6% of the autumn and spring microzooplankton community, respectively. *Mesodinium* von Stein was more abundant in autumn (9. 5 x 10^2 $\pm$ 5.7 x 10^2 particles L^{-1}) than spring (8.8 x 10^2 $\pm$ 4.9 x 10^2 particle L^{-1}), accounting for 35.7% and only 11.6% of the total microzooplankton community in autumn and spring, respectively. Copepod nauplii were relatively rare and accounted for 7.2% in autumn and 3.8% in spring.

Microzooplankton biomass was greater in autumn (62.3 $\pm$ 58.8 μg C L^{-1}) relative to spring (50.6 $\pm$ 42.4 μg C L^{-1}), with 85.7% and 64.4% of the autumn and spring

biomass attributed to large (>50 μm, ABD) copepod nauplii present in the samples (Figure 2.12C). Aloricate choreotrichid biomass was 6.7 $\pm$ 3.8 μg C L^{-1} in autumn, doubling in spring to 15.7 $\pm$ 8.5 μg C L^{-1}. Despite *Mesodinium* von Stein contributing significantly to the microzooplankton community structure, these ciliates accounted for only a small percentage (< 2%) of the microzooplankton biomass.

2.3.3 Canonical correspondence analysis

The summary for the Canonical Correspondence Analysis (CCA) and inter-set correlations of environmental variables with CCA axes are presented in Tables 2.7-2.8 for autumn and Tables 2.9-2.10 for spring, respectively. Eigenvalues generated for every CCA axis where CCA 1 and CCA 2 were the highest values in both seasons. Total inertia (i.e variance) was 0.318 in autumn (Table 2.8) and 0.497 in spring (Table 2.8), whereas the sum of all CCA eigenvalues was 0.158 (autumn) and 0.184 (spring), representing 49.7% and 37.1% of the total inertia of the two respective seasons. A majority of the biologically-important environmental variables were expressed in the first two axes and were plotted along an ordination diagram (Figure 2.13). Species environmental correlations were high for all CCA axes in both autumn (range = 0.894 – 0.858) and spring (range = 0.0.841 – 0.702) (Tables 2.8 and 2.10). The cumulative percentage of species variance totaled 40.1% and 32.0% for the first four axes, and the cumulative percentage of species-environmental data totaled 80.6% and 86.4% (Table 2.9 and 2.11).

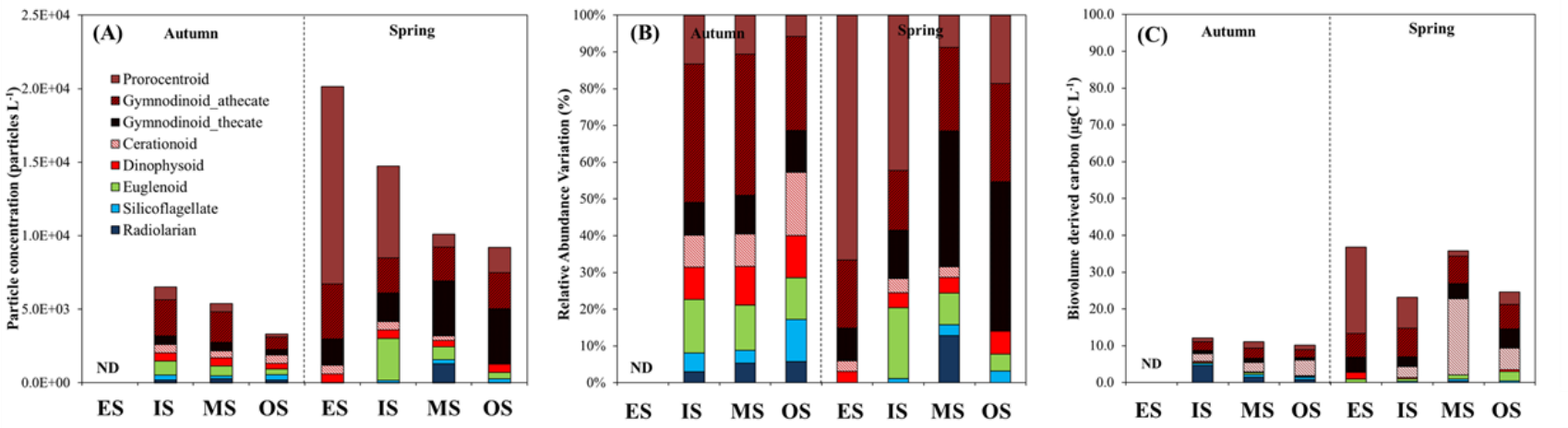

Figure 2.10 *Community composition for the different morphological based functional groups for Flagellates*

Stacked bars represent particle concentration (particles L-1), relative abundance variation (%), and biovolume-derived carbon (µg C L-1) for the different MBFGs of Non-flagellates (A-C) for each water type (ES = estuarine, IS = inner-shelf, MS = mid-shelf, OS = outer-shelf).

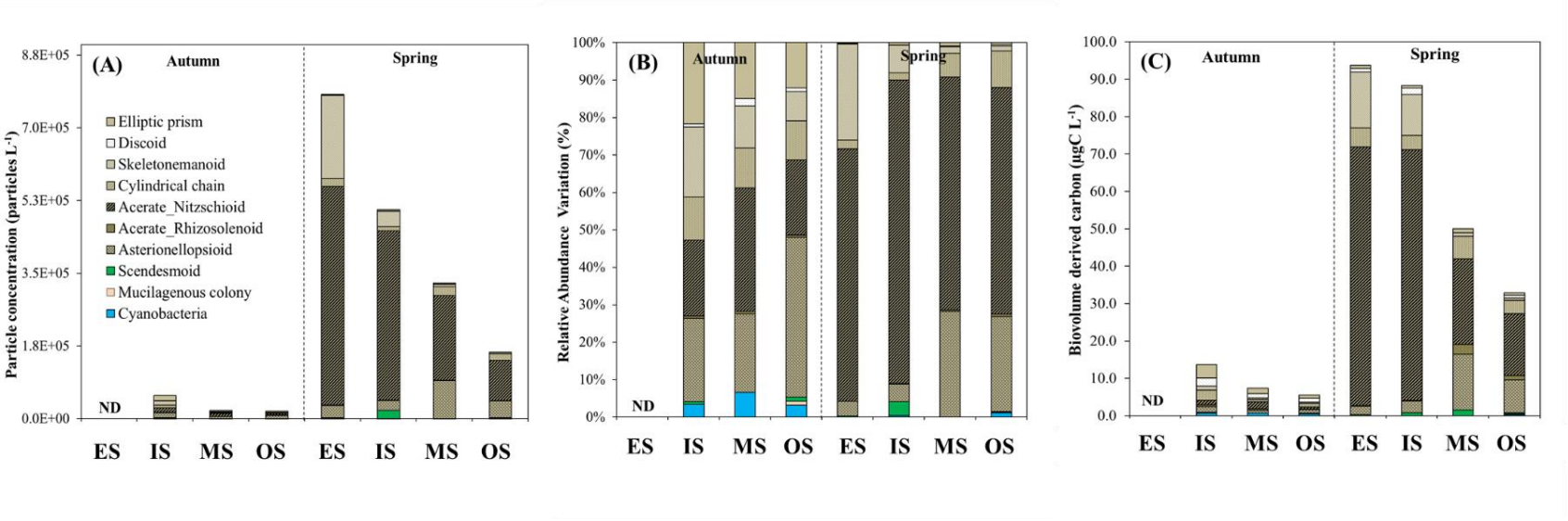

Figure 2.11 *Community composition for the different morphological based functional groups for Non-Flagellates*

Stacked bars represent particle concentration (particles L^{-1}), relative abundance variation (%), and biovolume-derived carbon (µg C L^{-1}) for the different MBFGs of *Non-flagellates* (A-C) for each water type (ES = estuarine, IS = inner-shelf, MS = mid-shelf, OS = outer-shelf).

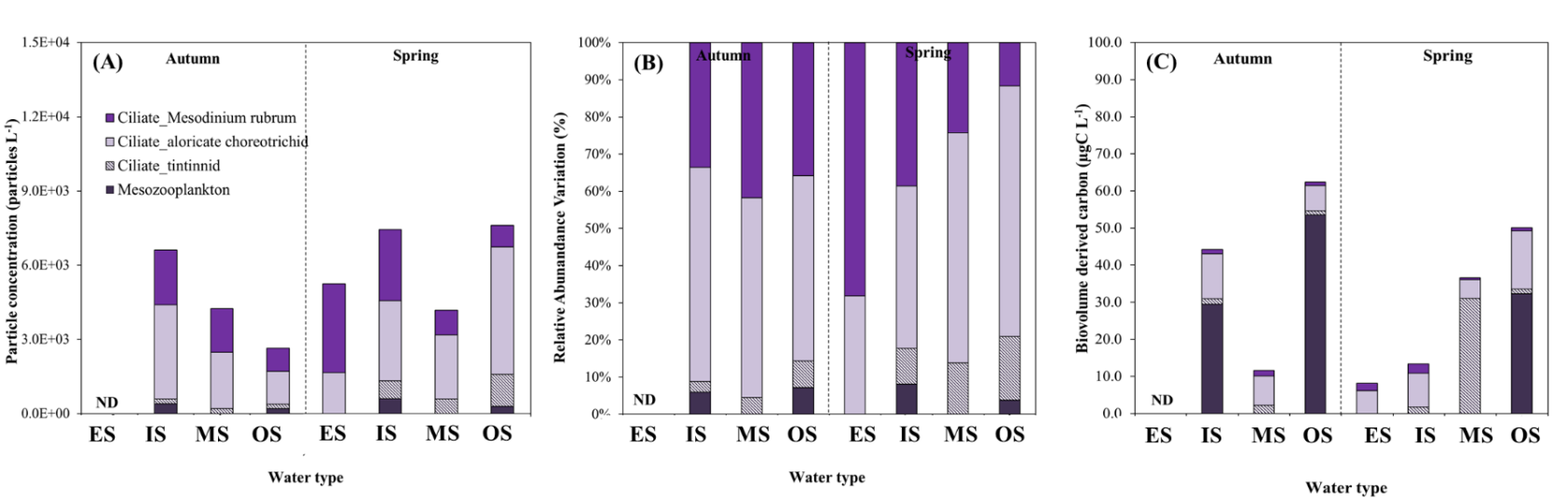

Figure 2.12 *Community composition for the different morphological based functional groups for Microzooplankton*

Stacked bars represent particle concentration (particles L^{-1}), relative abundance variation (%), and biovolume-derived carbon (µg C L^{-1}) for the different MBFGs of *Microzooplankton* (A-C) for each water type (ES = estuarine, IS = inner-shelf, MS = mid-shelf, OS = outer-shelf).

Table 2.8 *Summary of CCA for the biological and environmental data in autumn*

Summary of the CCA for the biological (21 MBFGs) and environmental data collected from the Mississippi Bight during the autumn CONCORDE cruise. All four eigenvalues reported are canonical and correspond to axes that are constrained by the explanatory (*i.e.* environmental) variables.

	CCA Axes				
	1	2	3	4	Total inertia
Eigenvalues	0.056	0.032	0.021	0.017	0.3175
Species-environment correlations	0.894	0.866	0.821	0.858	
Cumulative percentage variance					
of species	17.8	27.9	34.6	40.1	
of species-environment relation	35.8	56.1	69.6	80.6	
Sum of all unconstrained eigenvalues					0.3175
Sum of all canonical eigenvalues					0.1579

Table 2.9 *Inter-set correlations of environmental variables with CCA axes for autumn.*

Selected variables were significant in the Monte Carlo permutation test of F-ratios ($p < 0.05$). Bold values correspond to the variables that were biologically important ($r > |0.4|$).

	CCA axis 1	**CCA axis 2**	**CCA axis 3**	**CCA axis 4**
Selected variables				
Temperature	-0.3730	**0.5193**	0.1982	0.0399
Salinity	**-0.5397**	0.3506	0.1056	0.1943
Buoyancy frequency	**0.4914**	**-0.4369**	-0.0307	-0.0271
Chlorophyll *a*	**0.4674**	-0.0851	-0.0991	-0.3306
Nitrate + Nitrite	-0.0885	**0.6403**	-0.1639	0.0686
Ammonium	0.2930	0.2096	0.2834	**-0.4225**
Phosphate	**0.5168**	-0.0293	0.3618	**-0.5797**
Silicate	0.3944	0.0104	-0.3536	**-0.5076**

Table 2.10 *Summary of CCA for the biological and environmental data in spring.*

Summary of the CCA for the biological (21 MBFGs) and environmental data collected from the Mississippi Bight during the autumn CONCORDE cruise. All four eigenvalues reported are canonical and correspond to axes that are constrained by the explanatory (i.e environmental) variables.

	CCA Axes				
	1	2	3	4	Total inertia
Eigenvalues	0.074	0.039	0.026	0.021	0.4969
Species-environment correlations	0.841	0.84	0.725	0.702	
Cumulative percentage variance					
of species	14.8	22.7	27.9	32.0	
of species-environment relation	40.0	61.3	75.2	86.4	
Sum of all unconstrained eigenvalues					0.4969
Sum of all canonical eigenvalues					0.1843

Table 2.11 *Inter-set correlations of environmental variables with CCA axes for autumn.*

Selected variables were significant in the Monte Carlo permutation test of F-ratios ($p < 0.05$). Bold values correspond to the variables that were biologically important ($r > |0.4|$).

	CCA axis 1	**CCA axis 2**	**CCA axis 3**	**CCA axis 4**
Selected variables				
Temperature	0.2155	-0.2854	0.3586	0.2903
Salinity	**-0.7888**	0.1218	0.0886	-0.0924
Buoancy frequency	**0.7710**	-0.0725	-0.0398	-0.0531
Chlorophyll *a*	**0.7604**	0.0190	-0.2333	-0.0503
Nitrate + Nitrite	0.2550	**0.4230**	0.2572	-0.3460
Ammonium	-0.1873	-0.2619	-0.2633	-0.2910
Phosphate	-0.0970	**0.5384**	0.2702	-0.2500
Silicate	**0.7491**	-0.1289	-0.0169	-0.2678

Ordination diagrams were generated from CCA 1 and CCA 2 since these axes explained much of the variance of the biologically-relevant variables (Tables 2.8 and 2.10). Ordination diagrams of species and sample scores demonstrated that the temporal and spatial distribution of microplankton groups was strongly influenced by variations in the environmental conditions. Variables such as T, S, N^2, Chl *a*, $NO_2 + NO_3^-$, and PO_4^{3-} were important variables driving community variability in autumn (Figure 2.13A, Table 2.8), whereas S, N^2, Chl *a*, $NO_2 + NO_3^-$, PO_4^3-, and $Si(OH)_4$ were important in spring (Figure 2.13B, Table 2.10). The ordination diagrams of biologically-important environmental variables were represented by vectors and symbols, where direction and length of the vector represent the increased values of environmental variables and the angels denote correlations between individual environmental variables. Symbols represent group abundance, color-coded by water type, with the distances between symbols approximating the average dissimilarity of groups being compared. In general, the CCA plot of species scores classified by water types shows that a bulk of the autumn community responded to PO_4^{3-} and ammonium (NH_4^+) in inner-shelf waters, whereas T and S were considered driving variables for mid- and outer-shelf communities. Springtime estuarine and inner-shelf communities were scattered along the right side of the ordination space, suggesting that these waters were structured by $Si(OH)_4$, which can serve as a proxy for river discharge (Willén 1991), N^2, and T under higher stratified conditions. Mid- and outer-shelf communities responded to higher salinities and a greater influence by NH_4^+.

The structural composition and distribution of the microplankton communities responded strongly to seasonal variability of the 8 environmental conditions (Figures 2.14-2.16). The nanoplankton group was included with flagellates in this analysis. Environmental variables structuring the physical structure of the water column and regulating biological processes (i.e. T, S), stratification, and inorganic nutrients demonstrated that species with high values responded to changes in seasonal patterns within each water type. Ordination diagrams of constrained species scores for flagellates show that autumn communities clustered primarily along the left side of the ordination space, though this pattern was centered about the origin in spring (Figure 2.14). In general, flagellates responded to warmer, saltier water with lower nutrients in autumn, whereas nutrients were more important in spring. Autumn variability of prorocentroids and nanoplankton suggests that these groups were influenced largely by cooler, less saline waters with elevated ammonium concentration, whereas some of the less abundant groups such cerationoids, euglenoids, and Radiolarians responded more positively to warmer, saltier conditions. Nanoplankton and prorocentroids tended to predominate in estuarine and inner-shelf waters in spring, with some of the more rare groups (e.g. dinophysisoids, cerationoids) responding positively to inorganic nutrients. Thecate gymnodinoids responded more strongly to saltier, mid- and outer-shelf waters, whereas athecate gymnodinoids were more likely to be found along the inner shelf waters where $NO_2 + NO_3^-$ was greater.

Non-flagellates tended to respond positively to warmer, saltier conditions for acerate_rhizosolenoids, asterionellopsisoid, elliptic prism diatoms, and filamentous groups, whereas discoid diatoms responded positively to greater N^2. Springtime non-

flagellate communities responded mostly to inorganic nutrients for all groups (Figure 2.15). Within the ordination space microzooplankton clustered along the left side of the ordination space in autumn, suggesting a positive response to warmer, saltier conditions and moderate inorganic nitrogen. Springtime Microzooplankton communities also responded favorably to warmer, saltier conditions, with naupliiar mesozooplankton responding positively to NH_4^+.

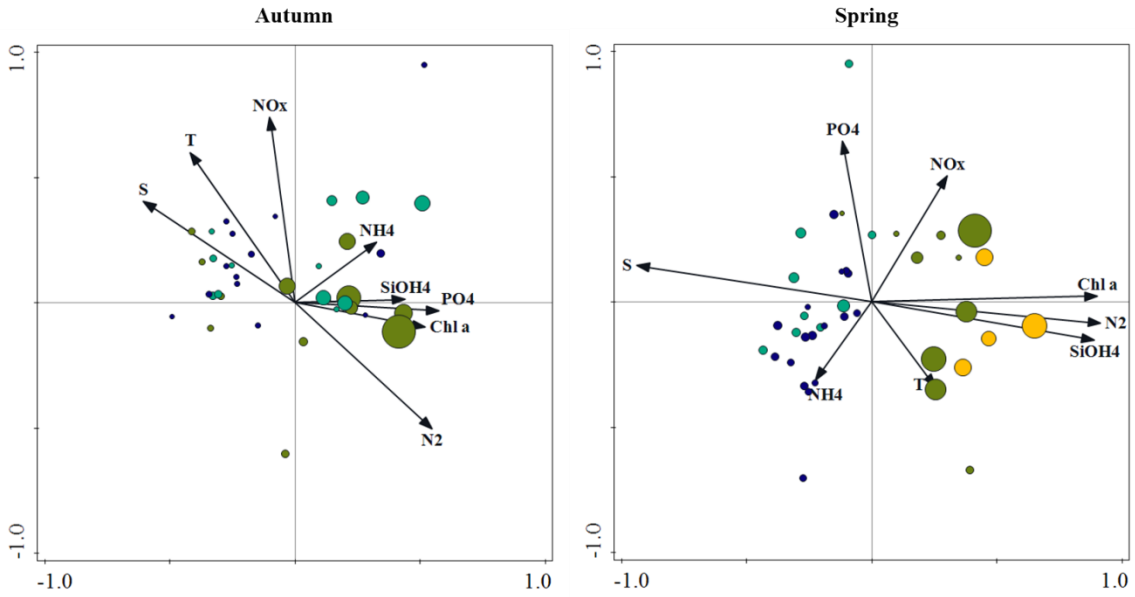

Figure 2.13 *Seasonal CCA biplots for environmental vectors and station data*

Station plots are color coded for estuarine (yellow), inner-shelf (green), mid-shelf (malachite), and outer-shelf (blue). Circle sizes are based on plot relative total abundance of untransformed values). Environmental variables used include temperature (T), salinity (S), buoyancy frequency (N2), chlorophyll *a* (Chl a), nitrite + nitrate (NOx), ammonium (NH4), orthophosphate (PO4), silicic acid (SiOH4).

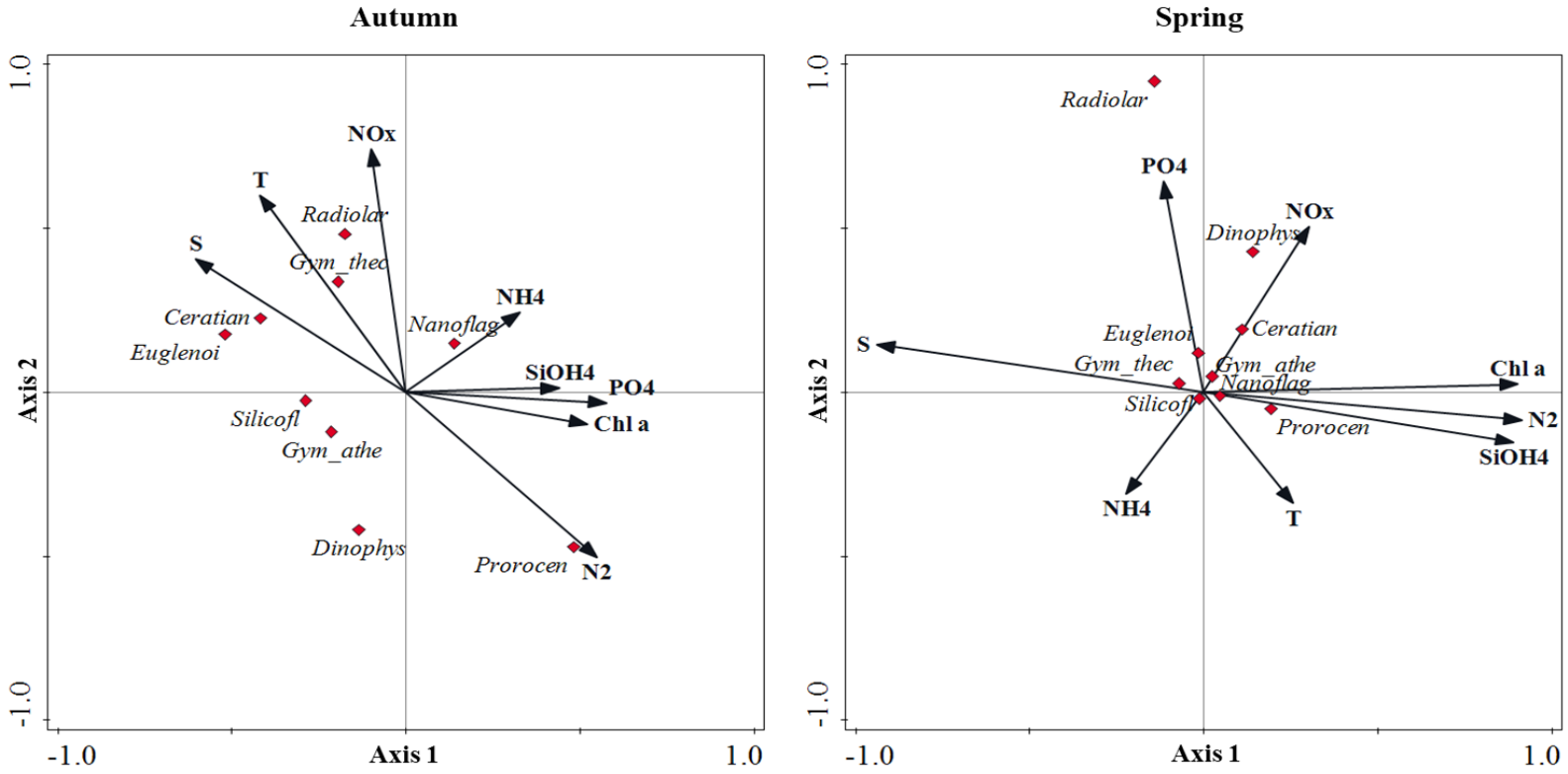

Figure 2.14 *Seasonal ordination diagrams of constrained species scores for Flagellates*

Ordination diagrams of constrained species scores for *Flagellates* (including *nanoplankton*) and environmental correlation vectors for autumn and spring. Environmental variables used include temperature (T), salinity (S), buoyancy frequency (N2), chlorophyll *a* (Chl a), nitrite + nitrate (NOx), ammonium (NH4), orthophosphate (PO4), silicic acid (SiOH4). Species (*i.e.* MBFGs) were represented by nanoplankton (Nanoflag), prorocentroids (Prorocen), athecate gymnodinoid (Gym_athe), thecate gymnodinoid (Gym_thec), cerationoids (Ceratian), dinophysioid (Dinophys), silicoflagellates (Silicofl), radiolarians (Radiolar), and euglenoids (Euglenoi).

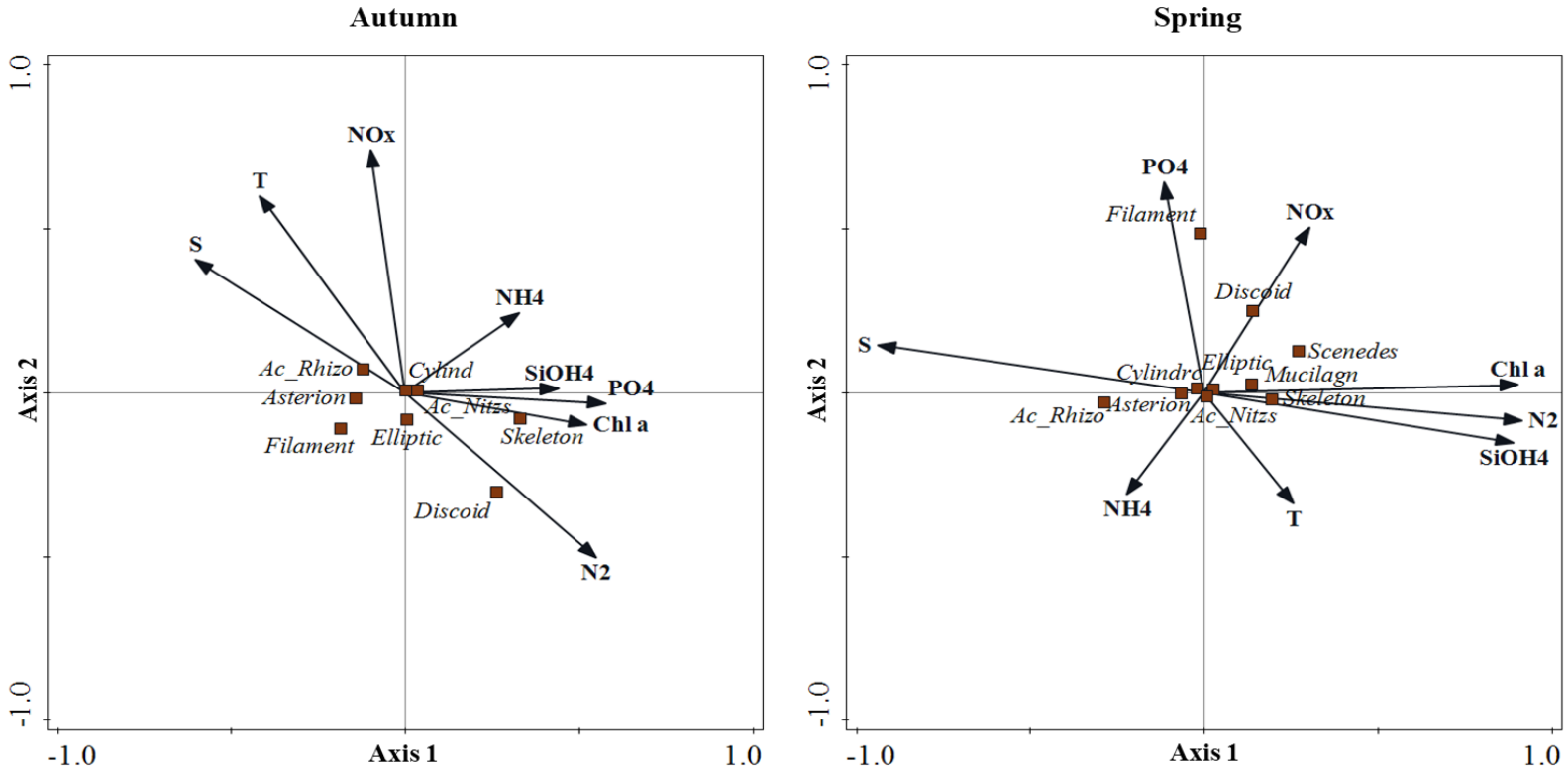

Figure 2.15 *Seasonal ordination diagrams of constrained species scores for Non-flagellates*

Ordination diagrams of constrained species scores for *Non-flagellates* and environmental correlation vectors for autumn and spring. Environmental variables used include temperature (T), salinity (S), buoyancy frequency (N2), chlorophyll *a* (Chl a), nitrite + nitrate (NOx), ammonium (NH4), orthophosphate (PO4), silicic acid (SiOH4). Species (*i.e.* MBFGs) were represented by elliptic prism (Elliptic), discoidal (Discoid), Skeletonemanoid (Skeleton), cylindrical chains (Cylind), acerate_nitzschioid (Ac_Nitzs), acerate_Rhizosolenoid (Ac_Rhizo), asterionellopsioid (Asterion), desmids (Scenedes), mucilaginous (Mucilagn), and filamentous (Filament).

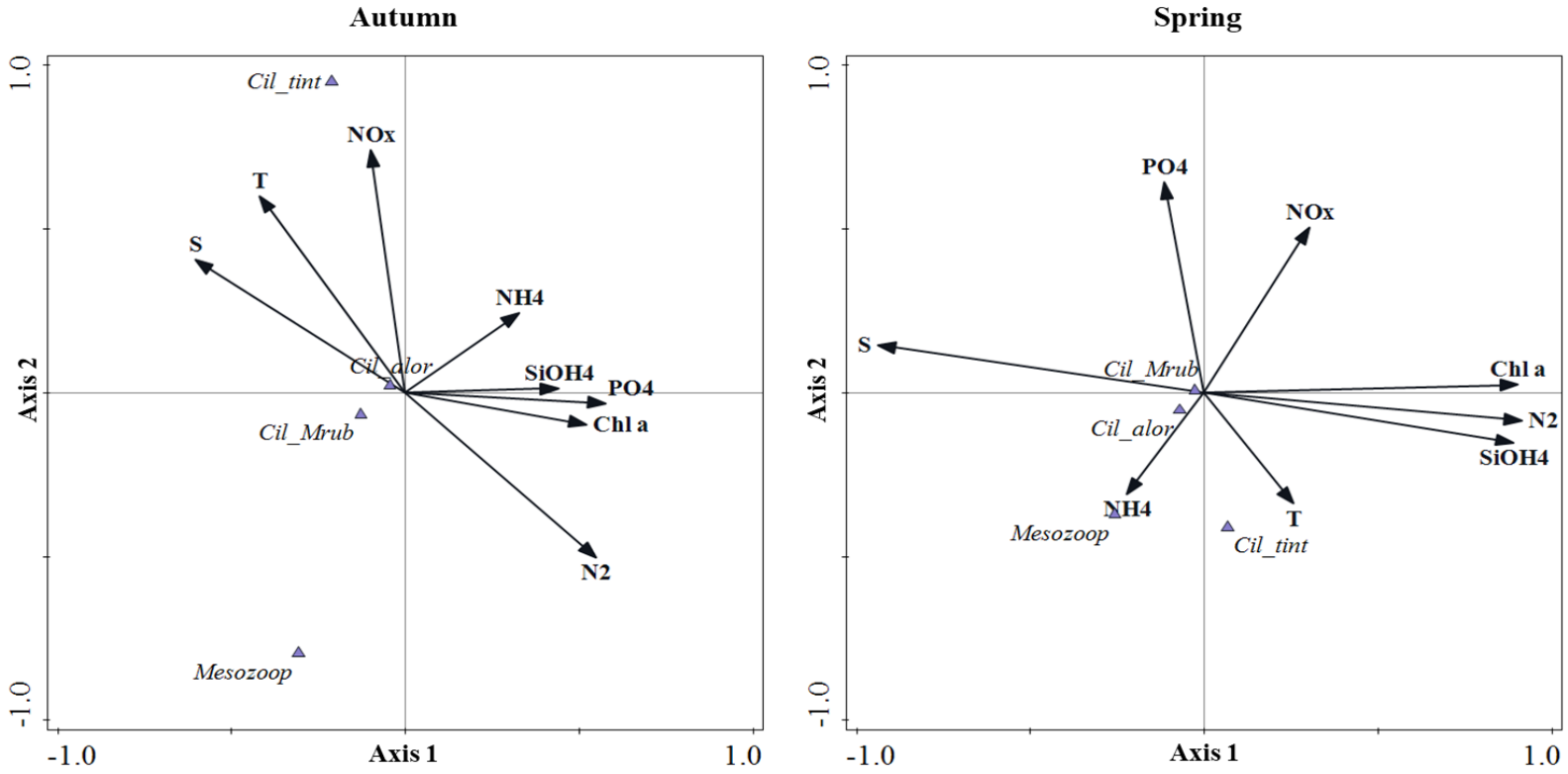

Figure 2.16 *Seasonal ordination diagrams of constrained species scores for Microzooplankton*

Ordination diagrams of constrained species scores for Non-flagellates and environmental correlation vectors for autumn and spring. Environmental variables used include temperature (T), salinity (S), buoyancy frequency (N2), chlorophyll a (Chl a), nitrite + nitrate (NOx), ammonium (NH4), orthophosphate (PO4), silicic acid (SiOH4). Species (*i.e.* MBFGs) were represented by the ciliates *Mesodinium* (Cil_Mrub), aloricate choreotrichids (Cil_alor), tintinnids (Cil_tint), and naupliiar mesozooplankton (Mesozoop).

2.4 DISCUSSION

The work presented here supports previous studies in the region which have documented similar patterns of planktonic response to physical forcing (e.g. Qian *et al.,* 2003, Chakraborty and Lohrenz 2015, Greer *et al.,* 2016). The hydrographic features in the river-dominated inner shelf of the northern Gulf of Mexico follow seasonal periodicity reflecting meteorological forcing patterns within the region and the Mississippi River and Mobile Bay-local watersheds in our region, and have been described in more detail elsewhere (see Dzwonkowski *et al.,* 2017, Parra *et al.,* 2020). This system transitioned from a mesotrophic state in autumn to a eutrophic-mesotrophic state in spring. Results presented here support our overarching hypothesis that microplankton communities exhibit seasonality and that variability is best explained in terms of environmental heterogeneity structured by the prevailing oceanographic conditions.

Physical mechanisms influencing water column structure and biogeochemistry are the primary forcing variables structuring microplankton communities in the river-dominated nGOM (Chakrabory and Lohrenz 2015). There were no attempts made to predict variability in morphological functional groups with environmental variability, but the study simply used the approach as a classification scheme. Here, the variability of the microplankton community is discussed within the context of the three primary hypotheses: (1) microplankton communities will differ seasonally and spatially with flagellate communities most abundant in the autumn, whereas diatoms will dominate in spring; (2) microplankton community size structure and carbon biomass vary such that estuarine and inner shelf waters can be characterized by large cells (> 30 μm, ABD) and

higher carbon biomass whereas mid- and outer-shelf waters are characterized by small cells (< 30 μm, ABD) and reduced carbon biomass; and (3) seasonal variability of microplankton community structure is best explained in terms of variables driven largely by physical conditions (e.g. T, S, stratification) in autumn and inorganic nutrients in spring.

2.4.1 Environmental drivers structuring microplankton communities

Autumn hydrographic conditions were influenced by the passage of the remnants of tropical cyclone Patricia, which completely mixed the water column and resulted in the flushing of estuarine waters from Mobile Bay onto the shelf (Dzwonkowski *et al*., 2017). Despite this being an extraordinary and anomalous event, its meteorological forcing was similar to passing cold fronts typical of conditions during this time of year (Dzwonkowski *et al*., 2017). River discharge into the MSB was higher in spring relative to autumn and was typical of patterns observed by others (e.g. Dzwonkowski *et al*., 2011, 2017, 2018).

Nutrient concentrations were elevated in spring relative to autumn and were concomitant with river discharge. These patterns followed seasonal variability observed by others in this region (e.g. Lohrenz *et al*., 1997, Qian *et al*., 2003, Chakraborty and Lohrenz 2015). In general, DIN and silicate concentrations were higher in estuarine and inner shelf waters and lower at stations along the outer shelf where river outflow exerts less influence. Stoichiometric ratios indicated that DIN likely was limiting in all water types in autumn, whereas PO_4^{3-} was limiting in estuarine and inner shelf waters in spring. However, absolute concentrations of DIN and PO_4^{3-} were at the threshold for limitation

along the inner shelf with potential silicate limitation in the mid and outer shelf waters in spring (Table 2.5).

2.4.2 Microplankton community structure

Three key results are highlighted from this research: (1) Nanoplankton and diatoms were the most dominant communities along the river-dominated nGOM continental shelf, with both communities increasing several orders of magnitude in abundance in spring; (2) there was a distinct seasonal shift in the diatom community, such that genera within acerate_nitzschioid cells (*i.e. Pseudeo-nitzschia* Pergallo spp.) and skeletonemanoid cells were the predominant groups in spring, whereas autumn diatom communities were more diverse. Ancillary to this is that nutrient stoichiometric ratios suggest that silicate limitation was likely in spring for mid and outer-shelf diatom communities; (3) aloricate choreotrichid ciliates were the most abundant microzooplankton group, but the prevalence of athecate and thecate dinoflagellates, coupled with the likely predominance of nanoflagellagtes suggests other groups may contribute significantly to the heterotrophic community in this system.

Seasonal succession of phytoplankton communities are common and have been described in various productive freshwater (Reynolds *et al*., 2002, Calijuri *et al*., 2002), coastal upwelling (Iriarte *et al*., 2012), estuarine (MacIntyre *et al*., 2011; Dorado *et al*.,, 2015; Novoveská and MacIntyre 2019), and river-dominated shelf (Qian *et al*., 2003, Chakrabory and Lohrenz 2015, Bargu *et al*., 2016) ecosystems. The results presented here partly support the initial hypothesis that flagellates will predominate in autumn and diatoms in spring. If we assume that nanoflagellate protists accounted for most of the nanoplankton community, as they often do (e.g. Iriarte *et al.*, 2012), and given that the

results show that the nano- microplankton community was comprised nearly equally of mixed assemblages of nanoplankton and diatoms in both seasons, this supports the first hypothesis. Many studies have shown that mixed assemblages of nanoflagellates account for a significant portion of the nanoplankton community (Sherr and Sherr 1994; Hahn and Hofle, 2001; Tsai *et al*., 2008; Iriarte *et al.*, 2012; Vargas *et al*., 2012).

Given these previous assumptions, we conclude that nanoflagellates play an equally important role to diatoms in terms of carbon biomass available for energy transfer in this system. Nanoflagellates are ubiquitous members of the heterotrophic, mixotrophic, and autotrophic planktonic communities, and are widely recognized as an important trophic intermediary of picoplankton in planktonic food webs (Sherr and Sherr 1994, Hahn and Hofle 2001, Tsai *et al*., 2008, Vargas *et al*., 2012). These groups often contribute significantly to total water column primary production (Iriarte *et al*., 2012), grazing (Sherr and Sherr, 1994; Jochem, 2003; Vargas *et al*., 2012), and biomass (Jochem 2003, Christaki *et al*., 2009; Iriarte *et al*., 2012; Vargas *et al*., 2007, 2012) in aquatic ecosystems. In the current study, estimates of nanoplankton (*i.e*.. nanoflagellate) biomass ranged from 3.7 to nearly 100 µg C L^{-1}, and are consistent with previous values of nanophytoplankton biomass reported in the literature. For instance, Jochem (2003) observed pico- and nanophytoplankton abundances as high as 91 µg C L^{-1} in the Mississippi River plume. Vargas *et al*., (2012) reported nanoflagellate biomass ranged from 1 to 43 µg C L^{-1} in the river-influenced coastal upwelling margin off Concepción, Chile. Earlier reports in that region found that bacterivorous nanoflagellates dominated the water column-integrated microbial biomass, ranging 17.1 to 51.4 µg C L^{-1}, throughout their study (Vargas *et al*., 2007).

Chakraborty and Lohrenz (2015) found similar patterns of community structure along inner shelf waters in the nGOM, where diatoms accounted for more than 50% of Chl *a* seasonally with important contributions from nanoplankton (*i.e.* cryptophytes, prymnesiophytes, chlorophytes) and cyanobacteria. Qian *et al*., (2003) also found that changes in river discharge and physical forcing drive phytoplankton community variability along the inner shelf of the nGOM. They showed that diatoms were a major contributor (6-13%) of Chl *a* in inner shelf waters, particularly in the vicinity of river mouths where inorganic nutrients are continuously supplied, whereas prymnesiophyte flagellates (25-40%) and prokaryotes (14-38%) were the major phytoplankton taxa throughout northeastern Gulf of Mexico continental margin. Wawrik and Paul (2004) found phytoplankton community structure was comprised mostly of diverse assemblages of diatoms along the productive inner shelf of the nGOM, whereas chlorophytes, prokaryotic *Synechococcus*, and to a lesser extent prymnesiophytes, dominated mid-river plume regions in the study area. A cross ecosystem comparison of productive, river-dominated estuarine and coastal habitats by Olli *et al*. (2015) found that diverse assemblages of diatoms were the most common phytoplankton at all ecological sites. Using a nonmetric multidimensional scaling to visualize communities, they identified the most diverse groups as diatoms (757 taxa), dinoflagellates (348 taxa), chlorophytes (216 taxa), and cyanobacteria (215 taxa). They also found that the diatoms *Chaetoceros* spp. (59 species) and *Nitzschia* spp. (70 species) accounted for the most diverse phytoplankton groups (Olli *et al*., 2015). In the current study, seasonal changes in the surface water microplankton community structure and abundance were driven largely from the influx inorganic nutrients from river sources, as determined from the CCA (Tables 2.8-2.11,

Figures 2.14-2.16). Diatoms were abundant along the inner shelf (including estuarine water types) where nutrients were abundant and in constant supply and have been readily described by others (Dortch and Whitledge, 1992; Chakrabory and Lohrenz 2015).

River-borne inorganic nutrients delivered to estuaries and along the nGOM inner shelf play an important role for the predominance of diatoms in river-influenced waters (Qian *et al*., 2003, Chakraborty and Lohrenz 2015). Results from the current study also provide strong evidence of diverse diatom groups associated with specific environmental conditions, particularly those influenced by river discharge. However, springtime diatom communities were predominantly acerate_nitzschioid (mostly *Pseudo-nitzschia* Pergallo spp.) and skeletonemanoid groups, which was a stark transition from autumn when the diatom community was significantly less abundant and more diverse (Figure 2.11). It is suggested that this transition was due to a combination of factors, including elevated nutrient concentrations coupled with reduced Si:DIN and Si:P stoichiometric ratios observed along shelf waters.

Many diatoms, such as *Skeletonema* Greville spp., *Thalassiosira* (Cleve) Hasle spp, and in particular *Pseudo-nitzschia* Pergallo spp., can decrease their silica content in order to maintain high growth rates under reduced Si:DIN and Si:P conditions, and thereby outcompete other heavily silicified diatoms whose silicate requirements are much greater (Parsons *et al*., 2002; Anderson *et al*., 2006; Leifer *et al*., 2009; Ajani *et al*., 2014; McNair *et al*., 2018). Strom and Strom (1996) identified *Pseudo-nitzschia* spp. and *Skeletonema* spp. as the dominant diatom genera along the Louisiana Shelf. Liefer *et al*. (2009) also observed that *Pseudo-nitzschia* Pergallo spp. accounted for more than two-thirds of the springtime phytoplankton samples collected along Alabama's coastal waters.

They attributed the proliferation of a toxic bloom of *Pseudo-nitzschia* Pergallo spp. was due to multiple factors, including submarine groundwater discharge, salinity, and changes in nutrient stoichiometry, where they found strong negative correlations between low Si:DIN and Si:P (Liefer *et al*. 2009). They suggested that *Pseudo-nitzschia* Pergallo spp. occupy a ruderal niche along coastal Alabama, where morphology and physiological characteristics (e.g. low silicate requirements, high growth rates) provide a competitive advantage over other phytoplankton communities (Liefer *et al*., 2009; MacIntyre *et al*., 2011). Previous studies (Dortch *et al*., 1997; Parsons *et al*., 2013), with more recent observations by Bargu *et al*. (2016), reported toxic blooms of *Pseudo-nitzschia* Pergallo spp. in Louisiana coastal waters. These studies observed highest cell numbers during in spring immediately following peak Mississippi River discharge, which was concomitant with elevated DIN concentrations and low Si:DIN ratios.

Increased anthropogenic input of inorganic N into coastal aquatic systems is driving Si limitations in many of these diatom-dominated coastal systems in the nGOM (Turner and Rabalais, 1991; Justić *et al*., 1995; Parsons *et al*., 2002; MacIntyre *et al*. 2011). These increased N loads are likely to select for lightly-silicified diatom communities, such as *Pseudo-nitzschia* Pergallo spp. (Bargu *et al*., 2016). The production of DA produced by some *Pseudo-nitzschia* Pergallo species has been linked to physiological stress and environmental variability, including salinity, dissolved inorganic carbon, and low Si concentrations (MacIntyre *et al*., 2011; Leifer *et al*., 2013). Leifer *et al*. (2013) reported that a bloom of *Pseudo-nitzschia* Pergallo spp. was linked to with increasing salinity and reduced nutrient concentrations along the inner Alabama shelf. They found that *Pseudo-nitzschia* Pergallo *subfraudulenta* DA production was linked to

reduced Si:DIN and Si:P (Leifer *et al*., 2013). Results from the current study also highlight that species (mostly *Pseudo-nitzschia* Pergallo spp) within the acerate_nitzschioid group became dominant in spring under elevated river discharge and reduced Si:DIN and Si:P scenarios, conditions that selected for toxic-forming species observed in other reports. Neither the presence/absence of harmful algal toxins (e.g. DA, brevetoxin), nor the identification of HAB-forming species within the *Pseudo-nitzschia* genus were quantified in this study. However, the results do support those of previous research in river-dominated systems, which showed that diatom communities shifted to lightly-silicified genera in response to variable nutrient and physical conditions driven by river discharge.

In addition to increasing the potential for toxic blooms of DA-producing diatoms, reduced Si:DIN due to eutrophication has the potential to shift the phytoplankton community from a diatoms to one largely dominated by dinoflagellates. This has a number of biogeochemical cycling and food web implications. In terms of the biological pump, the siliceous frustules of diatoms are readily remineralized at the seafloor, whereas dinoflagellate cells and their assimilated nutrients are recycled the productive euphotic zone (Kemp *et al.*, 2008). However, unlike the dissolution of diatom frustules deposited on the sea surface, cellulosic dinoflagellate cysts are resistant to degradation and are effectively removed from the benthic community (Kemp *et al.*, 2008). Moreover, many toxic dinoflagellates (e.g. *K. brevis*) produce hypnozygote resting cysts, which may act as a benthic seed stock and possible bloom initiation mechanism under ideal environmental conditions (Brand *et al.*, 2012).

Shifts in the siliceous phytoplankton communities could also have significant impacts on energy transfer to mesozooplankton (*i.e.*. copepods) (Gilpin *et al.*, 2004). For example, feeding efficiencies of copepods on diatoms of varying morphologies (*i.e.*. lightly/heavily silicified, absence/presence of spines), cellular lipid, protein and amino acid content, and differences in the cellular elemental composition would affect the overall energy transfer in planktonic food web (Gilpin *et al.*, 2004). Miralto *et al.* (1999) observed that copepod fecundity also was greatly reduced when feeding on lightly silicified diatoms *Skeletonema costaum* and *P. delicatissima*. They attributed this to three antiproliferative aldehydes produced by these diatoms, which inhibited copepod embryonic growth and cell-hatching rates (Miralto *et al.*, 1999). These aldehydes most likely are evolutionary anti-herbivory deterrents similar to the noxious secondary metabolites produced by terrestrial plants to discourage grazing (Miralto *et al.*, 1999). These effects likely would impact higher trophic levels and the regional aquatic food structure.

Carbon biomass for protozooplankton (dinoflagellates and ciliates) ranged from ~1 to 30.0 µg C L^{-1}, which is similar to values reported in other upwelling systems (Vargas *et al.*, 2012). These results are consistent with these values and show that dinoflagellates (i.e. flagellate group excluding euglenoids, silicoflagellates, and radiolarians) and ciliates (excluding *Mesodinium* Von Stein spp. and mesozooplankton) ranged 6.6 to 35.9 µg C L^{-1} and 6.1 to 36.1 µg C L^{-1}, respectively. However, the results presented here do not distinguish between heterotrophic, mixotrophic, or autotrophic groups. Consequently, it is assumed that the carbon biomass presented in the results is based on the size fraction < 20 μm of multiple groups exhibiting different trophic

strategies. Several studies have reported higher abundances of photosynthetic nanophytoplankton relative to mixotrophs or heterotrophic nanoplankton (Jochem 2003, Christaki *et al*., 2009, Vargas *et al*., 2012). It is suggested that this ecosystem is not unlike other river-dominated and upwelling environments where seasonal changes in river discharge influence nutrient concentrations and organic matter stimulate microbial (i.e. bacteria and picoeukaryotes) production, which in turn promote heterotrophic bacteriovory and herbivory. Microzooplantkon MBFGs were only a small fraction to the total microplankton abundance, yet results in the current study show that this group contributed a significant portion of the carbon in this system, particularly in autumn (Figure 6). This was due to the presence of large, rare individuals (i.e. tintinnids, radiolarians, copepod nauplii), which likely skewed our estimates (Figure 7). Strom and Strom (1996) found that the total microzooplankton (> 5μm) abundance (range = 5.0 x 10^3 to 6.2 x 10^4 cells L^{-1}) and total biomass (range = 2.2 to 18.9 μg C L^{-1}) were elevated at stations with higher Chl *a*. The microzooplankton community (> 5 μm) was comprised largely of aloricate choreotrichid ciliates and heterotrophic dinoflagellates (e.g. *Gyrodinium*, *Gymnodinium*, and *Protoperidinium*). Although ciliates were abundant, tintinnids played a minor role in community abundance. Cell volumes and carbon biomass generally were smaller in more oligotrophic waters, whereas cell sizes and carbon increased under more eutrophic conditions (Strom and Strom 1996). Aloricate choreotrichid ciliates were also the most abundant ciliate taxa in the MS-AL shelf waters.

2.5 CONCLUSION

The MBFG classification framework used in this study demonstrated that microplankton communities were closely related to environmental conditions. Despite

that this trait-based approach did not predict, nor was it intended to predict microplankton community dynamics within the context of environmental variability, this study highlighted how imaging systems, in combination with trait-based approaches and synoptic physico-chemical measurements, can be used to describe community succession and ecological variability under changing environmental scenarios.

The results presented here build upon and corroborate previous studies of microplankton community dynamics within the region. Analysis of the microplankton community composition in the nGOM revealed a highly structured and dynamic environment supporting diverse community of phytoplankton and microzooplankton. Diatoms are the predominant microplanktonic group in both seasons, with nanoflagellates likely playing an equally important role in terms of carbon availability and transfer efficiency to higher trophic levels. Further, the diatom community transitioned from a diverse mixed assemblage under low river discharge and DIN-limited conditions to a community dominated by *Pseudo-nitzschia* Peragallo spp. under elevated river discharge, high DIN, and Si-limiting conditions. This not only has profound implications on the biogeochemistry, increasing potential for HABs, and on the food web structure in this system, but also is indicative of the dominant mode of diatom variability in nGOM freshwater-dominated shelf ecosystems.

CHAPTER III – PRIMARY PRODUCTIVITY ALONG THE CONTINENTAL SHELF IN THE MISSISSIPPI BIGHT

3.1 INTRODUCTION

Aquatic phytoplankton primary production, mediated by energy from photosynthesis, is a key process in the transformation of dissolved inorganic carbon ($CO_2 + H_2O \rightarrow CO_3^{2-} \leftrightarrow HCO_3^{-} \leftrightarrow H_2CO_3$) into organic carbon. Variations in aquatic primary production and phytoplankton biomass, referred to hereafter as biomass, are related to the interaction between multiple environmental conditions (Lohrenz *et al*., 1997), including temperature (Eppley, 1972), light availability and quality (Kirk 1996, Falkowski and Raven, 2013), and inorganic nutrients (Harrison and Platt 1980; Kemp and Boynton, 1984; Cullen *et al*., 1992), cell size and physiology (Malone and Chervin, 1979; Joint and Pomeroy, 1981; Finkel *et al*., 2010), and the diversity of the resident phytoplankton community (Malone, 1980; Côté and Platt, 1984; Gallegos, 1992; Tilstone, *et al*., 2009). Ultimately, the phytoplankton community response to variations in environmental and physiological conditions influence how aquatic food webs are structured (Walsh, 1976; Lenz, 1992; Sin *et al*., 1999).

One approach to understanding phytoplankton dynamics is to examine phytoplankton assemblages within different size classes. Cell sizes influence autotrophic biomass concentrations and rates of primary production (Chisholm, 1992; Finkel *et al*., 2010). Prior studies have shown that nano- and microphytoplankton, as well as picophytoplankton (0.2-2.0 μm) (Malone *et al*., 1991; Iriarte1993; Sin *et al*., 1999), are the main contributors to autotrophic biomass and carbon assimilation in productive coastal and estuarine ecosystems (Iriarte and Purdie, 1994; Butrón *et al*., 2009),

mediators of biogeochemical cycling (Dugdale *et al*., 2007), and represent an important trophic link to heterotrophic grazers (Calbet *et al*., 2008). Tilstone *et al*., (1999) observed that microphytoplankton primary productivity was significantly higher (> 66%) than nanophytoplankton in coastal upwelling waters along northwest Spain. Similarly, Maguer *et al*. (2009) found that larger phytoplankton (>10 μm) accounted for most of the autuotrophic biomass in the Loire Estuary, North Biscay Bay. In the York River estuary, Sin *et al*. (2000) found that pico- and nanophytoplankton were the most abundant phytoplankton in terms of biomass throughout the year, whereas larger-celled microphytoplankton became dominant during sporadic winter and spring blooms.

Determining carbon content for phytoplankton cells in natural assemblages is a notoriously difficult and labor-intensive to determine directly, and is usually derived through numerous calculations and imprecise conversion factors (Geider *et al*., 1997; Felip and Catalan, 2000). A widely used proxy to estimate phytoplankton biomass is Chl *a*, as the presence of nonphytoplankton particulate organic matter often confounds direct measurements of phytoplankton carbon in aquatic ecosystems (Falkowski and Raven 2007). Another commonly used metric to estimate phytoplantkon biomass is the carbon to Chl *a* (C:Chl *a*) ratio. However, it is highly variable, ranging from ~ 10 to more than 200 (weight/weight), and is often driven by environmental factors, community taxonomic composition, temperature, nutrient limitation, and the irradiance quality and quantity (Falkowski and Raven 2007). Biovolume measurements of phytoplankton cells is another commonly used method to assess the relative biomass (Hillebrand *et al*., 2002), in which the carbon to volume relationship of multiple protist groups (Beers and Stewart, 1969; Verity and Langdon, 1984; Putt and Stoecker, 1989; Menden-Deuer and Lessard, 2000)

has been empirically derived. However, like the direct measurement of carbon, microscopy-based methods to calculate cell biovolume are laborious, time-consuming, and requires a special taxonomic skill set to identify multiple clades of organisms. These often require applications of multiple geometric models to determine biovolume (Hillebrand *et al*. 1999; Alvarez *et al*. 2012). Image-based automated sampling devices (e.g. FlowCAM) provide reasonable estimates (>75-90% accuracy) of abundance and sizes (i.e. diameter, biovolume) of plankton cells (Gorsky *et al*., 2010; Alvarez *et al*., 2012).

River-dominated coastal margins often are associated with nutrient enrichment and biogeochemical transformations, which often act in concert with physical processes (e.g. wind-driven mixing, convergence) to structure planktonic communities and enhance productivity. Phytoplankton production and the relationship to environmental forcing have been studied extensively throughout a variety of large temperate to subtropical estuaries (see Cloern 2014) including the Chesapeake Bay (Malone 1992; Harding *et al*., 1994; Adolf *et al*., 2006), San Francisco Bay (Cloern, 1996; Cloern *et al*., 2014), Neuse River estuary (Mallin *et al*., 1991, 1993; Boyer *et al*., 1993), Apalachicola Bay (Mortazavi *et al*., 2000; Caffrey 2004), San Antonio Bay (MacIntyre and Cullen 1996), Pearl River estuary (Cai *et al*., 2004) and coastal river-dominated ecosystems, such as the Amazon River plume (Smith and Demaster 1996; Stukel *et al*., 2014), Columbia River plume (Frame and Lessard 2009; Kudela *et al*., 2010), Changjiang River plume (Chen *et al*., 2004), Mississippi-Alabama shelf (Dzwonkowski *et al*., 2017), Louisiana continental shelf (Lohrenz *et al*., 1990, 1997, 1999, 2014) and Mississippi River plume (Lohrenz *et al*., 1990).

The waters along river-dominated continental shelf of the Mississippi Bight (MSB) in the northern Gulf of Mexico (nGOM) are highly productive and part of a biologically-rich region encompassing the Mississippi River outflow, which is often referred to as the "fertile fisheries crescent" (Gunter 1969, Grimes 2000). In this system buoyancy-driven flows of nutrient-rich river water drive seasonal ecosystem variability. Historically, phytoplankton production studies in the nGOM have been focused primarily in the northwestern region of the nGOM, encompassing the Louisiana-Texas continental shelf and slope (e.g. Lohrenz *et al*., 1990, 1992, 1994, 1997, 1999; Chen *et al*., 2000) and waters west of the Mississippi River (MSR) plume (Lohrenz *et al*., 1990; Chen *et al*., 2000). Lohrenz *et al*., (1994) found that seasonal productivity was related primarily to changes in temperature, whereas spatial variations influenced phytoplankton community growth rates. They speculated that this variability was related to a combination of reduced nutrient availability with increased distance from the river plume, as well as with shifts in phytoplankton community composition (Lohrenz *et al*., 1994). Similarly, Chen *et al*., (2000) found high phytoplankton biomass and production rates within the Louisiana inner shelf waters were influenced primarily by a combination of regional mesoscale circulation, nutrient sources, and light availability.

Collectively, these prior studies have provided excellent spatial and temporal trends in relating biological variability to physical processes in various coastal, river-dominated ecosystems. However, less well studied is the MSB region east of the Mississippi River birdfoot delta to the outflow of Perdido Bay near the Alabama and Florida border (Lohrenz *et al.*, 2014). Vandermeulen (2012) reported primary productivity (^{18}O-labeled O_2) estimates of 1.6 g C m^{-2} d^{-1} in Mississippi coastal waters.

Autumn productivity rates from Dzwonkowski *et al*., (2017) show that size fractionated (>0.6 μm, >5 μm) chlorophyll a and primary production rates exhibited both spatial and temporal variability across the Mississippi-Alabama shelf, and that the > 5μm size fraction phytoplankton accounted for more than 60 % total primary production. Phytoplankton primary production rates in this region are sparse and studies relating productivity to environmental variability are presently unknown. Furthermore, while the relationship between phytoplankton community structure and its relationship to primary productivity has been documented across multiple systems, there is a disparity relating carbon biomass to rates of carbon assimilation among nano- and microplankton groups. Efforts to relate size-fractionated biomass and productivity to imaged-based microplankton biovolume-carbon estimates have not been previously considered in this system.

In the present work, the spatial and temporal patterns of size-structured phytoplankton biomass and productivity were investigated under different hydrographic regimes. The overarching hypothesis was that size-fractionated autotrophic biomass and primary productivity will vary seasonally and spatially, such that the smaller size fraction (0.6-5 μm) will account for about half of the biomass and most (> 50%) of the primary productivity across the shelf in autumn, whereas the larger size fraction (>5 μm) will have greater biomass and production rates in spring within the near shore communities. It was also hypothesized that the size-fractionated biomass and productivity would be significantly correlated to C_{BV} (µg C L^{-1}) estimates from each plankton group (*i.e.* nanoplankton, flagellates, diatoms, microzooplankton). The implications from this analysis were that nanoplankton and diatoms would account for most of the >5 μm

primary productivity in autumn, whereas diatoms would contribute disproportionately more than other groups in spring. The objectives of this study were to (1) describe the seasonal and spatial variability in the phytoplankton biomass and primary productivity size structure (0.6-5 μm and >5 μm size fractions) along a cross-shelf environmental gradient, (2) relate observed biomass and productivity to the microplankton community biovolume-derived carbon estimates, and (3) identify potential mechanisms driving variability in phytoplankton biomass and productivity in the MSB.

Observations were made as part of CONCORDE and the Alabama Center for Ecological Resistance (ACER) projects, which provided for the comparison of microplankton community structure, biomass, and primary productivity relative to oceanographic and biogeochemical data collected simultaneously during the course of two research cruises in autumn 2015 and spring 2016 under differing hydrographic environments. This provided the setting to examine spatial and temporal variability of phytoplankton dynamics as it relates to the broader ecology of the region and other river-dominated ecosystems.

3.2 METHODS

3.2.1 Sampling

Sample depths were obtained from surface waters (~0.9-3.0 m), where the rosette was held at just below the surface for all samples. Water samples for depth-integrated productivity measurements were collected at depths approximating PAR from just below surface, mid (~50%), and bottom (~1%) intensities. Discrete water samples were obtained using a rosette sampler equipped with 12.0 L Niskin bottles, a SeaBird SBE911 plus conductivity-temperature-depth instrument profiler, and a WET Labs ECO-AFL

chlorophyll fluorometer. Acid-washed silicon tubing fitted with 200 μm Nitex mesh was placed onto each water collection valve, and the entire contents were dispensed into an acid-washed 4.0 L bottles for image analysis, inorganic nutrients, and size-fractionated (0.6 μm – 5 μm, > 5 μm) Chl *a* and primary productivity (PP). All size-fractionated samples are reported as 0.6 μm – 5 μm, which is the difference between > 0.6 μm and > 5μm size fractions, and > 5 μm. Autumn size-fractionated Chl *a* and PP were described previously in Dzwonkowski *et al*. (2017).

Samples for phytoplankton biomass (μg Chl *a* L^{-1}) were determined using two techniques: one for total chlorophyll a (Chl *a*), and the other for size-fractionated Chl *a*, where 0.6 μm– 5 μm (Chl $a_{0.6\text{-}5\mu m}$) and >5 μm (Chl $a_{>5\mu m}$) represent the different chlorophyll size fractions, respectively. Triplicate aliquots of 100-300 mL for Chl *a* were filtered onto 0.6 μm GF/F (Whatman), whereas single replicates for size-fractionated samples were filtered independently using an inline filtration apparatus in which a 100-300 mL water sample was filtered through a 5 μm polycarbonate membrane filter and a 0.6 μm GF/F. All filters for chlorophyll were placed immediately into cryo-vials and then into liquid nitrogen until laboratory analysis. Chl *a* was determined fluorometrically using methanol extraction (Welschmeyer 1994) and analyzed on a Turner 10-AU fluorometer, whereas size-fractionated Chl $a_{>0.6\mu m}$ and Chl $a_{>5\mu m}$ were determined using a 90% acetone extraction and acidification technique (Strickland and Parsons 1972) and analyzed on a Turner Trilogy Fluorometer. Due to a calibration error that potentially could affect the absolute quantity of chlorophyll, spring size-fractionated Chl $a_{>5\mu m}$ samples were estimated based on the percent >5μm relative to the Chl *a*, assuming that the proportional difference was not affected, and Chl $a_{>0.6\mu m}$ approximated Chl *a*. Chl *a*

0.6-5μm was calculated as the difference between the Chl $a_{>5\ \mu m}$ and Chl *a* values for >0.6 μm (autumn) and Chl *a* (spring).

Primary production rates were determined following standard procedures and have been described elsewhere (Brzezinski and Washburn 2011; Dzwonkowski *et al*., 2017). Briefly, 100 mLsamples were collected and dispensed into trace-metal clean 125 mL polycarbonate light and dark bottles, which were spiked with 100 μL of a 1 mCi mL^{-1} stock $NaH^{14}CO_3$ tracer (final activity = 1 μCi mL^{-1}) , then incubated 24 h in a deckboard incubator at ambient irradiance (Dzwonkowski *et al*., 2017). Light bottles were placed into shade bags approximating light intensities from sample depths. Productivity measurements were not replicated, though duplicate measurements from other studies (see Brzezinski and Washburn 2011) showed that duplicate measurements agreed within 10%. Following incubations, ^{14}C-labled samples were filtered onto 0.6 GF/F and 5 μm polycarbonate membrane filters, acidified to volatilize excess radioactive ^{14}C, then placed into scintillation vials containing 10mL EcoLume^{TM} liquid scintillation cocktail. Samples were counted on a Perkin Elmer TriCarb 3110 TR scintillation counter. Total primary production (TPP) was defined as the sum of the two size fractions (TPP = $PP_{0.6\text{-}5\mu m}$ + $PP_{>5\mu m}$). Size-fractionated production rates were normalized to the respective chlorophyll size fraction to provide biomass-specific rates (P^B) (*i.e.* assimilation number). Depth-integrated productivity measurements were calculated using the trapezoidal method.

3.2.2 Statistical Analysis

Statistical analyses were performed using SPSS (IBM SPSS Statistics 24.0) to evaluate the relationships between environmental and biological data. The data set was initially tested for normality using a Kolomogorov-Smirinov test. Non-parametric

statistics were used since most of the environmental and biological data did not follow a normal distribution ($p \leq 0.05$). Spearman's rank, r was used to identify significant ($p \leq 0.05$) correlations between variables. Variability between seasons and water types was evaluated using the Mann-Whitney U test to highlight significant ($p \leq 0.05$) differences between two independent groups of data (e.g. seasonal), whereas the Kruskal-Wallis test ($p \leq 0.05$) was used to compare three or more independent groups (e.g. water types). Wilcoxon signed-rank test was used to compare whether two related samples (e.g. size fractioned samples) were different. Depth-integrated productivity values were not used in any statistical analyses due to the small sample size in each water type; however, descriptive statistics were used to highlight ecological patterns.

Principle component analysis (PCA) was applied to the entire data set to examine whether other patterns between variables were evident. Subsequent PCAs were applied to each water type to identify relationships among environmental and biological variables to assess the relative importance of environmental and biological factors in controlling production among the two size fractions. Estuarine and inner-shelf water types were combined into a single dataset for this study. Each PCA used the Varimax with Kaiser normalization rotation method. Environmental variables included T, S, N^2, $NO_2 + NO_3^-$, $NH4^+$, $Si(OH)_4$, and PO_4^{3-}. Biological and taxonomic variables included size-fractionated Chl *a*, PP, and C_{BV}, with nanoplankton, flagellates, non-flagellates, and microzooplankton representing each of the taxonomic groups.

3.3 RESULTS

3.3.1 Size-fractionated particulate organic matter and biomass

Both size fractions of POC and PON were strongly correlated (Spearman's rank, $p \leq 0.01$, Tables A.16-A.17) to one another in each season. Seasonal trends for PON mirrored POC concentrations, such that greatest concentrations of $PON_{>5\mu m}$ and $PON_{0.6\text{-}5\mu m}$ were observed along inner shelf and estuarine waters. Total median $\pm$ MAD POC ranged from 185.5 $\pm$ 64.0 μg POC L^{-1} in autumn to 235.9 $\pm$ 66.5 μg POC L^{-1} in spring. Seasonal median POC/PON ratio for the smaller size fraction ranged from 6.1 $\pm$ 0.3 in autumn to 7.2 $\pm$ 1.1 in spring, whereas the larger size class ranged from 6.9 $\pm$ 1.1 in autumn to 7.0 $\pm$ 0.9 in spring (Figure 3.1, Table 3.3).

Size-fractionated Chl *a* was significantly greater (Mann-Whitney U, $p \leq 0.05$) in spring than autumn, with Chl $a_{>5\mu m}$ (range = 0.4 – 3.2 μg Chl *a* L^{-1} in autumn and 1.0 – 21.0 μg Chl *a* L^{-1} in spring) accounting for more than 80.0% of total Chl *a* (Table 3.1, Figure 3.4). Autumn size-fractionated Chl *a* median concentrations were 0.4 $\pm$ 0.3 μg Chl *a* L^{-1} (range = 0.1 – 2.9 μg Chl *a* L^{-1}) for Chl $a_{0.6\text{-}5\mu m}$ and 0.9 $\pm$ 0.2 μg Chl *a* L^{-1} (range = 0.4 – 3.2 μg Chl a L^{-1}) for Chl $a_{>5\mu m}$. Spring median concentrations and ranges increased to 1.4 + 0.9 μg Chl *a* L^{-1} (range = 0.1 – 14.3 μg Chl a L^{-1}) for Chl $a_{0.6\text{-}5\mu m}$ and 4.5 + 3.1μg Chl *a* L^{-1} (range = 1.0 – 21.0 μg Chl *a* L^{-1}) for Chl $a_{>5\mu m}$. In terms of absolute size-fractionated Chl *a* values relative to total Chl *a*, the upper limit for the smaller size fraction was attained at approximately 4 μg L^{-1}, whereas the larger size fraction increased to nearly 13 μg L^{-1}.

Both size-fractions for Chl *a* were greater within estuarine and inner-shelf waters and the lowest concentrations were measured in outer shelf waters (Figure 3.2). Despite

an observable seasonal cross shelf pattern, both size fractions did not differ significantly (Kruskal-Wallis, $p \leq 0.05$, Table 3.5) between water types in autumn, but this pattern shifted in spring with estuarine and inner shelf waters accounting for more than 76% of the total Chl *a*. Chl $a_{>5\mu m}$ increased nearly an order of magnitude from autumn in all water types and was significantly greater (Wilcoxon rank-sum, $p \leq 0.05$, Table 3.6) than smaller chlorophyll size fraction across the shelf.

Seasonal (autumn, spring) median POC/Chl *a* ratio was greater for the smaller size fraction (304.0 $\pm$ 84.0, 46.4 $\pm$ 11.2) than the larger size fraction (82.8 $\pm$ 16.4, 35.3 $\pm$ 8.0) in both seasons, and was greater in the autumn than in spring (Table 3.3). The POC/Chl *a* ratio did not deviate significantly from the seasonal medians, except for autumn mid- and outer-shelf water types, where the 0.6-5 μm size fraction was more than three times greater than the >5 μm size fraction.

Significant correlations (Spearman's rank, $p \leq 0.05$) between POC and PON with C_{BV} for nanoplankton, flagellates, diatoms, and microzooplankton are shown in the Appendix F. Nanoplankton was significantly correlated ($p \leq 0.05$) with $POC_{0.6\text{-}5\mu m}$ in autumn, whereas strong correlations ($p \leq 0.01$) between nanoplankton with $POC_{>5\mu m}$ and $PON_{>5\mu m}$ were evident in spring. Nanoplankton, flagellates, and diatoms also were positively correlated ($p \leq 0.05$) with $POC_{>5\mu m}$ in estuarine and inner-shelf waters, with diatoms also strongly correlated in outer-shelf waters. In mid-shelf waters, nanoplankton were also correlated with $POC_{>5\mu m}$ and $PON_{>5\mu m}$, though flagellates and diatoms were both correlated to the smaller POC size fraction.

Table 3.1 *Median ± MAD values for microplankton biovolume-carbon, and size-fractionated POC, and PON*

Biovolume-derived carbon for total microplankton (C_{Total}) was determined as the sum of all micro- (C_{Micro}) and nano- (C_{Nano}) plankton communities at each station, and the median ± MAD was calculated for each water type. Particulate organic carbon (POC) and particulate organic nitrogen (PON) were determined for the two size fractions 0.6-5 μm and > 5 μm.

Season	Region	Biovolume Carbon, C_{BV} (µg C L^{-1})			Particulate organic carbon, POC (µg L^{-1})		Particulate organic nitrogen, PON (µg L^{-1})	
		C_{Total}	C_{Micro}	C_{Nano}	0.6-5 µm	>5 µm	0.6-5 µm	>5 µm
Autumn	Inner-shelf	62.1 ± 8.6	35.4 ± 6.3	17.7 ± 4.9	97.0 + 41.5	129.0 ± 48.0	17.5 + 10.0	19.0 ± 7.0
	Mid-shelf	51.4 ± 14.5	24.8 ± 3.6	15.2 ± 4.5	154.0 +30.0	66.5 ± 15.0	22.0 + 3.0	11.5 ± 3.5
	Outer-shelf	24.7 ± 5.7	17.3 ± 1.9	3.7 ± 1.3	66.5 + 26.0	48.0 ± 13.5	14.0 + 2.0	9.5 ± 4.0
Spring	Estuarine	241.9 ± 10.8	162.7 ± 13.3	98.9 ± 8.5	139.2 + 129.2	440.0 ± 66.7	65.0 + 11.7	20.1 ± 13.4
	Inner-shelf	200.4 ± 57.8	181.5 ± 15.4	57.5 ± 14.9	53.9 + 26.0	286.7 ± 33.8	38.9 + 3.2	4.5 ± 2.6
	Mid-shelf	110.4 ± 28.2	101.7 ± 18.7	21.6 ± 7.7	49.9 + 30.9	139.2 ± 31.3	19.0 + 6.3	8.6 ± 2.3
	Outer-shelf	110.5 ± 13.4	98.5 ± 17.5	30.7 ± 11.3	69.9 + 20.5	163.5 ± 50.8	14.3 + 4.8	9.6 ± 1.7

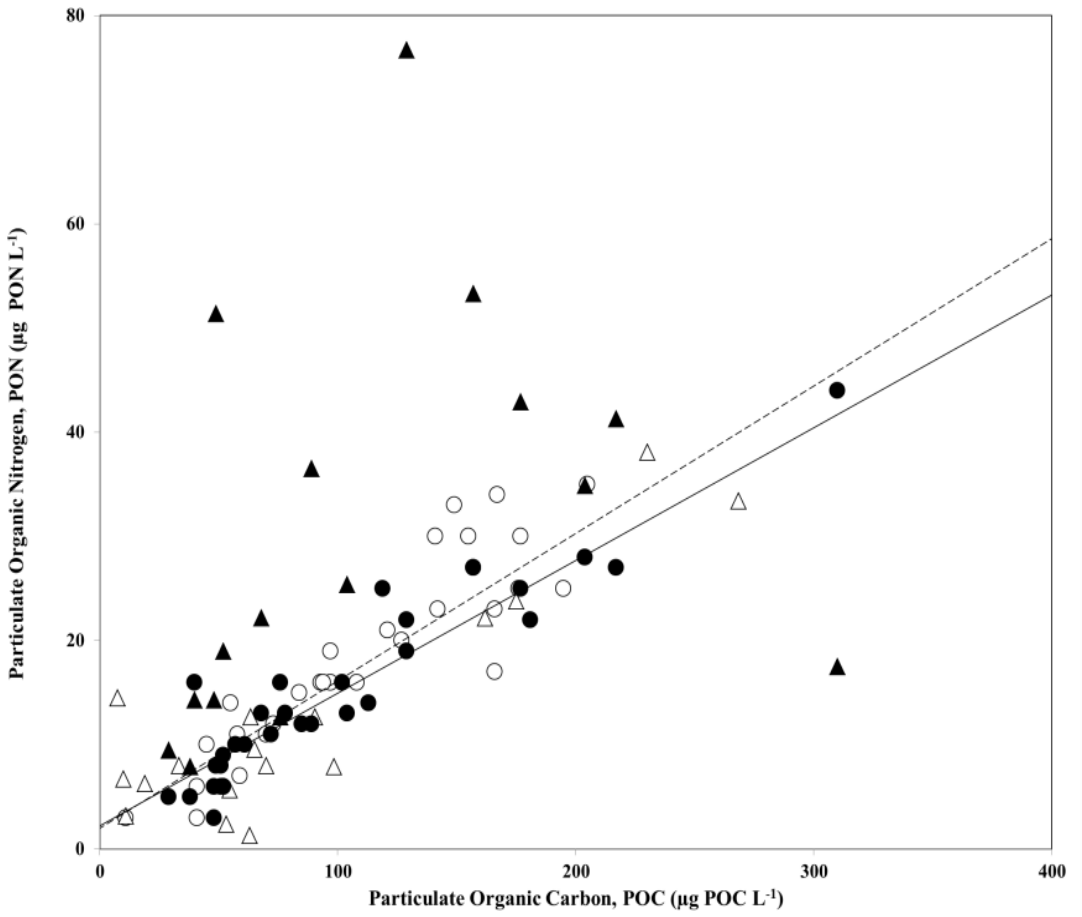

Figure 3.1 *Relationship between POC and PON in the Mississippi Bight*

Size-fractionated POC and PON in autumn (shaded) and spring (open) for the 0.6-5 μm (circles) and > 5 μm (triangles) linear regressions (model II). Dashed and solid lines are for the 0.6-5 μm ($y = 0.1415x + 2.012$, $r^2 = 0.80$) and > 5 μm ($y = 0.123x + 2.229$, $r^2 = 0.93$) size-fractions combined for both seasons, respectively.

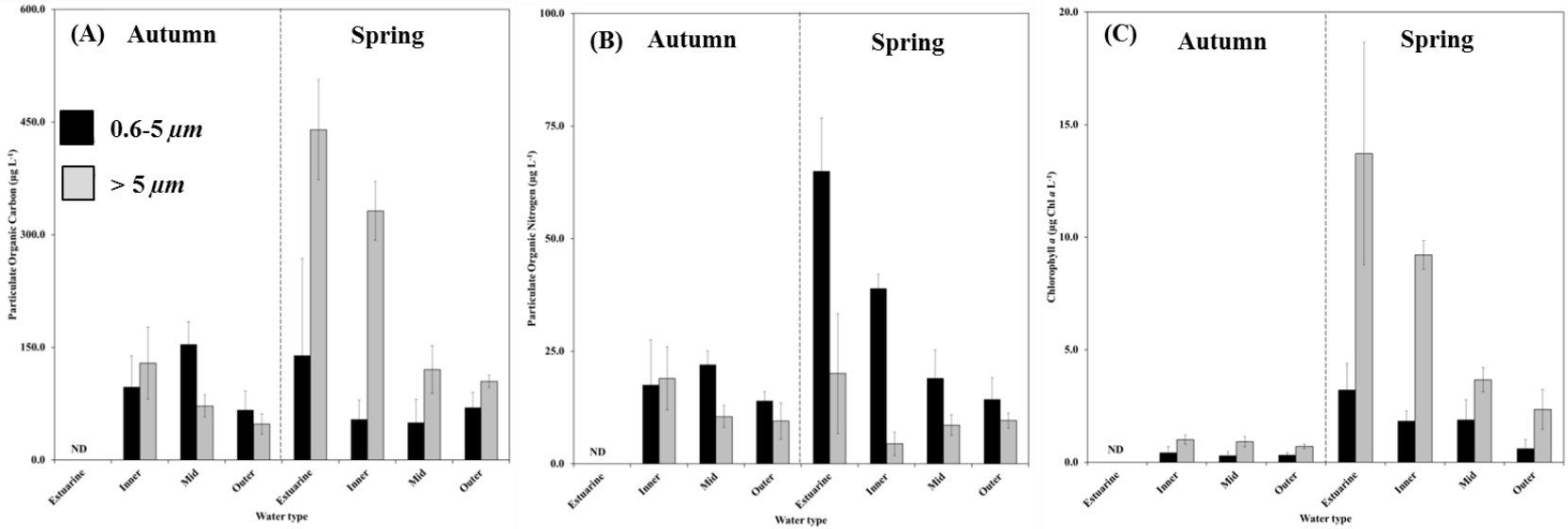

Figure 3.2 *Seasonal distributions of size-fractionated POC, PON, and Chl a across different water types*

Size-fractionated median values are represented in bar plots, with error bars representing the median absolute deviation (MAD) for particulate organic carbon (A), particulate organic nitrogen (B), chlorophyll *a* (C).

Table 3.2 *Median ± MAD values for size-fractionated Chl a, primary productivity, and Chl a-normalized productivity*

Median ± MAD values for size-fractionated (0.6-5 μm, >5 μm) and total (>0.6 μm) Chl *a*, size-fractionated rates of primary production and biomass-normalized production for each water type over the course of the study period.

Season	Region	Chlorophyll *a*, Chl *a* (µg Chl *a* L^{-1})			Primary production, PP (µg C L^{-1} d^{-1})		Chl *a*-normalized production, P^B (µg C (µg Chl *a*)$^{-1}$ d^{-1})	
		0.6-5 µm	>5 µm	Total	0.6-5 µm	>5 µm	0.6-5 µm	>5 µm
Autumn	Inner-shelf	2.1 + 1.5	1.0 ± 0.3	2.3 + 0.2	19.1 + 11.7	83.9 ± 42.8	12.5+ 8.3	38.2 + 30.5
	Mid-shelf	0.8 + 0.4	0.9 ± 0.2	1.7 + 0.3	11.3 + 5.0	20.2 ± 4.8	51.6 + 40.3	22.4 + 5.4
	Outer-shelf	1.2 + 0.3	0.7 ± 0.1	0.9 + 0.1	8.8 + 1.5	5.6 ± 2.3	21.1 + 17.9	7.1 + 2.9
Spring	Estuarine	3.2 + 1.2	13.7 ± 4.9	8.9 + 1.6	236.2 + 87.7	453.0 ± 22.2	92.8 + 78.8	29.6 + 3.1
	Inner-shelf	1.8 + 0.5	9.2 ± 0.6	7.2 + 0.5	26.3 + 6.5	66.7 ± 40.9	4.5 + 3.1	7.3 + 6.1
	Mid-shelf	1.9 + 0.9	3.7 ± 0.5	2.6 + 0.4	23.6 + 9.8	44.9 ± 16.7	15.9 + 7.4	22.0 + 11.5
	Outer-shelf	0.6 + 0.4	2.4 ± 0.9	1.9 + 0.4	18.6 + 8.7	26.8 ± 15.9	43.6 + 20.2	13.6 + 4.4

Table 3.3 *Median ± MAD values for ratios of POC/PON and POC/Chl a*

Season	Region	POC/PON		POC/Chl *a*	
		0.6-5 µm	>5 µm	0.6-5 µm	>5 µm
Autumn	Inner-shelf	6.0 ± 0.5	7.4 ± 1.0	285.2 ± 108.0	83.3 ± 20.6
	Mid-shelf	6.1 ± 0.3	6.1 ± 0.5	260.6 ± 51.3	71.0 ± 18.2
	Outer-shelf	6.2 ± 0.1	7.0 ± 1.2	349.2 ± 42.4	83.7 ± 10.0
Spring	Estuarine	5.8 ± 0.3	6.8 ± 0.2	35.3 ± 18.5	34.8 ± 7.6
	Inner-shelf	7.8 ± 0.6	8.4 ± 0.2	37.9 ± 3.6	38.5 ± 6.5
	Mid-shelf	5.9 ± 0.2	6.3 ± 0.3	51.5 ± 5.1	28.6 ± 0.1
	Outer-shelf	7.2 ± 0.8	6.1 ± 0.6	107.0 ± 21.8	43.3 ± 15.8

3.3.2 Primary productivity

Total primary productivity (TPP) varied seasonally, with median ± MAD production rates ranging from 15.5 ± 4.2 μg C L^{-1} d^{-1} (range = 4.0 – 377.7 μg C L^{-1} d^{-1}) in autumn to 96.3 ± 53.0 μg C L^{-1} d^{-1} (range = 26.7 – 637.5 μg C L^{-1} d^{-1}) in spring (Figure 3.9, Table 3.2). Productivity was greatest in spring, with the 0.6-5 μm and >5 μm size fractions accounting for 27.1% and 72.9%, respectively. Seasonal $PP_{>5\mu m}$ increased over an order of magnitude from 5.6 ± 2.3 μg C L^{-1} d^{-1} (range = 1.5 – 220.0 μg C L^{-1} d^{-1}) to 64.5 + 45.7 μg C L^{-1} d^{-1} (range = 10.2 – 494.6 μg C L^{-1} d^{-1}), whereas $PP_{0.6\text{-}5\mu m}$ more than doubled from 8.8 ± 1.5 μg C L^{-1} d^{-1} (range = 2.5 – 157.7 μg C L^{-1} d^{-1}) autumn to 20.2 ± 6.7 μg C L^{-1} d^{-1} (range = 0.6 – 394.4 μg C L^{-1} d^{-1}) in spring. Primary production also varied spatially and followed patterns similar to chlorophyll and POC (Figure 3.9). Production rates for both size fractions were greater within inner-shelf waters and were lower in mid- and outer shelf waters, though not statistically significant between water types (Kruskal-Wallis, $p \leq 0.05$, Table 3.5) or size fractions (Wilcoxon rank-sum, $p \leq 0.05$, Table 3.6). Productivity in estuarine waters was significantly greater (Kruskal-

Wallis, $p \leq 0.05$) than any other water type, accounting for 53% (0.6-5 μm) and 38% (>5 μm) of the respective size-fractions in spring.

There was no discernable seasonal pattern or statistical difference (Mann-Whitney U, $p \leq 0.05$, Table 3.4) in chlorophyll-normalized production (P^B) (i.e. assimilation number) for total production (P^B) , which had a lower autumn median value of 50.0 $\pm$ 31.3 μg C (μg Chl a)$^{-1}$ d^{-1} relative to 64.8 $\pm$ 15.3 μg C (μg Chl a)$^{-1}$ d^{-1} observed in spring (Figure 3.9). Seasonal median values of $P^B_{0.6\text{-}5\mu m}$ and $P^B_{>5\mu m}$ also were not statistically different between seasons (Mann-Whitney U, $p \leq 0.05$, Table 3.4) or size fractions (Wilcoxon rank-sum, $p < 0.05$, Table 3.6). Autumn $P^B_{0.6\text{-}5\mu m}$ median was 16.9 $\pm$ 14.6 μg C (μg Chl a)$^{-1}$ d^{-1}, whereas values of 21.3 + 17.6 μg C (μg Chl a)$^{-1}$ d^{-1} were observed for spring. $P^B_{>5\mu m}$ median decreased from 20.2 $\pm$ 13.2 μg C (μg Chl a)$^{-1}$ d^{-1} in autumn to 15.3 $\pm$ 8.8 μg C (μg Chl a)$^{-1}$ d^{-1} in spring. Spatial variability in P^B for both size fractions was not statistically significant between water types (Kruskal-Wallis, $p \leq 0.05$) in either season, nor were the size fractions significantly different across water types (Wilcoxon rank-sum, $p \leq 0.05$, Table 3.7).

Correlation analysis highlighted significant (Spearman's rank r, $p \leq 0.05$) positive correlations between $PP_{>5\mu m}$ and C_{BV} for nanoplankton and diatoms in autumn and spring, whereas diatoms and microzooplankton were significantly (r, $p \leq 0.05$) correlated with $PP_{0.6\text{-}5\mu m}$ in autumn and spring (Tables A.16-A.17). No significant relationships were evident between $P^B_{>5\mu m}$ and C_{BV} for the plankton groups.

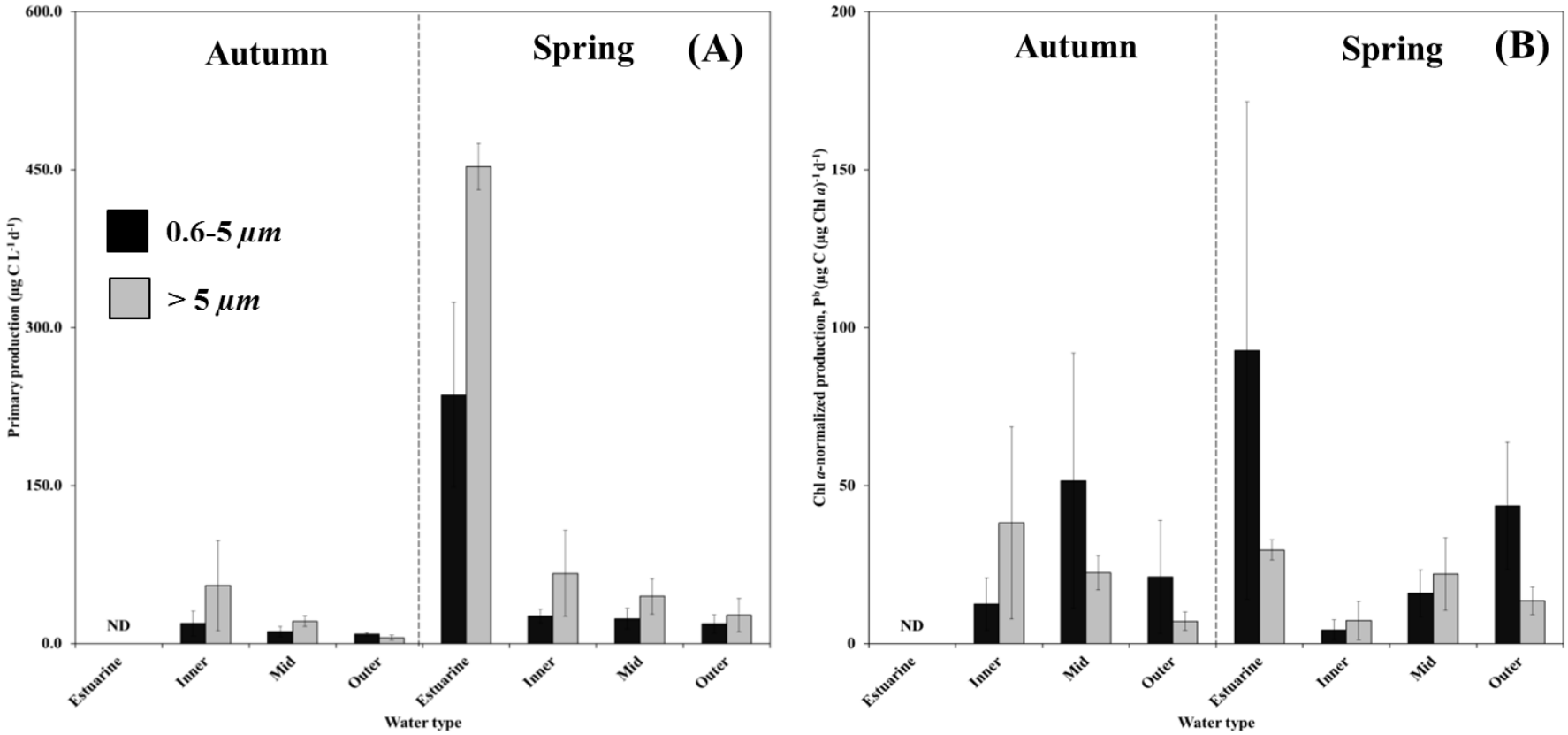

Figure 3.3 *Seasonal size-fractionated primary productivity across in the Mississippi Bight across different water types*

Size-fractionated primary productivity (A) and chlorophyll-normalized productivity (B) for each water type for autumn and spring. Bar plots represent median values with error bars representing MAD.

Table 3.4 *Mann-Whitney test for seasonal differences for biotic variables*

Mann-Whitney test for differences between autumn and spring for biological variables: size-fractionated (0.6-5 μm, > 5 μm) primary productivity (PP), Chl *a*-normalized productivity (P^B), chlorophyll *a* (Chl *a*), particulate organic carbon (POC), particulate organic nitrogen (PON), ratios of POC/PON, POC/Chl *a*, and the biovolume-derived carbon biomass (C_{BV}) for nanoplankton (nanof), microflagellates (microf), diatoms (diatom), and microzooplankton (mzp).

Parameter	U	Significance	N
$PP_{0.6\text{-}5\mu m}$ ($\mu g\ C\ L^{-1}\ d^{-1}$)	348	0.015*	66
$PP_{>5\mu m}$ ($\mu g\ C\ L^{-1}\ d^{-1}$)	271	0.001**	66
$P^B_{0.6\text{-}5\mu m}$ ($\mu g\ C\ (\mu g\ Chl\ a)^{-1}\ d^{-1}$)	128	0.007**	46
$P^B_{>5\mu m}$ ($\mu g\ C\ (\mu g\ Chl\ a)^{-1}\ d^{-1}$)	113	0.151	45
Chl $a_{0.6\text{-}5\mu m}$ ($\mu g\ Chl\ a\ L^{-1}$)	120	0.000**	55
Chl $a_{>5\mu m}$ ($\mu g\ Chl\ a\ L^{-1}$)	26	0.000**	52
Chl a_{tot} ($\mu g\ Chl\ a\ L^{-1}$)	279	0.000**	77
$POC_{0.6\text{-}5\mu m}$ ($\mu g\ POC\ L^{-1}$)	215	0.106	51
$POC_{>5\mu m}$ ($\mu g\ POC\ L^{-1}$)	121	0.001**	51
$PON_{0.6\text{-}5\mu m}$ ($\mu g\ PON\ L^{-1}$)	149	0.001**	47
$PON_{>5\mu m}$ ($\mu g\ PON\ L^{-1}$)	119	0.001**	50
$POC{:}PON_{0.6\text{-}5\mu m}$	280	0.952	51
$POC{:}PON_{>5\mu m}$	192	0.738	51
$POC{:}Chl_{0.6\text{-}5\mu m}$	13	0.000**	51
$POC{:}Chl_{>5\mu m}$	42	0.000**	49
$C_{BV_{nanof}}$ ($\mu g\ C\ L^{-1}$)	153	0.000**	78
$C_{BV_{microf}}$ ($\mu g\ C\ L^{-1}$)	268	0.000**	77
$C_{BV_{diatom}}$ ($\mu g\ C\ L^{-1}$)	115	0.000**	77
$C_{BV_{mzp}}$ ($\mu g\ C\ L^{-1}$)	710	0.901	76

Table 3.5 *Kruskal-Wallis analysis of spatial variability for biological variables*

Kruskal-Wallis analysis of spatial variability for biotic variables in autumn (df = 1) and spring (df =3). Significance between water types is given by χ^2 with a significance level $p \leq 0.01$ (**) and $p \leq 0.05$ (*). Variables include: size-fractionated (0.6-5 μm, > 5 μm) primary productivity (PP), Chl *a*-normalized productivity (P^B), chlorophyll *a* (Chl *a*), particulate organic carbon (POC), particulate organic nitrogen (PON), ratios of POC/PON, POC/Chl *a*, and the biovolume-derived carbon biomass (C_{BV}) for nanoplankton (nanof), microflagellates (microf), diatoms (diatom), and microzooplankton (mzp).

Parameter	Autumn		Spring	
	χ^2	p	χ^2	p
$PP_{0.6\text{-}5\mu m}$ ($\mu g\ C\ L^{-1}\ d^{-1}$)	1.409	0.235	7.369	0.054*
$PP_{>5\mu m}$ ($\mu g\ C\ L^{-1}\ d^{-1}$)	1.570	0.210	15.073	0.002**
$P^B_{0.6\text{-}5\mu m}$ ($\mu g\ C\ (\mu g\ Chl\ a)^{-1}\ d^{-1}$)	0.626	0.429	9.252	0.026*
$P^B_{>5\mu m}$ ($\mu g\ C\ (\mu g\ Chl\ a)^{-1}\ d^{-1}$)	1.917	0.166	3.417	0.332
Chl $a_{0.6\text{-}5\mu m}$ ($\mu g\ Chl\ a\ L^{-1}$)	0.909	0.340	9.668	0.022*
Chl $a_{>5\mu m}$ ($\mu g\ Chl\ a\ L^{-1}$)	0.963	0.326	11.373	0.010**
Chl a_{tot} ($\mu g\ Chl\ a\ L^{-1}$)	11.373	0.001**	28.633	0.000**
$POC_{0.6\text{-}5\mu m}$ ($\mu g\ POC\ L^{-1}$)	1.672	0.196	1.946	0.584
$POC_{>5\mu m}$ ($\mu g\ POC\ L^{-1}$)	1.445	0.229	13.344	0.004**
$PON_{0.6\text{-}5\mu m}$ ($\mu g\ PON\ L^{-1}$)	0.054	0.817	2.575	0.462
$PON_{>5\mu m}$ ($\mu g\ PON\ L^{-1}$)	0.461	0.497	12.423	0.006**
$POC{:}PON_{0.6\text{-}5\mu m}$	0.163	0.686	1.018	0.797
$POC{:}PON_{>5\mu m}$	6.166	0.013*	12.270	0.007**
$POC{:}Chl_{0.6\text{-}5\mu m}$	0.013	0.908	7.068	0.070*
$POC{:}Chl_{>5\mu m}$	0.046	0.498	1.168	0.761
$C_{BV_{nanof}}$($\mu g\ C\ L^{-1}$)	0.580	0.446	20.921	0.000**
$C_{BV_{microf}}$($\mu g\ C\ L^{-1}$)	1.149	0.284	5.852	0.119
$C_{BV_{diatom}}$($\mu g\ C\ L^{-1}$)	3.624	0.057*	10.193	0.017*
$C_{BV_{mzp}}$($\mu g\ C\ L^{-1}$)	0.959	0.328	4.249	0.235

Table 3.6 *Wilcoxon rank sum for seasonal comparison between size-fractions*

Wilcoxon rank sum combined water types for autumn and spring to compare between 0.6-5 μm and > 5 μm size fractions. Significance level set at $p \leq 0.01$ (**) and $p \leq 0.05$ (*). Variables include: size-fractionated (0.6-5 μm, > 5 μm) primary productivity (PP), Chl *a*-normalized productivity (P^B), chlorophyll *a* (Chl *a*), particulate organic carbon (POC), particulate organic nitrogen (PON), ratios of POC/PON,and POC/Chl *a*.

Parameter	Autumn	Spring
$PP_{0.6\text{-}5\mu m}$ ($\mu g\ C\ L^{-1}\ d^{-1}$) $PP_{>5\mu m}$ ($\mu g\ C\ L^{-1}\ d^{-1}$)	0.003**	0.000**
$P^B_{0.6\text{-}5\mu m}$ ($\mu g\ C\ (\mu g\ Chl\ a)^{-1}\ d^{-1}$) $P^B_{>5\mu m}$ ($\mu g\ C\ (\mu g\ Chl\ a)^{-1}\ d^{-1}$)	0.642	0.191
Chl $a_{0.6\text{-}5\mu m}$ (μg Chl $a\ L^{-1}$) Chl $a_{>5\mu m}$ (μg Chl $a\ L^{-1}$)	0.000**	0.000**
$POC_{0.6\text{-}5\mu m}$ ($\mu g\ POC\ L^{-1}$) $POC_{>5\mu m}$ ($\mu g\ POC\ L^{-1}$)	0.280	0.002**
$PON_{0.6\text{-}5\mu m}$ ($\mu g\ PON\ L^{-1}$) $PON_{>5\mu m}$ ($\mu g\ PON\ L^{-1}$)	0.016*	0.001**
$POC{:}PON_{0.6\text{-}5\mu m}$ $POC{:}PON_{>5\mu m}$	0.000**	0.000**
$POC{:}Chl_{0.6\text{-}5\mu m}$ $POC{:}Chl_{>5\mu m}$	0.000**	0.196

Table 3.7 *Wilcoxon rank sum for each water type across seasons*

Wilcoxon rank sum for the different water types for autumn and spring to compare between 0.6-5 µm and > 5 µm size fractions. Significance level set at $p < 0.01$ (**) and $p < 0.05$ (*). Variables include: size-fractionated (0.6-5 µm, > 5 µm) primary productivity (PP), Chl a-normalized productivity (PB), chlorophyll a (Chl a), particulate organic carbon (POC), particulate organic nitrogen (PON), ratios of POC/PON,and POC/Chl a.

Parameter	Autumn			Spring			
	Inner-shelf	**Mid-shelf**	**Outer-shelf**	**Estuarine**	**Inner-shelf**	**Mid-shelf**	**Outer-shelf**
$PP_{0.6\text{-}5\mu m}$ (µg C L^{-1} d^{-1}) $PP_{>5\mu m}$ (µg C L^{-1} d^{-1})	0.006**	0.005**	0.018*	0.018*	0.043*	0.180	0.018*
$P^{B}_{0.6\text{-}5\mu m}$ (µg C (µg Chl *a*)$^{-1}$ d^{-1}) $P^{B}_{>5\mu m}$ (µg C (µg Chl *a*)$^{-1}$ d^{-1})	0.308	0.180	0.180	0.180	0.317	0.180	0.180
Chl $a_{0.6\text{-}5\mu m}$ (µg Chl *a* L^{-1}) Chl $a_{>5\mu m}$ (µg Chl *a* L^{-1})	0.006**	0.074	0.499	0.068	0.008**	0.012**	0.020*
$POC_{0.6\text{-}5\mu m}$ (µg POC L^{-1}) $POC_{>5\mu m}$ (µg POC L^{-1})	0.002**	0.009**	0.018*	0.180	0.028*	0.180	0.180
$PON_{0.6\text{-}5\mu m}$ (µg PON L^{-1}) $PON_{>5\mu m}$ (µg PON L^{-1})	0.002**	0.034*	0.011**	0.180	0.028*	0.180	0.028*
$POC{:}PON_{0.6\text{-}5\mu m}$ $POC{:}PON_{>5\mu m}$	0.023*	0.021*	0.005**	0.180	0.080	0.180	0.398
$POC{:}Chl_{0.6\text{-}5\mu m}$ $POC{:}Chl_{>5\mu m}$	0.023*	0.002**	0.002**	1.000	1.000	1.000	1.000

Vertical profiles of primary production at select stations allowed for estimates of depth-integrated areal productivity, referred to hereafter as integrated productivity ($\int P$), for each size fraction (Figure 3.4). A single station for each water type accounted for autumn integrated productivity, whereas duplicate, single, and triplicate stations contributed to estuarine, inner-shelf, and outer-shelf water types in spring. There were no stations with vertical productivity measurements representing the mid-shelf water type in spring. Vertical profiles showed that production decreased markedly with depth, particularly for spring estuarine and inner shelf water stations. Integrated productivity for the different size fractions followed seasonal and spatial patterns similar to production and chlorophyll, with highest median values measured in spring and within estuarine and inner-shelf waters in spring. Median seasonal integrated productivity for the 0.6 – 5 μm and > 5μm size fractions ranged from 0.14 $\pm$ 0.02 g C m^{-2} d^{-1} and 0.07 $\pm$ 0.04 g C m^{-2} d^{-1} in autumn to 0.46 $\pm$ 0.25 g C m^{-2} d^{-1} and 0.96 $\pm$ 0.31 g C m^{-2} d^{-1} in spring, respectively. Estuarine, inner-shelf, and outer-shelf waters each contributed 41%, 22%, and 36% of the 0.6 – 5μm size fraction and 30%, 34%, and 36% of the > 5μm size fraction, respectively. Seasonal median for total integrated productivity ($\int P_{TOT}$) (i.e. sum of the two size fractions) ranged from 0.19 $\pm$ 0.02 g C $m^{-2}d^{-1}$ in autumn to 2.25 $\pm$ 0.52 g C $m^{-2}d^{-1}$ in spring.

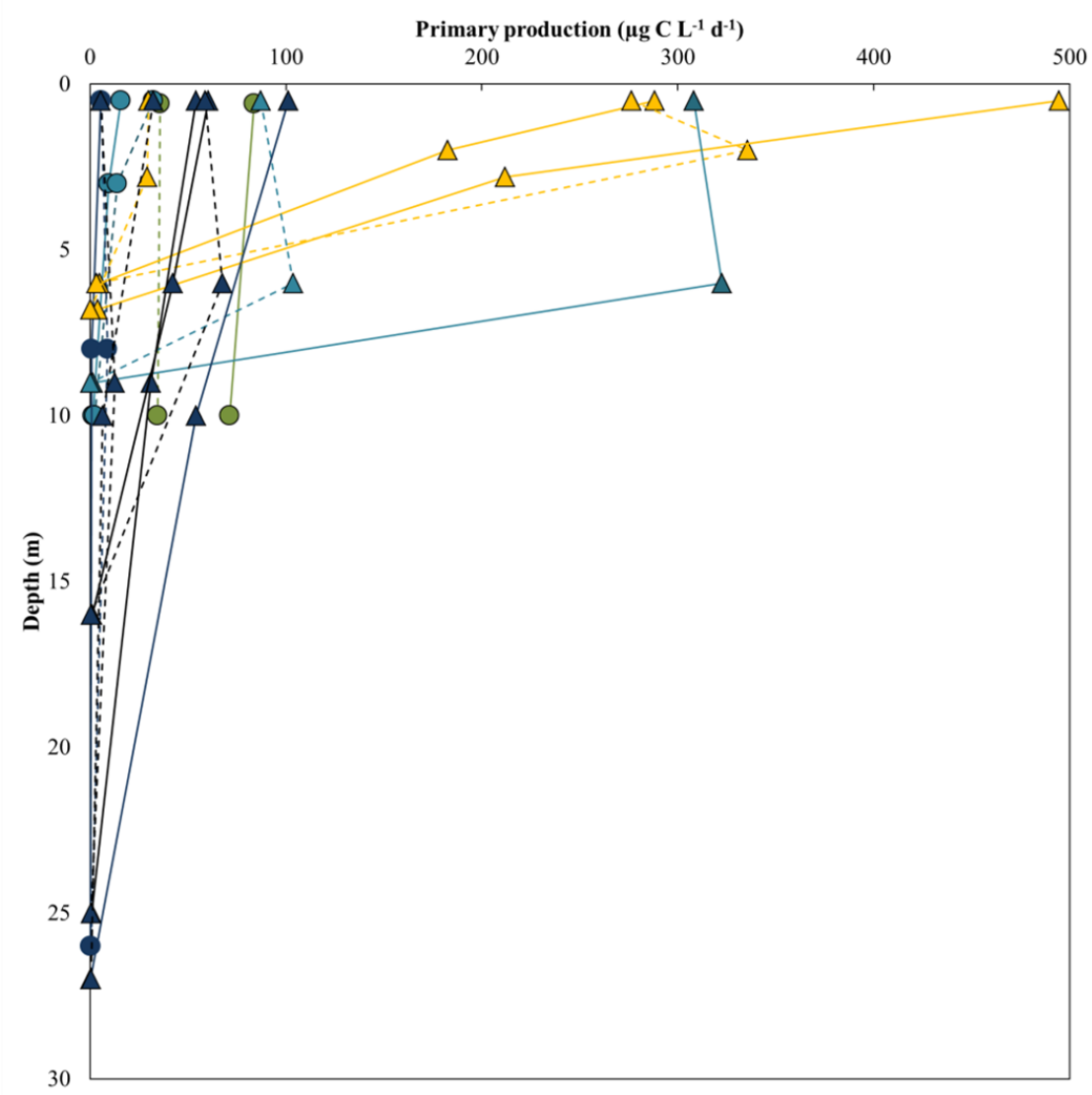

Figure 3.4 *Vertical profiles of primary productivity*

Vertical profiles of primary productivity (µg C L^{-1} d^{-1}). Values were used to calculate depth-integrated productivity using the trapezoidal method. Autumn (circles) an spring (triangles) for the different water types are represented by colors: estuarine (yellow), inner-shelf (green), mid-shelf (cyan), and outer-shelf (blue). Size fractions are indicated by dashed (0.6-5µm) or solid (> 5µm) lines.

3.3.3 Principal component analysis

The relationship between variables for the two seasons and different water types were examined using principal component analysis (PCA) (Figure 3.5, Tables 3.8-3.9). Eigenvectors expressed the relationships between individual environmental parameters and the derived components, which showed that the first two principal components (*i.e.* PC 1, PC 2) accounted for 71.9% of the variance in autumn and 62.7% of the variance in spring across all water types. While seasonal variability was less discernable, both seasons did exhibit similar loading patterns, with physical and biogeochemical constituents grouping into different water types. In both seasons, vector loadings associated with biological data grouped mostly along the positive component 1 and component 2 axes, which indicate estuarine and inner shelf end members. Abiotic variance (*i.e.*. S, T, PO_4^{3-}) was strongly and inversely associated with biological constituents, suggesting outer shelf end members.

The relationship between biological parameters and environmental variables derived from principal components was examined for each water type (Table 3.9). The first two components explained 70.1%, 93.1%, and 78.4% of the cumulative variability in estuarine and inner shelf (Figure 3.6), mid-shelf (Figure 3.7), and outer-shelf waters (Figure 3.8), respectively. The data clustered together such that autumn variables were correlated negatively with spring variables. There was a strong, positive correlation between environmental constituents in PC 1 and biological processes in estuarine and inner-shelf waters, suggesting that there were strong horizontal gradients associated with freshwater discharge (Figure 3.6). PC 1 was characterized positively by $Si(OH)_4$, N^2,

which is an index for stratification intensity, high primary production, biovolume-derived carbon, and chlorophyll a, whereas negative PC 1 was associated with inorganic nutrients PO_4^{3-}, $NO_2 + NO_3^-$, and NH_4^+. PC 2 was positively correlated with all nutrients and negatively with temperature, salinity, and biovolume-derived carbon for microzooplankton.

Variance partitioned similarly for mid-shelf waters. Diatom biovolume-derived carbon ($C_{BVdiatoms}$) strongly correlated with PC 1, as was the buoyancy frequency, Chl *a*, and PP, whereas T, S, and PO_4^{3-} were negatively associated with PC 1 (Figure 3.7). $Si(OH)_4$ and $NO_2 + NO_3^-$ comprised much of the positive variance in PC 2, whereas nanoplankton and microzooplankton C_{BV} characterized the negative PC 2. Salinity and temperature were inversely correlated with the N^2 and $Si(OH)_4$, indicating both seasonal and freshwater influences in mid-shelf waters.

Seasonal patterns were evident in outer-shelf waters (Figure 3.8), which showed a strong inverse relationship between temperature and salinity with biological data along the PC 1 axis. Temperature and salinity also were inversely correlated with the buoyancy frequency along PC 1, though temperature accounted for more variance than salinity along PC 2. This implied that a stronger relationship existed between T and the N^2, and that horizontal gradients driven by freshwater were less of an influence in outer shelf waters. All inorganic nutrients, except NH_4^+, clustered along the positive PC 2 axis and were strongly correlated with one another. Ammonium was positively correlated with biological data along PC 1.

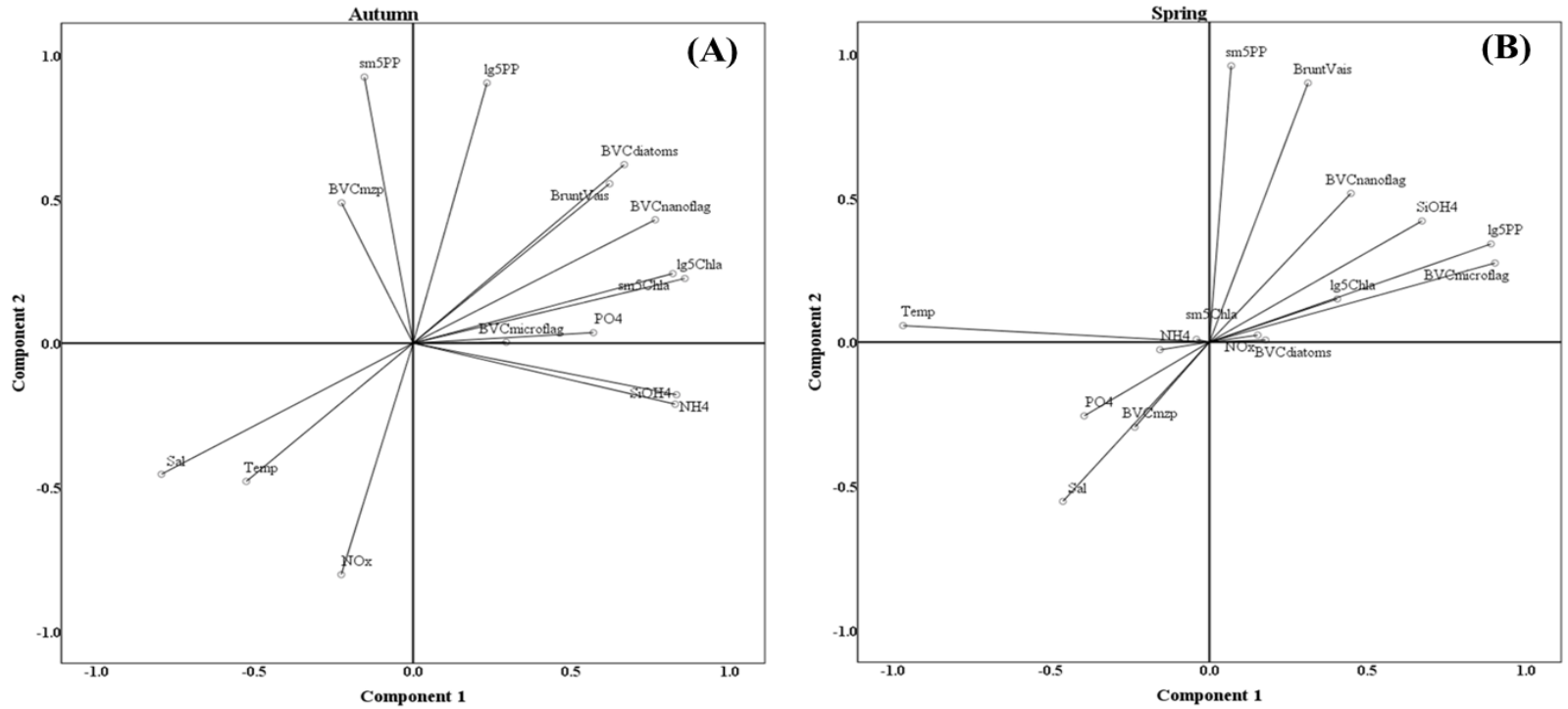

Figure 3.5 *Principal component analysis for autumn and spring*

Principal component analysis (PCA) for autumn (A) and spring (B). Water types were combined in each season to examine patterns in variability among environmental and phytoplankton community variables. Environmental variables include: temperature (Temp), salinity (Sal), ammonium (NH4), inorganic nitrogen, NO_2+NO_3^- (NOx), orthophosphate (PO4), silicic acid (SiOH4), and buoyancy frequency, N^2 (BruntVais). Phytoplankton community variables include: size-fractionated chlorophyll a for Chl a0.6-5µm (sm5Chla), Chl a>5µm (lg5Chla), primary productivity 0.6-5µm (sm5PP), primary productivity>5µm (lg5PP), and biovolume-derived carbon for nanoplankton (C_{BV}nanoflag), microflagellates (C_{BV}microflag), diatoms (C_{BV}diatoms), and microzooplankton (C_{BV}mzp).Autumn PC1 = 51.2%, PC2 = 20.7% of the variability, with a cumulative 71.9% of the variance accounted for in the first two components, and Spring PC 1=45.8%, PC2 = 17.0%, with 62.7% cumulative for the first two components.

Table 3.8 *PCA of environmental variables for autumn and spring*

Principal component analysis (PCA) variable loadings for environmental constituents for autumn and spring. (**) indicate the dominant variables in each loading.

	Autumn Percent variance (%)			**Spring** Percent variance (%)		
	PC 1	PC 2	Cumulative	PC 1	PC 2	Cumulative
	51.2%	20.7%	71.9%	45.8%	17.0%	62.7%
	Extracted eigenvalues			Extracted eigenvalues		
Variable	PC 1	PC 2	N	PC 1	PC 2	N
Temperature	-0.527**	-0.480	11	-0.968**	0.570	13
Salinity	-0.795**	-0.455	11	-0.463	-0.553**	13
Brunt Vaisala	0.620**	0.554	11	0.311	0.899**	13
NO_x	-0.227	-0.803**	11	0.152**	0.024	13
NH_4	0.832**	-0.179	11	-0.156**	-0.027	13
$Si(OH)_4$	0.827**	0.212	11	0.671**	0.420	13
PO_4^{3-}	0.569**	0.037	11	-0.396**	-0.256	13
Chl $a_{0.6\text{-}5\ \mu m}$	0.820**	0.242	11	-0.041	0.010	13
Chl $a_{>5\ \mu m}$	0.858**	0.225	11	0.404**	0.150	13
$PP_{0.6\text{-}5\ \mu m}$	-0.154	0.924**	11	0.069	0.959**	13
$PP_{>5\ \mu m}$	0.233	0.903**	11	0.889**	0.341	13
$C_{BV_{nanoflag}}$	0.765**	0.428	11	0.447	0.516**	13
$C_{BV_{microflag}}$	0.294**	0.003	11	0.902**	0.274	13
$C_{BV_{diatom}}$	0.667**	0.620	11	0.177**	0.007	13
$C_{BV_{mzp}}$	-0.226	-0.480**	11	-0.236	-0.295**	13

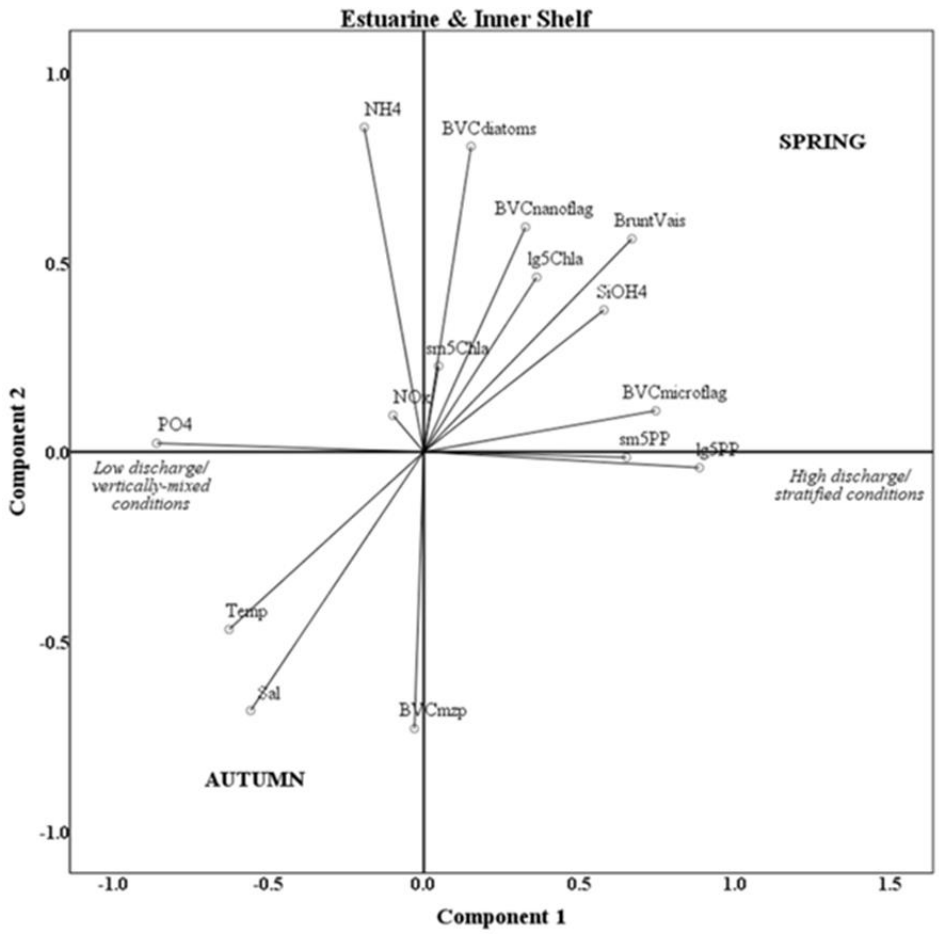

Figure 3.6 *Principal component analysis for estuarine and inner-shelf waters*

Principal component analysis (PCA) for estuarine and inner-shelf waters in the Mississippi Bight. Seasonal data were combined to assess water type influence on plankton community dyanamics. Environmental variables include: temperature (Temp), salinity (Sal), ammonium (NH4), inorganic nitrogen (NOx), orthophosphate (PO4), silicic acid (SiOH4), and buoyancy frequency (BruntVais). Phytoplankton community variables include: size-fractionated chlorophyll a for Chl a0.6-5µm (sm5Chla), Chl a>5µm (lg5Chla), primary productivity 0.6-5µm (sm5PP), primary productivity>5µm (lg5PP), and biovolume-derived carbon for nanoplankton (C_{BV}nanoflag), microflagellates (C_{BV}microflag), diatoms (C_{BV}diatoms), and microzooplankton (C_{BV}mzp).

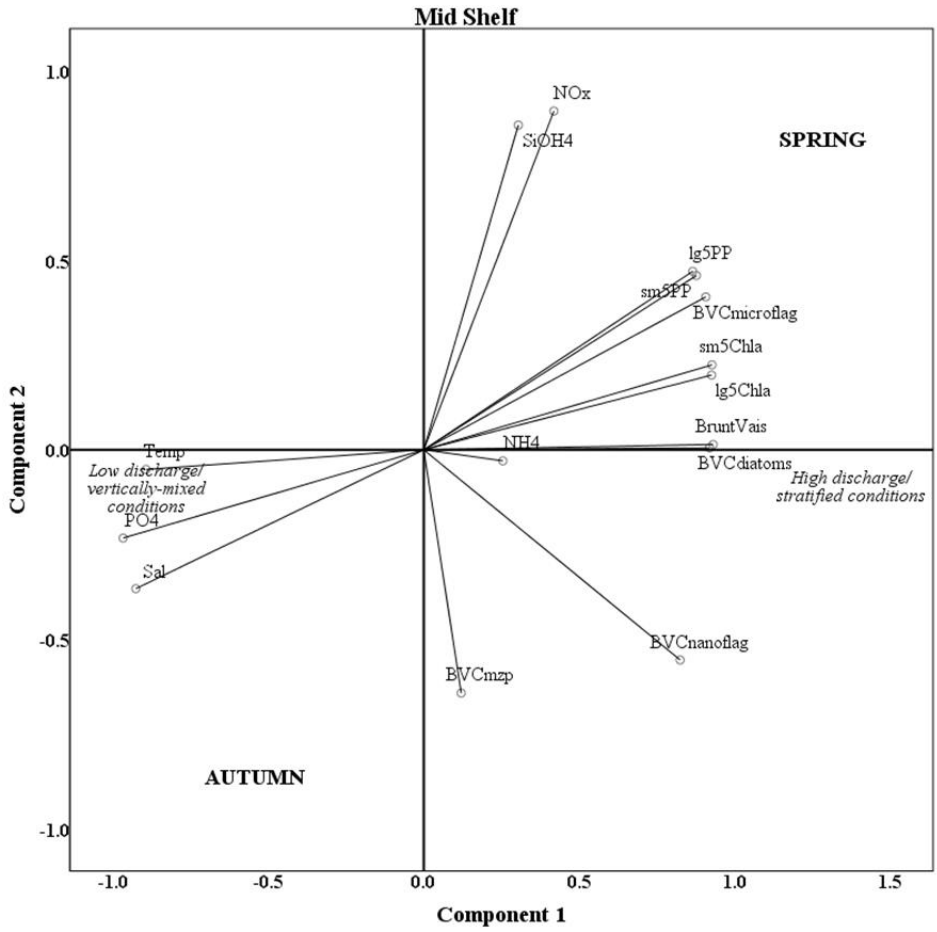

Figure 3.7 *Principal component analysis for mid-shelf waters*

Principal component analysis (PCA) for mid-shelf waters in the Mississippi Bight. Seasonal data were combined to assess water type influence on plankton community dyanamics. Environmental variables include: temperature (Temp), salinity (Sal), ammonium (NH4), inorganic nitrogen (NOx), orthophosphate (PO4), silicic acid (SiOH4), and buoyancy frequency (BruntVais). Phytoplankton community variables include: size-fractionated chlorophyll a for Chl a0.6-5µm (sm5Chla), Chl a>5µm (lg5Chla), primary productivity 0.6-5µm (sm5PP), primary productivity>5µm (lg5PP), and biovolume-derived carbon for nanoplankton (C_{BV}nanoflag), microflagellates (C_{BV}microflag), diatoms (C_{BV}diatoms), and microzooplankton (C_{BV}mzp).

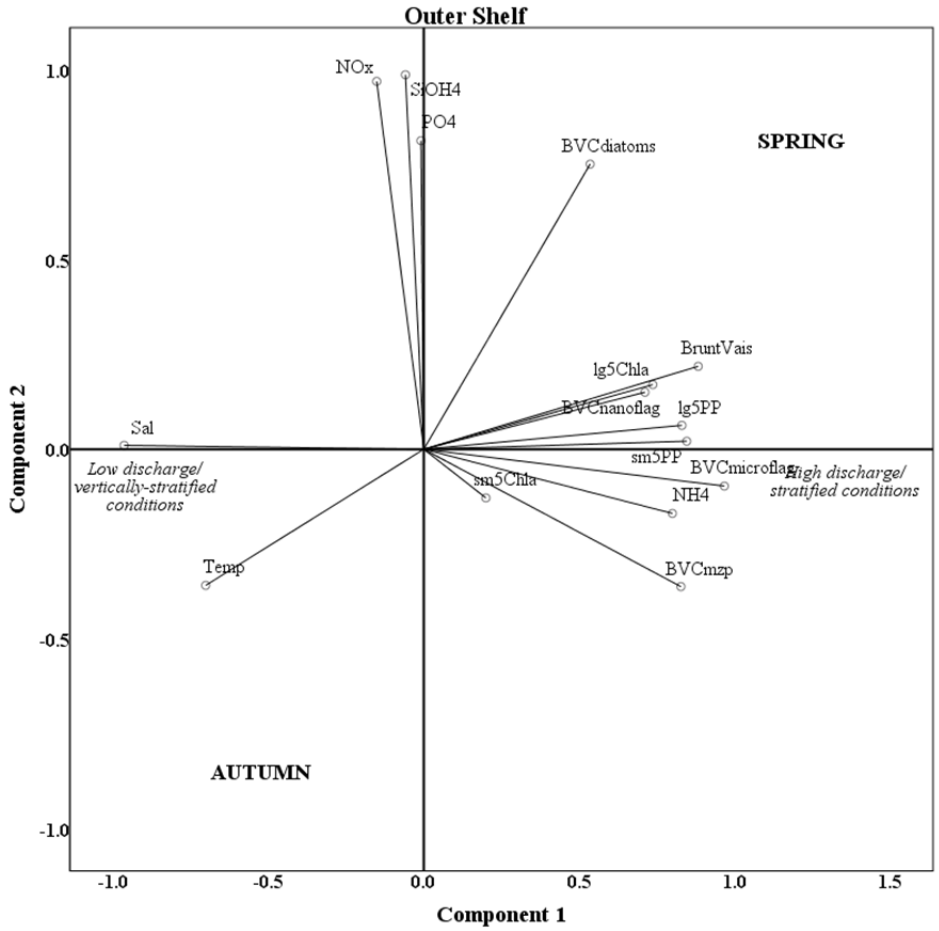

Figure 3.8 *Principal component analysis for outer-shelf waters*

Principal component analysis (PCA) for outer-shelf waters in the Mississippi Bight. Seasonal data were combined to assess water type influence on plankton community dyanamics. Environmental variables include: temperature (Temp), salinity (Sal), ammonium (NH4), inorganic nitrogen (NOx), orthophosphate (PO4), silicic acid (SiOH4), and buoyancy frequency (BruntVais). Phytoplankton community variables include: size-fractionated chlorophyll a for Chl a0.6-5µm (sm5Chla), Chl a>5µm (lg5Chla), primary productivity 0.6-5µm (sm5PP), primary productivity>5µm (lg5PP), and biovolume-derived carbon for nanoplankton (C_{BV}nanoflag), microflagellates (C_{BV}microflag), diatoms (C_{BV}diatoms), and microzooplankton (C_{BV}mzp).

Table 3.9 *PCA of environmental variables for the different water types*

Principal component analysis (PCA) variable loadings for environmental constituents for autumn and spring. (**) indicate the dominant variables in each loading.

	Estuarine & Inner Shelf Percent variance (%)			**Mid Shelf** Percent variance (%)			**Outer Shelf** Percent variance (%)		
	PC 1	PC 2	Cumulative	PC 1	PC 2	Cumulative	PC 1	PC 2	Cumulative
	52.0%	18.1%	70.1%	69.7%	23.4%	93.1%	54.8%	23.6%	78.4%
	Extracted eigenvalues			Extracted eigenvalues			Extracted eigenvalues		
Variable	PC 1	PC 2	N	PC 1	PC 2	N	PC 1	PC 2	N
Temperature	-0.627**	-0.469	12	-0.894**	-0.052	4	-0.702**	-0.359	8
Salinity	-0.557	-0.682**	12	-0.927**	-0.366	4	-0.964**	0.010	8
Brunt Vaisala	0.670**	0.562	12	0.931**	0.014	4	0.883**	0.218	8
NO_x	-0.099	0.096	12	0.419	0.894**	4	-0.152	0.969**	8
NH_4	-0.191	0.856**	12	0.254**	-0.029	4	0.800**	-0.169	8
$Si(OH)_4$	0.580**	0.374	12	0.304	0.856**	4	-0.059	0.987**	8
PO_4^{3-}	-0.860**	0.022	12	-0.967**	-0.233	4	-0.009	0.813**	8
Chl $a_{0.6\text{-}5\ \mu m}$	0.048	0.226**	12	0.927**	0.224	4	0.200	-0.128	8
Chl $a_{>5\ \mu m}$	0.363	0.460**	12	0.926**	0.197	4	0.737**	0.170	8
$PP_{0.6\text{-}5\ \mu m}$	0.652**	-0.015	12	0.877**	0.460	4	0.846**	0.021	8
$PP_{>5\ \mu m}$	0.887**	-0.042	12	0.865**	0.471	4	0.831**	0.063	8
$C_{BV_{nanoflag}}$	0.327	0.593**	12	0.825**	-0.554	4	0.712**	0.150	8
$C_{BV_{microflag}}$	0.747**	0.108	12	0.907**	0.403	4	0.967**	-0.097	8
$C_{BV_{diatom}}$	0.152	0.806**	12	0.919**	0.005	4	0.535	0.752**	8
$C_{BV_{mzp}}$	-0.030	-0.730**	12	0.120	-0.642**	4	0.827**	-0.362	8

3.4 DISCUSSION

A central goal of this study was to identify the environmental constituents that drive seasonal rates of phytoplankton primary production within MSB shelf waters. This study examined the spatial and temporal variability of size-fractionated (0.6-5 μm, > 5μm) POC, Chl *a*, and primary productivity, and how these size fractions were related to nano-microplankton community C_{BV}. Here, addressed is the overarching hypothesis that size-fractionated autotrophic biomass and primary productivity will vary seasonally and spatially, such that the smaller size fraction (0.6-5 μm) would account for half of the biomass and most (> 50%) of the primary productivity across the shelf in autumn, whereas the larger size fraction (>5 μm) will have greater biomass and production rates in spring. The reader is directed to Chapter II for taxonomic description of seasonal shifts in the microplankton community

Observations show that size-fractionated biomass was not statistically different (Wilcoxon rank sum, $p \leq 0.05$) from the respective size fractions in autumn, whereas the >5μm size fraction accounted for ~73% of the total biomass in spring. This pattern was also evident in the size-fractionated primary productivity measurements. In this study, we also examined whether size-fractionated biomass and productivity would be significantly correlated to C_{BV} estimates from each plankton group, such that nanoplankton and diatoms would account for most of the >5 μm primary productivity in autumn, whereas diatoms would contribute disproportionately more carbon than other groups in spring. A Spearman's rank correlation analysis between plankton group C_{BV} and size fractionated productivity highlighted highly significant ($p \leq 0.01$) relationships between nanoplankton

and diatoms with the >5 μm productivity size fraction in autumn, whereas diatoms were highly correlated ($p \leq 0.01$) with >5 productivity in spring (Appendix F). Interestingly, microzooplankton C_{BV} also was significantly ($p \leq 0.05$) correlated with productivity in the 0.6-5 μm size fraction in both seasons. Overall, the observations from these two cruises provide three fundamental conclusions about this system: (1) primary productivity in this system is high and is comparable to other highly productive shelf ecosystems, (2) river plume effects influence physical and biogeochemical processes up to 60 km offshore during the spring freshet, and (3) predation on small (0.6-5 μm) phytoplankton biomass likely is an important top-down control on pico- and nanoplankton in this system. Evidence for these conclusions is discussed below.

3.4.1 Primary productivity in the Mississippi Bight

Coastal river-dominated ecosystems are biological hot spots (Cloern *et al.*, 2014). In this study, estimates for daily median depth-integrated primary productivity for the Mississippi-Alabama Shelf was 1.7 $\pm$ 0.9 g C m^{-2} d^{-1}, with an annual estimate of 518.2 $\pm$ 162.5 g C m^{-2} y^{-1}. Despite having only two seasons measured, productivity was high and variable in this ecosystem and ranged from < 0.1 – 1.2 g C m^{-2} d^{-1} (< 37 - 500 g C m^{-2} y^{-1}), shifting from a mesotrophic (100-300 g C m^{-2} y^{-1}) state in autumn to a more eutrophic (300-500 g C m^{-2} y^{-1}) system in spring following the water quality classification of Nixon (1995). The results presented here are similar to rates of primary production measured in other temperate and subtropical eutrophic/mesotrophic ecosystems (see Cloern *et al.*, 2014). Studies along the continental shelf waters of Louisiana reported mean daily integrated primary production values ranging from 0.3 – 3.7 g C m^{-2} d^{-1} and up to 8.1 g C

m^{-2} d^{-1} within the Mississippi River plume (Redalje *et al*., 1994; Lohrenz *et al*., 1997; Chen *et al*., 2000). Brzezinski and Washburn (2011) observed ranges of daily integrated production from 0.4 g C m^{-2} d^{-1} to as high as 5.8 g C $m^{-2}d^{-1}$ in the Santa Barbara Channel (California Current). North Atlantic phytoplankton bloom values reported ranged from 0.5 – 1.0 g C m^{-2} d^{-1} (Bury *et al*., 2001).

The results presented in the present study also show that both size fractions (0.6-5 μm and > 5 μm) contribute statistically equivalent proportions to biomass and productivity during low discharge conditions in autumn, whereas the >5 μm size fraction contributed significantly more biomass and productivity under elevated freshwater discharge in spring. PCA for each of the seasons (Figures 3.5A-B) indicated that both productivity size-fractions were inversely related to inorganic nitrogen, temperature, and salinity in autumn, whereas biomass was positively related to nanoplankton and diatom biovolume-derived carbon. Thus, while much of the autotrophic biomass was contained in the nanoplankton and diatom community, autumn variability in size-fractionated productivity was regulated primarily by biotic (top-down) controls, as indicated by the positive correlation with microzooplankton C_{BV} along PC 2 and possibly other biological sources not addressed (e.g. bacterial production, viral lysis) in this system. However, spring >5 μm size-fractionated biomass and productivity were positively related to inorganic N and $Si(OH)_4$ in spring. This suggests that variability in the >5 μm autotrophic community is driven abiotically (bottom-up) by river discharge during the spring freshet, and is reflected in shifts in nanoplankton, microflagellate, and diatom community structure. Other studies have shown that pico- and nanophytoplankton biomass and

production contribute significantly to the overall production in marine systems. In the highly eutrophic Pearl River Estuary and adjacent near shore waters, Qui *et al*., (2010) reported that nano- and microphytoplankton dominated the phytoplankton community in autumn and spring. Gaulke *et al*., (2010) found that picophytoplankton (< 3 μm) contributed 35-44% of the total Chl *a* and 42-55% of the total primary production in the Neuse River Estuary. Seasonal variability for both size fractions (< 3 μm, > 3μm) was evident, with greater biomass and productivity in spring and summer, as indicated by the positive correlations with temperature (Gaulke *et al*., 2010).

3.4.2 Influence of river plumes on microplankton shelf communities

The timing and magnitude of nutrient loading via river discharge is a key factor in the controlling primary production in river influenced coastal margins (Caffery *et al.*, 2014). Seasonal variations in the water column physical structure were important in influencing biomass and primary production in autumn for the larger size fraction, as indicated by the negative correlations (Spearman's r, $p \leq 0.05$) between temperature and salinity with >5 μm size fraction. However, spring variability was largely influenced by salinity, as indicated by PCA (Figures 3.13A-B, Table 3.8) and correlation analysis (Spearman's r, $p \leq 0.05$). Except for PO_4^{3-}, inorganic nutrient concentrations were also were less important for seasonal variability in phytoplankton biomass and production for both size classes. Low salinity river plumes were dominant features of the estuarine and inner shelf surface waters in spring (refer to Figure 2.4, Chapter II). It was also expected that low salinity freshwater plumes would not influence mid- and outer-shelf communities, but rather, biomass would be influenced by slope waters where temperature

plays a much stronger role in structuring water column. However, PCA bi-plots (Figures 3.6-3.8) for spring water types show that the N^2 was controlled mostly by salinity in estuarine and inner shelf surface waters, whereas temperature determined the physical structure of the surface waters in outer shelf. Like the estuarine and inner shelf regions, mid shelf surface water buoyancy frequency was mostly regulated by salinity, as indicated by the inverse relationship between biological variables and salinity along the PC 1 axis. This suggests that freshwater river plumes likely were affecting nano- and microplankton community dynamics up to 60 km from the mouth of the Mobile Bay during the spring freshet.

Buoyant river plumes are distinguishing and ecologically relevant features along the nGOM continental shelf. Dzwonkowski *et al.*, (2015, 2017) observed that estuarine influences from Mobile Bay affect shelf waters via surface water discharge plumes. They found that the region of freshwater influence extended to approximately 30 km offshore following the passage of a post-tropical cyclone in autumn 2015 (Dzwonkowski *et al*., 2017). In this system, wind forcing, plume buoyancy, and river momentum act as the primary agents pushing river water onto the shelf (Dzwonkowski *et al.,* 2017), particularly in spring. This has significant implications for local biogeochemistry and trophic interactions in the MSB. Because freshwater river plumes are coherent structures, they serve as an efficient retention and transport mechanism for river-borne nutrients, trace metals, contaminants, and plankton along continental shelf margins (Banas, 2009; Kudela *et al.,* 2010; Dzwonkowski *et al.,* 2015). These plumes also serve as areas of enhanced trophic activity (i.e. floating bioreactors), where phytoplankton can maximize

their growth rates (Kudela *et al*. 2010). Further, enriched nutrient loads within river plumes have shown greater rates phytoplankton production (Banse, 1992; Lohrenz *et al*., 1995; Kudela *et al*., 2010), intrinsic growth rates (Murell *et al*., 2002; Frame and Lessard, 2009; Ortell and Ortmann, 2014), and enhanced trophic transfer (Dagg and Breed, 2003; Liu and Dagg, 2003; Dagg *et al*., 2004).

3.4.3 Phytoplankton biomass dynamics

Aquatic ecologists have long understood the importance herbivory plays in controlling phytoplankton biomass (Banse 1982). Suspended particulate matter plays a major role in biogeochemical cycling and energy flows in aquatic ecosystems, serving as a direct food source for many herbivorous grazers in the water column (Fuhrman, 1992). Further, in many coastal marine systems, the autotrophic biomass is dominated by a size spectrum ranging from 0.2 – 2 μm prokarytotic picoplankton (e.g. *Synechococcus* spp. and *Prochlorococcus* spp.) to > 20 μm microplanktonic protists (Gin *et al.*, 2000). While small cells tend to out-number large cells in terms of cell numbers, large cell dominate the photosynthetic biomass (*i.e.*. Chl *a*) and primary production in productive coastal regions (Cloern, 2018). This system is not unlike other productive, coastal ecosystems. Spatial and seasonal variability was evident for both size fractions, and the results show that 0.6 – 5 μm and >5 μm phytoplankton biomass values were not statistically different (Wilcoxon rank sum, $p < 0.05$) in autumn (Figure 3.2C, Table 3.2). The pattern was different in spring, with the larger size fraction biomass accounting for more than 76% of the total biomass across all water types.

There were also distinct patterns between water types with biomass concentrations and ratios of POC, PON, and Chl *a* for each of the size fractions (Figures 3.2A-C), distributions which are typical of coastal, river-dominated shelf systems in the region (Lohrenz *et al*., 1990; Redalje *et al*., 1994; Dagg *et al*. 2004). Although the chemical composition of the resident phytoplankton community was not quantified, the proportions of POC/PON were examined, as this ratio is often used to infer carbon and nitrogen assimilation ratio of phytoplankton (Eppley *et al*., 1979). In the current study, the ratios of POC/PON for the two size fractions were significantly different (Wilcoxon rank sum, $p < 0.05$) from one another. Median POC/PON was lower (6.1 ± 0.3) for the 0.6-5μm size fraction, but was higher (6.8 ± 0.5) for the larger size fraction. This suggests that a strong detrital component was evident in the water column in both seasons. Studies in the Lake Pontchartrain estuary have shown that elevated POC/PON ratios (> 7) point to high allochthounous input from terrestrially-derived carbon sources (Bianchi and Agyron, 1997). The MSB is influenced by multiple larger rivers, which are likely sources of terrigenous carbon sources, and particularly during the spring freshet. In autumn, the likely source of allochthonous carbon may have been through resuspension of bottom sediments during the passage of post-tropical storm Patricia. This event mixed the entire water column along the shelf and likely played a role in resuspending carbon-rich organic sediments into the surface waters.

One notable pattern was the prevalence of spring $POC_{>5\mu m}$ relative to $POC_{0.6\text{-}5\mu m}$ and the inverse pattern for PON size fractions. This suggests a significant source of $PON_{0.6\text{-}5\mu m}$ size fraction to the PON pool, and likely is an indication of extensive bacterial

colonization of particles (Cifuetues *et al*., 1999). Bacteria tend to have low (~3-5) carbon-to-nitrogen elemental ratios and can supplement N-requirements with organic N (e.g. urea) or by respiring much of the assimilated carbon to reduce growth efficiency (Cifuentes *et al*., 1999). However, low (< 3) POC/PON ratios coupled with high organic matter indicate a rich medium for enhanced bacterial growth (Cifuentes *et al*., 1999). These organically-rich aggregates serve as miniature bioreactors important for driving elemental transformations in the microbial loop (Azam *et al*., 1983), as well as serving as food sources for multiple trophic levels, including microzooplankton, mesozooplankton, and ichthyoplankton (Kiørbe 2001). Previous results from coastal regions also show that pico- and nanoplankton may account for >70% of the total organic biomass (Rossi *et al*, 2013). In autumn, the ratio POC:Chl *a* for the 0.6-5μm size fraction was significantly greater in the mid- and outer-shelf waters than at stations along the inner-shelf region (Table 3.3). This reflects either the presence of carbon-rich organic matter resulting from estuarine flushing and resuspension from post tropical cycolone Patricia or the predominance of bacterioplankton and/or heterotrophic protists (*i.e.* ciliates, heterotrophic dinoflagellates) in the surface waters. While neither group was quantified, image-based classification of microzooplankton consisted of mixed assemblages of ciliates, tintinnids, and copepod nauplii, which accounted for ~16% of the total imaged nano-microplankton community carbon biomass in autumn (Table 3.1). Autumn mid- and outer-shelf waters were characterized by low 0.6-5 μm size-fractionated Chl *a* concentrations and very high (>200) POC:Chl *a* ratios. Therefore, we suggest that

microzooplankton herbivory (and bacteriovory) likely were key processes in controlling 0.6-5μm phytoplankton biomass.

It is widely accepted that small cells grow faster than large cells (Kiørbe, 2008). Gin *et al*. (2003) and studies cited therein, found that growth rates of different phytoplankton size classes tend to follow rectangular hyperbolic trends (e.g. Michaelis-Menten or Mondad kinetics; Thingstad and Sakshaug, 1990), with maximal growth rates inversely proportional to size (Peters 1983). Others (e.g. Finkel *et al*., 2010; Ward *et al*., 2012) observed that oligotrophic waters were dominated by pico- and nanophytoplankton, where a tight coupling exists between growth, mortality, and nutrient regeneration. However, unlike "semi-closed systems" like those found in oligotrophic open ocean ecosystems where production is maintained through nutrient recycling, high-nutrient coastal regimes support new production of large cells, which are usually diatom-dominated communities. Kiørbe (2003) found that large phytoplankton cells become dominant in "resource-saturated" environments, whereas others (e.g. Jochem, 2003; Cermño *et al*., 2005) suggest that large cells may be more physiologically fit to outgrow small cells. Cermño *et al*. (2005) found that large cells were dominant in coastal regions and these cells were able to maintain more biomass due to favorable conditions (*i.e.* luxury N-uptake and higher light- utilization efficiency). However, Cloern (2018) identified top-down grazing pressure on small cells as a reason why large cells dominate coastal and estuarine ecosystems. Large cells are grazed slower than small cells, due primarily to the time lag between the growth rate of large phytoplankton and their grazers, which include both protists and larger metazoan mesozooplankton (Cloern,

2018). Further, heavily silicified diatoms may serve as a mechanical defense to deter or slow the rates of herbivory (Spillane, 2016; Zhang *et al.*, 2017).

Herbivorous microzooplankton are the consummate consumers of phytoplankton biomass in aquatic ecosystems and are essential components of marine food webs (Calbet and Landry, 2004). The impact of microzooplankton (< 200 μm) herbivory on phytoplankton communities has been well documented and underscores the important role that heterotrophic protists play in a diversity of aquatic environments (Beers *et al*., 1980; Smetacek *et al*., 1981; Paranjape, 1990; Landry and Hassett, 1982; Verity *et al*., 1993; Neuer and Cowles, 1994; Sherr and Sherr, 1994; Landry *et al*., 1993, 1994, 1997, 1998, 2000, 2002; Strom *et al*., 2001; Calbet and Landry, 2004). In the coastal NW Mediterranean Sea, Calbet *et al*. (2008) found that microzooplankton grazing on < 10 μm phytoplankton production often exceeds 100% seasonally, whereas herbivory on > 10 μm phytoplankton production was about 30-60%. They observed that herbivorous grazers, comprised of < 20 μm-sized heterotrophic flagellates and small ciliates, exerted significant top-down control on < 10 μm phytoplankton biomass (Calbet *et al*. 2008). Although this contrasts with studies (e.g. Sherr and Sherr, 1992; Strom and Strom, 1996; Jeon *et al*., 2005; Leising *et al*., 2005a), which highlight the greater top-down role microzooplankton and flagellated protists play in controlling larger-celled phytoplankton communities, it nevertheless highlights the important role that small (<10 μm) heterotrophic flagellates and ciliates play in controlling small (<10 μm) phytoplankton production (Calbet *et al*., 2008). A study of trophic interactions in the western Arabian Sea also showed that the grazing pressure of nano- and microzooplankton on

phytoplankton (2.0 – >20 μm) daily productivity ranged from 38% to 102%, but more relevant is that picophytoplankton (0.2 – 2 μm) growth greatly increased upon removal of nanozooplankton grazers during a series of dilution experiments (Reckermann and Veldhuis 1997). Christaki *et al*. (2001) indicated that consumption of *Synechococcus* and *Prochlorococcus* picoprokaryotes by nanoplankton heterotrophic grazers exceeded 45% daily in the Mediterranean Sea.

While there is a tendency to view the microbial trophic web as a linear cascade based on a size class approach (e.g. picoplankton – small heterotrophic nanoplankton – microzooplankton ciliates and larger flagellated protists), protists often feed at multiple trophic levels, as well as upon other herbivorous protists (Dolan, 1991; Dolan *et al*., 2000). In the present study, Chl *a*-normalized PP in both size fractions were similar, yet their biomass were significantly different. This is a strong indication that grazing could be controlling the small cells in this system. Therefore, it is under this assumption that we suggest herbivory by nano- and microzooplankton protists, including flagellates, exert significant top-down grazing pressure on small (0.6-5 µm) phytoplankton biomass and productivity throughout the year in this system.

3.5 CONCLUSION

This study has provided evidence that river discharge, through the influence of buoyant river plumes, has a strong influence on the spatial and temporal variability of primary productivity, biogeochemistry, and trophic interactions in surface waters along the MS-AL shelf. Previous studies (e.g. Lohrenz *et al.*, 1990; Smith and Demaster, 1996; Dagg *et al.*, 2004; Kudela *et al.*, 2010) also highlight the importance freshwater discharge

plays in structuring planktonic communities and biogeochemical transformations in coastal river-dominated ecosystems. Observations from this study also show that the influence of river plumes greatly affects planktonic communities in shelf waters up to 30 km offshore during periods of low discharge and more than 60 km during the spring freshet. The MSB is a highly productive ecosystem, oscillating from eutrophic conditions during high river discharge and elevated nutrient concentrations, to a mesotrophic state under reduced discharge and nutrients. It should be noted that most of the production is concentrated within the upper 2 meters of the surface waters. Unlike productive upwelling systems where primary production is distributed through more than 50 m of the water column, river dominated systems such as the MSB have very high production rates and autotrophic biomass concentrated in the surface waters. Like the MSR-influenced Louisiana Shelf, much of the water column within the MSB is light limited, particularly during periods of high river discharge. It is during the spring freshet when rivers deliver high concentrations of inorganic nutrients, especially N, to the surface waters. This stimulates phytoplankton growth and acts to reset and sustain the system during periods of reduced river discharge.

While pigment-labelled production incubations were not conducted, it is suggested that seasonal variability in primary productivity is linked to changes in the phytoplankton community. Image analysis indicated that mixed assemblages of nanoplankton and diatoms were the predominant protist community in autumn, but transitioned to a diatom-dominated community across the shelf in spring (see Chapter II), which explains the springtime increase in phytoplankton productivity. Despite a reduced

nutrient load in autumn, inorganic nutrients, and likely organic recycled nutrients, phytoplankton biomass, productivity, and growth remains high year-round, which addresses why this region is part of the "fertile fisheries cresecent." High phytoplankton production usually is significantly and positively correlated with fisheries production (Nixon *et al.*, 1986). Further studies which examine size-fractionated ^{14}C- pigment-labeled phytoplankton coupled with ^{15}N and ^{13}C stable isotopes should be conducted to quantify phytoplankton growth and trophic transfer throughout this system. Ultimately, this information will assist ecosystem modeling efforts for visualizing the movement of carbon and nitrogen through multiple trophic levels.

CHAPTER IV – MICROZOOPLANKTON GRAZING IN THE MISSISSIPPI BIGHT

4.1 INTRODUCTION

Improved understanding of plankton community dynamics and trophic connectivity between primary producers and heterotrophic protists, and their relationship within their physical setting, is a central tenet to plankton ecological studies. Microzooplankton (20 - 200 μm) herbivory on phytoplankton communities has been well documented throughout different aquatic ecosystems and highlights the important role microzooplankton play in structuring marine food webs (Smetacek, 1981, Landry and Hassett 1982, Paranjape 1990, Verity *et al*. 1993, Landry *et al*. 1993, 1995, 1998, 2000, 2002, Neuer and Cowles 1994, Sherr and Sherr, 1994, 2007; Strom *et al*. 2007, Calbet and Landry 2004).

Microzooplankton are the main consumers of autotrophic biomass and primary production (Calbet and Landry, 2004), play a key role in the microbial loop (Azam *et al*., 1983; Sherr and Sherr, 2008), and they serve as intermediaries between phytoplankton and mesozooplankton predators (Gifford, 1991; Calbet, 2008). Grazing by microzooplankton may account for most or all of the daily phytoplankton production (Landry and Hasset 1982, Gifford 1988, Olson and Strom 2002, Calbet and Landry 2004), and because they often have generation times on the same order as their prey, microzooplankton often serve as the primary top-down control on phytoplankton biomass most aquatic systems (Landry and Hassett 1982, Paranjape 1990, Verity *et al*. 1993, Landry *et al*. 1993, 1995, 1998, 2000, 2002, Calbet and Landry 2004). As regenerators of inorganic nutrients, microzooplankton can return up to 70% of regenerated nutrients to

the dissolved or particulate pool for subsequent use by bacterioplankton and phytoplankton (McManus and Santoferrara, 2013). Microzooplankton also serve also as prey items for larger mesozooplankton grazers and ichthyoplankton, and thus serving as the primary conduit to for transferring carbon from primary producers to higher trophic levels (Calbet and Saiz, 2015).

Although the impact of microzooplankton herbivory on phytoplankton has been documented extensively throughout many regions of the world's oceans and coastal margins (see Calbet and Landry 2004 review), these studies tend to be underrepresented in the Gulf of Mexico, particularly along the biologically-rich Mississippi-Alabama shelf waters. Results observing the seasonal grazing impact of microzooplankton on phytoplankton in Fourleague Bay, Louisiana showed significant top-down control on phytoplankton, with more than 95% total photosynthetic biomass being grazed by microheterotrophic protists (Dagg 1995). Fahnenstiel *et al*. (1995) found higher grazing rates (range 0.6-1.5 d^{-1}) on smaller (< 15μm) phytoplankton size fractions and grazing rates not significantly different from zero for larger size fractions (e.g. diatoms) in the MSR plume region. Strom and Strom (1996) reported significant grazing rates (>1 d^{-1}) on two phytoplankton size fractions (< 8 μm and > 8 μm), consuming approximately 30% of autotrophic biomass. Microzooplankton herbivory in MSR plume waters has been found to exert significant top-down control on phytoplankton biomass (Dagg, 1995; Fahnenstiel *et al*., 1995; Strom and Strom, 1996). Strom and Strom (1996) found significant grazing impacts by microheterotrophic protists on phytoplankton communities, predominantly large diatoms, on the Louisiana continental shelf, and suggested that grazing-induced

mortality can exert substantial control on phytoplankton populations in relatively eutrophic coastal ecosystems. Liu and Dagg (2003) also observed significant grazing and phytoplankton growth rates in the plume field of the Mississippi River on the Louisiana Shelf. Microzooplankton grazing studies east of the Mississippi River Birdfoot Delta include the Saint Louis Bay (McGhee and Redlaje, 2016), Mobile Bay (Lehrter *et al*., 1999; Ortmann *et al*. 2011; Ortell and Ortmann 2014), Pensacola Bay (Murrell *et al*. 2002), Santa Rosa Sound (Juhl and Murrell 2005), and the Suwannee River estuary (Jett 2004).

In the present study the impact of microzooplankton herbivory on phytoplankton was determined in the river-dominated inner shelf and adjacent outer shelf waters of the Mississippi Bight. Observations were made as part of the CONCORDE project, which provided for the comparison of microplankton community structure and trophic dynamics (i.e. primary productivity and herbivory) to physical and biogeochemical data collected simultaneously during the course of two research cruises in two seasons and under differing hydrographic regimes. The primary objective of this study was to determine the impact microzooplankton grazing has on seasonal phytoplankton production across the continental shelf of the northern Gulf of Mexico (nGOM). The findings of this study highlight the quantitative importance microzooplankton herbivory, particularly by ciliates, plays in controlling phytoplankton biomass and productivity.

4.2 METHODS

In this study, the impact microzooplankton grazing has on phytoplankton productivity using two approaches: the seawater dilution technique and in-flow imaging-

based ciliate potential grazing on nanoplankton was examined. The seawater dilution method developed by Landry and Hassett (1982) has been applied in a variety of environments to measure grazing control of phytoplankton and predator-prey interactions (Murrell *et al.* 2002). While this technique integrates the net functioning of the plankton (< 200 μm) community, it is cumbersome and time-consuming, often providing low spatial and temporal resolution. Alternatively, in-flow imaging-based (*i.e.* FlowCAM) indirect methods to predict microzooplankton herbivory based on taxonomic and phenotypic characteristics provides greater spatio-temporal resolution, as well as information on the community structure and dynamics. Potential grazing of ciliates on nanoplankton was based on prey density relative to body size dependency of maximum ingestion and clearance rates, and has been used in a variety of aquatic ecosystems (Hansen *et al.*, 1997; Haraguchi *et al.*, 2018). Each of these techniques was applied to estimate the fate of primary production and carbon flow through microzooplankton in this system.

4.2.1 Sampling

The CONCORDE study area is bounded to the north and west by a series of barrier islands and situated between the two largest river systems in terms of discharge into the Gulf of Mexico: the Mississippi-Atchafalaya River system (MSR) to the west and the Alabama and Tombigbee Rivers via Mobile Bay to the east (Figure 4.1). Samples were obtained from surface waters (~0.9-3.0 m), where the rosette was held at just below the surface for all samples. Two consecutive discrete surface water samples, one for ancillary measurements (i.e. plankton imaging, nutrients, chlorophyll a, productivity

incubations) and one for microzooplankton grazing experiments, were obtained at night using a rosette sampler equipped with 12.0 L Niskin bottles, a SeaBird SBE911 plus conductivity-temperature-depth instrument profiler, and a WET Labs ECO-AFL chlorophyll fluorometer. Acid-washed silicon tubing fitted with 200 μm Nitex mesh was placed onto each water collection valve to remove large grazers, and the entire contents were dispensed into an acid-washed 4.0 L bottle for image analysis, inorganic nutrients, Chl *a*, and a 25 L opaque carboys for microplankton grazing incubations. A total of 78 (autumn = 38, spring = 40) discrete samples were taken for ancillary measurements, whereas only 12 (autumn = 4, spring = 8) stations were sampled for microzooplankton grazing estimates.

Methods for determining inorganic nutrient concentrations, phytoplankton biomass (i.e. Chl *a*), microplankton community structure using in-flow imaging (i.e. FlowCAM), and size-fractionated primary productivity were described previously in Chapter II and Chapter III, respectively.

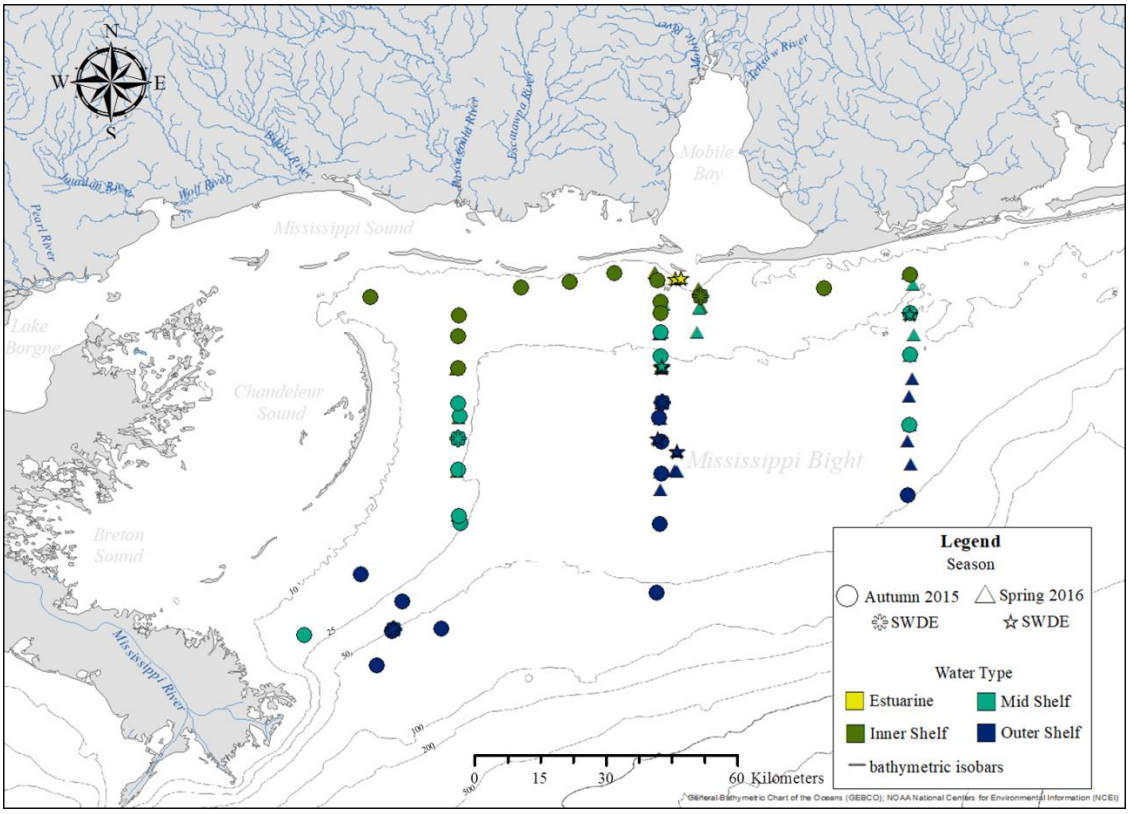

Figure 4.1 *Station map of surface sampling stations for microplankton imaging and seawater dilution experiments (SWDE) for autumn and spring*

4.2.2 Seawater dilution experiments

Microzooplankton grazing rates were quantified using modified seawater dilution experiments (SWDE) (Landry and Hassett, 1982), which included a highly diluted fraction (90-95%) of particle free seawater (PFSW) to adjust for the non-linear feeding (Gallegos, 1989) expected in these highly productive waters. Three assumptions were accounted for to estimate microzooplankton grazing and phytoplankton growth: 1) phytoplankton growth rates were not density-dependent, 2) phytoplankton cell mortality was linearly related to microzooplankton cell density, and 3) phytoplankton growth was not nutrient limited (Landry and Hassett, 1982). Non-linear functional feeding responses

and potential trophic cascades were addressed using a highly diluted (10% and 5%) whole seawater (WSW) diluent (Gallegos, 1989).

All tubing, containers, and materials were pre-cleaned with 10% HCl and diluted micro, then rinsed three times with deionized water following the trace metal clean procedures of Fitzwater *et al.* (1982). The current study used 1.078 L clear, polycarbonate wide-mouthed bottles and neutral density screen for shading in the incubator. Once the CTD rosette was on-deck and secured water samples for grazing experiments were prescreened through 202 μm Nitex mesh and dispensed into a 25 L carboy. Particle free seawater (PFSW) diluent was prepared via filtration through a Whatman 0.22 μm filter cartridge, inorganic nutrients (final concentration = 5 μM KNO_3/ 0.5 μM KPO_4) were added to ensure no nutrient limitation of phytoplankton growth occurred. An additional set of non-nutrient amended whole seawater (WSW) was incubated as well. Triplicate treatments were carried out in an on-deck clear acrylic incubator with circulating ambient surface seawater. Bottles were placed into 12% neutral density screening to approximate irradiance intensities just below the water surface.

Chl *a* was used to determine change in phytoplankton biomass over 24 hour incubation. Triplicate 100-300 mL aliquots from each bottle treatment were used to determine Chl *a* concentration following a methanol extraction technique (Welschmeyer, 1984). Phytoplankton net growth rate is represented by Equation 4.1 and its linear relationship (model II linear regression) along the dilution gradient (D) provides measures of grazing (g) and intrinsic phytoplankton growth in theoretical absence of grazers (μ), where g and μ are the slope and ordinal intercept, respectively (Figure 4.2),

Equation 4.1

$$\left({}^{1}/_{t}\right) ln\left({}^{P_t}/_{P_0}\right) = k - g$$

where, P_0 and P_t is the change in phytoplankton biomass over time, *t*, at the beginning and end of the experiment, respectively, *k* is the nutrient-augmented apparent phytoplankton growth rate, *g* is the rate of phytoplankton mortality due to grazing. Phytoplankton apparent growth rate in the absence of nutrients (k_0) was used to calculate phytoplankton intrinsic growth in experiments without nutrient enrichment (μ_0) in the undiluted 100% WSW fraction, where $\mu_0 = \mu + g$. Estimates μ_0 were used to compare microzooplankton grazing to *in situ* phytoplankton growth to microzooplankton grazing. Nutrient limitation was determined as the ratio of $\mu_0{:}\mu$, where ratios < 1 indicate nutrient limitation. The ratio of microzooplankton grazing to non-nutrient amended phytoplankton net growth rates ($g{:}\mu_0$) served as a first-order approximation of the fraction of primary production consumed daily by microzooplankton (Strom *et al.*, 2007). The percent daily phytoplankton biomass grazed (%PBG) and daily primary production consumed (%PPG) was estimated following Murrell *et al.* (2002):

Equation 4.2

$$\%PBG = (1 - e^{-g}) * 100\%$$

Equation 4.3

$$\%PPG = ((e^{\mu} - e^{(\mu - g)})/e^{\mu - 1}) * 100\%$$

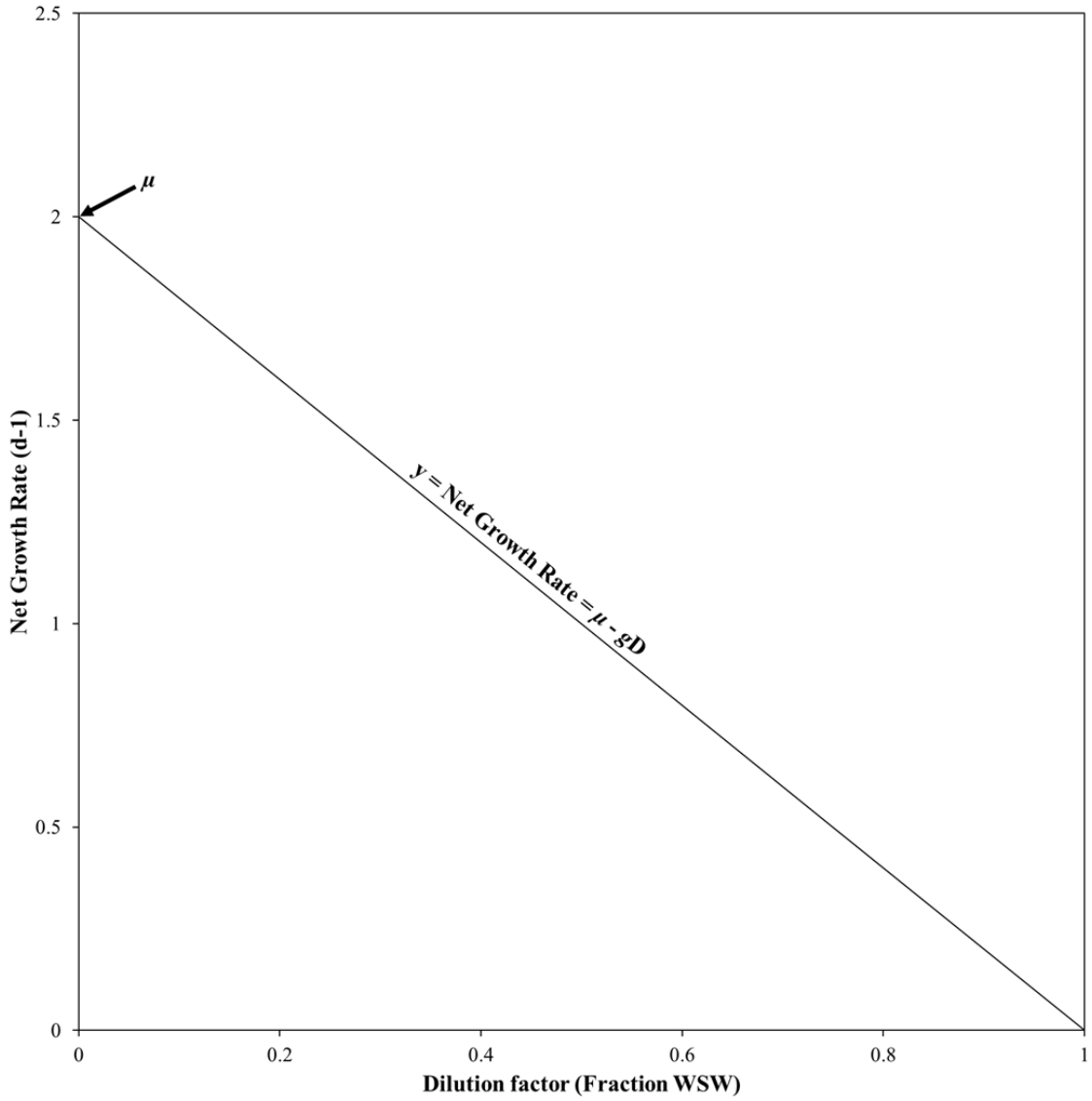

Figure 4.2 *Idealized seawater dilution model*

Idealized dilution model describing the linear relationship between phytoplankton net growth rate and the dilution factor (*i.e.* fraction of undiluted seawater (whole seawater, WSW)). Specific phytoplankton growth rate (*i.e.* intrinsic growth rate) is denoted by μ (ordinal intercept) and phytoplankton mortality due to microzooplankton grazing, g (slope).

4.2.3 Ciliate potential grazing

Water samples were imaged using FlowCAM® and manually classified into one of twenty-two categories of microplankton (see Chapter II, Table 2.1). Nanoplankton and microzooplankton particle dimensions (*i.e.* area based diameter (ABD), biovolume) and abundances were estimated using the Visual Spreadsheet software.

4.2.3.1 Microzooplankton herbivory trophic strategy definitions

Microzooplankton herbivores were broadly classified into two primary categories: ciliates and other microzooplankton grazers (e.g. naupliiar copepods). Ciliates were further classified into three sub-categories based on their morphology and trophic strategy following Haraguchi *et al*. (2018) (see Chapter II, Table 2.1): (i) *Mesodinium* (Lohman 1908) sp., a genus that includes mixotrophs that acquire chloroplasts (*i.e.* kleptoplasty) for photosynthesis from specific prey (*Teleaulux* spp.) and selective herbivores preying mainly on nanoplankton (Smith and Hansen 2007; Peltomaa and Johnson, 2017; Haraguchi *et al*., 2018); (ii) aloricate choriotrichids, which includes both generic and selective herbivores, and general non-constitutive mixotrophs that feed primarily on picoeukaryotes and nanoplankton (Smith and Hansen, 2007; Peltomaa and Johnson, 2017; Haraguchi *et al*., 2018); and (iii) tintinnids, which have a conspicuous lorica and feed selectively on picoeukaryotes and nanoplankton (Montanges 2013, Haraguchi *et al*., 2018), although this group was assumed to be a generic herbivore in this study. The strategy was based on the ciliate nutritional modes and predation defined by Haraguchi *et al*., (2018), which defined "predation" to include grazing by any organism requiring an external food source, whether it is to obtain the photosynthetic apparatus (i.e.

chloroplast) of phytoplankton (e.g. *Mesodinium* spp. ingesting *Teleaulax* spp.) or purely carnivorous. Other microzooplankton grazers were not used to estimate potential grazing.

4.2.3.2 Prey definitions

Prey were defined as nanoplankton (2-20 μm), which were imaged using FlowCAM®. Some representative taxa include genera from Chlorophyte and Chromophyte functional groups. Studies (e.g. Smith and Hansen, 2007; Johnson, 2011; Schoener and McManus, 2012; Montagnes, 2013; Peltomaa and Johnson, 2017) have shown that picoeukaryotes and nanoplanktonic flagellates are the primary food sources for ciliates and tintinnids.

4.2.3.3 Potential grazing rates

Potential grazing rates (PG, μg C L^{-1} d^{-1}) by ciliates were estimated by calculating the generic maximum ingestion and clearance rates of nanoplankton following methods outlined by Hansen *et al*. (1997) and Haraguchi *et al*. (2018). Generic maximum ingestion rate (I_{max}) is equivalent to the prey items, presented here as the total sum of the nanoplankton biovolume (spheroid), ingested per unit time. The generic maximum clearance rate (C_{max}) is equivalent to the volume of water cleared or filtered of prey (i.e. nanoplankton biovolume) per unit time. The relationship between grazer activity and prey density were described by Michaelis-Menten kinetics, where the ingestion rate approaches a maximum rate (I_{max}) at high prey densities and maximum clearance (C_{max}) rate is obtained at low prey densities (Hansen *et al*., 1997). Both I_{max} and C_{max} were normalized to predator biovolume following the 20^{o}C temperature standard and ciliate biovolume parameters from Hansen *et al*. (1997) (Haraguchi *et al*., 2018).

Equation 4.4

$$I_{max} = 50.1 \cdot V_{cil}^{-0.225}$$

Equation 4.5

$$C_{max} = 70.6 \cdot 10^{-6} \cdot V_{cil}^{-0.225}$$

The half-saturation food density (K_m) was calculated following Equation 4.6.

Equation 4.6

$$K_m = \frac{I_{max}}{C_{max}}$$

Volume-normalized cell-specific ingestion rates, $I(d,T,V_{cil})$ for the entire ciliate group were calculated following methods by Haraguchi *et al.* (2018) (Equation 4.7).

Equation 4.7

$$I(d,T,V_{cil}) = \frac{1}{V_{sample}} \cdot \left(\frac{I_{max} \cdot d}{(K_m + d)} \cdot Q_{10}^{\frac{(T-20)}{10}} \right)$$

Here, d, Q_{10} , and T are the prey density (μm^3 mL^{-1}), temperature quotient equivalent to 2.8 (Hansen *et al.* 1997), and the water temperature (^oC), respectively. For simplicity, the water temperature was assumed to be constant at 20^{o}C.

The impact of ciliate potential grazing on nanoplankton primary productivity (PP_{nano}, μg C L^{-1} d^{-1}) was determined as the ratio of PG: PP_{nano}, where PP_{nano} was estimated as a function of the nanoplankton percent contribution of image-based biovolume-derived carbon (C_{BVnano}) to the total microplankton community biovolume-derived carbon ($C_{BVtotal}$). The percent contribution for nanoplankton to total microplankton used was 20.2%, 33.7%,4.6%, for autumn and 41.6%, 30.8%,

15.0%,22.2%, for spring. The >5 μm size fraction was used to estimate PP since imaged plankton < 5 μm were not quantified.

4.2.4 Data analysis

Descriptive statistics for the data set are presented as median $\pm$ MAD. For the SWDE, a t-test was used to test whether slope of the regression was significantly different ($p \leq 0.05$) from zero and a Wilcoxon rank sum to test whether nutrient augmented non-diluted replicates were significantly different (Wilcoxon rank, $p \leq 0.05$) from non-nutrient addition undiluted replicates. Mann-Whitney U test was used to determine whether seasons were statistically different. All statistical analyses were conducted with SPSS software program at the significance level $\alpha = 0.05$.

4.3 RESULTS

4.3.1 Microzooplankton grazing rates

Results of seasonal rates of microzooplankton grazing SWDE for each water type are summarized in Table 4.1. Overall, three out of twelve (autumn = 1, spring = 2) dilution experiments showed regression slopes significantly different from zero ($p < 0.05$), saturated feeding kinetics was observed in one experiment in autumn (Figure 4.3), and a positive slope was observed at a single experiment in spring (Figures 4.4-4.5).

Microzooplantkon grazing rates (g) ranged from 0.2 to 1.1 d^{-1}, with nutrient-augmented phytoplankton growth rates (μ) ranging from -0.81 to 2.5 d^{-1} (Table 4.1). Median g and μ across water types and seasons was 0.38 $\pm$ 0.14 d^{-1} and 0.87 $\pm$ 0.5 d^{-1}, respectively, with the non-nutrient amended phytoplankton net growth (μ_0) equivalent to 0.8 $\pm$ 0.3 d^{-1}. Phytoplankton net growth also was greater than grazing in both seasons,

with μ increasing from 0.8 $\pm$ 0.3 d^{-1} in autumn to 1.1 $\pm$ 0.7 d^{-1}, whereas the microzooplankton grazing pressure did not differ between autumn (0.4 $\pm$ 0.1 d^{-1}) and spring (0.4 $\pm$ 0.2 d^{-1}). Autumn grazing rates were higher along the inner- and outer-shelf stations, whereas phytoplankton growth rates were greatest at the mid-shelf station (Table 4.1, Figure 4.3). In spring grazing rates tended to be greater along mid- and outer-shelf water types, ranging from 0.8 $\pm$ 0.4 to 0.7 $\pm$ 0.3 d^{-1}, respectively (Table 4.1). Phytoplankton growth rates also were greater along mid- and outer-shelf waters in both seasons, ranging from 1.3 $\pm$ 0.9 to 2.5 $\pm$ 0.0 d^{-1}, respectively. A single station along the inner-shelf in autumn exhibited potential nutrient limitation, with phytoplankton apparent growth rate k_0 equivalent to 0.2 $\pm$ 0.1 d^{-1}, whereas, six stations in spring exhibited potential nutrient limitation. However, μ_0 indicated that *in situ* phytoplankton growth was likely enhanced due to nutrient addition at the mid-shelf station in autumn, and estuarine and outer-shelf stations in spring. Nutrient limitation was examined using the μ_0:μ ratio. Ratios ranged from -1.3 to 1.8 over the course of the study, with an overall study median of 0.9 $\pm$ 0.4. Negative ratios were due to negative μ and μ_0 in autumn and spring, respectively. Nutrient limitation was observed at mid-shelf stations in autumn and at estuarine and inner-shelf stations in spring.

The g:μ_0 ratio ranged from 0.6 $\pm$ 0.2 in autumn to 0.5 $\pm$ 0.1 in spring, with an overall study median equivalent to 0.5 $\pm$ 0.2. Ratios did not differ between water types in either season or between seasons, except in estuarine waters where g:μ_0 (1.1 $\pm$ 0.1) was significantly greater than any other water type in either season (Table 4.1).

The overall study percent phytoplankton biomass (%PBG) consumed was 33.9 $\pm$ 11.4% and did not differ seasonally (Table 4.1). Similarly, the percent phytoplankton production grazed (%PPG) for the study was 48.1 $\pm$ 9.2% and was not statistically significant (Mann Whitney U, $p \leq 0.05$) between seasons, ranging 47.2 $\pm$ 12.4% to 48.1 $\pm$ 9.2% in autumn and spring, respectively. The negative %PBG and %PPG in estuarine water type resulted from negative grazing rates (i.e. positive slope) at one of the stations (Figure 4.4B). Excluding this station, %PBG and %PPG for the remaining estuarine station was 38.1% and 79.8%, respectively.

Table 4.1 *Microzooplankton grazing and phytoplankton growth in the Mississippi Bight*

Results from seawater dilution experiments (SWDE) for microzooplankton grazing rates (d^{-1}) on total chlorophyll separated by water types (ES = estuarine, IS = inner-shelf, MS = mid-shelf, OS = outer-shelf) and seasons in the Mississippi Bight. Parameters are given for microzooplankton grazing (g), phytoplankton intrinsic growth rate in nutrient augmented (μ) and natural seawater (μ_0), phytoplankton apparent growth in the absence of nutrients (k_0), index for nutrient limitaions ($\mu:\mu_0$), ratio of microzooplankton grazing:phytoplankton growth ($g:\mu_0$), percent phytoplankton biomass grazed (%PBG), and primary production grazed (%PPG). Values are reported as median ± MAD. Where n = 1, results from SWDE are given as single values.

Season	Water-type	g (d^{-1})	μ (d^{-1})	μ_0 (d^{-1})	k_0 (d^{-1})	$\mu_0:\mu$	$g:\mu_0$	%PBG	%PPG
Autumn	IS	0.45	0.87	0.80	0.16 ± 0.07	0.92	0.56	29.1%	41.6%
	MS	0.24	1.44	0.33	1.19 ± 0.08	0.23	0.73	46.4%	28.0%
	OS	0.58 ± 0.02	0.52 ± 0.26	0.78 ± 0.01	0.22 ± 0.05	0.98 ± 0.51	0.54 ± 0.13	38.1 ± 0.6%	62.9 ± 10.2%
Spring	ES	-0.10 ± 0.40	0.60 ± 0.28	-0.14 ± 0.37	-0.18 ± 0.14	-0.66 ± 0.93	1.05 ± 0.12	-18.2 ± 41.9%	-86.6 ± 126.9%
	IS	0.38 ± 0.46	0.90 ± 0.46	0.98 ± 0.17	-0.06 ± 0.58	1.34 ± 0.49	0.37 ± 0.08	29.6 ± 9.1%	55.1 ± 2.6%
	MS	0.75 ± 0.37	1.33 ± 0.93	1.49 ± 0.37	0.03 ± 0.04	1.81 ± 0.98	0.47 ± 0.13	49.2 ± 17.5%	61.5 ± 17.8%
	OS	0.64 ± 0.27	2.45 ± 0.01	1.50 ± 0.42	-0.34 ± 0.13	0.62 ± 0.17	0.41 ± 0.07	48.0 ± 11.8%	52.4 ± 13.0%

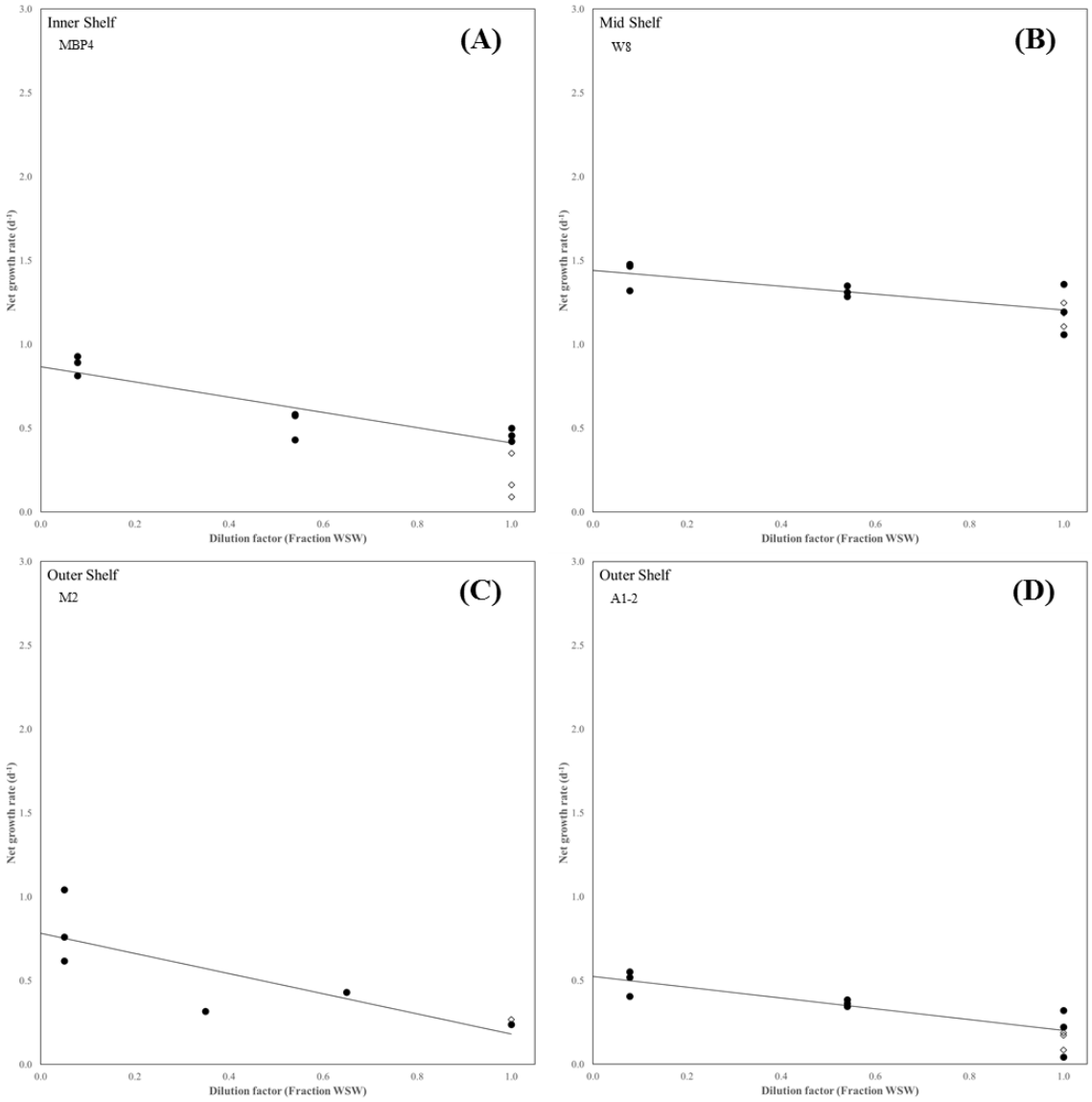

Figure 4.3 *Seawater dilution experiments for autumn*

Net growth rates along a dilution gradient for autumn inner-shelf (A), mid-shelf (B), and outer-shelf (C-D) water types. SWDE in panel C was conducted along a four-point dilution gradient.

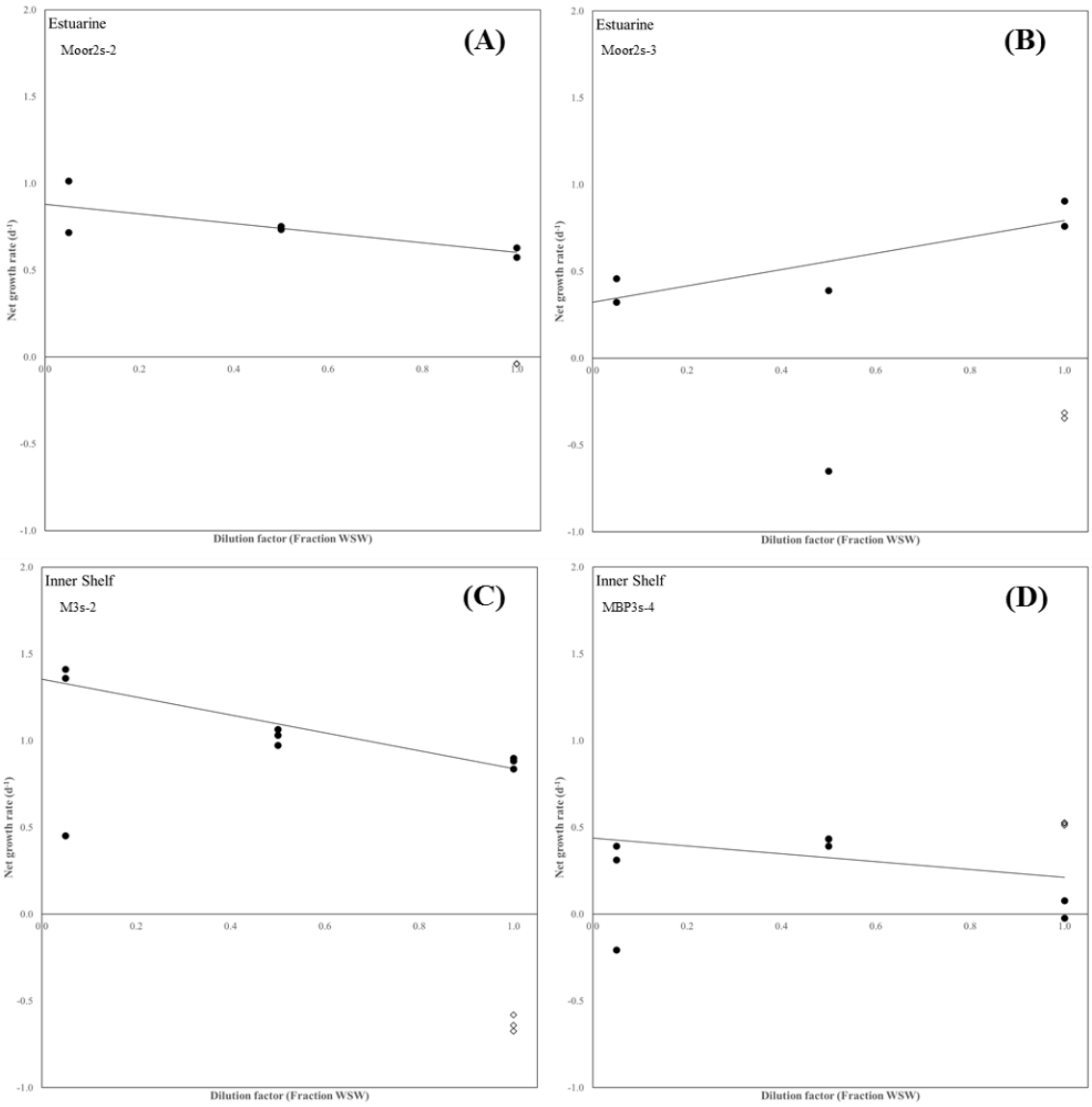

Figure 4.4 *Seawater dilution experiments for spring estuarine and inner-shelf waters*

Net growth rates along a dilution gradient for spring estuarine (A-B) and inner-shelf (C-D) waters.

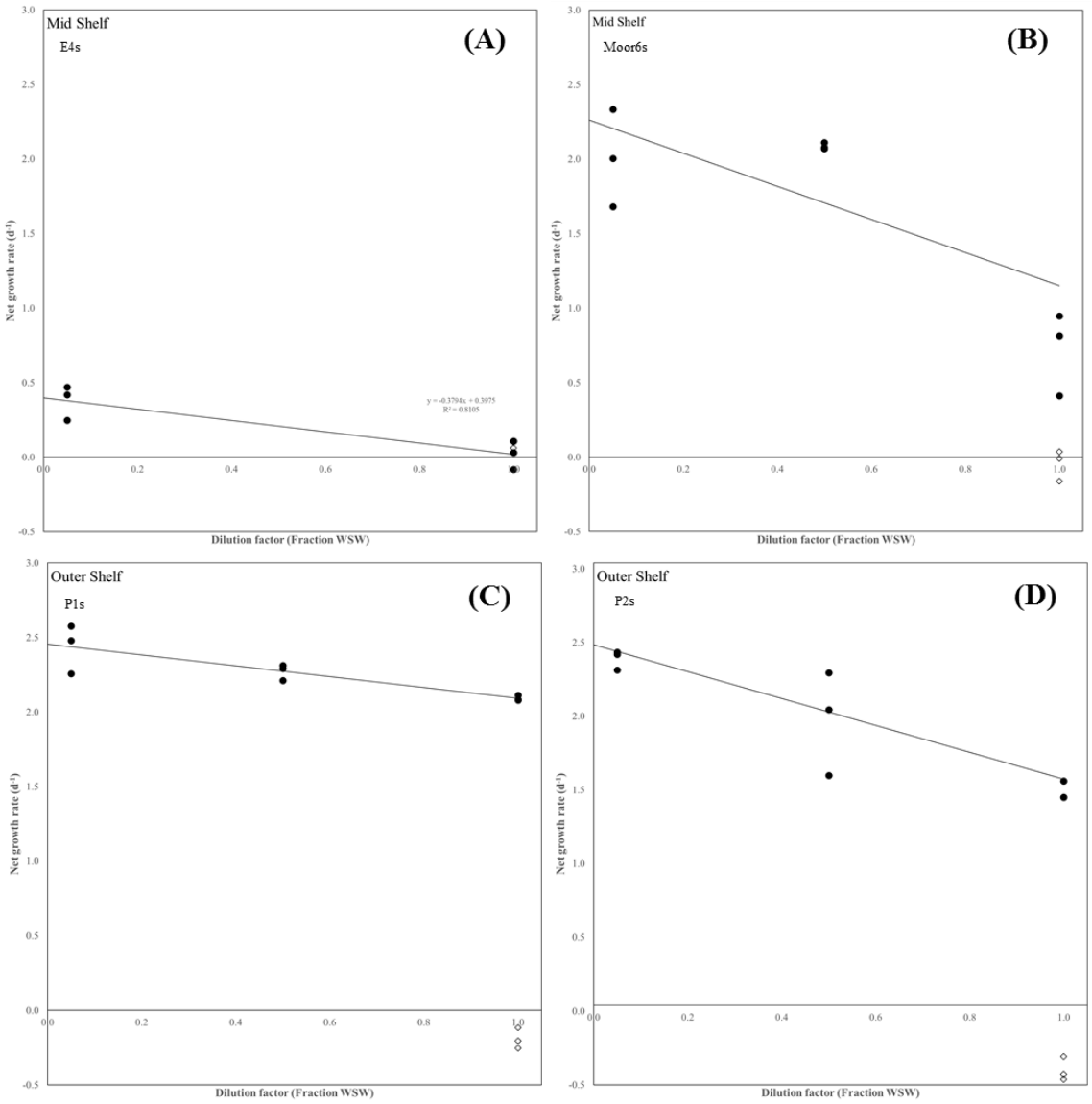

Figure 4.5 *Seawater dilution experiments for spring mid-shelf and outer-shelf waters*

Net growth rates along a dilution gradient for spring mid-shelf (A-B) and outer-shelf (C-D) waters.

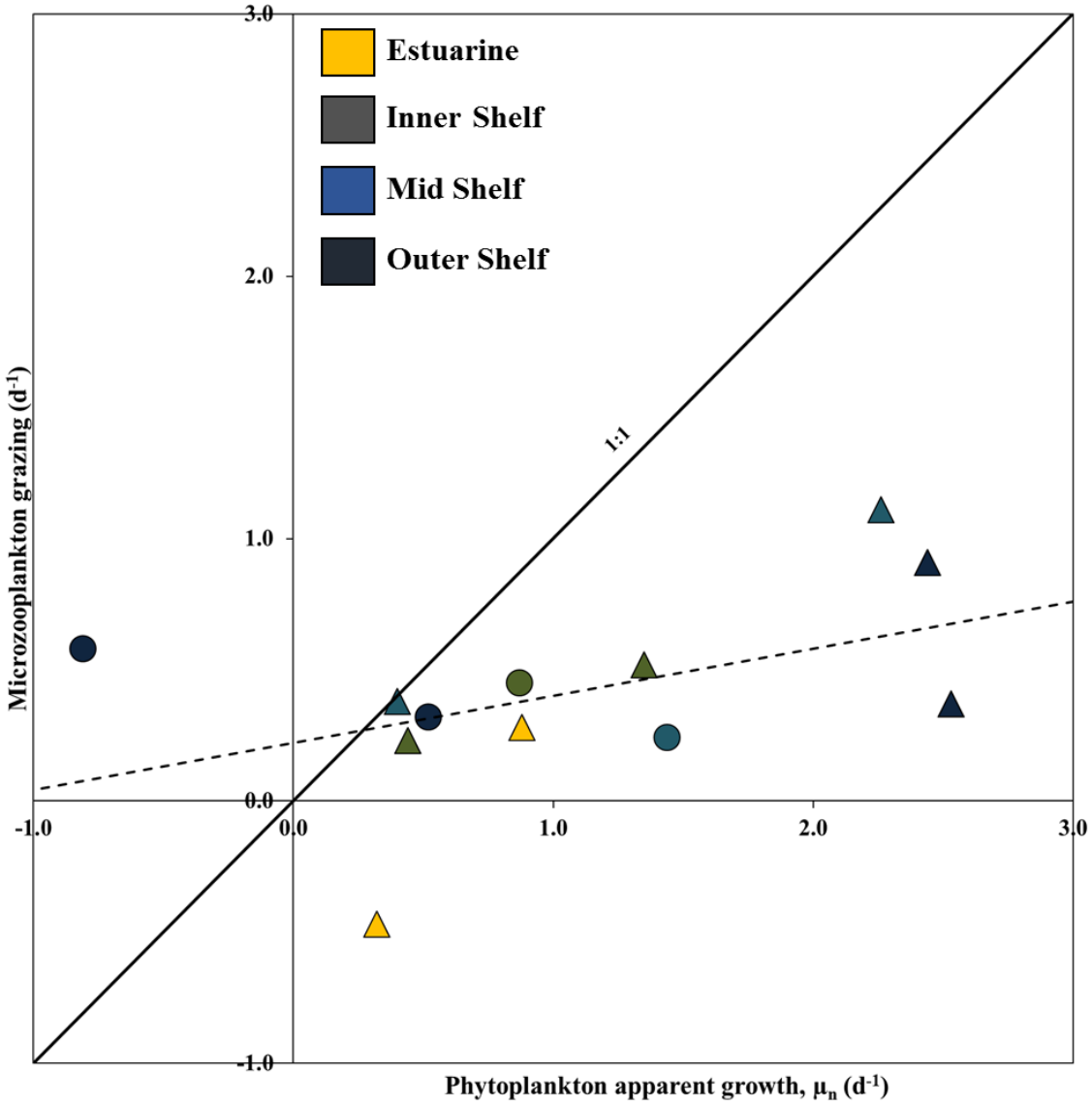

Figure 4.6 *Phytoplankton apparent growth rate versus grazing rate*

Phytoplankton apparent growth rate versus grazing rate. The 1:1 is the solid line indicates a perfectly coupled system. Regression between growth and grazing is given by a dashed line (R2 = 0.2147). Seasonal median (MAD) for u:m was 1.78 (1.66) for autumn and 2.32 (0.61) for spring. The study median (mad) was 1.98 (0.81). Seawater Dilution experiments: x-axis is the nutrient augmented phytoplankton apparent growth rate, y-axis is phytoplankton mortality due to microzooplankton grazing. Points represent rates, with the symbols denoting the seasons, colors for the different water types. The solid 1:1 line shows that all of the growth was greater than the grazing. The dashed line shows that growth is greater than grazing. Model II regression showin ghe best fit for all of the data. Except for a single data point in the autumn outer shelf where there was negative growth. This likely was due to error in the incubation.

4.3.2 Nanoplankton biomass, primary productivity, and ciliate community biomass

The reader is directed to Chapter II and Chapter III for a description of the microplankton community biovolume-derived carbon (C_{BV}) estimates of nanoplankton and microzooplankton biomass and patterns of size-fractionated primary productivity used in this study. Briefly, nanoplankton C_{BV} was greater in spring (41.1 $\pm$ 18.8 μg C L^{-1}) than autumn (12.8 $\pm$ 6.6 μg C L^{-1}). The percent contribution of nanoplankton C_{BV} to total microplankton community C_{BV} was 20.2%, 33.7%, and 4.6% for inner-, mid-, and outer-shelf waters in autumn, and 41.6%, 30.8%, 15.0%, 22.2% for estuarine, inner-, mid-, and outer-shelf waters in spring, respectively. Ciliate biomass, determined as the total biovolume-derived carbon (C_{BV}) did not differ significantly between seasons or across water types, ranging from 1.1-40.9 μg C L^{-1} in autumn and 1.2- 60.5 μg C L^{-1}. Nanoplankton biomass differed seasonally, ranging from 1.8 to 58.4 μg C L^{-1} in autumn to 6.5-117.6 μg C L^{-1} in spring (Table 4.2).

Primary productivity varied seasonally and spatially, with patterns similar to inorganic nutrients and Chl *a*. Primary production rates for >5μm size-fraction, with highest productivity at along estuarine and inner shelf waters and decreasing across the shelf in mid- and outer shelf waters (Table 4.2). The percent contribution of nanoplankton C_{BV} to productivity values are presented in Table 3. Nanoplankton estimated productivity mirrored seasonal and spatial productivity, with greatest rates in spring and along estuarine and inner-shelf waters, whereas lowest values were in autumn and at outer-shelf stations.

Microzooplankton ciliate C_{BV} did not differ seasonally between seasons (autumn = 11.1 ± 41.5 μg C L^{-1}; spring = 10.3 ± 6.4 μg C L^{-1}), but accounted for ~31% of the total microplantkon C_{BV} in autumn, and just 6% in spring. Aloricate choretrochids *Strombidium* Claparède and Lachmann and *Strombilidium* sp. and *Mesodinium* Lohman spp. were the most abundant ciliate groups, collectively contributing over 95% and 86% of the microzooplankton community in autumn and spring, respectively. Aloricate choreotrichs accounted for a 59% of the springtime biomass. Tintinnids were rare in both seasons, although they were more abundant in spring than autumn. Microzooplankton biomass increased over 30% in spring, and was attributed to a single large tintinnid belonging to the *Tintinnopsis* Stein genus. Aloricate choreotrichid biomass did not differ between seasonally, but was greater in autumn (8.0 ± 3.1 μg C L^{-1}) relative to spring (5.0 ± 1.3 μg C L^{-1}). Despite *Mesodinium* Lohman spp. being highly abundant in both seasons, they contributed only 12.0% of the autumn microzooplankton biomass, and only a fraction (<1.5%) of the biomass in spring mid-shelf waters. Ciliate abundance was greatest in outer-shelf stations in both seasons, with *Strombidium* Claparède and Lachmann spp. accounting for 49.9% and 67.6% of the autumn and spring microzooplankton community, respectively.

4.3.3 Potential grazing rates by ciliates

Potential grazing rates (PG) varied considerably over the course of the study (median ± MAD = 28.0 ± 26.7 μg C L^{-1} d^{-1}), with median ± MAD seasonal variations in PG ranging from 9.7 ± 9.0 μg C L^{-1} d^{-1} (range = 0.2 – 160.9 μg C L^{-1} d^{-1}) in autumn and 87.8 ± 67.0 μg C L^{-1} d^{-1} (range = 0.5 – 842.7 μg C L^{-1} d^{-1}) in spring (Table 4.2, Figure

4.8). Potential grazing of nanoplankton biomass reflected ciliate abundances and was greatest along inner- and mid-shelf waters in autumn, and estuarine, inner- and outer-shelf stations in spring. Despite ciliate C_{BV} greater at mid-shelf spring stations, which was attributed to the large *Tintinnopsis* Stein, mid-shelf PG was lower than other water types due to the abundance of smaller ciliates (see Chapter II, Figure 2.10).

The ratio of PG to the percent contribution of nanoplankton productivity ($PG:PP_{nano}$) estimated potential grazing pressure consuming primary productivity by the nanoplankton community. The ratio of $PG:PP_{nano}$ exceeded 1.0 at nearly all stations, ranging from 0.1 to 68.8. Seasonal medians ranged from 3.9 + 2.4 in autumn to 6.3 $\pm$ 5.0 in spring, with ratios lowest along the inner shelf and greatest at outer shelf stations (Table 4.2). Because PG is related to the encounter rate, which is a function of prey density, and the cell-specific ingestion and clearance rates based on empirical values from the literature, ratios > 1 were not unexpected since ciliates consume cells ranging from < 1 μm to cells equivalent to their own size (Stoecker *et al*. 1984; Sherr *et al*., 1989; Dolan, 1991; Verity, 1991; Christaki *et al*., 1999), in addition to heterotrophic organisms without chlorophyll. PP_{nano} only accounted for the fraction of primary productivity attributed to nanoplankton > 5μm. However, comparison of the ratio of potential grazing to total primary productivity (PP_{TOT}), the ratios of $PG:PP_{TOT}$ ranged from 0.3 $\pm$ 0.3 in autumn to 0.7 $\pm$ 0.6 in spring, with an overall study median of 0.6 $\pm$ 0.4. This indicates that approximately 30% to > 60% of primary production potentially could be consumed daily by ciliates.

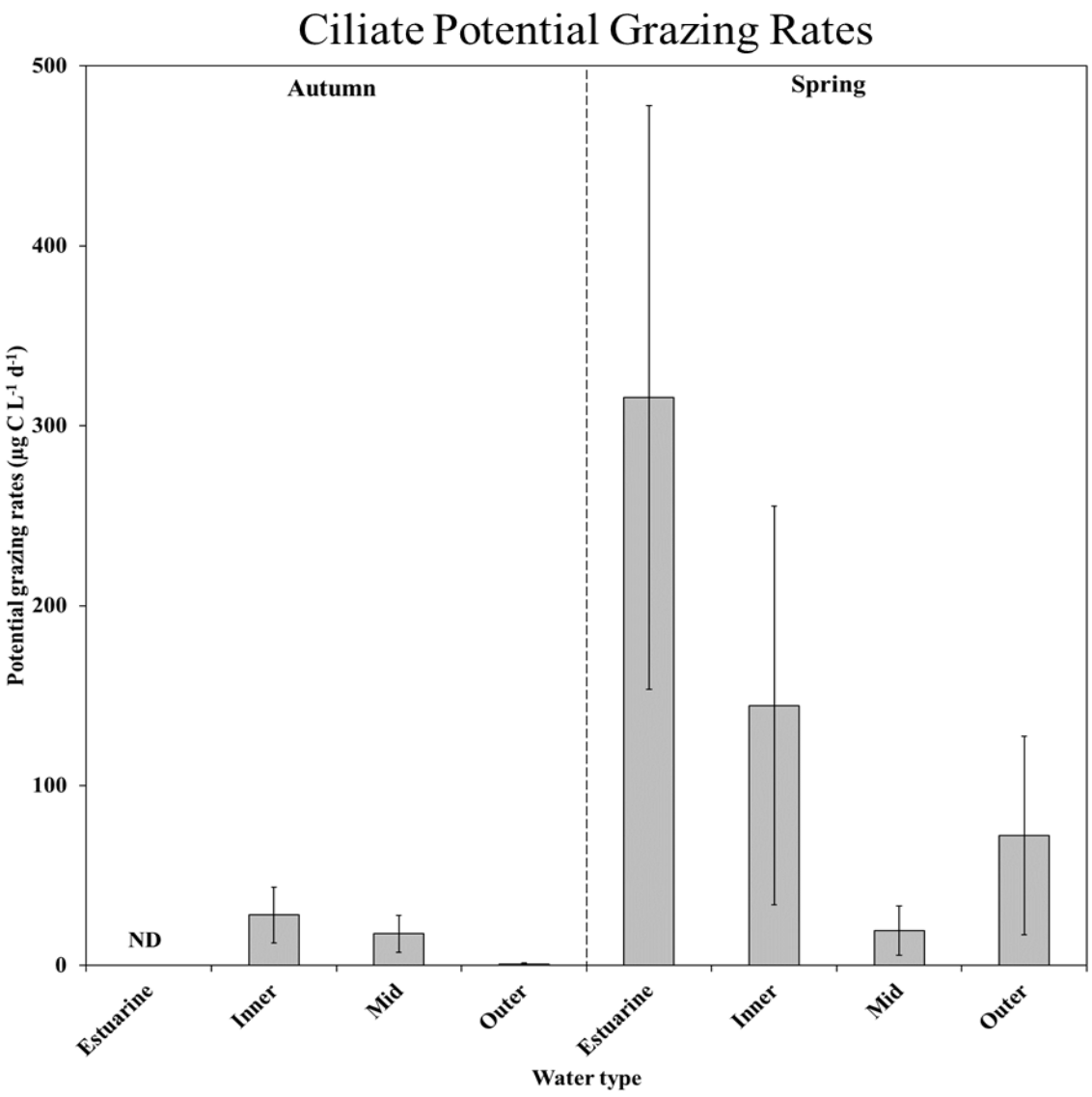

Figure 4.7 *Seasonal ciliate potential grazing rates between water types*

Median potential grazing rates within each water type are given in the bar plots, with median absolute deviation (MAD) values represented by error bars.

Table 4.2 *Potential grazing rates, biovolume-derived carbon for microplankton community, and primary productivity*

Biovolume-derived carbon (µg C L^{-1}) for nanoplankton, ciliates, and sum total microplankton community for each season and water type (ES = estuarine, IS = inner-shelf, MS = mid-shelf, OS = outer-shelf) are represented by the C_{BVnano}, $C_{BVcilitate}$, TC_{BVnano}, and $TC_{BVciliate}$, respectively. Potential grazing rates by ciliates (PG), total primary productivity from on deck size fractionated incubations (PP_{total}), primary productivity by nanoplankton (PP_{nano}), and the ratio of potential grazing by ciliates:primary productivity of nanoplankton ($PG:PP_{nano}$), where PP_{nano} was estimated as the product between PP_{total} and the percent of nanoplankton of TC_{BV} in each water type each group. The percent contribution for nanoplankton used was 20.2%, 33.7%,4.6%, for autumn and 41.6%, 30.8%, 15.0%,22.2%, for spring. Values are median + MAD, except TC_{BV}, which are sum totals. Values are given as the median ± MAD.

Season	Water-Type	$C_{BV_{nano}}$ (µg C L^{-1})	$C_{BV_{ciliate}}$ (µg C L^{-1})	$TC_{BV_{nano}}$ (µg C L^{-1})	$TC_{BV_{ciliate}}$ (µg C L^{-1})	PG (µg C L^{-1} d^{-1})	PP_{TOT} (µg C L^{-1} d^{-1})	PP_{nano} (µg C L^{-1} d^{-1})	$PG:PP_{nano}$
Autumn	IS	17.7 ± 4.9	15.1 ± 7.7	272.7	218.9	28.0 ± 15.6	79.8 ± 41.8	16.1 ± 8.4	2.9 + 2.1
	MS	15.2 ± 4.5	11.9 ± 3.8	192.1	190.2	17.6 ± 10.3	30.9 ± 10.7	10.4 ± 1.3	2.9 + 2.2
	OS	3.7 ± 1.3	7.8 ± 4.6	77.9	99.1	0.9 ± 0.5	15.5 ± 4.2	0.7 ± 0.2	12.3 ± 4.7
Spring	ES	98.9 ± 8.5	8.1± 2.1	404.7	37.9	315. 7 ± 162.2	630.8 ± 40.7	248.3 ± 16.9	1.9 ± 0.6
	IS	57.5 ± 14.9	12.2 ± 9.2	647.0	202.5	144.5 ± 110.9	94.2 ± 51.8	38.7 ± 26.0	2.7 ± 1.8
	MS	21.6 ± 7.7	5.8 ± 1.8	244.1	88.7	19.4 ± 13.8	75.2 ± 29.4	23.0 ± 3.2	3.9 ± 2.5
	OS	30.7 ± 11.3	16.0 ± 6.3	572.9	253.5	72.3 ± 55.2	45.3 ± 17.3	9.4 ± 3.5	7.8 ± 6.8

Table 4.3 *Summary of microplankton biomass compared Chl a concentrations*

Microplankton biomass was determined from biovolume-derived carbon, whereas Chl *a* concentrations were determined fluorometrically. Data were binned into two groups based on trophic state following Sherr and Sherr (2009) criteria. Values are given as the median ± MAD and range (minimum – maximum) for each water type.

Season	Water-Type	Trophic State	Chl*a* (μg L^{-1})	Phytoplankton biomass (μg C L^{-1})	Microzooplankton biomass (μg C L^{-1})	Phytoplankton:MZP biomass ratio
Autumn	IS	mesotrophic	2.5 ± 0.7	39.4 ± 7.1	17.2 ± 12.6	2.2 ± 1.5
			(1.0-3.6)	(25.6-93.6)	(3.0-52.6)	(0.7-18.5)
	MS	mesotrophic	1.7 ± 0.3	33.0 ± 19.8	11.9 ± 6.0	3.4 ± 1.9
			(1.1-2.1)	(12.6-118.8)	(2.1-38.1)	(0.9-6.1)
	OS	mesotrophic	1.0 ± 0.2	14.3 ± 4.7	7.8 ± 3.7	2.3 ± 1.0
			(0.8-1.6)	(5.0-57.4)	(1.1-123.8)	(0.5-26.7)
Spring	ES	eutrophic	9.7 ± 3.3	234.9 ± 16.7	8.1 ± 2.1	41.0 ± 17.8
			(6.8-14.3)	(214.4-460.2)	(4.4-17.3)	(12.4-61.1)
	IS	eutrophic	7.1 ± 0.8	8.0 ± 7.1	12.3 ± 8.5	8.0 ± 7.1
			(5.7-8.7)	(0.5-129.2)	(1.2-38.8)	(0.5-129.2)
	MS	mesotrophic	2.6 ± 0.5	96.2 ± 19.2	5.8 ± 1.8	17.2 ± 7.2
			(2.0-3.5)	(44.2-134.6)	(1.2-38.8)	(2.3-38.0)
	OS	mesotrophic	1.9 ± 0.9	94.9 ± 8.4	16.0 ± 11.2	6.1 ± 4.0
			(0.9-3.9)	(56.0-268.0)	(3.6-53.7)	(1.3-56.0)

Table 4.4 *Microzooplankton grazing in sub-tropical river dominated ecosystems*

Reports of microzooplankton grazing (g), phytoplankton growth (μ), and percent phytoplankton productivity grazed from other subtropical river-dominated coastal ecosystems.

Region		**g** (d^{-1})	***μ*** (d^{-1})	**Percent phytoplankton grazed**
Suwanee River Estuary, FL	Jett, 2004		-0.15 – 3.2	13.0 – 71.0 %
Pensacola Bay, FL	Murrell et al., 2002	0.51 – 0.54	1.00 – 1.02	23.0 – 56.0 %
Mobile Bay, AL	Lehrter et al., 1999	-0.03 – 2.44	-0.09 – 2.87	71.0 – 83.0 %
	Ortell and Ortmann, 2014	0.00 – 2.40	-0.60 – 2.40	79.7 – 83.0 %
Alabama Shelf	Lehrter et al., 1999	-0.09 – 2.93	0.01 – 3.45	64.0 %
	Ortell and Ortmann, 2014	-0.20 – 2.00	-0.6 – 2.40	79.7 – 83.0 %
Saint Louis Bay	McGehee and Redalje, 2016	0.00 – 0.49	0.14 – 0.93	0.0 – 37.5%
Louisiana Shelf	Strom and Strom, 1996	-0.10 – 0.67	0.53 – 2.22	40.1 $\pm$ 10.0 %
Mississippi River Plume	Lui and Dagg, 2003	0.17 – 1.82	0.42 – 2.23	71.2 $\pm$ 41.1 %
Mississippi Bight	Present study	0.38 $\pm$ 0.46	0.90 $\pm$ 0.46	48.1 $\pm$ 9.2 %

4.4 DISCUSSION

The results presented here were comparable to other studies using the seawater dilution technique to determine phytoplankton growth and microzooplankton grazing rates. While it was not the intention of the present study to compare methods to estimate grazing rates, the two methods used to determine microzooplankton herbivory on phytoplankton biomass and production provided estimates similar to each other and to literature values reported across other coastal and oceanic systems. The fraction of primary production grazed by microzooplankton ranged from 28% to 63% across all water types and was similar to estimates reported in other productive coastal ecosystems (Table 4.4). Despite decoupled rates of phytoplankton growth and grazing, protistan herbivory, particularly by ciliates, is central to controlling phytoplankton in the highly productive Mississippi Bight (MSB) region. This study also highlights the fundamental role ciliates play in making available < 20 μm phytoplankton carbon to higher level trophic communities. It was estimated that more than 60% of > 0.6 μm size fractionated primary production could potentially be grazed by ciliates in the study region.

4.4.1 Microzooplankton herbivory on phytoplankton in the Mississippi Bight

This system is not unlike other eutrophic-mesotrophic marine systems. Results from seawater dilution experiments (SWDE) indicate that microzooplankton grazing accounted for nearly half of the phytoplankton biomass and over 60% of primary production over the course of the study. Median microzooplankton grazing rates ranged from 0.5 $\pm$ 0.1 d^{-1} in autumn (n = 4) to 0.4 $\pm$ 0.1 d^{-1} in spring (n = 8) and were not different between seasons, nor were they significantly ($p \leq 0.05$) different between water

types (Table 4.1). However, phytoplankton growth rates were significantly ($p < 0.05$) greater in spring ($\mu = 1.1 \pm 0.8$ d^{-1}) than autumn ($\mu = 0.8 \pm 0.3$ d^{-1}). The ratio $g:\mu_0$ provided a first order estimate grazing control on phytoplankton production, and indicated that 53.7% ± 0.19% of the phytoplankton production was consumed daily by microzooplankton, whereas percent phytoplankton biomass (%PBG) and production (%PPG) grazed estimates were 33.9 ± 11.4 % and 48.1 + 9.2 %, respectively (Table 4.1).

In the current study, a positive slope ($g = -0.5$ d^{-1}) was observed at one of estuarine SWDE stations (Figure 4), which also resulted in a negative percent phytoplankton biomass (-60.0%) and percent phytoplankton production grazed (-213.5) % (Table 4.1). Excluding these values, the other estuarine station indicated strong decoupling between phytoplankton growth (0.9 d^{-1}) and grazing (0.3 d^{-1}) rates, with microzooplankton grazing consuming 23.7% and 40.4% of the phytoplankton biomass and production, respectively. The interpretation of positive slopes is difficult to understand, as the increasing apparent growth rate with microzooplankton predators violates one of the assumptions of the dilution technique (Ortmann *et al*., 2011; Calbet and Saiz 2013). The apparent phytoplankton growth is assumed to remain constant along the dilution gradient, while the change in biomass results solely from grazing pressure. Positive slopes resulting from dilution experiments may arise from complex interactions between external and internal nutrient pools (Landry, 1993; Calbet and Saiz, 2013), nutrient recycling by viruses or grazers (Ortmann *et al*., 2011), mixotrophy (Calbet and Saiz 2013), or experimental artefacts (e.g. self-shading, contamination of filtered seawater) (Landry *et al*., 2000).

Landry and Calbet (2004) summarized results from 788 seawater dilution experiments from 66 studies across different estuarine (including coastal bays), coastal (overlying the continental shelf), and oceanic environments. According to their literature synthesis, mean $\pm$ standard deviation phytoplankton growth and grazing mortality rates ranged from 1.0 ± 0.1 d^{-1} and 0.5 ± 0.0 d^{-1} in estuarine waters (n = 136) to 0.7 ± 0.1 d^{-1} and 0.4 ± 0.0 d^{-1} in coastal waters (n = 142), respectively. The report suggests that grazing accounted for approximately 60% of the daily primary production throughout the world's estuarine and coastal waters (Landry and Calbet, 2004). However, Dolan and McKeon (2005) suggested that these values likely were inflated due to artifacts associated with dilution experiments, and suggest that microzooplankton grazing rates are closer to < 50% of primary production. Nevertheless, these estimates are comparable to the values reported in the present study. Studies in similar subtropical river-dominated environments reported grazing impacts on phytoplankton biomass averaged 68% in the Amazon River Plume (Conroy *et al*., 2016), 64-83% within the Mobile Bay and Alabama inner shelf (Lehrter *et al*., 1999; Ortmann *et al*. 2011), 30% along the Louisiana Shelf in the northern Gulf of Mexico (Strom and Strom, 1996), 23-56% in Pensacola Bay (Murell *et al*., 2002), 17% in Saint Louis Bay estuary, MS (McGehee and Redalje, 2016), and up to 71 % in Suwanee River Estuary, FL (Jett, 2004) (Table 4.4).

In the present study, it was expected that phytoplankton growth rates would be greater in the spring relative to autumn, concomitant with inorganic nutrient concentrations following increased river discharge in spring. Phytoplankton growth rates are a function of physiological conditions (e.g. photophysiology, internal nutrient pools)

of the prevailing phytoplankton community (Falkowski and Raven, 2007). While light conditions were not quantified in this study, nutrient limitation in SWDE was inferred by examining the ratio of μ_0:μ, where a ratio < 1 indicates the potential nutrient limitation. The potential for nutrient limitation was apparent only along the mid-shelf station in autumn, whereas nearly all stations exhibited $\mu_0 < \mu$ in spring. Comparisons of ambient nutrient concentrations with those concentrations likely to limit nutrient uptake were addressed previously in Chapter II. These ratios indicated that DIN was limiting in autumn at all stations, whereas in spring PO_4^{3-} was limiting along the inner shelf waters and $Si(OH)_4$ was limiting at mid and outer shelf stations. Hydrographic and biogeochemical settings were considerably different seasonally, and were the primary drivers associated with the phytoplankton community shifting from predominantly nanoplankton in autumn to a nanoplankton and > 20μm diatom-dominated community in spring. This likely was reflected in the phytoplankton growth rates, as diatoms often have higher growth rates under nutrient replete conditions and can outcompete other phytoplankton groups (Banse, 1982; Strom and Strom, 1996). Moreover, the apparent phytoplankton growth (k_0) was nutrient limited in spring, and the addition of inorganic nutrients may have stimulated growth rates in observed in spring SWDE (Table 4.1). Strom and Strom (1996) reported increased growth rates of large phytoplankton (i.e. diatoms) following nutrient additions to seawater dilution experiments. They suggested that this was due to the fact that diatoms are ubiquitous along continental shelves and have a high growth rate potential following nutrient inputs (Strom and Strom, 1996). Results from the dilution experiments indicated that phytoplankton intrinsic growth (μ)

was greater than microzooplankton in both seasons, particularly in spring (Table 4.1, Figure 4.7). This could result from either nutrient-enhanced phytoplankton growth rates, shifts in the phytoplankton community structure, top-down predation of mesozooplankton on microzooplankton (Calbet and Saiz, 2015), or a combination of any of these.

While microzooplankton grazing rates were not statistically different ($p < 0.05$) between water types in either season, phytoplankton growth rates were up to three times greater in outer-shelf waters relative to estuarine and inner-shelf waters (Table 4.1). This may be attributed to a combination of environmental (e.g. increased light availability for photosynthesis) and ecological (e.g. phytoplankton community structure, reduced grazing pressure) conditions in offshore waters relative to estuarine and inner-shelf waters. Moreover, like the seawater dilution experiments, increased river discharge dilutes coastal shelf waters and influences predator-prey encounter ratios. The impact of microzooplankton grazing on phytoplankton biomass varied seasonally and spatially, with grazing rates accounting for ~34% and 48% of the phytoplankton biomass and primary production over the course of the study, respectively. Lehrter *et al*. (1999) also reported a cross-shelf increase in phytoplankton growth rates and decrease in microzooplankton grazing concomitant with increasing salinity, where highest percent production grazed was observed in the Mobile Bay (83%) and lowest estimates (63%) approximately 10 km offshore from the mouth of the bay. They observed that coupling was strongest within the turbid bay, where growth rates were reduced due to low light levels and where saturated feeding responses (i.e. grazing rates) were greatest (Lehrter *et al*., 1999). The opposite pattern was observed by Ortmann *et al*. (2011), where

phytoplantkon growth and mortality were tightly coupled along the Alabama shelf and decoupled within the bay. Results from the present study showed that phytoplankton growth and grazing were tightly coupled in estuarine waters, but decoupling was greatest within inner shelf waters and decreased across the shelf.

Coupling between phytoplankton growth and microzooplankton herbivory in productive ecosystems tends to fluctuate with environmental conditions, whereas in tightly coupled systems (e.g. subarctic Pacific, ocean gyres), there tends to be a linear response in microzooplankton grazing with any changes in phytoplankton biomass (Landry *et al*. 1995; Strom 2002). This pattern reflects the physical and biogeochemical dynamics structuring planktonic communities: static environments (i.e. "semi-closed" systems) tend to be tightly coupled, whereas dynamic ecosystems (i.e. "open" systems) are characteristically variable, having locally high gradients in hydrology and biogeochemistry. Microzooplankton protists have growth rates similar to phytoplankton (Sherr and Sherr, 1994), and as a result, they are able to maintain control on phytoplantkon biomass, particularly in tightly coupled "closed systems." In river-dominated coastal environments, pulsed nutrient loading and biogeochemical variability drive phytoplankton community dynamics. Invariably, these drivers structure the microzooplankton community. The microzooplankton grazing rates along the river-dominated coastal shelf of the northern Gulf of Mexico did not differ between two hydrographically and biogeochemically disparate regimes. Regression slopes of phytoplankton growth along the dilution gradient, an indication of phytoplankton mortality due to grazing (g), were not significantly different from zero ($p < 0.05$) in most

cases and saturated feeding kinetics was observed in at least one experiment (Figure 4.4), but likely occurred more frequently, as indicated by multiple insignificant regression slopes. These patterns suggest that microzooplankton grazing was saturated due to elevated concentration of phytoplankton biomass and productivity present throughout the study. As grazing approaches saturation, phytoplankton biomass begins to decouple from microzooplankton. Thus, decoupling is driven primarily by shifts in phytoplankton growth rates, which are a function of community dynamics and prevailing environmental conditions. Lui and Dagg (2003) observed similar patterns in the meso-eutrophic Mississippi River plume, where saturated grazing was observed on nano- and microphytoplankton, but not in the ultraphytoplankton size fraction. They attributed this to microzooplankton efficiently consuming <5 μm size fraction, thereby preventing accumulation of ultraphytoplankton biomass (Lui and Dagg, 2003).

4.4.2 Grazing potential of ciliates on phytoplankton productivity

The current study also estimated the potential grazing rates (PG) by ciliates on size fractionated phytoplankton productivity. Primary productivity for >5 μm size fraction was significantly correlated (Spearman's r, $p \leq 0.05$, Appendix F) to nanoplankton and diatom biomass, whereas microzooplankton biomass were significantly correlated ($p \leq 0.05$) to productivity in the 0.6-5 μm (ultraphytoplankton) size fraction over the course of the study (see Chapter III). Estimates of nanoplankton contribution to primary productivity (PP_{nano}) indicated that this group was an important component to the >5 μm size fraction of primary producers. However, the ratio of $PG:PP_{nano}$ was > 1 at all stations, which suggests that ciliates could potentially consume significantly more

nanoplankton based on > 5 μm size-fraction primary productivity alone. Results from Chapter III showed that primary productivity differed seasonally and between size fractions, with the > 5 μm size fractions significantly greater than 0.6-5μm size fraction, yet productivity normalized to Chl *a* (P^B) was not different between size fractions or between seasons (Table 3.2, Chapter III). It was concluded that herbivory was an important control on ultraphytoplankon (0.6-5 μm) fraction. The ratio between PG and the productivity of the total phytoplankton > 0.6 μm community (PP_{TOT}) indicated that more than 60% of primary production could potentially be consumed daily by ciliates. Pico- and ultraphytoplankton had production rates similar to microphytoplankton on a Chl *a* -normalized basis, and thus, phytoplankton within these size groups appear to play a disproportionately greater role as prey items for ciliates in this system.

Previous studies have described trophic interactions of ciliates in coastal and estuarine systems. In Roskilde Fjord estuary ciliate seasonal average percent biomass herbivory ranging from 9 % to > 55% on picoeukaryotes and nanoplankton biomass, while the seasonal averages of biomass potentially consumed ranged from 2.1 – 22.6 μg C L^{-1} d^{-1} (Haraguchi *et al*., 2018). Median ciliate potential grazing rates in the present study was 28.0 $\pm$ 26.7 μg C L^{-1} d^{-1} and were well within the 95% confidence intervals to those reported by Haraguchi *et al*. (2018). Ciliates in the South Slough estuary, Oregon significantly impacted total phytoplankton assemblage when nanoplankton dominated the >5 μm phytoplankton biomass (Cowlishaw, 2002). Strom *et al*. (2007) reported that nearly 100% of nanophytoplankton were consumed by microzooplankton in the Gulf of Alaska and Prince William Sound. The study estimated that ciliates accounted for 13.4 %

(1.3 – 11.0 μg C L^{-1}) of the microzooplankton (ciliates + heterotrophic dinoflagellates) biomass, values similar to those reported in the present study (Table 4.4). Microzooplankton grazing rates on < 20 μm phytoplankton along the Louisiana Shelf also have shown that ciliates are an important pathway for phytoplankton biomass in hydrographically complex coastal waters. Strom and Strom (1996) found that microzooplankton grazing on nanophytoplantkon communities was highly variable, accounting for 10% to >100% of daily production, and indicated that ciliates comprised about half of the microzooplankton community biomass. Previous studies in the same region reported that microzooplankton exclusively grazed on nanophytoplantkon, accounting for nearly 100% of the phytoplankton daily standing stock (Fahnenstiel *et al*. 1995).

Ciliates are not always the main grazers in productive ecosystems. In fact, studies have shown that heterotrophic dinoflagellates, particularly gymnodinoid genera, have clearance rates as great as ciliates, potentially consuming upwards of 50% of the autotrophic biomass in productive waters (e.g. Neuer and Cowles, 1995; Strom and Strom, 1996; Archer *et al*., 1996; Stelfox-Widdicombe *et al*., 2004; Jeong *et al*., 2005a, 2005b; Saito *et al*., 2006; Sherr and Sherr, 2007; Calbet, 2008). Although the present study did not quantify trophic strategies of dinoflagellates, the predominace of athecate (e.g. *Gyrodinium* Kofoid and Swezy spp.) and thecate (e.g. *Protoperidinium* Bergh spp.) Gymnodinoids suggests that these groups likely were contributing to the microzooplankton biomass (Figure 4.10). Biomass values for dinoflagellates and ciliates were similar to those observed in other productive marine systems, such as coastal

upwelling (Neuer and Cowles 1994, Vargas *et al*., 2007), polar (Levinsen *et al*., 1999, Sherr and Sherr 2007), sub-Arctic (Howell-Kubler *et al*., 1996, Sherr and Sherr 2007), and river-dominated shelf ecosystems (Strom and Strom 1996, Tsai *et al*., 2008). Sherr and Sherr (2007) also suggest that heterotrophic dinoflagellates are important groups contributing to the microzooplankton biomass. In their review of productive systems, they show that both thecate and athecate forms of dinoflagellates comprise more than one half of the microzooplankton biomass, particularly in association with diatom blooms (Sherr and Sherr 2007). They suggest that most of these heterotrophic dinoflagellates, which are mostly gymnodinoid species, are associated with elevated concentrations of Chl *a*. Sherr and Sherr (2007) discussed anecdotal evidence for the presence of heterotrophic dinoflagellates under conditions of high Chl *a*, particularly during coastal diatom blooms. Microzooplankton biomass ranged nearly two orders of magnitude (0.1 to 109 μg C L^{-1}) in the Bering Sea under bloom and non-bloom conditions, of which *Strombidium, Strombilidium,* and *Laboea* were the predominant ciliates, and thecate and athecate dinoflagellates. A similar correlation (Spearman's r, $p \leq 0.05$, Tables F.3, F.5) was observed in the current study, in which the relationship between phytoplankton biomass (i.e. Chl *a*) and flagellate biomass (i.e. C_{BVflag}) were significantly correlated ($p \leq 0.05$) to one another. Given the predominance of athecate and thecate gymnodinoid dinoflagellates as contributors to the overall flagellate biomass, coupled with the significant correlations to Chl *a*, dinoflagellates could play an equally important, if not greater role than ciliates, as the primary herbivores of ultra-, pico-, nano-, and microphytoplankton in the MSB system, and this should be examined in future work.

4.5 CONCLUSION

The results presented in this study highlight the important role that microzooplankton grazing play in structuring the planktonic food web within the river-dominated continental shelf waters of the northern Gulf of Mexico. The impact of microzooplankton grazing on phytoplankton growth and carbon cycling in this system is similar to other marine systems (Calbet and Landry, 2004). Microzooplankton grazing accounted for 29-59% of phytoplankton biomass and 30-63% of the daily primary production. Despite decoupled growth and saturated grazing determined by the seawater dilution experiments, ciliates imposed significant grazing impacts on ultra- and nanoplankton, consuming potentially > 60% of daily primary production of this size fraction. Comparison of Chl *a* to microzooplankton biomass (see Sherr and Sherr, 2007) suggests that heterotrophic dinoflagellates likely play an equally important role as that of microzooplankton in this food web. Trophic pathways of phytoplankton production in this system depends on the direct interplay between nutrient inputs structuring phytoplankton communities (i.e. composition, body size, nutritional composition) and energy efficiency at each trophic transfer (First *et al*., 2009). Carbon movement through system needs to be better understood, particularly among protists. Future studies should quantify the role heterotrophic dinoflagellates play as consumers of phytoplankton biomass, particularly of pico- and ultraplankton groups, in addition to mixotrophic plasticity and what environmental conditions drive this variability among protists.

CHAPTER V – GENERAL SUMMARY AND CONCLUSIONS

A key objective of ocean ecology is the understanding of processes and patterns of marine organisms across broad scales and gradients involving space and time (Banse, 2002). Variability in physical and biogeochemical processes shapes microplankton communites and trophic interactions, which ultimately helps structure higher-order trophic levels through time and space (Margalef, 1978; Smayda, 1980). Primary producers reflect immediate (<1 day) changes in physical and biogeochemical pressures in the environment. The ecological niches associated with the rapid succession of these communites can alter secondary production, which invariably can affect higher trophic levels throughout the food web. Therefore, understanding what mechanisms are currently influencing microplantkon communitity variability and energy transfer through the different trophic levels is critical to perceiving changes that occur in the future. Prior to this study, much of the research focusing on phytoplankton community structure, primary productivity, growth and mortality due to micrzooplankton grazing were focused on the Louisiana and Texas shelf, and along the west Florida shelf. This dissertation fills a gap in our understanding of the microplanktonic trophic dynamics in the ecologically and economically vital MSB. Specifically, it identifies buoyant river plumes as the primary mechanism driving protist variability across spatial and temporal scales in this system.

Observations presented in this dissertation show that the river-dominated MSB is a highly dynamic ecosystem driven largely by river discharge. Biological productivity in the MSB is driven by the spring freshet. High river discharge supplies abundant inorganic nutrients, which stimulates phytoplankton (mostly diatoms and nanophytoplankton)

growth and biomass. During this time, phytoplankton growth decouples from microzooplankton grazing pressure and autrophic biomass accumulates. Microzooplankton grazing rates do not increase presumably because food is plentiful. The floating bounty of microplanktonic biomass likely serves as food sources for larger zooplankton and ichthyoplankton. For instance, the timing of many larval fish (e.g. menhaden) moving inshore to grow follows this proliferation of microplankton. The cycle of river discharge and the subsequent patterns of phytoplankton productivity and growth drive the biological productivity in this system. Further, stable buoyant freshwater plumes during the spring freshet can act as a barrier for surface offshore waters to come into the MSB up to 60km across the shelf. These freshwater plumes increase water column stratification, which further enhances advection of saline offshore waters via an estuarine circulation dynamic. Will this layered system further exacerbate hypoxia in the region? The magnitude and importance of these possible impacts under these exceptional conditions are presently unknown.

High discharge events are analogous to upwelling systems, in which nutrient-rich waters stimulate phytoplankton growth and biomass accumulates. However, unlike many upwelling systems where iron limitation could be changing Si:N ratio of source waters, river dominated shelf margins like the MSR-influenced Lousisana shelf are becoming Si-limited as N pollution becomes more widespread throughout many river watersheds (Parsons *et al.*, 2002; Bargu *et al.*, 2016). This has profound impacts on the biogeochemistry, which greatly influences the food web structure in these systems. The MSB appears to be experiencing similar eutrophication processes and increased potential

for recurrent HABs and hypoxia. This is apparent through the shift in phytoplankton community structure in which the diatom community transitioned from a diverse mixed assemblage under low river discharge and DIN-limited conditions to a community dominated by lightly-silicified and potentially toxic *Pseudo-nitzschia* and gymnodinoid dinoflagellate species under elevated river discharge, high DIN and Si-limiting conditions. This presents a few questions and challenges. For example, if toxic species of *Pseudo-nitzschia* are proliferating throughout the region, why is there not widespread toxicosis from domic acid (DA) in fish, birds, and mammals? Does the presence of dissolved organic matter (DOM), lignins, tannins from the local rivers influence DA persistence in these waters, unlike those of the west coast that are relatively low in DOM?

While sea level rise will likely influence Mississippi River discharge patterns impacting the nGOM over the long term, more immediate shifts in precipitation patterns throughout the MSR and local river watersheds will influence the spatial and temporal distribution of low salinity waters in the MSB. Increased river discharge and flood control diversions (e.g. BCS) will likely have a broader distribution and persistent low salinity surface waters throughout the region. For example, the BCS has been opened four out of the last five years, with only 10 prior openings since it was built in 1937. The 2019 opening marked the first time the spillway was opened twice in the same year, with combined openings equivalent to the largest freshwater diversion into Lake Pontchartrain (Army Corps of Engineers, 2019). This large pulse of N-rich MSR freshwater initiated widespread noxious cyanobacteria (*Dolichospermum* sp. and *Microcystis* sp.) blooms that persisted for several weeks along coastal Mississippi (Mississippi Department of Marine

Resources, 2019). This prompted the closure of beaches and recreational activities during the summer tourist season, which greatly impacted local and state economies. Although cyanobacteria-induced toxicosis to marine life was not observed, over 130 dolphins and 154 sea turtles were found dead along the beaches and marshes, and was attribitued to prolonged exposure to low salinity water (Institute of Marine Mammal Studies, 2019). The freshwater diversion also reduced commercial blue crab and shrimp landings to 25% and 40% of the five year average, respectively, and it caused >90% mortality of oyster reefs in coastal Mississippi and Louisiana (Mississippi Department of Marine Resources, 2019). Are these new discharge patterns indicative of a new paradigm? Climate change will influence precipitation patterns throughout the MSR and local river watersheds. Can we expect more frequent freshwater diversions impacting the MSB? Will increased N loading further drive Si-limited conditions in this system? If so, will these conditions shift the phytoplankton community from a diatom-dominated to one dominated by dinoflagellates or recurrent, noxious cyanobacteria blooms? Besides causing HABs, cyanobacteria are poor food sources for meso- and ichthyoplankton (Anderson *et al.*, 2008). How will this impact fisheries yields such as menhaden? It is uncertain how a shift to Si-limiting ultimately will impact nutrient cycling, fisheries yields, or the formation of HABs in this system, but ecological models can use the data from this body of research to assess multiple scenarios and potential consequences.

River discharge clearly is an important process for the transport and delivery of inorganic nutrients, dissolved organic matter, and particulate material to the MSB. The influence of the prevailing hydrographic conditions, coupled with biogeochemical

processes, structures microplanktonic communities and subsequent trophic interactions in this system. The MSB is experiencing significant environmental stressors that are selecting for eutrophication processes, particularly HABs. The MSB needs a long-term plankton monitoring system to serve as an advanced warning to HABs, as well as to observe the ecological changes driven by anthropogenic modifications and natural variability. It is recommended that a monitoring strategy to aid in the prevention and help mitigate the losses that occur from HABs. Such a strategy will provide information on the initiation of HABs occurring in the MSB and the potential ecological impacts affecting biological communiteis in the region. Imaging technologies, coupled with MBFG trait-based approaches, *in situ* physico-chemical measurements, and satellite derived products can provide a comprehensive temporal and spatial assessment of microplankton community dynamics.The data can then be assimilated into high resolution biophysical models to provide near-real time information and forecast trajectories of HABs. This will enable resource managers and public health officials to make informed decisions protecting human well-being and environmental health. To date, the combination of *in situ* biogeochemical measuments, real-time imaging and satellite remote sensing has not been implemented in Mississippi as part of a strategic plan to observe and mitigate potential HABs occurring in this region. Finally, improved understanding of the role mixotrophy plays in the carbon trophic transfer will be of paramount importance as biogeochemical models begin to incorporate trait-based approaches. These are a diverse, yet enigmatic group of protists that likely have significant impacts on the energy flow and ecosystem function in this system. In closing, it is importatnt to understand that

ecosystem resiliency is measured not by the degree to which communities are stable, but rather it is a continuum of the dynamic adaptability of its constituents.This dissertation provided a framework to better understand and predict ecosystem variablilty within the context of environmental forcing: processes which ultimately affect energy flows throughout marine food webs.

APPENDIX A– ENVIRONMENTAL DATA

Table A.1 Environmental Data for Autumn 2015

Date (ddmmmyy)	**Water Type**	**Station ID**	**LON** (dd)	**LAT** (dd)	**Sample Depth** (m)	**Bottom Depth** (m)	**T** (^{o}C)	**S** (PSU)	**PAR** (mol photon m^{-2} d^{-1})
29-Oct-15	IS	W4	-88.607	30.094	1.3	17.0	23.6	33.5	32.9
2-Nov-15	IS	WM6	-88.459	30.161	1.4	10.0	23.6	33.8	27.0
3-Nov-15	IS	W10	-88.609	29.968	1.0	24.0	24	34.5	25.9
3-Nov-15	IS	W11	-88.608	30.045	1.2	22.0	23.8	34.1	25.9
3-Nov-15	IS	G1	-88.817	30.138	1.0	15.0	23.4	34.1	25.9
30-Oct-15	IS	M5	-88.126	30.127	0.9	18.0	23.9	33.6	31.4
31-Oct-15	IS	M10	-88.126	30.100	1.3	15.8	24.2	33.9	34.4
1-Nov-15	IS	MBP4	-88.030	30.139	0.9	18.0	23.9	34.4	32.0
2-Nov-15	IS	WM3	-88.133	30.179	1.2	11.0	23.7	33.6	27.0
2-Nov-15	IS	WM4	-88.235	30.194	0.9	16.0	23.3	32.2	27.0
2-Nov-15	IS	WM5	-88.343	30.174	1.5	11.0	23.7	33.8	27.0
1-Nov-15	IS	E5	-87.530	30.192	1.6	13.0	24.2	34.5	32.0
1-Nov-15	IS	ME3	-87.734	30.159	1.6	9.0	24.1	34.5	32.0
29-Oct-15	MS	W1	-88.603	29.599	1.2	24.0	24.4	34.6	32.9
29-Oct-15	MS	W2	-88.608	29.726	1.3	26.0	24.1	34.4	32.9
29-Oct-15	MS	W3	-88.604	29.854	1.2	21.0	23.9	34.2	32.9
2-Nov-15	MS	W7	-88.607	29.617	1.8	21.0	24.7	35.1	27.0
3-Nov-15	MS	W8	-88.609	29.800	1.3	24.0	24.4	34.9	25.9
3-Nov-15	MS	W9	-88.608	29.884	1.3	24.0	24.3	34.8	25.9
30-Oct-15	MS	M4	-88.125	30.053	1.0	22.6	24.2	35.3	31.4

Table A.1 (continued)

Date (ddmmmyy)	Water Type	Station ID	LON (dd)	LAT (dd)	Sample Depth (m)	Bottom Depth (m)	T (ºC)	S (PSU)	PAR (mol photon m^{-2} d^{-1})
31-Oct-15	MS	M9	-88.126	29.996	1.3	23.0	24.2	34.8	34.4
1-Nov-15	MS	E2	-87.532	29.834	2.0	36.0	24.9	35	32.0
1-Nov-15	MS	E3	-87.530	30.000	1.6	20.0	24.4	34.7	32.0
1-Nov-15	MS	E4	-87.530	30.099	1.5	20.5	24.5	34.8	32.0
5-Nov-15	MS	A7	-88.976	29.334	1.5	16.0	23.9	33.8	34.7
29-Oct-15	OS	M1	-88.123	29.717	1.5	36.0	25.5	35.5	32.9
30-Oct-15	OS	M2	-88.122	29.886	1.2	36.0	25.1	35.3	31.4
30-Oct-15	OS	M6	-88.135	29.434	1.2	47.8	25.5	35.5	31.4
31-Oct-15	OS	M7	-88.127	29.597	1.5	37.0	25.5	35.5	34.4
31-Oct-15	OS	M8	-88.124	29.794	1.5	32.5	25.1	35.3	34.4
2-Nov-15	OS	M11	-88.129	29.851	1.4	36.0	24.9	35.2	27.0
31-Oct-15	OS	E1	-87.535	29.666	2.8	46.0	25	35.3	34.4
4-Nov-15	OS	A5_1	-88.742	29.413	1.1	38.0	25	35.4	36.0
4-Nov-15	OS	A1_1	-88.763	29.345	1.1	48.0	25.1	35.4	36.0
4-Nov-15	OS	A2_1	-88.802	29.259	1.2	50.0	25	35.4	36.0
4-Nov-15	OS	A6_1	-88.649	29.349	1.6	56.0	25.5	35.5	36.0
5-Nov-15	OS	A1_2	-88.766	29.343	1.2	49.0	25.3	35.5	34.7
5-Nov-15	OS	A9	-88.841	29.477	1.2	11.5	25.1	35.1	34.7

Table A.1 (continued).

Date (ddmmmyy)	Water Type	Station ID	LON (dd)	LAT (dd)	NO_2^- (µM)	NO_3^- (µM)	NH_4^+ (µM)	PO_4^{3-} (µM)	$Si(OH)_4$ (µM)
29-Oct-15	IS	W4	-88.607	30.094	0.1	0.1	--	0.4	9.0
2-Nov-15	IS	WM6	-88.459	30.161	0.1	0.5	0.7	0.3	7.4
3-Nov-15	IS	W10	-88.609	29.968	0.1	0.8	0.2	0.2	5.6
3-Nov-15	IS	W11	-88.608	30.045	0.1	0.8	0.4	0.3	6.4
3-Nov-15	IS	G1	-88.817	30.138	0.0	0.3	0.0	0.2	2.3
30-Oct-15	IS	M5	-88.126	30.127	0.1	0.2	--	0.3	6.1
31-Oct-15	IS	M10	-88.126	30.100	0.1	0.2	--	0.4	5.9
1-Nov-15	IS	MBP4	-88.030	30.139	0.1	0.1	--	0.3	3.8
2-Nov-15	IS	WM3	-88.133	30.179	0.1	0.1	--	0.4	5.0
2-Nov-15	IS	WM4	-88.235	30.194	0.1	0.3	0.7	0.3	7.5
2-Nov-15	IS	WM5	-88.343	30.174	0.1	0.8	0.5	0.3	7.3
1-Nov-15	IS	E5	-87.530	30.192	0.1	0.1	--	0.3	3.4
1-Nov-15	IS	ME3	-87.734	30.159	0.0	0.2	--	0.3	3.7
29-Oct-15	MS	W1	-88.603	29.599	0.0	--	--	0.4	5.4
29-Oct-15	MS	W2	-88.608	29.726	0.1	0.0	--	0.3	4.4
29-Oct-15	MS	W3	-88.604	29.854	0.0	0.1	--	0.4	6.3
2-Nov-15	MS	W7	-88.607	29.617	0.0	0.7	0.0	0.3	4.1
3-Nov-15	MS	W8	-88.609	29.800	0.2	0.8	0.6	0.3	6.1
3-Nov-15	MS	W9	-88.608	29.884	0.1	0.6	0.3	0.3	4.3
30-Oct-15	MS	M4	-88.125	30.053	0.1	--	--	0.3	4.4

Table A.1 (continued).

Date (ddmmmyy)	Water Type	Station ID	LON (dd)	LAT (dd)	NO_2^- (µM)	NO_3^- (µM)	NH_4^+ (µM)	PO_4^{3-} (µM)	$Si(OH)_4$ (µM)
31-Oct-15	MS	M9	-88.126	29.996	0.1	0.1	--	0.4	4.0
1-Nov-15	MS	E2	-87.532	29.834	0.1	0.1	--	0.4	3.8
1-Nov-15	MS	E3	-87.530	30.000	0.0	0.1	--	0.4	5.9
1-Nov-15	MS	E4	-87.530	30.099	0.0	0.0	--	0.4	4.6
5-Nov-15	MS	A7	-88.976	29.334	0.1	0.4	0.3	0.3	7.9
29-Oct-15	OS	M1	-88.123	29.717	0.0	0.1	--	0.3	2.2
30-Oct-15	OS	M2	-88.122	29.886	0.0	0.0	--	0.3	3.2
30-Oct-15	OS	M6	-88.135	29.434	0.0	--	--	0.3	2.3
31-Oct-15	OS	M7	-88.127	29.597	0.0	0.1	--	0.3	2.4
31-Oct-15	OS	M8	-88.124	29.794	0.0	0.1	--	0.3	2.7
2-Nov-15	OS	M11	-88.129	29.851	--	--	--	--	--
31-Oct-15	OS	E1	-87.535	29.666	0.1	0.5	0.2	0.2	2.7
4-Nov-15	OS	A5_1	-88.742	29.413	0.0	0.8	0.3	0.2	2.2
4-Nov-15	OS	A1_1	-88.763	29.345	0.1	0.4	0.4	0.3	1.9
4-Nov-15	OS	A2_1	-88.802	29.259	0.1	0.8	0.5	0.2	2.3
4-Nov-15	OS	A6_1	-88.649	29.349	0.1	1.3	0.2	0.2	2.3
5-Nov-15	OS	A1_2	-88.766	29.343	0.1	0.6	0.4	0.4	2.4
5-Nov-15	OS	A9	-88.841	29.477	--	1.0	0.1	0.2	4.7

Table A.2 Environmental Data for Spring 2016

Date (ddmmmyy)	**Water Type**	**Station ID**	**LON** (dd)	**LAT** (dd)	**Sample Depth** (m)	**Bottom Depth** (m)	**T** (^{o}C)	**S** (PSU)	**PAR** (mol photon m^{-2} d^{-1})
5-Apr-16	ES	WM1S	-88.137	30.195	2.3	9.0	19.9	21.4	46.8
5-Apr-16	ES	WM3S	-88.130	30.179	2.4	9.5	19.5	19.7	46.8
8-Apr-16	ES	MOOR2S_2	-88.088	30.182	1.8	8.0	20.2	20.9	48.3
9-Apr-16	ES	MOOR2S_3	-88.076	30.183	1.6	8.0	17.4	20.4	44.1
2-Apr-16	IS	W2S	-88.610	29.723	2.4	21.7	21.1	23.0	45.6
2-Apr-16	IS	W3S	-88.606	29.851	2.9	20.0	20.9	17.8	45.6
2-Apr-16	IS	W10S	-88.613	29.967	3.2	21.5	20.4	23.3	45.6
5-Apr-16	IS	M3S_2	-88.122	29.971	2.2	26.0	19.9	24.7	46.8
5-Apr-16	IS	M4S_2	-88.122	30.054	1.9	19.0	20.3	24.3	46.8
5-Apr-16	IS	M5S_2	-88.123	30.125	2.9	13.0	20.1	23.9	46.8
8-Apr-16	IS	WM1S_2	-88.138	30.196	1.7	12.0	20.4	26.2	48.3
8-Apr-16	IS	MBP3S_4	-88.030	30.114	2.7	18.0	21.3	24.8	48.3
9-Apr-16	IS	MBP1S_3	-88.033	30.159	2.3	11.0	20.3	24.4	44.1
7-Apr-16	IS	MBP3S_2	-88.028	30.115	2.2	16.0	21.2	23.3	47.9
3-Apr-16	MS	MOOR6S	-88.121	29.974	2.6	24.9	20.1	33.0	47.2
3-Apr-16	MS	MOOR4S	-88.117	30.121	2.4	15.4	19.6	28.4	47.2
3-Apr-16	MS	MBP2S	-88.037	30.054	2.1	22.0	19.6	29.8	47.2
3-Apr-16	MS	MBP3S	-88.031	30.110	2.4	16.0	19.6	28.4	47.2
31-Mar-16	MS	E3S	-87.530	30.000	3.4	22.0	19.8	32.8	11.7
31-Mar-16	MS	E4S	-87.530	30.098	2.0	22.4	19.9	32.2	11.7

Table A.2 (continued)

Date (ddmmmyy)	Water Type	Station ID	LON (dd)	LAT (dd)	Sample Depth (m)	Bottom Depth (m)	T (°C)	S (PSU)	PAR (mol photon m^{-2} d^{-1})
31-Mar-16	MS	E5S	-87.533	30.195	2.5	12.0	19.7	31.0	11.7
4-Apr-16	MS	E10S	-87.520	30.049	1.8	23.5	19.6	32.1	47.7
4-Apr-16	MS	E11S	-87.521	30.169	1.9	20.0	19.3	30.6	47.7
1-Apr-16	OS	W7S	-88.609	29.618	3.1	21.0	20.7	29.0	3.9
31-Mar-16	OS	M12S	-88.126	29.721	2.5	32.0	20.6	33.5	11.7
1-Apr-16	OS	M8S	-88.122	29.886	3.2	31.0	21.0	31.2	3.9
1-Apr-16	OS	M2S	-88.122	29.885	2.5	35.0	21.1	29.2	3.9
1-Apr-16	OS	M3S	-88.124	29.969	2.1	21.1	20.9	28.7	3.9
1-Apr-16	OS	M4S	-88.127	30.051	2.5	18.2	20.6	28.3	3.9
2-Apr-16	OS	M14S	-88.126	29.679	2.4	33.7	20.3	33.2	45.6
3-Apr-16	OS	M11S	-88.125	29.848	2.9	36.0	20.2	32.9	47.2
30-Mar-16	OS	E6S	-87.534	29.795	3.0	35.2	19.9	33.2	12.7
31-Mar-16	OS	E7S	-87.531	29.901	2.3	31.2	19.7	32.5	11.7
3-Apr-16	OS	E8S	-87.527	29.739	2.2	34.5	20.4	33.1	47.2
4-Apr-16	OS	E2S	-87.530	29.833	2.4	35.0	20.4	33.0	47.7
4-Apr-16	OS	E9S	-87.523	29.945	2.2	35.0	19.8	32.0	47.7
6-Apr-16	OS	P1S	-88.086	29.771	1.9	32.0	20.5	29.4	28.4
6-Apr-16	OS	P2S	-88.130	29.801	1.8	30.0	20.9	29.6	28.4
7-Apr-16	OS	P3S	-88.090	29.726	2.1	30.0	20.4	30.9	47.9
7-Apr-16	OS	P9S	-88.086	29.723	2.0	36.0	20.3	30.0	47.9

Table A.2 (continued).

Date (ddmmmyy)	Water Type	Station ID	LON (dd)	LAT (dd)	NO_2^- (µM)	NO_3^- (µM)	NH_4^+ (µM)	PO_4^{3-} (µM)	$Si(OH)_4$ (µM)
5-Apr-16	ES	WM1S	-88.137	30.195	1.0	2.9	0.6	0.2	31.5
5-Apr-16	ES	WM3S	-88.130	30.179	0.5	1.7	0.7	0.2	28.2
8-Apr-16	ES	MOOR2S_2	-88.088	30.182	0.2	1.1	0.4	0.2	28.6
9-Apr-16	ES	MOOR2S_3	-88.076	30.183	0.4	2.9	0.9	0.2	45.3
2-Apr-16	IS	W2S	-88.610	29.723	0.3	1.3	0.0	0.2	5.5
2-Apr-16	IS	W3S	-88.606	29.851	0.2	0.5	1.2	0.0	24.8
2-Apr-16	IS	W10S	-88.613	29.967	--	--	--	--	--
5-Apr-16	IS	M3S_2	-88.122	29.971	0.1	0.2	0.6	0.2	9.7
5-Apr-16	IS	M4S_2	-88.122	30.054	--	--	--	--	--
5-Apr-16	IS	M5S_2	-88.123	30.125	0.0	0.1	0.7	0.2	9.9
8-Apr-16	IS	WM1S_2	-88.138	30.196	--	--	--	--	--
8-Apr-16	IS	MBP3S_4	-88.030	30.114	0.5	2.5	1.3	0.3	19.7
9-Apr-16	IS	MBP1S_3	-88.033	30.159	0.8	7.7	1.1	0.3	28.0
7-Apr-16	IS	MBP3S_2	-88.028	30.115	0.1	0.4	3.5	0.3	20.5
3-Apr-16	MS	MOOR6S	-88.121	29.974	0.2	0.6	1.2	0.2	1.8
3-Apr-16	MS	MOOR4S	-88.117	30.121	0.4	5.1	0.2	0.2	7.2
3-Apr-16	MS	MBP2S	-88.037	30.054	0.3	0.8	0.6	0.2	8.9
3-Apr-16	MS	MBP3S	-88.031	30.110	1.2	0.9	1.3	0.2	10.0
31-Mar-16	MS	E3S	-87.530	30.000	0.0	0.5	4.1	0.2	1.9
31-Mar-16	MS	E4S	-87.530	30.098	0.4	6.8	0.6	0.4	1.2

Table A.2 (continued).

Date (ddmmmyy)	Water Type	Station ID	LON (dd)	LAT (dd)	NO_2^- (µM)	NO_3^- (µM)	NH_4^+ (µM)	PO_4^{3-} (µM)	$Si(OH)_4$ (µM)
31-Mar-16	MS	E5S	-87.533	30.195	0.0	--	--	0.3	0.8
4-Apr-16	MS	E10S	-87.520	30.049	0.0	0.1	0.1	0.3	1.3
4-Apr-16	MS	E11S	-87.521	30.169	--	0.2	1.4	0.2	0.5
1-Apr-16	OS	W7S	-88.609	29.618	0.3	1.8	1.0	0.2	3.3
31-Mar-16	OS	M12S	-88.126	29.721	0.2	0.6	0.3	0.3	2.0
1-Apr-16	OS	M8S	-88.122	29.886	0.2	0.6	0.5	0.2	2.5
1-Apr-16	OS	M2S	-88.122	29.885	0.1	0.4	0.4	0.3	1.6
1-Apr-16	OS	M3S	-88.124	29.969	--	--	--	--	--
1-Apr-16	OS	M4S	-88.127	30.051	0.2	0.2	0.4	0.3	2.7
2-Apr-16	OS	M14S	-88.126	29.679	--	--	--	--	--
3-Apr-16	OS	M11S	-88.125	29.848	0.3	6.7	0.3	0.5	12.9
30-Mar-16	OS	E6S	-87.534	29.795	0.0	0.8	3.8	0.2	1.9
31-Mar-16	OS	E7S	-87.531	29.901	0.0	0.5	4.1	0.2	1.5
3-Apr-16	OS	E8S	-87.527	29.739	0.1	0.1	0.0	0.2	1.1
4-Apr-16	OS	E2S	-87.530	29.833	0.1	1.8	0.8	0.1	0.8
4-Apr-16	OS	E9S	-87.523	29.945	0.1	0.3	0.4	0.1	0.5
6-Apr-16	OS	P1S	-88.086	29.771	1.0	--	1.1	0.2	1.0
6-Apr-16	OS	P2S	-88.130	29.801	0.0	0.1	0.8	0.3	0.4
7-Apr-16	OS	P3S	-88.090	29.726	--	0.1	0.7	0.3	0.5
7-Apr-16	OS	P9S	-88.086	29.723	0.0	0.2	0.8	0.2	0.7

APPENDIX B–SIZE-FRACTIONATED BIOMASS AND PRIMARY PRODUCTIVITY

Table B.1 Size-fractionated biomass and primary productivity for Autumn 2015

Date (ddmmmyy)	**Water Type**	**Station ID**	**POC$_{>0.6\mu m}$** (µg L^{-1})	**POC$_{>5\mu m}$** (µg L^{-1})	**PON$_{>0.6\mu m}$** (µg L^{-1})	**PON$_{>5\mu m}$** (µg L^{-1})	**Chl a_{tot}** (µg L^{-1})	**Chl $a_{>0.6\mu m}$** (µg L^{-1})	**Chl $a_{>5\mu m}$** (µg L^{-1})
29-Oct-15	IS	W4	124.0	113.0	17.0	14.0	2.2	0.7	1.0
2-Nov-15	IS	WM6	135.0	51.0	21.0	6.0	2.5	0.7	0.8
3-Nov-15	IS	W10	227.0	157.0	38.0	27.0	2.3	1.3	1.1
3-Nov-15	IS	W11	187.0	129.0	33.0	22.0	2.4	1.5	0.7
3-Nov-15	IS	G1	111.0	52.0	13.0	6.0	1.0	0.4	0.6
30-Oct-15	IS	M5	278.0	181.0	38.0	22.0	2.2	0.2	2.2
31-Oct-15	IS	M10	149.0	52.0	25.0	6.0	2.1	0.6	0.9
1-Nov-15	IS	MBP4	--	--	--	--	2.4	--	--
2-Nov-15	IS	WM3	332.0	177.0	55.0	25.0	3.6	0.7	3.0
2-Nov-15	IS	WM4	361.0	204.0	55.0	28.0	3.6	0.9	2.6
2-Nov-15	IS	WM5	270.0	129.0	49.0	19.0	3.4	0.9	1.6
1-Nov-15	IS	E5	256.0	89.0	46.0	12.0	2.3	0.8	0.9
1-Nov-15	IS	ME3	198.0	49.0	41.0	8.0	2.0	0.3	0.9
29-Oct-15	MS	W1	51.0	217.0	10.0	27.0	1.1	0.6	0.8
29-Oct-15	MS	W2	252.0	76.0	41.0	16.0	1.4	1.0	0.7
29-Oct-15	MS	W3	289.0	--	-16.0	-16.0	1.7	1.1	0.7
2-Nov-15	MS	W7	173.0	52.0	30.0	9.0	1.3	0.8	0.7
3-Nov-15	MS	W8	184.0	57.0	30.0	10.0	1.4	1.1	1.0
3-Nov-15	MS	W9	238.0	61.0	40.0	10.0	2.1	1.2	0.9
30-Oct-15	MS	M4	273.0	78.0	38.0	13.0	1.7	1.1	1.3

Table B.1 (continued).

Date (ddmmmyy)	**Water Type**	**Station ID**	**POC$_{>0.6\mu m}$** ($\mu g\ L^{-1}$)	**POC$_{>5\mu m}$** ($\mu g\ L^{-1}$)	**PON$_{>0.6\mu m}$** ($\mu g\ L^{-1}$)	**PON$_{>5\mu m}$** ($\mu g\ L^{-1}$)	**Chl a_{tot}** ($\mu g\ L^{-1}$)	**Chl $a_{>0.6\mu m}$** ($\mu g\ L^{-1}$)	**Chl $a_{>5\mu m}$** ($\mu g\ L^{-1}$)
31-Oct-15	MS	M9	217.0	51.0	31.0	8.0	1.4	0.4	1.6
1-Nov-15	MS	E2	154.0	119.0	25.0	25.0	2.1	0.3	1.4
1-Nov-15	MS	E3	165.0	72.0	27.0	11.0	2.0	0.5	1.2
1-Nov-15	MS	E4	227.0	85.0	35.0	12.0	1.9	0.9	0.9
5-Nov-15	MS	A7	79.0	38.0	11.0	5.0	1.7	0.3	0.4
29-Oct-15	OS	M1	102.0	29.0	17.0	5.0	0.8	0.2	0.8
30-Oct-15	OS	M2	198.0	104.0	29.0	13.0	1.1	0.6	1.1
30-Oct-15	OS	M6	100.0	40.0	16.0	16.0	0.9	0.3	0.5
31-Oct-15	OS	M7	125.0	48.0	--	--	0.8	0.4	0.8
31-Oct-15	OS	M8	176.0	68.0	29.0	13.0	1.1	0.7	0.8
2-Nov-15	OS	M11	283.0	310.0	44.0	44.0	1.2	0.3	3.2
31-Oct-15	OS	E1	253.0	48.0	41.0	6.0	1.6	0.8	1.0
4-Nov-15	OS	A5_1	103.0	48.0	17.0	3.0	1.1	0.3	0.6
4-Nov-15	OS	A1_1	--	--	--	--	0.8	0.4	0.5
4-Nov-15	OS	A2_1	--	--	--	--	0.8	--	--
4-Nov-15	OS	A6_1	--	--	--	--	0.9	0.3	0.4
5-Nov-15	OS	A1_2	97.0	52.0	16.0	6.0	0.9	0.2	0.6
5-Nov-15	OS	A9	143.0	102.0	19.0	16.0	1.1	0.3	0.7

Table B.1 (continued).

Date (ddmmmyy)	**Water Type**	**Station ID**	**Chl *a*$_{\%>5\mu m}$** (%)	**Chl *a*'$_{>5\mu m}$** (µg L^{-1})	**PP$_{>0.6\mu m}$** (mg C m^{-3} d^{-1})	**PP$_{>5\mu m}$** (mg C m^{-3} d^{-1})
29-Oct-15	IS	W4	--	--	4.0	1.5
2-Nov-15	IS	WM6	--	--	96.4	85.6
3-Nov-15	IS	W10	--	--	2.6	22.9
3-Nov-15	IS	W11	--	--	5.2	26.1
3-Nov-15	IS	G1	--	--	50.0	200.0
30-Oct-15	IS	M5	--	--	48.0	83.9
31-Oct-15	IS	M10	--	--	109.6	97.4
1-Nov-15	IS	MBP4	--	--	--	--
2-Nov-15	IS	WM3	--	--	62.3	220.0
2-Nov-15	IS	WM4	--	--	110.8	175.6
2-Nov-15	IS	WM5	--	--	6.7	10.7
1-Nov-15	IS	E5	--	--	36.2	18.4
1-Nov-15	IS	ME3	--	--	27.1	13.5
29-Oct-15	MS	W1	--	--	14.1	11.0
29-Oct-15	MS	W2	--	--	29.5	23.0
29-Oct-15	MS	W3	--	--	48.0	15.7
2-Nov-15	MS	W7	--	--	8.6	20.2
3-Nov-15	MS	W8	--	--	4.4	15.4
3-Nov-15	MS	W9	--	--	--	--
30-Oct-15	MS	M4	--	--	73.5	36.3

Table B.1 (continued).

Date (ddmmmyy)	**Water Type**	**Station ID**	**Chl *a*$_{\%>5\mu m}$** (%)	**Chl *a*'$_{>5\mu m}$** ($\mu g\ L^{-1}$)	**PP$_{>0.6\mu m}$** ($mg\ C\ m^{-3}\ d^{-1}$)	**PP$_{>5\mu m}$** ($mg\ C\ m^{-3}\ d^{-1}$)
31-Oct-15	MS	M9	--	--	61.8	34.5
1-Nov-15	MS	E2	--	--	30.0	17.6
1-Nov-15	MS	E3	--	--	28.4	22.3
1-Nov-15	MS	E4	--	--	17.6	26.0
5-Nov-15	MS	A7	--	--	--	--
29-Oct-15	OS	M1	--	--	12.9	5.6
30-Oct-15	OS	M2	--	--	--	--
30-Oct-15	OS	M6	--	--	11.3	2.2
31-Oct-15	OS	M7	--	--	15.5	5.8
31-Oct-15	OS	M8	--	--	25.5	16.7
2-Nov-15	OS	M11	--	--	--	--
31-Oct-15	OS	E1	--	--	17.9	11.3
4-Nov-15	OS	A5_1	--	--	--	--
4-Nov-15	OS	A1_1	--	--	--	--
4-Nov-15	OS	A2_1	--	--	--	--
4-Nov-15	OS	A6_1	--	--	11.3	5.6
5-Nov-15	OS	A1_2	--	--	20.7	3.3
5-Nov-15	OS	A9	--	--	--	--

Table B.2 Size-fractionated biomass and primary productivity for Spring 2016

Date (ddmmmyy)	**Water Type**	**Station ID**	**POC$_{>0.6\mu m}$** ($\mu g\ L^{-1}$)	**POC$_{>5\mu m}$** ($\mu g\ L^{-1}$)	**PON$_{>0.6\mu m}$** ($\mu g\ L^{-1}$)	**PON$_{>5\mu m}$** ($\mu g\ L^{-1}$)	**Chl a_{tot}** ($\mu g\ L^{-1}$)	**Chl $a_{>0.6\mu m}$** ($\mu g\ L^{-1}$)	**Chl $a_{>5\mu m}$** ($\mu g\ L^{-1}$)
5-Apr-16	ES	WM1S		--	--	--	7.9	7.9	--
5-Apr-16	ES	WM3S		--	--	--	9.9	9.9	--
8-Apr-16	ES	MOOR2S_2	363.3	373.3	60.0	53.3	6.8	6.8	8.8
9-Apr-16	ES	MOOR2S_3	238.3	506.7	43.3	76.7	14.3	14.3	18.7
2-Apr-16	IS	W2S	--	--	--	--	5.7	--	--
2-Apr-16	IS	W3S	--	--	--	--	6.5	--	--
2-Apr-16	IS	W10S	--	--	--	--	6.3	--	--
5-Apr-16	IS	M3S_2	284.1	295.2	33.3	36.5	7.6	7.6	9.2
5-Apr-16	IS	M4S_2	348.4	401.6	40.5	42.9	7.7	7.7	5.7
5-Apr-16	IS	M5S_2	235.9	290.5	29.2	34.9	6.8	6.8	--
8-Apr-16	IS	WM1S_2	--	--	--	--	7.3	--	--
8-Apr-16	IS	MBP3S_4	303.5	311.1	51.0	36.5	7.2	7.2	21.0
9-Apr-16	IS	MBP1S_3	207.8	382.9	27.6	51.4	8.7	8.7	9.9
7-Apr-16	IS	MBP3S_2	289.3	352.4	40.0	41.3	7.5	7.5	9.2
3-Apr-16	MS	MOOR6S	107.9	88.9	19.0	12.7	2.3	2.3	3.1
3-Apr-16	MS	MOOR4S	--	230.2	--	38.1	3.1	3.1	--
3-Apr-16	MS	MBP2S	170.5	120.6	27.6	19.0	3.0	3.0	4.2
3-Apr-16	MS	MBP3S	--	--	--	--	2.6	2.6	--
31-Mar-16	MS	E3S	--	--	--	--	2.2	--	--
31-Mar-16	MS	E4S	--	--	--	--	2.8	--	--

Table B.2 (continued).

Date (ddmmmyy)	**Water Type**	**Station ID**	**POC$_{>0.6\mu m}$** ($\mu g\ L^{-1}$)	**POC$_{>5\mu m}$** ($\mu g\ L^{-1}$)	**PON$_{>0.6\mu m}$** ($\mu g\ L^{-1}$)	**PON$_{>5\mu m}$** ($\mu g\ L^{-1}$)	**Chl a_{tot}** ($\mu g\ L^{-1}$)	**Chl $a_{>0.6\mu m}$** ($\mu g\ L^{-1}$)	**Chl $a_{>5\mu m}$** ($\mu g\ L^{-1}$)
31-Mar-16	MS	E5S	--	--	--	--	3.5	--	--
4-Apr-16	MS	E10S	--	--	--	--	2.0	--	--
4-Apr-16	MS	E11S	--	--	--	--	2.2	--	--
1-Apr-16	OS	W7S	--	--	--	--	2.2	--	--
31-Mar-16	OS	M12S	112.7	47.6	17.5	7.9	0.9	0.9	2.4
1-Apr-16	OS	M8S	130.2	60.3	17.5	9.5	1.1	1.1	1.0
1-Apr-16	OS	M2S	238.1	139.7	17.5	25.4	2.2	2.2	3.2
1-Apr-16	OS	M3S	195.2	104.8	27.0	14.3	3.4	3.4	4.8
1-Apr-16	OS	M4S	163.5	100.0	27.0	14.3	2.8	2.8	3.4
2-Apr-16	OS	M14S	274.6	112.7	44.4	22.2	2.1	2.1	1.9
3-Apr-16	OS	M11S	73.0	106.3	9.5	17.5	1.9	1.9	2.3
30-Mar-16	OS	E6S	--	--	--	--	1.4	--	--
31-Mar-16	OS	E7S	--	--	--	--	1.8	--	--
3-Apr-16	OS	E8S	--	--	--	--	--	--	--
4-Apr-16	OS	E2S	--	--	--	--	1.7	--	--
4-Apr-16	OS	E9S	--	--	--	--	1.5	--	--
6-Apr-16	OS	P1S	--	--	--	--	1.9	--	--
6-Apr-16	OS	P2S	--	--	--	--	2.5	--	--
7-Apr-16	OS	P3S	--	--	--	--	1.5	--	--
7-Apr-16	OS	P9S	--	--	--	--	3.9	--	--

Table B.2 (continued).

Date (ddmmmyy)	**Water Type**	**Station ID**	**Chl *a*$_{\%>5\mu m}$** (%)	**Chl *a*'$_{>5\mu m}$** (µg L^{-1})	**PP$_{>0.6\mu m}$** (mg C m^{-3} d^{-1})	**PP$_{>5\mu m}$** (mg C m^{-3} d^{-1})
5-Apr-16	ES	WM1S	--	--	624.1	450.2
5-Apr-16	ES	WM3S	--	--	754.2	455.8
8-Apr-16	ES	MOOR2S_2	1.3	8.8	564.4	288.1
9-Apr-16	ES	MOOR2S_3	1.3	18.7	464.9	494.6
2-Apr-16	IS	W2S	--	--	71.5	83.8
2-Apr-16	IS	W3S	--	--	84.4	51.6
2-Apr-16	IS	W10S	--	--	94.2	66.7
5-Apr-16	IS	M3S_2	1.2	9.2	157.1	156.5
5-Apr-16	IS	M4S_2	0.7	5.7	236.9	210.6
5-Apr-16	IS	M5S_2	--	--	214.3	181.6
8-Apr-16	IS	WM1S_2	--	--	--	--
8-Apr-16	IS	MBP3S_4	2.9	21.0	40.0	25.9
9-Apr-16	IS	MBP1S_3	1.1	9.9	42.4	25.8
7-Apr-16	IS	MBP3S_2	1.2	9.2	94.2	66.7
3-Apr-16	MS	MOOR6S	1.3	3.1	47.6	32.8
3-Apr-16	MS	MOOR4S	--	--	137.7	145.6
3-Apr-16	MS	MBP2S	1.4	4.2	174.5	141.0
3-Apr-16	MS	MBP3S	--	--	--	--
31-Mar-16	MS	E3S	--	--	81.2	47.1
31-Mar-16	MS	E4S	--	--	7.6	18.7

Table B.2 (continued).

Date (ddmmmyy)	**Water Type**	**Station ID**	**Chl $a_{\%>5\mu m}$** (%)	**Chl $a'_{>5\mu m}$** ($\mu g\ L^{-1}$)	**$PP_{>0.6\mu m}$** ($mg\ C\ m^{-3}\ d^{-1}$)	**$PP_{>5\mu m}$** ($mg\ C\ m^{-3}\ d^{-1}$)
31-Mar-16	MS	E5S	--	--	84.2	51.0
4-Apr-16	MS	E10S	--	--	44.1	23.5
4-Apr-16	MS	E11S	--	--	69.2	42.6
1-Apr-16	OS	W7S	--	--	33.7	32.6
31-Mar-16	OS	M12S	2.6	2.4	29.2	10.2
1-Apr-16	OS	M8S	0.9	1.0	26.7	11.7
1-Apr-16	OS	M2S	1.5	3.2	79.4	58.0
1-Apr-16	OS	M3S	1.4	4.8	163.4	101.6
1-Apr-16	OS	M4S	1.2	3.4	98.4	62.2
2-Apr-16	OS	M14S	0.9	1.9	40.0	25.9
3-Apr-16	OS	M11S	1.2	2.3	42.4	25.8
30-Mar-16	OS	E6S	--	--	61.1	22.7
31-Mar-16	OS	E7S	--	--	44.7	26.5
3-Apr-16	OS	E8S	--	--	44.7	27.1
4-Apr-16	OS	E2S	--	--	14.9	8.3
4-Apr-16	OS	E9S	--	--	45.8	21.9
6-Apr-16	OS	P1S	--	--	54.1	59.7
6-Apr-16	OS	P2S	--	--	133.5	101.3
7-Apr-16	OS	P3S	--	--	--	--
7-Apr-16	OS	P9S	--	--	119.3	60.4

APPENDIX C–PARTICLE IMAGING USING FLOWCAM

Table C.1 FlowCAM Imaging Particle Counts for Autumn 2015

Particle values represent the summation of particles at each station. Values are given in particles per milliliter (mL).

Date (ddmmmyy)	**Water Type**	**Station ID**	**Classified particles** (particles mL^{-1})	**Unclassified particles** (particles mL^{-1})	**Total particles** (particles mL^{-1})
29-Oct-15	IS	W4	468.5	238.7	707.2
2-Nov-15	IS	WM6	464.9	964.7	1429.5
3-Nov-15	IS	W10	76.0	64.3	140.3
3-Nov-15	IS	W11	81.5	187.4	268.9
3-Nov-15	IS	G1	130.2	127.0	257.2
30-Oct-15	IS	M5	522.6	580.0	1102.6
31-Oct-15	IS	M10	163.7	135.0	298.7
1-Nov-15	IS	MBP4	88.1	107.3	195.4
2-Nov-15	IS	WM3	802.2	738.0	1540.2
2-Nov-15	IS	WM4	1154.8	1755.5	2910.3
2-Nov-15	IS	WM5	340.4	629.5	969.9
1-Nov-15	IS	E5	90.8	44.7	135.4
1-Nov-15	IS	ME3	81.8	49.0	130.8
29-Oct-15	MS	W1	213.8	33.7	247.5
29-Oct-15	MS	W2	421.1	207.8	629.0
29-Oct-15	MS	W3	353.2	175.4	528.7
2-Nov-15	MS	W7	413.7	73.2	487.0
3-Nov-15	MS	W8	38.0	46.6	84.6
3-Nov-15	MS	W9	25.9	113.5	139.4
30-Oct-15	MS	M4	459.2	231.3	690.5

Table C.1 (continued)

Date (ddmmmyy)	**Water Type**	**Station ID**	**Classified particles** (particles mL^{-1})	**Unclassified particles** (particles mL^{-1})	**Total particles** (particles mL^{-1})
31-Oct-15	MS	M9	43.0	52.8	95.8
1-Nov-15	MS	E2	131.8	22.7	154.5
1-Nov-15	MS	E3	106.6	43.1	149.7
1-Nov-15	MS	E4	127.0	26.1	153.0
5-Nov-15	MS	A7	50.6	15.7	66.2
29-Oct-15	OS	M1	137.4	18.4	155.8
30-Oct-15	OS	M2	49.9	23.0	72.9
30-Oct-15	OS	M6	36.1	9.1	45.2
31-Oct-15	OS	M7	26.7	3.8	30.5
31-Oct-15	OS	M8	55.0	6.6	61.6
2-Nov-15	OS	M11	42.6	19.1	61.8
31-Oct-15	OS	E1	67.0	49.4	116.4
4-Nov-15	OS	A5_1	22.3	7.0	29.3
4-Nov-15	OS	A1_1	23.0	4.5	27.5
4-Nov-15	OS	A2_1	26.1	9.8	35.9
4-Nov-15	OS	A6_1	43.2	3.2	46.5
5-Nov-15	OS	A1_2	17.2	6.2	23.4
5-Nov-15	OS	A9	41.1	4.7	45.8

Table C.2 FlowCAM Imaging Particle Counts for Spring 2016

Particle values represent the summation of particles at each station. Values are given in particles per milliliter (mL).

Date (ddmmmyy)	**Water Type**	**Station ID**	**Classified particles** (particles mL^{-1})	**Unclassified particles** (particles mL^{-1})	**Total particles** (particles mL^{-1})
5-Apr-16	ES	WM1S	1837.2	1764.5	3601.7
5-Apr-16	ES	WM3S	1908.7	2802.5	4711.2
8-Apr-16	ES	MOOR2S_2	3006.3	6252.0	9258.3
9-Apr-16	ES	MOOR2S_3	1574.0	744.0	2318.0
2-Apr-16	IS	W2S	607.3	177.7	785.0
2-Apr-16	IS	W3S	457.4	954.0	1411.4
2-Apr-16	IS	W10S	111.2	437.0	548.2
5-Apr-16	IS	M3S_2	82.0	49.0	131.0
5-Apr-16	IS	M4S_2	45.4	42.0	87.4
5-Apr-16	IS	M5S_2	1095.3	447.0	1542.3
8-Apr-16	IS	WM1S_2	2467.6	1301.0	3768.6
8-Apr-16	IS	MBP3S_4	3072.5	1298.0	4370.5
9-Apr-16	IS	MBP1S_3	4333.8	5762.0	10095.8
7-Apr-16	IS	MBP3S_2	2436.4	5473.7	7910.2
3-Apr-16	MS	MOOR6S	534.3	119.5	653.8
3-Apr-16	MS	MOOR4S	429.0	391.0	820.0
3-Apr-16	MS	MBP2S	529.4	271.0	800.4
3-Apr-16	MS	MBP3S	1163.5	971.0	2134.5
31-Mar-16	MS	E3S	501.4	215.2	716.5
31-Mar-16	MS	E4S	519.9	90.8	610.7

Table C.2 (continued).

Date (ddmmmyy)	**Water Type**	**Station ID**	**Classified particles** (particles mL^{-1})	**Unclassified particles** (particles mL^{-1})	**Total particles** (particles mL^{-1})
31-Mar-16	MS	E5S	539.3	210.0	749.3
4-Apr-16	MS	E10S	864.6	79.0	943.6
4-Apr-16	MS	E11S	884.1	200.0	1084.1
1-Apr-16	OS	W7S	512.9	140.4	653.3
31-Mar-16	OS	M12S	370.6	106.3	477.0
1-Apr-16	OS	M8S	289.4	179.7	469.1
1-Apr-16	OS	M2S	400.5	148.1	548.5
1-Apr-16	OS	M3S	363.3	177.5	540.8
1-Apr-16	OS	M4S	443.8	302.0	745.8
2-Apr-16	OS	M14S	564.8	352.8	917.6
3-Apr-16	OS	M11S	645.7	114.0	759.7
30-Mar-16	OS	E6S	469.5	380.4	849.9
31-Mar-16	OS	E7S	546.8	249.4	796.2
3-Apr-16	OS	E8S	551.7	256.3	807.9
4-Apr-16	OS	E2S	376.3	197.5	573.8
4-Apr-16	OS	E9S	448.2	123.0	571.2
6-Apr-16	OS	P1S	213.9	7.5	221.4
6-Apr-16	OS	P2S	328.3	91.7	420.0
7-Apr-16	OS	P3S	87.6	1048.0	1135.6
7-Apr-16	OS	P9S	166.8	0.6	167.3

APPENDIX D–MICROPLANKTON CLASSIFICATION AND PARTICLE PROPERTIES

Table D.1 Microplankton Morphological-Based Functional Groups (MBFGs) Reference

MBFG					FunctionalGroup	Representative Taxa	TL
Flagellates	1	Nanoplankton			Chromophyte*/ Chlorophyte	*Heterocapsa, Scrippsiella, Chroomonas, Rhodomonas, , Actinomonas, Dictyocha, Dinobryon, Ochromonas, Ciliphyrs, Meringosphaera, Octactis, Isochrysis, Chrysochromulina, Prymnesium, Phaeocystis, Pavlova, Chlamydomonas, Choanoplankton*	a, m, h
	2	Prorocentroid			Dinophyceae	*Prorocentrum**	m
	3	Gymnodinoid	3a	athecate		*Gymnodinium, Karenia*, Akishiwo*, Gyrodinium*, Torodinium*	m, h
			3b	thecate		*Alexandrium*, Oxyphsis, Gamberidiscus*, Protoperidinium*	m, h
	4	Cerationoid				*Ceratium, Ceratoperidinium, Brachydinium*	a, m
	5	Dinophysoid				*Dinophysis*, Phalacroma, Oxyphysis, Oxytoxum**	a, m
	6	Euglenoid			Chlorophyceae	*Eutrepia, Euglena, Eutreptiella*	a
	7	Silicoflagellates			Chromophyta	*Dicyocha, Octactis, Mesocena, Ebria*	a
	8	Radiolarians			Radiolaria	*Acanthometra, Amphilonche*	a
Non-flagellates	9	Elliptic prism			Bacillariophyceae	*Navicula, Pleurosigma, Gyrosigma, Entomoneis*	a
	10	Discoid				*Coscinodiscus, Azpeitia, Hemidiscus, Actinocychus, Roperia*	a
	11	Skeletonemanoid	11a	small		*Skeletonema, Lauderia, Thalassiosira*	a
			11b	large		*Odontella, Hemiaulus*	a
	12	Cylindrical chains				*Dactyliosolen, Guinardia, Leptocylindrus, Corethron, Muneria*	a
	13	Acerate cells	13a	Nitzschioid		*Pseudo-nitzschia*, Nitzschia, Cylindrotheca*	a
			13b	Rhizosolenoid		*Rhizosolenia, Proboscia, Ditylum*	a
	14	Aserionellopsioid				*Asterionellopsis, Chaetoceros, Thalassionema, Lioloma*	a
	15	Desmids			Chlorophyceae	*Scendesmus, Desmodesmus, Pediastrum*	a
	16	Mucilagenous			Chlorophyceae	*Oocystis*	a

	17	Filamentous			Cyanophyta	*Dolichospermum*, Aphanizomenon*, Merismopedia*	a

Table D.1 (continued).

MBFG					FunctionalGroup	Representative Taxa	TL
Microzooplankton	18	Ciliates	18a	*Mesodinium*	Ciliophora	*Mesodinium*	m
			18b	aloricate choreotrichids		*Laboea, Strombilidium, Strombidium, Euplotes, Diophrys*	m, h
			18c	tintinnids		*Favella, Tintinniopsis, Heliocostomella*	m, h
	19	mesozooplankton			mesozooplankton	copepod nauplii, rotifers, larvaceans	h
Other	20	particulate matter (PM)	20a	unidentified particles < 20 μm	PM	unidentified cells, dead fragments, appendages, fecal pellets, exuvia	NA
			20b	unidentified particles > 20 μm			NA

Table D.2 Microplankton MBFGs Particle Counts for Autumn 2015

Particle values represent the summation of particles at each station. Values are given in particles per milliliter (mL), whereas values presented throughout the text were given in particles per liter (L), which was calculated by multiplying the particles mL^{-1} by 10^3.

Station ID	**MBFG_1**	**MBFG_2**	**MBFG_3a**	**MBFG_3b**	**MBFG_4**	**MBFG_5**	**MBFG_6**	**MGFB_7**	**MGFB_8**
	part. mL^{-1}	part. mL^{-1}	part. mL^{-1}	part. mL^{-1}	part. mL^{-1}	part. mL^{-1}	part. mL^{-1}	part. mL^{-1}	part. mL^{-1}
W4	422.0	2.9	2.9	1.9	0.2	--	0.2	--	--
WM6	401.0	--	0.4	0.2	0.2	0.4	1.0	--	--
W10	36.3	0.2	2.1	0.4	0.8	--	1.0	0.4	--
W11	33.7	0.2	2.7	0.4	0.2	--	0.4	0.6	0.2
G1	43.7	0.8	2.7	--	--	1.0	--	0.2	--
M5	466.0	2.7	2.7	0.9	--	--	0.4	--	--
M10	28.0	0.9	1.1	0.9	1.4	--	0.9	--	--
MBP4	26.0	--	3.6	2.1	--	--	3.8	--	--
WM3	679.7	--	1.0	0.6	--	--	--	0.2	--
WM4	1047.5	1.2	1.2	0.3	--	--	--	0.3	--
WM5	255.0	0.9	0.3	--	--	0.6	--	--	--
E5	25.0	--	2.9	0.6	0.8	--	2.7	0.6	--
ME3	31.3	0.8	2.5	2.3	0.6	--	5.3	--	--
W1	190.0	0.2	2.1	0.2	0.2	--	0.4	0.2	0.4
W2	371.7	3.4	3.4	--	--	--	0.8	--	0.2
W3	331.0	2.1	2.1	4.2	0.4	--	0.2	--	--
W7	384.0	--	0.3	0.3	--	--	0.3	--	--
W8	19.3	--	0.8	0.8	--	--	1.0	--	--
W9	11.6	--	--	--	--	--	--	--	--
M4	429.0	0.2	1.0	0.6	--	--	--	--	--

Table D.2 (continued).

Station ID	MBFG_1	MBFG_2	MBFG_3a	MBFG_3b	MBFG_4	MBFG_5	MBFG_6	MGFB_7	MGFB_8
	part. mL^{-1}	part. mL^{-1}	part. mL^{-1}	part. mL^{-1}	part. mL^{-1}	part. mL^{-1}	part. mL^{-1}	part. mL^{-1}	part. mL^{-1}
M9	9.9	--	2.1	1.1	0.6	--	1.0	--	--
E2	47.3	--	1.1	0.2	--	--	5.3	0.2	--
E3	41.0	--	0.2	0.2	--	--	3.3	0.2	--
E4	29.3	--	16.7	2.5	0.6	0.6	0.6	0.4	--
A7	22.0	0.6	2.3	--	--	--	0.6	0.2	--
M1	115.0	1.1	1.1	0.4	0.2	--	0.2	0.4	0.2
M2	9.6	--	4.1	0.4	--	--	--	0.4	0.2
M6	10.2	--	0.8	--	--	--	0.2	--	--
M7	5.7	--	1.1	--	--	--	0.6	0.4	--
M8	11.2	0.2	0.2	0.4	0.6	--	0.6	--	0.2
M11	6.6	0.2	0.9	0.2	--	--	--	--	0.2
E1	17.3	--	3.0	0.4	--	0.6	2.5	--	--
A5_1	4.4	--	0.2	--	0.6	0.2	--	--	--
A1_1	2.3	--	0.8	--	--	--	0.4	0.4	--
A2_1	11.0	--	1.1	--	--	--	0.6	0.6	0.6
A6_1	40.0	--	--	0.2	--	--	--	--	--
A1_2	4.5	--	0.4	--	--	--	0.2	--	0.2
A9	9.5	--	0.6	0.2	--	--	0.2	0.2	--

Table D.2 (continued).

Station ID	MBFG_9	MBFG_10	MBFG_11a	MBFG_11b	MBFG_12	MBFG_13a	MBFG_13b	MGFB_14	MGFB_15
	part. mL^{-1}	part. mL^{-1}	part. mL^{-1}	part. mL^{-1}	part. mL^{-1}	part. mL^{-1}	part. mL^{-1}	part. mL^{-1}	part. mL^{-1}
W4	3.6	--	2.7	--	7.7	13.6	2.7	3.0	--
WM6	13.7	--	12.6	--	4.0	14.3	0.3	12.5	--
W10	7.8	0.4	--	--	0.8	2.7	0.3	9.2	--
W11	12.2	0.2	4.1	--	1.7	4.6	0.1	12.0	--
G1	21.3	0.8	6.0	--	6.4	5.2	0.0	22.8	--
M5	11.6	--	13.7	--	5.4	13.3	0.1	0.9	--
M10	18.5	0.9	31.6	--	22.5	14.4	0.3	31.6	--
MBP4	7.5	0.2	2.2	--	7.5	2.1	4.5	20.6	0.4
WM3	29.3	1.2	20.7	--	12.8	17.7	0.5	32.6	--
WM4	20.0	0.9	22.0	--	9.5	35.5	--	10.6	--
WM5	16.9	0.3	12.4	--	6.6	11.5	0.4	27.0	--
E5	5.5	0.6	8.8	--	4.9	5.5	0.5	17.4	--
ME3	8.3	0.4	2.3	--	2.2	2.2	0.3	12.3	--
W1	1.3	--	3.9	--	3.9	4.6	0.1	2.7	--
W2	2.7	0.2	1.6	--	6.7	15.1	0.0	10.4	--
W3	1.3	0.4	1.0	--	0.8	3.4	--	0.6	--
W7	2.3	--	5.3	--	1.4	12.6	--	2.1	--
W8	2.7	--	--	--	0.3	2.9	--	6.2	--
W9	3.4	0.3	1.5	--	--	3.2	--	3.3	--
M4	2.5	--	8.6	--	6.6	8.2	0.0	0.3	--

Table D.2 (continued).

Station ID	MBFG_9	MBFG_10	MBFG_11a	MBFG_11b	MBFG_12	MBFG_13a	MBFG_13b	MGFB_14	MGFB_15
	part. mL^{-1}	part. mL^{-1}	part. mL^{-1}	part. mL^{-1}	part. mL^{-1}	part. mL^{-1}	part. mL^{-1}	part. mL^{-1}	part. mL^{-1}
M9	3.6	--	4.1	--	2.9	5.2	--	5.1	--
E2	7.3	1.0	2.3	--	1.2	13.6	0.2	31.5	--
E3	11.0	--	2.3	--	0.3	13.0	0.4	15.7	--
E4	7.0	0.4	4.5	--	9.0	17.8	0.5	27.5	--
A7	4.4	0.6	1.7	--	--	1.9	--	3.4	--
M1	1.0	0.4	1.9	--	6.6	6.2	--	2.0	--
M2	3.6	0.2	0.4	--	1.2	7.7	--	19.3	0.2
M6	2.8	--	--	--	--	5.2	0.1	11.9	--
M7	0.8	0.2	0.7	--	2.6	3.7	0.2	7.6	--
M8	1.9	--	2.7	--	3.2	3.6	--	22.9	--
M11	2.5	0.2	0.9	--	1.2	5.3	0.1	18.1	--
E1	4.7	--	0.2	--	1.4	7.2	--	20.8	--
A5_1	1.9	--	2.3	--	2.3	2.3	0.0	5.9	--
A1_1	1.1	--	--	--	6.1	1.5	--	6.9	--
A2_1	1.7	0.2	--	--	0.9	1.9	0.1	3.9	--
A6_1	--	--	0.2	--	1.2	0.1	--	--	--
A1_2	2.6	0.4	2.1	--	1.1	1.6	0.1	2.5	--
A9	6.0	0.2	3.0	--	3.5	2.1	0.2	7.7	--

Table D.2 (continued).

Station ID	MBFG_16	MBFG_17	MBFG_18a	MBFG_18b	MBFG_18c	MBFG_19	MBFG_20a	MGFB_20b
	part. mL^{-1}	part. mL^{-1}	part. mL^{-1}	part. mL^{-1}	part. mL^{-1}	part. mL^{-1}	part. mL^{-1}	part. mL^{-1}
W4	--	0.2	1.5	3.3	0.2	--	218.3	20.3
WM6	--	0.4	2.1	1.9	--	--	885.0	79.7
W10	--	2.7	3.4	7.4	--	0.2	50.3	14.0
W11	--	1.9	2.1	4.2	--	--	164.0	23.3
G1	--	5.6	8.2	5.0	--	0.6	100.3	26.7
M5	--	0.4	2.2	2.3	--	--	547.3	32.7
M10	--	9.2	0.9	0.9	--	--	102.5	32.5
MBP4	--	0.6	5.7	1.3	--	--	79.7	27.7
WM3	--	0.8	2.7	1.9	0.2	0.4	652.3	85.7
WM4	--	0.6	1.5	3.8	--	--	1618.5	137.0
WM5	--	2.3	1.7	4.6	--	--	534.5	95.0
E5	--	6.5	3.4	5.3	--	--	26.7	18.0
ME3	--	3.2	3.0	4.9	--	--	20.3	28.6
W1	--	0.8	0.4	2.7	--	--	28.7	5.0
W2	--	0.6	2.1	2.1	0.2	--	195.0	12.8
W3	--	0.2	1.0	--	0.8	3.4	--	0.6
W7	--	1.2	5.3	--	1.4	12.6	--	2.1
W8	--	1.5	--	--	0.3	2.9	--	6.2
W9	--	0.9	1.5	--	--	3.2	--	3.3
M4	--	0.2	8.6	--	6.6	8.2	0.0	0.3

Table D.2 (continued).

Station ID	MBFG_16	MBFG_17	MBFG_18a	MBFG_18b	MBFG_18c	MBFG_19	MBFG_20a	MGFB_20b
	part. mL^{-1}	part. mL^{-1}	part. mL^{-1}	part. mL^{-1}	part. mL^{-1}	part. mL^{-1}	part. mL^{-1}	part. mL^{-1}
M9	--	4.0	0.9	2.5	--	--	39.7	13.1
E2	--	6.5	5.9	8.3	--	--	13.3	9.4
E3	--	11.3	4.6	3.1	0.2	--	30.0	13.1
E4	--	2.7	4.9	1.9	0.2	--	16.3	9.8
A7	--	2.3	2.3	8.5	--	--	10.2	5.5
M1	--	0.2	--	0.6	--	--	16.7	1.7
M2	0.2	0.6	0.8	1.0	0.2	--	15.0	8.0
M6	--	0.6	1.0	3.2	0.2	--	4.9	4.2
M7	--	0.4	0.4	2.5	--	--	2.1	1.7
M8	--	0.9	2.8	3.6	--	--	4.7	1.9
M11	--	1.9	1.9	2.5	--	--	11.0	8.2
E1	--	2.8	2.5	3.6	--	--	17.3	32.0
A5_1	--	--	0.8	1.1	0.2	0.2	5.1	1.9
A1_1	--	0.3	1.9	1.3	--	--	3.2	1.3
A2_1	--	1.7	1.1	0.8	--	--	5.7	4.2
A6_1	--	--	0.4	1.1	--	--	2.1	1.1
A1_2	2.6	0.4	0.4	1.0	--	--	4.5	1.7
A9	6.0	0.2	0.9	5.5	--	--	2.5	2.3

Table D.3 Microplankton MBFGs Particle Counts for Spring 2016

Particle values represent total number of particles at each station for each MBFG. Values are given in particles per milliliter (mL), whereas values presented throughout the text were given in particles per liter (L), which was calculated by multiplying the particles mL^{-1} by 10^3.

Station ID	**MBFG_1**	**MBFG_2**	**MBFG_3a**	**MBFG_3b**	**MBFG_4**	**MBFG_5**	**MBFG_6**	**MGFB_7**	**MGFB_8**
	part. mL^{-1}	part. mL^{-1}	part. mL^{-1}	part. mL^{-1}	part. mL^{-1}	part. mL^{-1}	part. mL^{-1}	part. mL^{-1}	part. mL^{-1}
WM1S	935.5	3.9	3.0	0.3	--	--	--	--	--
WM3S	1239.5	2.4	4.5	1.8	--	--	--	--	--
MOOR2S_2	1053.0	23.0	15.0	4.9	--	0.6	--	--	--
MOOR2S_3	1030.0	52.0	1.8	--	0.6	--	--	--	--
W2S	441.0	8.5	5.8	6.1	--	--	1.7	--	--
W3S	257.0	6.2	0.6	2.1	--	--	--	--	--
W10S	74.0	1.2	--	--	--	--	--	--	--
M3S_2	31.3	0.8	2.5	2.3	0.6	--	5.3	0.2	--
M4S_2	21.0	--	2.3	--	--	--	2.8	--	--
M5S_2	319.5	0.9	5.5	0.3	--	--	--	--	--
WM1S_2	1664.0	22.0	2.4	1.2	0.6	0.6	--	--	--
MBP3S_4	632.0	8.3	1.8	1.8	--	--	--	--	--
MBP1S_3	1789.0	4.3	10.0	4.3	--	--	4.3	--	--
MBP3S_2	576.0	7.7	2.3	0.9	0.2	--	0.5	0.2	--
MOOR6S	261.5	1.4	2.0	3.5	--	--	--	--	--
MOOR4S	242.5	2.6	4.9	4.0	0.3	0.3	0.9	--	--
MBP2S	247.5	0.9	5.2	1.4	--	--	0.9	--	--
MBP3S	436.5	0.9	1.8	0.3	--	--	--	0.3	--
E3S	439.0	--	1.2	3.5	--	--	--	--	--
E4S	128.5	0.9	3.5	5.5	--	0.6	--	--	2.3

Table D.3 (continued).

Station ID	**MBFG_1**	**MBFG_2**	**MBFG_3a**	**MBFG_3b**	**MBFG_4**	**MBFG_5**	**MBFG_6**	**MGFB_7**	**MGFB_8**
	part. mL^{-1}	part. mL^{-1}	part. mL^{-1}	part. mL^{-1}	part. mL^{-1}	part. mL^{-1}	part. mL^{-1}	part. mL^{-1}	part. mL^{-1}
E5S	83.0	--	2.3	4.6	--	--	--	--	--
E10S	87.0	0.9	2.0	3.8	--	--	0.9	--	--
E11S	68.5	--	2.9	6.3	--	--	1.7	--	0.3
W7S	407.0	7.8	8.4	5.8	--	--	0.3	--	--
M12S	293.0	--	0.3	7.4	--	--	--	--	--
M8S	180.0	--	2.9	1.4	--	--	--	--	--
M2S	137.0	--	6.0	2.6	--	--	--	--	--
M3S	200.5	--	--	2.6	--	--	--	--	--
M4S	219.5	--	4.0	12.0	--	--	0.6	--	--
M14S	339.0	0.6	2.0	3.5	--	--	--	0.3	--
M11S	217.0	--	4.6	6.9	--	0.6	--	--	--
E6S	356.3	--	6.6	0.4	--	--	1.0	--	--
E7S	263.0	--	2.0	2.0	--	--	0.3	--	--
E8S	296.0	--	1.5	6.1	--	--	0.3	0.3	--
E2S	174.5	0.6	0.3	4.0	--	--	0.3	--	--
E9S	93.0	0.6	0.6	6.3	--	--	--	--	--
P1S	47.0	1.7	4.0	14.0	--	--	3.4	--	--
P2S	95.0	2.9	1.7	3.4	--	--	0.6	--	--
P3S	59.0	1.7	--	2.8	--	--	--	--	--
P9S	161.0	--	--	--	--	--	--	--	--

Table D.3 (continued).

Station ID	MBFG_9	MBFG_10	MBFG_11a	MBFG_11b	MBFG_12	MBFG_13a	MBFG_13b	MGFB_14	MGFB_15
	part. mL^{-1}	part. mL^{-1}	part. mL^{-1}	part. mL^{-1}	part. mL^{-1}	part. mL^{-1}	part. mL^{-1}	part. mL^{-1}	part. mL^{-1}
WM1S	1.8	--	263.5	--	16.7	585.7	0.1	20.2	--
WM3S	1.8	1.5	137.0	--	17.5	467.6	--	27.9	--
MOOR2S_2	7.4	--	998.5	--	36.5	822.4	--	41.9	1.8
MOOR2S_3	1.2	0.6	45.0	--	19.7	387.7	0.1	32.3	--
W2S	0.6	0.3	3.2	--	8.3	122.3	--	2.6	--
W3S	2.7	--	6.4	--	5.0	154.6	--	17.7	--
W10S	0.6	3.4	10.3	--	2.4	7.1	0.3	10.3	--
M3S_2	8.3	0.4	2.3	--	2.2	2.2	0.3	12.3	--
M4S_2	6.8	0.6	0.6	--	1.1	--	0.6	0.6	--
M5S_2	0.9	--	98.5	--	11.5	564.7	0.7	53.2	36.0
WM1S_2	1.8	0.6	64.4	--	42.4	619.9	--	38.2	1.2
MBP3S_4	7.1	--	533.7	--	42.8	1813.9	--	29.9	--
MBP1S_3	9.7	1.8	1981.2	--	33.4	407.8	0.6	85.7	--
MBP3S_2	3.2	--	261.9	--	27.0	1242.4	--	309.1	--
MOOR6S	2.6	--	0.9	--	30.5	159.8	0.6	66.6	--
MOOR4S	2.3	--	5.8	--	17.7	133.8	0.4	6.7	--
MBP2S	6.9	--	8.6	--	39.4	125.1	0.5	91.4	--
MBP3S	4.4	--	103.7	--	13.7	546.6	--	55.4	--
E3S	1.2	--	--	--	5.0	0.5	--	45.9	--
E4S	0.9	0.9	4.5	--	20.9	203.6	1.3	143.5	--

Table D.3 (continued).

Station ID	**MBFG_9**	**MBFG_10**	**MBFG_11a**	**MBFG_11b**	**MBFG_12**	**MBFG_13a**	**MBFG_13b**	**MGFB_14**	**MGFB_15**
	part. mL^{-1}	part. mL^{-1}	part. mL^{-1}	part. mL^{-1}	part. mL^{-1}	part. mL^{-1}	part. mL^{-1}	part. mL^{-1}	part. mL^{-1}
E5S	6.9	--	5.4	--	19.6	213.2	5.4	195.4	--
E10S	2.9	--	2.4	--	48.3	272.0	12.1	428.1	--
E11S	4.6	--	5.7	--	48.8	341.0	13.8	386.9	--
W7S	0.3	--	2.2	--	9.7	51.0	--	9.5	--
M12S	0.3	--	--	--	0.5	36.0	0.1	20.0	--
M8S	--	0.3	--	--	2.5	55.5	0.7	39.2	--
M2S	0.9	0.6	1.4	--	15.8	114.3	1.2	113.0	0.3
M3S	0.3	--	0.3	--	4.4	132.1	0.9	18.8	--
M4S	0.3	0.9	0.6	--	16.5	95.7	1.8	87.1	--
M14S	1.5	--	--	--	21.3	158.1	0.3	34.0	--
M11S	4.6	--	--	--	15.6	200.6	0.1	191.7	--
E6S	1.4	--	2.3	--	1.4	62.4	0.6	29.4	--
E7S	1.4	--	1.7	--	15.1	117.4	2.5	137.8	--
E8S	1.2	--	3.7	--	24.8	97.3	1.4	109.9	--
E2S	0.9	0.3	2.3	--	15.8	119.9	7.9	42.4	--
E9S	0.6	--	9.6	--	28.2	156.5	8.0	141.9	--
P1S	4.0	--	1.9	--	25.9	79.2	0.3	19.7	--
P2S	0.6	0.6	8.7	--	32.2	132.6	--	43.2	0.6
P3S	1.7	--	--	--	4.3	13.4	0.6	4.1	--
P9S	0.6	--	--	--	1.5	2.7	1.0	--	--

Table D.3 (continued).

Station ID	MBFG_16	MBFG_17	MBFG_18a	MBFG_18b	MBFG_18c	MBFG_19	MBFG_20a	MGFB_20b
	part. mL^{-1}	part. mL^{-1}	part. mL^{-1}	part. mL^{-1}	part. mL^{-1}	part. mL^{-1}	part. mL^{-1}	part. mL^{-1}
WM1S	--	--	3.6	3.0	--	--	1714.0	50.5
WM3S	0.3	0.3	4.5	2.1	--	--	2754.5	48.0
MOOR2S_2	--	--	--	1.2	--	--	6125.0	127.0
MOOR2S_3	--	--	2.4	0.6	--	--	705.0	39.0
W2S	--	--	2.9	4.1	--	--	174.5	3.2
W3S	--	--	2.1	2.1	0.9	--	849.0	105.0
W10S	--	--	--	1.7	--	--	426.0	11.0
M3S_2	--	3.2	3.0	4.9	--	--	20.3	28.6
M4S_2	--	0.6	2.8	5.1	0.6	--	20.0	22.0
M5S_2	--	--	0.9	2.9	--	--	423.5	23.5
WM1S_2	--	--	4.2	3.6	--	0.6	1223.0	78.0
MBP3S_4	--	--	--	1.2	--	--	1278.0	20.0
MBP1S_3	--	--	--	1.8	--	--	5572.0	190.0
MBP3S_2	--	--	--	4.5	0.7	--	5202.0	271.7
MOOR6S	--	--	1.2	3.2	0.6	--	111.0	8.5
MOOR4S	--	--	4.6	2.3	--	--	363.0	28.0
MBP2S	--	--	0.9	0.9	--	--	228.0	43.0
MBP3S	--	--	--	--	--	--	927.0	44.0
E3S	--	--	0.6	4.7	--	--	207.0	8.2
E4S	--	1.2	1.4	0.6	--	--	88.5	2.3

Table D.3 (continued).

Station ID	MBFG_16	MBFG_17	MBFG_18a	MBFG_18b	MBFG_18c	MBFG_19	MBFG_20a	MGFB_20b
	part. mL^{-1}	part. mL^{-1}	part. mL^{-1}	part. mL^{-1}	part. mL^{-1}	part. mL^{-1}	part. mL^{-1}	part. mL^{-1}
E5S	--	--	0.9	2.6	--	--	196.5	13.5
E10S	--	--	1.2	3.2	--	--	68.0	11.0
E11S	--	0.3	0.6	2.6	--	--	173.5	26.5
W7S	--	--	7.5	3.5	--	--	137.5	2.9
M12S	--	--	7.2	5.3	0.6	--	102.5	3.8
M8S	--	--	1.2	5.5	--	0.3	172.5	7.2
M2S	--	--	0.6	6.9	--	--	138.5	9.6
M3S	--	--	0.6	0.9	2.0	--	158.0	19.5
M4S	--	--	1.5	3.5	--	--	284.0	18.0
M14S	--	--	0.9	3.5	--	--	343.0	9.8
M11S	--	1.7	--	2.3	--	--	98.0	16.0
E6S	0.2	--	0.4	7.2	--	--	374.0	6.4
E7S	--	--	0.9	2.6	--	--	238.5	10.9
E8S	--	--	0.9	8.5	--	--	249.0	7.3
E2S	--	--	0.9	6.3	--	--	187.0	10.5
E9S	--	--	--	2.9	--	--	104.0	19.0
P1S	--	--	1.7	11.0	--	--	6.9	0.6
P2S	--	--	1.1	5.1	--	--	86.0	5.7
P3S	--	--	--	--	--	--	1020.0	28.0
P9S	--	--	--	--	--	--	0.6	--

Table D.4 Microplankton MBFGs Biovolume for Autumn 2015

Biovolume values were derived using the area based diameter (ABD) biovolume represent the average cell size of MBFG classified cells. Values for unclassified particles were not determined.

Station ID	**MBFG_1**	**MBFG_2**	**MBFG_3a**	**MBFG_3b**	**MBFG_4**	**MBFG_5**	**MBFG_6**	**MGFB_7**	**MGFB_8**
	$\mu m^3 cell^{-1}$	$\mu m^3 cell^{-1}$	$\mu m^3 cell^{-1}$	$\mu m^3 cell^{-1}$	$\mu m^3 cell^{-1}$	$\mu m^3 cell^{-1}$	$\mu m^3 cell^{-1}$	$\mu m^3 cell^{-1}$	$\mu m^3 cell^{-1}$
W4	134.7	5602.2	4496.8	4001.9	16865.9	--	472.0	--	--
WM6	154.3	--	2899.2	11189.9	10419.8	1260.3	837.2	--	--
W10	1300.4	13772.9	3740.3	1851.6	9092.4	--	932.7	6161.2	--
W11	1389.9	4144.0	3775.8	2094.3	8609.0	--	1154.5	13375.5	153594.6
G1	1118.4	7731.8	3205.1	--	--	1061.3	--	13270.8	--
M5	150.6	3219.8	5865.7	1686.1	--	--	854.0	--	--
M10	1375.7	9407.9	3428.0	3573.0	19741.1	--	6033.4	--	--
MBP4	1237.4	--	3033.8	3072.5	--	--	946.4	--	--
WM3	131.2	--	4353.1	1380.5	--	--	--	10771.9	299681.6
WM4	134.0	7364.1	4833.0	7846.2	--	--	--	8511.0	--
WM5	663.0	3613.5	7623.4	--	--	1027.9	--	--	--
E5	1265.2	--	9384.7	5039.0	18210.2	--	859.2	1466.2	--
ME3	1258.3	3423.5	4876.1	2721.4	8063.3	--	1061.3	--	--
W1	243.7	21026.9	4733.7	4651.7	42437.6	--	--	11042.6	41919.0
W2	148.4	7610.2	7947.2	--	--	--	977.4	--	23813.3
W3	150.6	13693.0	4531.2	2881.6	14101.8	--	1004.8	--	--
W7	154.7	--	15377.7	5531.4	--	--	1330.5	--	--
W8	1141.8	3986.5	2494.3	6784.8	--	2173.0	1837.5	--	--
W9	1514.8	--	--	--	--	--	--	--	--
M4	110.3	3691.8	4433.7	3542.9	--	--	--	--	--

Table D.4 (continued).

Station ID	MBFG_1	MBFG_2	MBFG_3a	MBFG_3b	MBFG_4	MBFG_5	MBFG_6	MGFB_7	MGFB_8
	$\mu m^3 cell^{-1}$	$\mu m^3 cell^{-1}$	$\mu m^3 cell^{-1}$	$\mu m^3 cell^{-1}$	$\mu m^3 cell^{-1}$	$\mu m^3 cell^{-1}$	$\mu m^3 cell^{-1}$	$\mu m^3 cell^{-1}$	$\mu m^3 cell^{-1}$
M9	1466.8	4792.8	4160.9	--	26704.5	--	1909.7	--	39547.5
E2	1078.7	--	5668.2	8332.9	--	--	1285.9	17139.3	--
E3	1230.5	--	9166.4	3895.3	--	--	961.2	13345.8	--
E4	1261.8	--	5946.7	2403.4	16419.3	1159.6	2098.9	8832.8	--
A7	887.1	20448.6	4518.2	3222.3	--	--	4123.1	17061.0	--
M1	182.2	2369.6	5358.4	6691.8	36879.5	--	1202.0	13038.3	14609.2
M2	1206.3	--	4063.7	2704.0	--	--	--	8748.4	5720.5
M6	1444.0	18421.9	5827.3	--	--	--	2368.0	--	8972.1
M7	1265.2	--	7700.6	--	--	--	1654.3	11164.6	--
M8	1328.8	18277.0	21429.3	1936.8	12989.5	--	1295.8	--	245.0
M11	1303.1	9953.6	9275.2	4422.1	--	--	--	--	20901.8
E1	1199.5	--	4649.3	2759.9	--	--	1174.2	--	20630.4
A5_1	1176.2	--	18019.6	--	20320.8	1447.8	--	--	--
A1_1	203.5	--	3028.2	3489.4	--	--	1502.4	3007.7	--
A2_1	1282.8	--	8636.8	--	--	--	801.5	1373.0	20546.1
A6_1	171.1	--	--	4056.1	--	--	--	--	--
A1_2	191.9	--	6787.8	--	--	--	--	--	--
A9	1448.3	--	5398.4	4862.5	--	--	1519.9	13208.4	--

Table D.4 (continued).

Station ID	MBFG_9	MBFG_10	MBFG_11a	MBFG_11b	MBFG_12	MBFG_13a	MBFG_13b	MGFB_14	MGFB_15
	$\mu m^3 cell^{-1}$	$\mu m^3 cell^{-1}$	$\mu m^3 cell^{-1}$	$\mu m^3 cell^{-1}$	$\mu m^3 cell^{-1}$	$\mu m^3 cell^{-1}$	$\mu m^3 cell^{-1}$	$\mu m^3 cell^{-1}$	$\mu m^3 cell^{-1}$
W4	1934.1	--	1937.8	--	1192.8	422.7	--	2310.0	--
WM6	1437.9	--	765.8	--	3736.9	463.1	646.3	3278.1	--
W10	2081.3	7155.8	6537.5	--	2478.6	1151.0	7103.4	8239.2	--
W11	2142.1	19640.8	2785.3	--	17945.1	1129.7	7353.4	4483.9	--
G1	1659.7	28169.3	1486.7	--	2986.3	766.4	2218.0	1470.3	--
M5	1209.3	--	453.7	--	609.4	478.9	3246.8	7674.8	--
M10	1448.1	--	1601.2	--	5853.8	1069.4	8470.7	3490.1	--
MBP4	1835.0	31932.0	11641.6	--	7727.1	1051.9	3792.9	4178.4	1416.7
WM3	1490.4	19287.3	1487.4	--	1821.1	583.0	7036.5	3263.7	--
WM4	1372.3	126468.6	870.8	--	2371.7	772.8	--	1389.3	--
WM5	1674.8	13563.1	1237.8	--	1232.8	799.1	1867.3	3017.8	--
E5	2274.2	79354.6	2828.2	--	26164.9	1989.4	12383.2	3676.6	--
ME3	1667.9	13522.9	2566.5	--	2476.2	1169.9	7978.7	9822.8	--
W1	1812.8	--	655.7	--	9026.5	1686.0	3399.2	6169.7	--
W2	1757.4	23144.4	2098.1	--	791.0	1037.7	561.7	1162.1	--
W3	1748.2	48175.7	1811.9	--	968.7	163.2	1810.5	3406.8	--
W7	3330.2	--	650.6	--	3061.2	408.3	664.7	2938.5	--
W8	1416.8	--	1067.6	--	1561.5	880.3	--	5448.2	--
W9	1904.5	29372.3	7040.0	--	--	1185.5	--	2310.8	--
M4	2107.2	--	980.0	--	1487.3	570.1	2244.5	1637.1	--

Table D.4 (continued).

Station ID	MBFG_9	MBFG_10	MBFG_11a	MBFG_11b	MBFG_12	MBFG_13a	MBFG_13b	MGFB_14	MGFB_15
	$\mu m^3 cell^{-1}$	$\mu m^3 cell^{-1}$	$\mu m^3 cell^{-1}$	$\mu m^3 cell^{-1}$	$\mu m^3 cell^{-1}$	$\mu m^3 cell^{-1}$	$\mu m^3 cell^{-1}$	$\mu m^3 cell^{-1}$	$\mu m^3 cell^{-1}$
M9	2219.7	130777.1	3054.1	--	2074.1	1288.1	7714.5	3264.0	--
E2	2258.4	8653.0	2017.9	--	2981.7	1641.4	9552.5	2161.4	--
E3	1874.8	--	6722.8	--	2174.6	1369.9	6179.0	3132.5	--
E4	2498.9	9792.8	4015.9	--	5728.9	1636.8	2027.8	4425.5	--
A7	2483.7	19847.6	9692.0	--	--	1603.5	--	49431.3	--
M1	1511.9	93827.9	805.8	--	7042.3	637.8	--	903.5	--
M2	2508.4	82247.7	738.2	--	2298.3	1373.9	--	3432.2	4420.0
M6	2740.3	--	--	--	2917.3	999.5	1188.9	3450.1	--
M7	3145.2	12431.5	12182.2	--	12969.1	1628.9	7178.5	4302.8	--
M8	2934.9	--	5248.6	--	5651.7	1608.1	3368.8	3524.6	--
M11	3287.3	13553.7	5056.9	--	1971.8	999.6	1736.7	2080.8	--
E1	1958.6	--	305.8	--	13130.2	1357.8	6716.7	2365.2	--
A5_1	2925.8	--	2772.1	--	5467.1	2072.7	2781.3	4018.6	--
A1_1	1962.3	--	791.7	--	2856.0	2616.6	32774.1	4609.9	--
A2_1	4234.4	1874.0	--	--	5658.6	1168.9	2345.7	6855.0	--
A6_1	--	--	1736.2	--	12081.5	990.7	--	--	--
A1_2	2234.5	6183.2	703.5	--	--	829.6	--	2140.9	--
A9	2079.5	298807.2	8774.5	--	10028.5	3289.5	25877.4	2073.3	--

Table D.4 (continued).

Station ID	MBFG_16	MBFG_17	MBFG_18a	MBFG_18b	MBFG_18c	MBFG_19
	$\mu m^3 cell^{-1}$	$\mu m^3 cell^{-1}$	$\mu m^3 cell^{-1}$	$\mu m^3 cell^{-1}$	$\mu m^3 cell^{-1}$	$\mu m^3 cell^{-1}$
W4	1660.2	10813.3	7431.7	--	1660.2	10813.3
WM6	930.7	6459.1	--	--	930.7	6459.1
W10	2085.2	14383.6	--	--	2085.2	14383.6
W11	1980.1	5650.9	--	--	1980.1	5650.9
G1	2167.9	9851.9	--	105240.1	2167.9	9851.9
M5	1588.9	2828.9	--	--	1588.9	2828.9
M10	2999.5	13117.1	--	--	2999.5	13117.1
MBP4	1669.4	9887.8	--	--	1669.4	9887.8
WM3	1425.7	25637.8	23717.5	142437.6	1425.7	25637.8
WM4	1549.8	11492.2	--	--	1549.8	11492.2
WM5	1176.1	11248.2	--	--	1176.1	11248.2
E5	2734.2	10842.7	--	--	2734.2	10842.7
ME3	2782.5	8099.4	--	--	2782.5	8099.4
W1	1995.7	2920.2	--	--	1995.7	2920.2
W2	1582.9	14159.2	34919.0	--	1582.9	14159.2
W3	2281.3	6041.7	--	--	2281.3	6041.7
W7	1734.6	7903.2	10145.4	--	1734.6	7903.2
W8	1998.9	14609.1	--	--	1998.9	14609.1
W9	1660.2	10813.3	7431.7	--	1660.2	10813.3
M4	930.7	6459.1	--	--	930.7	6459.1

Table D.4 (continued).

Station ID	MBFG_16	MBFG_17	MBFG_18a	MBFG_18b	MBFG_18c	MBFG_19
	$\mu m^3 cell^{-1}$	$\mu m^3 cell^{-1}$	$\mu m^3 cell^{-1}$	$\mu m^3 cell^{-1}$	$\mu m^3 cell^{-1}$	$\mu m^3 cell^{-1}$
M9	1823.1	16018.4	--	--	1823.1	16018.4
E2	2531.9	9432.0	--	--	2531.9	9432.0
E3	3951.8	10660.9	14382.0	--	3951.8	10660.9
E4	2899.4	13280.4	50392.4	--	2899.4	13280.4
A7	1797.5	5990.3	--	--	1797.5	5990.3
M1	--	5312.4	--	--	--	5312.4
M2	2568.8	15635.9	14335.6	--	2568.8	15635.9
M6	2010.8	4479.9	14982.2	--	2010.8	4479.9
M7	3252.3	7504.7	--	--	3252.3	7504.7
M8	2823.9	3635.2	--	--	2823.9	3635.2
M11	2661.2	4310.5	--	--	2661.2	4310.5
E1	2256.9	5537.3	--	--	2256.9	5537.3
A5_1	2190.9	9380.0	16588.7	105471.3	2190.9	9380.0
A1_1	2469.7	3280.2	--	--	2469.7	3280.2
A2_1	3307.0	7446.5	--	752.8	3307.0	7446.5
A6_1	2583.2	6256.1	--	--	2583.2	6256.1
A1_2	3143.1	3383.0	--	--	3143.1	3383.0
A9	3880.0	6380.9	--	--	3880.0	6380.9

Table D.5 Microplankton MBFGs Biovolume for Spring 2016

Biovolume values were derived using the area based diameter (ABD) biovolume represent the average cell size of MBFG classified cells. Values for unclassified particles were not determined.

Station ID	**MBFG_1**	**MBFG_2**	**MBFG_3a**	**MBFG_3b**	**MBFG_4**	**MBFG_5**	**MBFG_6**	**MGFB_7**	**MGFB_8**
	$\mu m^3 cell^{-1}$	$\mu m^3 cell^{-1}$	$\mu m^3 cell^{-1}$	$\mu m^3 cell^{-1}$	$\mu m^3 cell^{-1}$	$\mu m^3 cell^{-1}$	$\mu m^3 cell^{-1}$	$\mu m^3 cell^{-1}$	$\mu m^3 cell^{-1}$
WM1S	302.6	5557.0	5425.4	5426.6	--	--	--	--	--
WM3S	320.5	25022.5	2749.5	4462.5	--	--	--	--	--
MOOR2S_2	343.1	11937.7	6781.0	4940.2	--	15853.3	1385.4	--	--
MOOR2S_3	244.6	18338.6	5529.4	--	--	--	--	--	--
W2S	237.5	1463.9	8678.4	2710.8	--	--	2214.4	--	--
W3S	248.2	3634.4	6378.6	4918.2	--	--	--	5119.3	--
W10S	229.0	8365.2	7486.9	2987.5	--	--	--	--	--
M3S_2	250.2	8609.3	5988.4	5576.0	25448.8	2057.6	5081.0	--	--
M4S_2	312.8	3200.9	11674.9	2613.7	95803.1	--	--	--	--
M5S_2	352.2	6895.9	4619.6	4387.8	--	--	--	--	--
WM1S_2	332.7	3301.8	12233.9	3866.8	31405.3	6908.7	--	--	--
MBP3S_4	343.1	10552.7	9112.2	15066.9	--	--	--	--	--
MBP1S_3	164.9	4232.9	20629.6	3890.5	--	--	2042.2	--	--
MBP3S_2	243.7	22355.9	5527.7	5887.0	16140.6	--	1121.0	3307.5	--
MOOR6S	330.4	6180.8	5106.7	4756.9	--	--	--	--	--
MOOR4S	291.2	3751.3	10644.7	3690.1	202436.6	--	2397.9	--	--
MBP2S	245.2	5421.2	8935.7	2701.9	--	--	4407.8	--	--
MBP3S	263.9	18273.1	5853.6	5360.4	--	--	--	10223.0	--
E3S	206.0	--	7674.1	3369.2	--	--	1930.0	--	--
E4S	1502.2	9183.6	12678.4	4388.1	--	--	4237.5	--	--

Table D.5 (continued).

Station ID	MBFG_1	MBFG_2	MBFG_3a	MBFG_3b	MBFG_4	MBFG_5	MBFG_6	MGFB_7	MGFB_8
	$\mu m^3 cell^{-1}$	$\mu m^3 cell^{-1}$	$\mu m^3 cell^{-1}$	$\mu m^3 cell^{-1}$	$\mu m^3 cell^{-1}$	$\mu m^3 cell^{-1}$	$\mu m^3 cell^{-1}$	$\mu m^3 cell^{-1}$	$\mu m^3 cell^{-1}$
E5S	249.9	--	6554.6	4372.0	--	--	--	--	--
E10S	388.1	4115.1	12612.0	2409.0	--	--	3478.8	--	--
E11S	635.8	--	7799.9	2782.5	--	--	7178.8	--	6219.7
W7S	280.7	2706.2	5539.4	2091.6	--	--	1384.1	--	--
M12S	252.8	27285.9	7555.0	3513.4	--	--	5236.9	--	--
M8S	239.7	33611.3	14276.4	4181.3	--	--	4699.7	--	--
M2S	339.7	--	6324.0	3454.1	--	--	--	--	--
M3S	342.0	4943.3	4793.2	4964.9	25448.8	--	--	--	--
M4S	397.3	2594.1	15268.0	3270.7	--	--	4724.0	--	--
M14S	351.5	7123.9	6189.3	4513.5	--	--	--	8018.2	--
M11S	303.0	--	3975.8	--	--	3860.7	--	--	--
E6S	190.3	--	6092.1	2970.0	--	--	5452.3	--	--
E7S	237.0	--	8878.4	3236.7	--	--	6690.7	--	--
E8S	348.9	28085.7	7153.6	3066.4	--	--	4469.6	--	--
E2S	479.7	11545.8	6006.9	2839.9	--	--	3617.5	--	--
E9S	474.2	14624.8	29668.2	3833.3	--	--	--	--	--
P1S	599.6	3613.8	5192.9	3761.5	81178.7	--	3581.8	--	--
P2S	409.1	4065.6	6134.3	6980.7	--	--	14011.3	--	--
P3S	234.7	3888.9	--	4927.5	--	--	--	--	--
P9S	229.4	--	--	--	--	--	--	--	--

Table D.5 (continued).

Station ID	MBFG_9	MBFG_10	MBFG_11a	MBFG_11b	MBFG_12	MBFG_13a	MBFG_13b	MGFB_14	MGFB_15
	$\mu m^3 cell^{-1}$	$\mu m^3 cell^{-1}$	$\mu m^3 cell^{-1}$	$\mu m^3 cell^{-1}$	$\mu m^3 cell^{-1}$	$\mu m^3 cell^{-1}$	$\mu m^3 cell^{-1}$	$\mu m^3 cell^{-1}$	$\mu m^3 cell^{-1}$
WM1S	1279.6	--	521.9	--	2277.9	1042.0	1003.2	772.4	--
WM3S	1478.2	6786.8	370.3	--	1293.0	644.8	--	1764.3	--
MOOR2S_2	4103.2	--	361.6	--	1087.6	584.3	--	1098.1	600.8
MOOR2S_3	2045.5	13768.3	319.7	--	905.1	494.1	--	--	--
W2S	2580.4	60047.0	1202.3	--	827.7	1020.8	--	614.3	--
W3S	3139.6	--	320.8	--	2437.7	826.9	--	3361.2	--
W10S	10004.4	9960.4	280.1	--	2063.7	390.6	538.2	1171.0	--
M3S_2	2397.6	15837.7	742.1	--	2332.8	2627.5	1016.7	2396.9	--
M4S_2	2212.4	--	644.3	--	1747.4	1845.5	2342.0	2623.5	6805.0
M5S_2	3231.7	--	536.5	--	1571.3	1861.4	14232.9	2897.6	--
WM1S_2	2435.2	7796.8	469.8	--	2033.1	1072.7	--	1848.2	3781.2
MBP3S_4	1922.2	--	620.9	--	1803.1	1938.0	--	1916.7	--
MBP1S_3	2166.6	5339.9	592.3	--	--	--	--	--	--
MBP3S_2	1964.5	--	738.1	--	2306.8	3671.0	--	2872.6	--
MOOR6S	1783.0	--	2604.2	--	1575.3	2893.6	8436.4	2060.7	--
MOOR4S	4396.7	--	625.9	--	2560.2	1998.9	2981.0	916.5	--
MBP2S	3217.5	--	824.6	--	1580.6	1249.1	1919.8	2010.5	--
MBP3S	1857.6	--	830.9	--	3707.4	1953.9	--	1134.2	--
E3S	--	--	380.8	--	423.7	937.6	--	1079.9	--
E4S	2251.2	--	9984.6	--	2529.5	1085.8	2791.8	2174.8	15953.1

Table D.5 (continued).

Station ID	MBFG_9	MBFG_10	MBFG_11a	MBFG_11b	MBFG_12	MBFG_13a	MBFG_13b	MGFB_14	MGFB_15
	$\mu m^3 cell^{-1}$	$\mu m^3 cell^{-1}$	$\mu m^3 cell^{-1}$	$\mu m^3 cell^{-1}$	$\mu m^3 cell^{-1}$	$\mu m^3 cell^{-1}$	$\mu m^3 cell^{-1}$	$\mu m^3 cell^{-1}$	$\mu m^3 cell^{-1}$
E5S	2473.2	--	1038.9	--	1147.4	478.9	5612.7	2011.9	--
E10S	1606.0	--	1605.1	--	1156.9	1448.2	5434.1	3416.1	--
E11S	2813.1	--	894.7	--	523.7	640.0	2100.5	2006.1	--
W7S	2590.1	--	491.9	--	3522.2	1646.2	--	1412.2	--
M12S	6724.3	--	780.4	--	1908.5	1597.4	--	1556.3	--
M8S	1154.0	23324.2	489.7	--	886.6	1967.2	8900.8	2130.3	--
M2S	1604.1	16823.5	2076.4	--	2346.8	2233.3	666.1	2344.5	2764.0
M3S	2316.2	--	1166.7	--	2614.6	2654.6	1042.1	2301.5	--
M4S	1973.5	25201.6	738.9	--	517.2	442.6	--	1243.7	--
M14S	8923.3	--	967.0	--	5205.0	3100.6	2937.7	4524.7	--
M11S	1782.9	--	868.9	--	4824.5	3963.2	2182.0	2984.4	--
E6S	2446.4	--	2060.9	--	7930.1	1696.9	17436.9	1582.1	--
E7S	3759.2	2588.4	1176.2	--	2558.0	1909.1	5509.3	2447.2	--
E8S	3358.0	--	4224.4	--	1017.9	1960.5	1562.4	2328.6	--
E2S	4799.8	15454.8	1689.9	--	738.8	1371.0	3358.1	1457.1	--
E9S	2892.4	--	799.8	--	859.8	1005.8	4562.5	2709.0	--
P1S	2290.8	--	1257.6	--	976.5	2794.2	--	--	--
P2S	1718.7	18767.2	2176.9	--	2195.6	1777.0	--	1770.7	8002.2
P3S	4211.8	--	--	--	773.8	628.9	8067.3	825.1	--
P9S	1022.1	--	--	--	267.9	747.3	--	--	--

Table D.5 (continued).

Station ID	MBFG_16	MBFG_17	MBFG_18a	MBFG_18b	MBFG_18c	MBFG_19
	$\mu m^3 cell^{-1}$	$\mu m^3 cell^{-1}$	$\mu m^3 cell^{-1}$	$\mu m^3 cell^{-1}$	$\mu m^3 cell^{-1}$	$\mu m^3 cell^{-1}$
WM1S	--	--	2654.2	20409.8	--	--
WM3S	1861.2	810.4	1674.7	12457.7	--	--
MOOR2S_2	--	--	3088.7	28089.8	--	--
MOOR2S_3	--	--	--	--	--	--
W2S	--	--	1842.9	4855.7	--	--
W3S	--	--	2765.7	11159.2	34804.7	--
W10S	--	--	1521.9	21707.4	--	--
M3S_2	--	807.1	2506.1	5930.5	16057.6	--
M4S_2	--	--	1941.9	10377.9	35153.4	--
M5S_2	--	--	2911.0	10691.6	--	--
WM1S_2	--	--	8412.8	6222.7	--	213412.0
MBP3S_4	--	--	--	14303.0	--	--
MBP1S_3	--	--	--	--	--	--
MBP3S_2	--	--	--	9421.6	--	--
MOOR6S	--	331.7	3864.6	5452.5	288405.0	--
MOOR4S	--	--	2797.8	5565.0	--	--
MBP2S	--	--	2101.9	23992.1	--	--
MBP3S	--	--	--	9421.6	--	--
E3S	--	--	2802.9	3291.9	--	--
E4S	--	--	1953.6	8009.4	--	--

Table D.5 (continued).

Station ID	MBFG_16	MBFG_17	MBFG_18a	MBFG_18b	MBFG_18c	MBFG_19
	$\mu m^3 cell^{-1}$	$\mu m^3 cell^{-1}$	$\mu m^3 cell^{-1}$	$\mu m^3 cell^{-1}$	$\mu m^3 cell^{-1}$	$\mu m^3 cell^{-1}$
E5S	--	--	1455.4	5757.3	--	--
E10S	--	--	1870.2	4326.6	--	--
E11S	--	117.5	1637.9	3176.1	--	--
W7S	--	--	3282.6	5939.0	--	--
M12S	--	25217.2	2914.4	5691.1	16720.1	--
M8S	--	--	3262.6	3439.7	--	323597.9
M2S	--	2295.5	3383.2	5388.4	--	--
M3S	--	418.5	3952.4	5208.6	16057.6	--
M4S	2977.4	--	1754.1	8778.8	--	--
M14S	--	--	4238.0	7208.6	--	--
M11S	--	3478.9	4248.4	4469.5	--	--
E6S	5001.3	--	1689.2	4240.6	--	--
E7S	--	--	4065.4	4857.7	--	--
E8S	--	--	2001.0	4176.0	--	--
E2S	--	--	1441.9	4502.6	--	--
E9S	--	672.7	1148.2	4056.9	--	--
P1S	--	--	--	--	--	--
P2S	--	--	2287.1	5519.5	--	--
P3S	--	--	--	--	--	--
P9S	--	--	--	--	--	--

Table D.6 Microplankton MBFGs Area Based Diameter (ABD) for Autumn 2015

Diameter values represent the average cell diameter (μm, ABD) of MBFG classified cells. Values for unclassified particles were not determined

Station ID	**MBFG_1**	**MBFG_2**	**MBFG_3a**	**MBFG_3b**	**MBFG_4**	**MBFG_5**	**MBFG_6**	**MGFB_7**	**MGFB_8**
	μm	μm	μm	μm	μm	μm	μm	μm	μm
W4	6.9	22.1	23.9	18.8	35.5	--	10.9	--	--
WM6	7.2	--	17.7	27.1	32.7	14.3	13.3	--	--
W10	14.0	33.6	23.6	15.6	27.1	--	13.6	22.7	--
W11	14.0	21.9	21.6	16.2	26.6	--	14.3	29.7	--
G1	12.1	27.9	19.3	--	--	12.5	--	28.1	--
M5	6.8	20.6	26.6	15.2	--	--	12.3	--	--
M10	10.5	28.4	25.7	19.7	32.3	--	26.2	--	--
MBP4	13.7	--	21.1	17.2	--	--	14.8	--	--
WM3	8.7	--	22.4	14.3	--	--	--	26.2	68.2
WM4	6.8	22.7	23.4	25.0	--	--	--	21.8	--
WM5	10.1	20.7	24.5	--	--	13.8	--	--	--
E5	12.2	--	27.3	21.8	37.4	--	12.9	14.1	--
ME3	12.7	18.3	25.0	17.2	27.4	--	14.3	--	--
W1	9.7	37.0	23.8	21.0	--	--	--	28.4	48.1
W2	7.3	23.1	26.9	--	--	--	16.0	--	29.8
W3	7.1	31.1	22.8	18.3	31.4	--	15.1	--	--
W7	7.1	--	36.9	21.9	--	--	15.1	--	--
W8	13.4	--	17.5	22.1	--	18.9	16.2	--	--
W9	15.1	--	--	--	--	--	--	--	--
M4	6.4	20.2	23.8	22.5	--	--	--	--	--

Table D.6 (continued).

Station ID	MBFG_1	MBFG_2	MBFG_3a	MBFG_3b	MBFG_4	MBFG_5	MBFG_6	MGFB_7	MGFB_8
	μm	μm	μm	μm	μm	μm	μm	μm	μm
M9	6.4	--	25.1	18.8	--	--	12.1	--	--
E2	13.5	--	28.5	25.1	--	--	14.6	31.5	--
E3	12.8	--	26.1	20.9	--	--	14.0	30.7	--
E4	13.2	--	23.1	16.8	31.6	14.7	18.1	25.3	--
A7	6.6	--	--	31.6	--	--	--	--	--
M1	7.6	15.4	25.7	23.2	44.7	--	17.4	28.9	27.7
M2	13.6	--	20.8	17.6	--	--	--	25.1	21.8
M6	9.7	--	22.5	--	--	--	19.4	--	--
M7	9.8	--	29.9	--	--	--	24.7	--	--
M8	7.0	21.2	19.4	19.1	--	--	15.9	--	40.7
M11	14.0	28.8	28.0	20.6	--	--	--	--	31.3
E1	7.0	--	23.0	22.0	--	16.5	18.7	--	--
A5_1	15.0	--	--	--	33.6	--	--	--	--
A1_1	7.7	--	23.5	19.2	--	--	16.9	22.9	--
A2_1	14.2	--	31.8	--	--	--	15.3	--	35.9
A6_1	7.5	--	--	20.2	--	--	--	--	--
A1_2	14.2	--	22.6	--	--	--	14.2	--	--
A9	14.1	--	21.5	21.3	--	--	16.9	29.4	--

Table D.6 (continued).

Station ID	MBFG_9	MBFG_10	MBFG_11a	MBFG_11b	MBFG_12	MBFG_13a	MBFG_13b	MGFB_14	MGFB_15
	μm	μm	μm	μm	μm	μm	μm	μm	μm
W4	21.0	--	--	--	18.8	11.3	--	25.1	--
WM6	16.5	--	--	--	37.9	10.8	13.9	22.2	--
W10	18.8	21.9	--	--	20.0	14.8	25.1	27.0	--
W11	18.5	32.9	--	--	36.7	16.1	34.4	27.1	--
G1	1.0	40.9	--	--	32.3	15.3	20.0	19.5	--
M5	1.0	--	--	--	15.7	10.6	29.1	31.6	--
M10	16.8	56.7	--	--	25.0	12.5	46.9	22.9	--
MBP4	18.9	45.5	--	--	35.9	18.1	25.6	28.7	14.3
WM3	16.5	46.9	--	--	24.3	12.2	38.2	23.7	--
WM4	16.8	62.8	--	--	21.2	13.0	--	17.9	--
WM5	17.0	31.5	--	--	20.7	13.4	21.2	22.2	--
E5	2.5	54.3	--	--	51.8	22.7	29.8	32.1	--
ME3	16.4	35.0	--	--	26.5	26.0	35.6	43.0	--
W1	16.5	--	21.9	--	25.7	29.2	22.6	27.1	--
W2	18.6	39.9	16.3	--	17.4	17.0	14.7	21.3	--
W3	17.4	40.4	14.7	--	18.0	10.6	17.6	25.7	--
W7	22.5	--	--	--	25.3	11.5	11.1	26.3	--
W8	19.5	--	--	--	16.0	15.1	--	29.4	--
W9	16.4	44.5	--	--	--	15.4	--	20.7	--
M4	1.0	--	--	--	17.1	12.3	19.8	14.1	--

Table D.6 (continued).

Station ID	MBFG_9	MBFG_10	MBFG_11a	MBFG_11b	MBFG_12	MBFG_13a	MBFG_13b	MGFB_14	MGFB_15
	μm	μm	μm	μm	μm	μm	μm	μm	μm
M9	8.9	--	--	--	14.7	9.5	--	30.9	--
E2	17.9	26.2	--	--	24.5	23.5	--	25.2	--
E3	18.8	--	--	--	23.5	20.0	33.9	27.7	--
E4	22.0	27.5	--	--	35.0	20.2	23.6	27.7	--
A7	16.4	32.8	--	--	--	10.7	--	--	--
M1	--	60.3	--	--	30.1	14.7	--	11.5	--
M2	1.0	62.2	--	--	19.0	15.7	--	22.2	25.8
M6	15.4	--	--	--	--	12.9	22.3	19.3	--
M7	18.8	34.1	--	--	32.0	15.5	21.2	20.6	--
M8	22.1	43.1	--	--	17.5	12.3	--	12.1	--
M11	27.0	43.9	--	--	22.7	19.7	26.9	22.6	--
E1	15.0	--	--	--	37.8	13.3	--	19.7	--
A5_1	33.9	--	--	--	26.5	28.5	--	27.5	--
A1_1	19.4	--	--	--	43.7	22.5	60.4	31.6	--
A2_1	18.7	17.3	16.9	--	31.6	18.4	28.7	27.3	--
A6_1	--	--	--	--	33.6	17.4	--	--	--
A1_2	19.6	37.1	27.4	--	31.9	18.6	--	27.6	--
A9	20.3	55.2	--	--	37.2	23.5	50.5	22.2	--

Table D.6 (continued).

Station ID	MBFG_16	MBFG_17	MBFG_18a	MBFG_18b	MBFG_18c	MBFG_19
	μm	μm	μm	μm	μm	μm
W4	--	10.8	14.8	30.6	26.4	--
WM6	--	8.8	12.2	26.7	--	--
W10	--	17.1	16.7	30.0	--	--
W11	--	19.7	15.8	23.4	--	--
G1	--	15.9	16.4	29.7	--	57.2
M5	--	32.5	15.0	21.9	--	--
M10	--	17.0	16.5	26.0	--	--
MBP4	--	20.9	15.0	26.0	--	--
WM3	--	20.9	14.4	36.0	39.1	60.6
WM4	--	16.7	14.3	28.1	--	--
WM5	--	16.2	13.2	27.0	--	--
E5	--	16.2	16.6	34.8	--	--
ME3	--	16.5	17.4	25.7	--	--
W1	--	15.9	16.1	21.6	--	--
W2	--	25.9	16.0	29.8	44.9	--
W3	--	28.9	15.8	24.8	--	--
W7	--	6.4	14.7	28.3	--	--
W8	--	18.7	16.0	28.8	--	--
W9	--	19.6	15.0	23.6	--	--
M4	--	28.6	13.9	21.0	--	--

Table D.6 (continued).

Station ID	MBFG_16	MBFG_17	MBFG_18a	MBFG_18b	MBFG_18c	MBFG_19
	μm	μm	μm	μm	μm	μm
M9	--	--	14.0	19.7	--	--
E2	--	16.3	17.0	25.4	--	--
E3	--	13.1	18.9	26.3	30.6	--
E4	--	21.0	18.0	27.0	51.5	--
A7	--	16.6	16.3	21.3	--	--
M1	--	31.3	--	20.5	--	--
M2	21.1	27.5	16.4	30.1	37.9	--
M6	--	41.8	12.8	23.5	33.6	--
M7	--	21.7	18.3	25.0	--	--
M8	23.5	16.5	14.5	22.0	--	--
M11	--	20.8	16.2	26.8	--	--
E1	--	9.5	15.6	24.3	--	--
A5_1	--	--	15.8	18.9	--	62.9
A1_1	--	14.7	17.0	20.1	24.0	--
A2_1	--	15.3	17.7	26.0	--	--
A6_1	--	--	17.3	20.1	--	--
A1_2	--	16.0	13.9	39.3	--	--
A9	--	28.1	20.3	24.5	--	--

Table D.7 Microplankton MBFGs Area Based Diameter (ABD) for Spring 2016

Diameter values represent the average cell diameter (µm, ABD) of MBFG classified cells. Values for unclassified particles were not determined.

Station ID	MBFG_1	MBFG_2	MBFG_3a	MBFG_3b	MBFG_4	MBFG_5	MBFG_6	MGFB_7	MGFB_8
	µm	µm	µm	µm	µm	µm	µm	µm	µm
WM1S	8.6	27.4	22.8	22.0	--	--	--	--	--
WM3S	8.7	34.6	18.1	21.1	--	--	--	--	--
MOOR2S_2	8.5	27.2	22.7	23.0	--	--	--	--	--
MOOR2S_3	9.0	31.1	31.4	21.3	--	33.9	15.8	--	--
W2S	8.3	16.5	29.7	18.0	--	--	17.2	--	--
W3S	8.1	22.9	30.6	20.9	--	--	--	21.2	--
W10S	8.0	25.1	27.5	18.6	--	--	--	--	--
M3S_2	8.4	25.1	27.3	21.1	39.1	17.7	--	--	--
M4S_2	8.6	22.6	29.6	17.5	59.7	--	--	--	--
M5S_2	8.8	22.5	21.0	23.0	--	--	--	--	--
WM1S_2	8.5	22.2	22.1	22.0	--	--	--	--	--
MBP3S_4	8.7	--	22.9	20.3	--	--	--	--	--
MBP1S_3	7.2	27.3	31.8	19.1	--	--	18.8	--	--
MBP3S_2	7.7	25.4	22.5	22.7	33.0	--	15.8	18.4	--
MOOR6S	9.0	24.1	23.7	20.3	--	--	--	--	--
MOOR4S	8.8	19.4	29.8	20.7	72.9	--	18.4	--	--
MBP2S	8.4	20.9	27.2	18.0	--	--	21.8	--	--
MBP3S	8.4	27.5	22.9	20.3	--	--	--	26.0	--
E3S	7.8	--	28.5	18.7	--	--	17.1	--	--
E4S	14.7	28.2	30.8	20.2	--	--	22.2	--	--

Table D.7 (continued).

Station ID	MBFG_1	MBFG_2	MBFG_3a	MBFG_3b	MBFG_4	MBFG_5	MBFG_6	MGFB_7	MGFB_8
	μm	μm	μm	μm	μm	μm	μm	μm	μm
E5S	8.7	--	26.5	20.5	--	--	--	--	--
E10S	9.9	25.3	35.2	19.2	--	--	19.3	--	--
E11S	10.7	--	25.4	17.4	--	--	23.2	--	23.7
W7S	8.7	19.6	25.0	16.1	--	--	14.6	--	--
M12S	8.4	29.1	24.3	19.3	--	--	22.3	--	--
M8S	8.2	42.1	30.8	20.3	--	--	20.8	--	--
M2S	8.9	--	26.8	19.6	--	--	--	--	--
M3S	9.2	21.9	22.7	20.0	39.1	--	--	--	--
M4S	9.5	--	32.0	20.0	--	--	20.0	--	--
M14S	9.2	24.2	24.4	24.0	--	--	--	27.3	--
M11S	8.9	--	23.7	--	--	19.1	--	--	--
E6S	7.7	--	24.9	19.1	--	--	22.4	--	--
E7S	8.1	--	28.4	19.1	--	--	22.8	--	--
E8S	9.1	37.6	25.9	17.9	--	--	21.1	--	--
E2S	9.9	27.7	22.5	17.5	--	--	20.0	--	--
E9S	10.4	31.4	39.9	19.1	--	--	--	--	--
P1S	12.5	22.2	27.9	19.6	57.3	--	19.8	--	--
P2S	9.9	24.1	20.8	23.8	--	--	30.5	--	--
P3S	8.0	25.6	--	21.6	--	--	--	--	--
P9S	8.0	--	--	--	--	--	--	--	--

Table D.7 (continued).

Station ID	MBFG_9	MBFG_10	MBFG_11a	MBFG_11b	MBFG_12	MBFG_13a	MBFG_13b	MGFB_14	MGFB_15
	μm	μm	μm	μm	μm	μm	μm	μm	μm
WM1S	16.7	--	9.9	--	21.3	16.5	15.9	14.2	--
WM3S	16.8	21.8	9.3	--	16.4	13.4	--	22.2	--
MOOR2S_2	16.5	12.9	9.6	--	17.1	11.6	11.5	10.2	15.0
MOOR2S_3	23.0	--	9.8	--	17.3	12.7	--	19.9	11.5
W2S	18.8	61.3	13.1	--	16.4	17.0	--	11.1	--
W3S	20.2	--	8.4	--	21.5	14.9	--	26.5	--
W10S	30.6	21.8	9.1	--	24.2	10.2	12.1	18.7	--
M3S_2	20.1	28.0	12.0	--	21.0	25.1	27.4	27.7	--
M4S_2	17.2	--	11.1	--	18.7	21.2	33.1	27.1	24.0
M5S_2	20.5	--	10.6	--	17.7	20.7	52.7	25.7	--
WM1S_2	14.2	--	10.4	--	21.9	17.0	15.9	16.9	--
MBP3S_4	21.9	--	11.7	--	23.5	20.0	--	--	--
MBP1S_3	19.2	27.3	10.3	--	17.2	15.6	27.9	22.7	--
MBP3S_2	17.1	--	12.0	--	17.9	21.3	--	27.5	--
MOOR6S	15.7	--	17.1	--	21.5	24.8	35.2	22.2	--
MOOR4S	22.6	--	13.8	--	22.5	21.5	19.2	12.6	--
MBP2S	22.3	--	14.6	--	19.9	18.2	23.5	23.1	--
MBP3S	18.2	--	11.8	--	20.3	18.9	--	12.3	--
E3S	--	--	9.0	--	17.6	17.8	--	17.2	--
E4S	18.5	--	28.9	--	19.3	15.6	25.6	19.7	28.0

Table D.7 (continued).

Station ID	MBFG_9	MBFG_10	MBFG_11a	MBFG_11b	MBFG_12	MBFG_13a	MBFG_13b	MGFB_14	MGFB_15
	μm	μm	μm	μm	μm	μm	μm	μm	μm
E5S	19.6	--	17.3	--	21.3	15.5	36.8	21.9	--
E10S	15.7	--	14.6	--	22.0	20.3	34.6	27.8	--
E11S	19.3	--	16.2	--	13.6	16.3	25.0	23.3	--
W7S	18.3	--	11.3	--	23.0	19.1	--	18.7	--
M12S	30.0	--	11.8	--	18.4	21.6	--	18.2	--
M8S	11.6	38.3	8.7	--	20.1	24.3	35.8	23.5	--
M2S	17.6	37.8	15.6	--	22.4	25.5	13.5	26.1	17.9
M3S	19.4	--	12.7	--	24.7	23.6	24.0	23.7	--
M4S	17.4	31.2	14.0	--	14.9	18.9	18.8	22.9	--
M14S	33.5	--	9.7	--	28.0	24.9	26.2	29.5	--
M11S	16.2	--	11.1	--	25.7	27.6	20.4	25.0	--
E6S	21.7	--	22.4	--	31.5	22.7	51.7	21.9	--
E7S	21.2	16.6	14.0	--	27.0	22.5	36.9	24.7	--
E8S	22.9	--	23.6	--	18.1	22.3	18.8	22.6	--
E2S	23.5	30.0	16.8	--	16.7	20.2	24.7	20.2	--
E9S	20.4	--	13.8	--	18.6	17.8	28.9	23.2	--
P1S	20.0	--	13.6	--	15.4	23.7	33.7	22.7	--
P2S	15.0	34.8	18.9	--	21.5	21.9	--	22.0	26.5
P3S	21.6	--	--	--	15.1	17.9	38.2	14.8	--
P9S	11.7	--	--	--	10.1	15.0	--	--	--

Table D.7 (continued).

Station ID	MBFG_16	MBFG_17	MBFG_18a	MBFG_18b	MBFG_18c	MBFG_19
	μm	μm	μm	μm	μm	μm
WM1S	--	--	19.8	32.2	--	--
WM3S	15.3	10.6	15.9	27.9	--	--
MOOR2S_2	--	--	--	22.4	--	--
MOOR2S_3	--	--	18.7	38.1	--	--
W2S	--	--	15.5	28.1	--	--
W3S	--	--	18.0	31.3	45.3	--
W10S	--	--	15.4	38.2	--	--
M3S_2	--	13.5	17.4	22.6	32.4	--
M4S_2	--	--	16.3	29.7	44.2	--
M5S_2	--	--	18.0	27.6	--	--
WM1S_2	--	--	21.0	32.7	--	--
MBP3S_4	--	--	--	25.0	--	--
MBP1S_3	--	--	--	20.2	--	--
MBP3S_2	--	--	--	25.0	--	--
MOOR6S	--	9.0	19.6	22.2	78.3	--
MOOR4S	--	--	17.9	25.9	--	--
MBP2S	--	--	16.1	30.9	--	--
MBP3S	--	--	--	25.0	--	--
E3S	--	--	17.3	18.2	--	--
E4S	--	--	17.6	23.5	--	--

Table D.7 (continued).

Station ID	MBFG_16	MBFG_17	MBFG_18a	MBFG_18b	MBFG_18c	MBFG_19
	μm	μm	μm	μm	μm	μm
E5S	--	--	13.9	25.4	--	--
E10S	--	--	15.3	24.0	--	--
E11S	--	6.1	15.1	19.7	--	--
W7S	--	--	18.6	24.1	--	--
M12S	--	37.8	20.8	28.3	39.4	--
M8S	--	--	19.1	24.2	--	74.1
M2S	--	15.3	18.2	26.0	--	--
M3S	--	8.4	19.7	22.3	32.4	--
M4S	--	18.6	15.8	27.2	--	--
M14S	--	--	19.6	30.2	--	--
M11S	--	19.2	20.3	23.6	--	--
E6S	21.2	--	17.0	20.7	--	--
E7S	--	--	19.7	21.6	--	--
E8S	--	--	15.4	22.0	--	--
E2S	--	--	14.4	22.4	--	--
E9S	--	10.6	13.9	20.9	--	--
P1S	--	--	16.0	21.1	--	--
P2S	--	--	16.3	29.2	--	--
P3S	--	--	--	--	--	--
P9S	--	--	--	--	--	--

APPENDIX E–SERIAL DILUTION EXPERIMENTS

Table E.1 Serial dilution experiment chlorophyll a and net growth rate for Autumn 2015

Fraction whole seawater (WSW) with asterisk (*) is the non-nutrient augmented treatment.

Water Type	**Station ID**	**Surface Sample Depth**	**Fraction WSW**	**P_0**	**P_t**	**k_n**
		(m)	(%)	(µg Chl *a* L^{-1})	(µg Chl *a* L^{-1})	(d^{-1})
Inner-shelf	MBP4	0.9	1.00*	2.70	3.82	0.35
			1.00*	2.70	2.95	0.09
			1.00*	2.70	3.17	0.16
			1.00	2.70	4.45	0.50
			1.00	2.70	4.26	0.46
			1.00	2.70	4.11	0.42
			0.54	1.46	2.61	0.58
			0.54	1.46	2.59	0.57
			0.54	1.46	2.24	0.43
			0.08	0.21	0.51	0.89
			0.08	0.21	0.53	0.93
			0.08	0.21	0.47	0.81

Table E.1 (continued)

Water Type	**Station ID**	**Surface Sample Depth**	**Fraction WSW**	**P_0**	**P_t**	**k_n**
		(m)	(%)	(µg Chl *a* L^{-1})	(µg Chl *a* L^{-1})	(d^{-1})
Mid-shelf	W8	1.3	1.00*	0.61	1.84	1.11
			1.00*	0.61	2.00	1.19
			1.00*	0.61	2.12	1.25
			1.00	0.61	2.37	1.36
			1.00	0.61	1.76	1.06
			1.00	0.61	2.01	1.19
			0.54	0.33	1.19	1.29
			0.54	0.33	1.27	1.35
			0.54	0.33	1.22	1.31
			0.08	0.05	0.18	1.32
			0.08	0.05	0.21	1.48
			0.08	0.05	0.21	1.47

Table E.1 (continued).

Water Type	**Station ID**	**Surface Sample Depth**	**Fraction WSW**	**P_0**	**P_t**	**k_n**
		(m)	(%)	(µg Chl *a* L^{-1})	(µg Chl *a* L^{-1})	(d^{-1})
Outer-shelf	M2	1.2	1.00*	1.38	1.81	0.27
			1.00	1.38	1.76	0.24
			0.65	0.90	1.38	0.43
			0.35	0.48	0.67	0.32
			0.05	0.07	0.13	0.62
			0.05	0.07	0.15	0.76
			0.05	0.07	0.20	1.04
Outer-shelf	A6_1	0.5	1.00*	0.60	0.25	-0.89
			1.00*	0.60	0.28	-0.76
			1.00*	0.60	0.31	-0.65
			1.00	0.60	0.68	0.12
			1.00	0.60	0.36	-0.52
			1.00	0.60	0.46	-0.27
			0.10	0.06	0.02	-0.91
			0.10	0.06	0.04	-0.50
			0.10	0.06	0.03	-0.83

Table E.1 (continued).

Water Type	**Station ID**	**Surface Sample Depth**	**Fraction WSW**	**P_0**	**P_t**	**k_n**
		(m)	(%)	(µg Chl *a* L^{-1})	(µg Chl *a* L^{-1})	(d^{-1})
Outer-shelf	A1_2	1.2	1.00*	0.80	0.96	0.19
			1.00*	0.80	0.95	0.17
			1.00*	0.80	0.87	0.08
			1.00	0.80	0.84	0.04
			1.00	0.80	1.00	0.22
			1.00	0.80	1.10	0.32
			0.54	0.43	0.61	0.34
			0.54	0.43	0.62	0.36
			0.54	0.43	0.63	0.39
			0.08	0.06	0.09	0.41
			0.08	0.06	0.10	0.52
			0.08	0.06	0.11	0.55

Table E.2 Serial dilution experiment chlorophyll a and net growth rate for Spring 2016

Fraction whole seawater (WSW) with asterisk (*) is the non-nutrient augmented treatment.

Water Type	**Station ID**	**Surface Sample Depth**	**Fraction WSW**	**P_0**	**P_t**	**k_n**
		(m)	(%)	(µg Chl *a* L^{-1})	(µg Chl *a* L^{-1})	(d^{-1})
Estuarine	MOOR2S_2	0.5	1.00*	9.46	9.08	-0.04
			1.00*	9.46	9.10	-0.04
			1.00	8.60	16.13	0.63
			1.00	8.60	15.28	0.57
			0.50	4.30	9.12	0.75
			0.50	4.30	8.97	0.74
			0.05	0.43	0.88	0.72
Estuarine	MOOR2S_3	0.5	0.05	0.43	1.18	1.01
			1.00*	9.69	7.08	-0.31
			1.00*	9.69	6.85	-0.35
			1.00	5.59	11.95	0.76
			1.00	5.59	13.82	0.91
			0.50	2.80	1.46	-0.65
			0.50	2.80	4.13	0.39
			0.05	0.28	0.39	0.32
			0.05	0.28	0.44	0.46

Table E.2 (continued).

Water Type	**Station ID**	**Surface Sample Depth**	**Fraction WSW**	**P_0**	**P_t**	**k_n**
		(m)	(%)	(µg Chl *a* L^{-1})	(µg Chl *a* L^{-1})	(d^{-1})
Inner-shelf	M3S_2	2.2	1.00*	7.29	3.84	-0.64
			1.00*	7.29	3.71	-0.67
			1.00*	7.29	4.08	-0.58
			1.00	6.68	16.15	0.88
			1.00	6.68	16.42	0.90
			1.00	6.68	15.42	0.84
			0.50	3.34	8.84	0.97
Inner-shelf	MBP3S_4	2.7	0.50	3.34	9.37	1.03
			0.50	3.34	9.68	1.06
			0.05	0.33	1.30	1.36
			0.05	0.33	0.52	0.45
			0.05	0.33	1.37	1.41
			1.00*	2.93	4.94	0.52
			1.00*	2.93	4.89	0.51
			1.00*	2.93	4.96	0.53
			1.00	3.15	3.08	-0.02

Table E.2 (continued).

Water Type	Station ID	Surface Sample Depth	Fraction WSW	P_0	P_t	k_n
		(m)	(%)	(µg Chl *a* L^{-1})	(µg Chl *a* L^{-1})	(d^{-1})
Mid-shelf	MOOR6S	2.6	1.00*	0.80	0.83	0.04
			1.00*	0.80	0.79	-0.01
			1.00*	0.80	0.68	-0.16
			1.00	0.80	2.06	0.95
			1.00	0.80	1.81	0.82
			1.00	0.80	1.21	0.41
			0.50	0.40	3.30	2.11
			0.50	0.40	3.17	2.07
			0.50	0.40	3.20	2.08
			0.05	0.04	0.41	2.33
			0.05	0.04	0.30	2.00
			0.05	0.04	0.21	1.68
Mid-shelf	E4S	2.0	1.00*	2.32	2.47	0.06
			1.00*	2.32	2.56	0.10
			1.00	2.50	2.30	-0.08
			1.00	2.50	2.58	0.03
			1.00	2.50	2.78	0.11
			0.05	0.13	0.20	0.47
			0.05	0.13	0.19	0.42
			0.05	0.13	0.16	0.25

Table E.2 (continued).

Water Type	Station ID	Surface Sample Depth	Fraction WSW	P_0	P_t	k_n
Outer-shelf	P1S	1.9	1.00*	1.43	1.27	-0.12
			1.00*	1.43	1.11	-0.25
			1.00*	1.43	1.17	-0.20
			1.00	1.55	12.40	2.08
			1.00	1.55	12.82	2.11
			1.00	1.55	12.46	2.08
			0.50	0.78	7.67	2.29
			0.50	0.78	7.07	2.21
			0.50	0.78	7.83	2.31
			0.05	0.08	1.02	2.58
			0.05	0.08	0.93	2.48
			0.05	0.08	0.74	2.26

Table E.2 (continued).

Water Type	Station ID	Surface Sample Depth	Fraction WSW	P_0	P_t	k_n
Outer-shelf	P2S	1.8	1.00*	2.15	1.30	-0.50
			1.00*	2.15	1.34	-0.47
			1.00*	2.15	1.52	-0.35
			1.00	1.93	7.91	1.41
			1.00	1.93	14.65	2.03
			1.00	1.93	8.83	1.52
			0.50	0.97	9.18	2.25
			0.50	0.97	7.15	2.00
			0.50	0.97	4.59	1.56
			0.05	0.10	1.06	2.39
			0.05	0.10	1.04	2.38
			0.05	0.10	0.94	2.27

APPENDIX F-SPEARMAN'S RANK CORRELATION ANALYSIS

Table F.1 Spearman's rank correlation analysis for Autumn 2015

Correlation is significant at the 0.01 level (**) and 0.05 level (*) (2-tailed).

Autumn	Temp	Sal	BruntVais	PARSSC	Chla	NOx	NH4	PO4	SiOH4	lg5POC	sm5POC	lg5PON	sm5PON
Temp	1												
Sal	.942**	1											
BruntVais	-.709**	-.701**	1										
PARSSC	.516**	.436**	-0.242	1									
Chla	-.792**	-.819**	.496**	-.547**	1								
NOx	-0.058	-0.031	-0.01	-0.023	0.031	1							
NH4	-0.294	-0.289	-0.099	-0.029	0.36	-0.114	1						
PO4	-0.245	-.354*	0.216	0.074	.331*	-.546**	.706**	1					
SiOH4	-.713**	-.803**	.554**	-.398*	.725**	0.102	0.434	.410*	1				
lg5POC	-.364*	-.438*	0.321	-.419*	.490**	0.087	0.238	0.25	.518**	1			
sm5POC	-0.158	-0.103	0.221	-0.137	0.243	-0.16	0.288	0.042	-0.005	0.037	1		
lg5PON	-0.189	-0.265	0.299	-.399*	.366*	-0.106	0.233	0.192	.382*	.891**	0.006	1	
sm5PON	-0.058	-0.038	0.054	-0.204	.368*	-0.23	0.347	0.117	-0.122	0.067	.919**	0.14	1
lg5Chla	-0.307	-0.325	0.072	-.455**	.556**	-0.182	0.377	.368*	.374*	.580**	0.295	.502**	.510**
sm5Chla	-0.119	-0.158	0.216	-0.153	0.229	-0.111	0.326	.398*	0.161	.370*	-0.057	.422*	0.157
lg5PP	-.586**	-.554**	.401*	-.458*	.512**	0.099	0.023	0.065	0.34	0.323	0.251	0.098	0.081
sm5PP	-.416*	-0.282	0.363	-.408*	0.296	0.06	-0.159	0.035	0.05	0.185	0.023	0.114	0.054
C_{BV}nano	-.695**	-.705**	.690**	-.359*	.634**	-0.206	0.134	.388*	.618**	0.29	.348*	0.241	0.293
C_{BV}flag	-.333*	-0.257	0.31	-0.066	0.271	-.406*	0.109	0.229	0.157	0.025	0.267	-0.065	0.203
C_{BV}diatoms	-.469**	-.468**	.327*	-0.252	.497**	-0.025	-0.039	0.072	0.298	0.221	0.005	0.003	0.005
C_{BV}mzp	-.468**	-.373*	0.307	-0.276	.364*	-0.015	-0.215	0.033	0.298	0.167	-0.284	0.166	-0.173

Table F.1 (continued)

Autumn	**lg5Chla**	**sm5Chla**	**lg5PP**	**sm5PP**	**C_{BV}nano**	**C_{BV}flag**	**C_{BV}diatoms**	**C_{BV}mzp**
lg5Chla	1							
sm5Chla	.578**	1						
lg5PP	0.361	0.144	1					
sm5PP	0.248	0.297	.655**	1				
C_{BV}nano	.358*	0.134	.494**	0.172	1			
C_{BV}flag	0.146	0.061	0.291	0.238	0.259	1		
C_{BV}diatoms	0.194	0.095	.657**	.371*	.329*	.408*	1	
C_{BV}mzp	0.08	0.048	0.292	.400*	.370*	.337*	.497**	1

Table F.2 Spearman's rank correlation analysis for Spring 2016

Correlation is significant at the 0.01 level (**) and 0.05 level (*) (2-tailed).

Spring	Temp	Sal	BruntVais	PARSSC	Chla	NOx	NH4	PO4	SiOH4	lg5POC	sm5POC	lg5PON	sm5PON
Temp	1												
Sal	-0.098	1											
BruntVais	0.068	-.952**	1										
PARSSC	-0.173	-0.122	0.218	1									
Chla	-0.047	-.850**	.850**	0.209	1								
NOx	-0.162	-0.197	0.279	-0.09	0.315	1							
NH4	-0.065	-0.024	0.041	-0.046	0.034	0.025	1						
PO4	0.247	.359*	-0.309	-0.178	-0.16	-0.071	-0.014	1					
SiOH4	-0.035	-.675**	.695**	0.033	.681**	.605**	0.019	-0.243	1				
lg5POC	-0.208	-.858**	.895**	0.389	.899**	0.304	0.433	-0.253	.854**	1			
sm5POC	-0.039	0.053	-0.073	-.622**	-0.032	0.171	-0.181	-0.135	-0.104	-0.003	1		
lg5PON	-0.261	-.843**	.886**	0.408	.849**	0.357	0.289	-0.362	.817**	.976**	0.074	1	
sm5PON	-0.124	0.178	-0.14	-0.246	-0.051	.640*	-0.243	0.07	0.118	-0.058	.598**	0.026	1
lg5Chla	-0.072	-.832**	.871**	0.366	.912**	0.258	.619*	-0.208	.698**	.785**	-0.153	.767**	0.112
sm5Chla	-0.275	-.663**	.698**	.472*	.609**	0.138	0.333	-.556*	.503*	.651**	-0.164	.629**	-0.025
lg5PP	-0.158	-.759**	.717**	0.108	.752**	-0.064	-0.048	-.364*	.475**	.623**	-0.083	.630**	-0.216
sm5PP	-0.207	-0.297	0.297	0.01	0.306	-0.178	0.115	-0.083	0.183	0.104	-0.01	0.08	-0.153
C_{BV}nano	-0.152	-.438**	.478**	0.265	.599**	0.028	0.104	-0.021	.396*	.670**	-0.282	.563*	-0.364
C_{BV}flag	.386*	0.023	-0.075	-0.228	-0.107	-0.295	-.433*	-0.098	-0.248	-0.443	0.243	-0.443	-0.145
C_{BV}diatoms	-.469**	-.468**	.327*	-0.252	.497**	-0.025	-0.039	0.072	0.298	0.221	0.005	0.003	0.005
C_{BV}mzp	-.468**	-.373*	0.307	-0.276	.364*	-0.015	-0.215	0.033	0.298	0.167	-0.284	0.166	-0.173

Table F.2 (continued).

Spring	**lg5Chla**	**sm5Chla**	**lg5PP**	**sm5PP**	**C_{BV}nano**	**C_{BV}flag**	**C_{BV}diatoms**	**C_{BV}mzp**
lg5Chla	1							
sm5Chla	.829**	1						
lg5PP	.541*	.629**	1					
sm5PP	0.143	0.133	.449**	1				
C_{BV}nano	.747**	0.33	.412*	0.211	1			
C_{BV}flag	-.568*	-0.414	0.018	-0.083	-.365*	1		
C_{BV}diatoms	0.194	0.095	.657**	.371*	.329*	.408*	1	
C_{BV}mzp	0.08	0.048	0.292	.400*	.370*	.337*	.497**	1

Table F.3 Spearmans rank correlation analysis for estuarine and inner-shelf waters

Correlation is significant at the 0.01 level (**) and 0.05 level (*) (2-tailed).

Estuarine & Inner Shelf	Temp	Sal	BruntVais	PARSSC	Chla	NOx	NH4	PO4	SiOH4	lg5POC	sm5POC	lg5PON	sm5PON
Temp	1												
Sal	.870**	1											
BruntVais	-.850**	-.958**	1										
PARSSC	-.675**	-.713**	.724**	1									
Chla	-.878**	-.800**	.803**	.700**	1								
NOx	-.548**	-.526**	.553**	0.279	.667**	1							
NH4	-0.256	-0.356	0.324	0.379	.525*	0.14	1						
PO4	.667**	.574**	-.562**	-.436*	-.536**	-.463*	0.154	1					
SiOH4	-.813**	-.843**	.834**	.675**	.831**	.609**	.566*	-.481*	1				
lg5POC	-.781**	-.865**	.886**	.641**	.900**	.561*	0.542	-0.438	.824**	1			
sm5POC	0.287	0.219	-0.217	-0.383	-0.029	0.042	0.236	0.3	-0.206	-0.113	1		
lg5PON	-.773**	-.833**	.853**	.635**	.898**	.570*	0.499	-.508*	.815**	.975**	-0.116	1	
sm5PON	0.42	0.376	-0.351	-0.356	-0.168	0.056	0.176	0.317	-0.316	-0.267	.830**	-0.242	1
lg5Chla	-.717**	-.828**	.851**	.732**	.860**	.507*	.741**	-0.237	.744**	.891**	-0.018	.879**	-0.08
sm5Chla	-.602**	-.740**	.797**	.579**	.659**	0.24	0.505	-0.24	.593**	.766**	-0.17	.742**	-0.104
lg5PP	-.610**	-.517**	.548**	0.304	.487*	0.228	-0.061	-0.396	0.387	.454*	-0.051	0.404	-0.136
sm5PP	-0.355	-.423*	.523**	0.139	0.283	0.208	0.01	-0.35	0.269	0.339	0.099	0.319	-0.005
C_{BV}nano	-.857**	-.903**	.908**	.664**	.865**	.621**	.510*	-.452*	.858**	.858**	-0.068	.834**	-0.265
C_{BV}flag	-.609**	-.676**	.673**	.644**	.659**	.525**	0.275	-.537**	.610**	.649**	-0.123	.708**	-0.172
C_{BV}diatoms	-.780**	-.701**	.723**	.739**	.853**	.455*	.571*	-.486*	.675**	.740**	-0.18	.711**	-0.302
C_{BV}mzp	0.057	0.112	-0.162	-0.286	-0.184	-0.127	-.605*	-0.133	-0.398	-0.346	0.013	-0.341	-0.029

Table F.3 (continued).

Estuarine & Inner Shelf	**lg5Chla**	**sm5Chla**	**lg5PP**	**sm5PP**	**C_{BV}nano**	**C_{BV}flag**	**C_{BV}diatoms**	**C_{BV}mzp**
lg5Chla	1							
sm5Chla	.789**	1						
lg5PP	0.286	.528*	1					
sm5PP	0.125	.463*	.663**	1				
C_{BV}nano	.826**	.644**	.500*	0.394	1			
C_{BV}flag	.605**	0.353	0.213	0.104	.635**	1		
C_{BV}diatoms	.700**	.595**	.489*	0.211	.744**	.670**	1	
C_{BV}mzp	-.511*	-0.328	-0.08	0.104	-0.143	-0.168	-0.27	1

Table F.4 Spearman's correlation analysis for mid-shelf waters

Correlation is significant at the 0.01 level (**) and 0.05 level (*) (2-tailed).

Mid Shelf	Temp	Sal	BruntVais	PARSSC	Chla	NOx	NH4	PO4	SiOH4	lg5POC	sm5POC	lg5PON	sm5PON
Temp	1												
Sal	.915**	1											
BruntVais	-.755**	-.689**	1										
PARSSC	-.491*	-.481*	.457*	1									
Chla	-.655**	-.734**	0.362	0.079	1								
NOx	-0.403	-.521*	0.189	0.012	.563*	1							
NH4	-0.338	-0.256	0.315	-0.132	0.329	0.07	1						
PO4	.573**	.528*	-0.299	-0.385	-0.429	-.520*	-0.24	1					
SiOH4	0.093	-0.038	0.044	0.235	-0.148	0.118	-0.196	-0.129	1				
lg5POC	-0.192	-0.395	0.38	0.409	0.495	0.148	0.214	-0.21	0.116	1			
sm5POC	-0.138	0.102	0.277	-0.221	-0.196	-0.137	-0.429	-0.075	0.108	0.101	1		
lg5PON	-0.171	-0.325	0.464	0.34	0.389	0.036	0.252	-0.129	0.117	.955**	0.205	1	
sm5PON	0.067	0.277	0.143	-0.331	0.028	-0.172	-0.464	-0.051	-0.242	0.143	.934**	0.243	1
lg5Chla	-0.1	0.033	-0.059	0.204	0.477	0.297	0.771	-0.172	-0.319	0.407	-0.294	0.281	-0.151
sm5Chla	-.599*	-.560*	0.472	.631**	.675**	0.497	0.381	-0.266	0.171	0.451	0.035	0.452	0.139
lg5PP	-.657**	-.557*	0.309	0.233	.628**	0.176	0.133	-.651**	-0.135	0.217	0.28	0.147	0.311
sm5PP	-0.409	-0.141	0.236	-0.056	0.286	-0.135	0.433	-0.251	-0.294	-0.154	-0.221	-0.224	-0.037
C_{BV}nano	-0.341	-0.354	.558**	0.017	0.414	0.154	0.161	-0.289	-0.036	.609*	-0.051	.620*	0.014
C_{BV}flag	-0.296	-0.195	0.356	0.187	0.2	-0.176	-0.091	0.095	-0.083	0.451	.600*	0.434	0.572
C_{BV}diatoms	-.661**	-.567**	0.343	0.291	.665**	0.079	0.231	-0.381	-0.371	.534*	-0.106	0.453	-0.085
C_{BV}mzp	0.359	0.407	-0.149	0.139	-0.308	-.519*	-0.503	0.373	0.073	-0.015	-0.343	0.015	-0.229

Table F.4 (continued).

Mid Shelf	**lg5Chla**	**sm5Chla**	**lg5PP**	**sm5PP**	**C_{BV}nano**	**C_{BV}flag**	**C_{BV}diatoms**	**C_{BV}mzp**
lg5Chla	1							
sm5Chla	.682**	1						
lg5PP	.601*	.564*	1					
sm5PP	0.497	0.253	.503*	1				
C_{BV}nano	0.231	0.439	0.43	0.267	1			
C_{BV}flag	0.22	0.214	0.418	0.185	0.144	1		
C_{BV}diatoms	0.336	0.262	.595**	0.375	0.27	.447*	1	
C_{BV}mzp	-0.024	-0.206	-0.29	-0.141	0.134	0.083	-0.035	1

Table F.5 Spearman's rank correlation analysis for outer-shelf waters

Correlation is significant at the 0.01 level (**) and 0.05 level (*) (2-tailed).

Outer Shelf	Temp	Sal	BruntVais	PARSSC	Chla	NOx	NH4	PO4	SiOH4	lg5POC	sm5POC	lg5PON
Temp	1											
Sal	.700**	1										
BruntVais	-.630**	-.888**	1									
PARSSC	-0.117	0.304	-0.246	1								
Chla	-.674**	-.864**	.801**	-0.189	1							
NOx	-0.207	-0.052	0.074	0.032	0.01	1						
NH4	-.449*	-.493*	.441*	-0.237	0.406	-0.149	1					
PO4	0.37	0.226	-0.254	-0.118	-0.198	-.386*	-0.326	1				
SiOH4	.443*	0.267	-0.36	-0.286	-0.231	0.307	-0.392	0.345	1			
lg5POC	-.548*	-.633**	0.258	-0.058	.713**	0.252	0.101	0.089	0.523	1		
sm5POC	-0.004	-0.08	0.1	-0.151	0.245	-.568*	0.293	-0.164	-0.218	-0.017	1	
lg5PON	-0.382	-0.496	0.329	-0.118	.521*	-0.047	-0.013	0.242	0.345	.798**	-0.149	1
sm5PON	0.048	0.275	-0.439	0.179	0.249	-.579*	-0.034	0.012	0.063	-0.135	.642*	-0.281
lg5Chla	-.760**	-.813**	0.453	-.554*	.721**	-0.034	0.255	0.331	0.25	.627**	0.162	0.481
sm5Chla	-0.285	-0.337	0.237	-.510*	0.278	-0.091	0.005	0.398	-0.029	0.263	-0.21	0.27
lg5PP	-.498*	-.886**	.832**	-0.309	.920**	-0.057	0.307	-0.108	-0.255	.842**	0.33	0.575
sm5PP	-0.411	-0.401	.512*	-0.144	0.413	-0.157	0.08	0.177	-0.367	0.539	-0.33	0.386
C_{BV}nano	-.715**	-.676**	.668**	-0.35	.647**	0.218	0.354	-0.284	-0.139	0.15	0.431	0.143
C_{BV}flag	-.514**	-.629**	.554**	-0.301	.514**	0.072	0.269	-0.297	-0.208	0.265	0.159	0.035
C_{BV}diatoms	-.706**	-.724**	.727**	-0.142	.713**	0.191	0.172	-0.262	-0.333	.506*	-0.002	0.264
C_{BV}mzp	-0.291	-.443*	0.366	-0.244	0.378	0.034	0.062	-0.063	-0.161	0.049	-0.123	0.06

Table F.5 (continued).

Outer Shelf	lg5Chla	sm5Chla	lg5PP	sm5PP	C_{BV}nano	C_{BV}flag	C_{BV}diatoms	C_{BV}mzp
lg5Chla	1							
sm5Chla	.713**	1						
lg5PP	.876**	0.317	1					
sm5PP	.776**	.653*	.500*	1				
C_{BV}nano	.647**	0.212	.550**	0.291	1			
C_{BV}flag	.612**	0.299	.548**	0.017	.660**	1		
C_{BV}diatoms	.630**	0.333	.729**	.491*	.625**	.718**	1	
C_{BV}mzp	0.253	0.043	0.342	0.245	0.31	.606**	0.322	1

REFERENCES

Ajani P. A., A.P. Allen, T. Ingleton, L. Armand L. (2014). "A decadal decline in relative abundance and a shift in microphytoplankton composition at a long-term coastal station off southeast Australia." *Limnology and Oceanography*, 59:519-531.

Álvarez E, Á. López-Urrutia, E. Nogueira. (2012). "Improvement of plankton biovolume estimates derived from image-based automatic sampling devices: application to FlowCAM." *Journal of Plankton Research*, 34:454-469.

Álvarez, E., Á. López-Urrutia, E. Nogueira, S. Fraga. (2011). "How to effectively sample the plankton size spectrum? A case study using FlowCAM." *Journal of Plankton Research*, 33:1119-1133.

Álvarez, E., M. Moyano, Á. López-Urrutia, E. Nogueira, R. Scharek. (2013). "Routine determination of plankton community composition and size structure: a comparison between FlowCAM and light microscopy." *Journal of Plankton Research*, 36(1): 170-184.

Anderson, D. M., J. M. Burkholder, W. P. Cochlan, P. M. Gilbert, C. J. Gobler, C. A. Heil, R. Kudela, M. L. Parsons, J. E. Jack Rensel, D. W. Townsend, V. L. Trainer, and G. A. Vargo. (2008). "Harmful algal blooms and eutrophication: examining linkages from selected coastal regions of the United States." *Harmful Algae*. 8(1): 39-53.

Azam, F., T. Fenchel, J. Field, J. Gray, L. Meyer-Reil, F. Thinstad. (1983). "The ecological role of water-column microbes in the sea." *Marine Ecology Progress Series*, 10: 257-263.

Banas, N. S. (2009). "The Columbia River plume as along-shelf barrier and cross-shelf

exporter: a Lagrangian model study." *Continental Shelf Research*. 29: 292-301.

Banse, K. (1992). "Grazing, temporal changes of phytoplankton concentrations, and the microbial loop in the open sea." In: Falkowski, P. and A. D. Woodhead (eds) *Primary Productivity and Biogeochemical Cycles in the Sea*. New York: Plenum. 550pp.

Bargu, S., M. M. Baustian, N. N. Rabalais, R. Del Rio, B. Von Korff, and R. E. Turner. (2016). "Influence of the Mississippi River on *Pseudo-nitzschia* spp abundance and toxicity in Louisiana coastal waters. *Estuaries and Coasts,* 39(5): 1345-1356.

Beers, J. R. and G. L. Stewart. (1969). "Microzooplankton and its abundance relative to the larger zooplankton and other seston components." *Marine Biology,* 4: 182-189.

Beers, J. R., F. M. H. Reid, and G. L. Stewart. (1980). "Microplankton population structure in Southern California nearshore waters in late spring." *Marine Biology,* 60 (2): 209-226.

Bianchi, T. and M. Argyrou. (1997). "Temporal and spatial dynamics of particulate organic carbon in the Lake Pontchartrain estuary, southeast Louisiana, U.S.A." *Estuaries, Coasts and Shelf Science,* 45: 165-176.

Boyer, J. N., R. R. Christian, D. W. Stanley. (1993). "Patterns of phytoplankton primary production in the Neuse River estuary, North Carolina, USA." *Marine Ecology Progress Series*, 97: 287-297.

Brand, L. E., L. Campbell, and E. Bresnan. (2012). "*Karenia*: the biology and ecology of a toxic genus." *Harmful Algae,* 14:156-178.

Brzezinski, M. A. and L. Washburn. (2011). "Phytoplankton primary productivity in the

Santa Barbara Channel: effects of wind-driven upwelling and mesoscale eddies." *Journal of Geophysical Research*, 116(C12).

Butrón, A., A. Iriarte, I. Madariaga. (2009). "Size-fractionated phytoplankton biomass, primary production and respiration in the Nervión-Ibaizabal estuary: A comparison with other nearshore coastal and estuarine ecosystems from the Bay of Biscay." *Continental Shelf Research,* 29(8): 1088-1102.

Bury, S. J., P. W. Boyd, T. Preston, G. Savidge, and N. J. P. Owens. (2001). "Size-fractionated primary production and nitrogen uptake during a North Atlantic phytoplankton bloom: implications for carbon export estimates." *Deep Sea Research I,* 48: 689-720.

Caffrey, J. M. (2004). "Factors controlling net ecosystem metabolism in U. S. estuaries." *Estuaries*. 27(1): 90-101.

Caffrey, J. M., M. C. Murrell, K. S. Amaacker, J. W. Harper, S. Phipps, M. S. Woodrey. (2014). "Seasonal and inter-annual patterns in primary production, respiration, and net ecosystem metabolism in three estuaries in the northeast Gulf of Mexico." *Estuaries and Coasts*, 37: 222-241.

Cai, W. J., M. Dai, Y. Wang, W. Zhai, T. Huang, S. Chen, F. Zhang, Z. Chen, Z. Wang. (2004). "The biogeochemistry of inorganic carbon and nutrients in the Pearl River estuary and the adjacent Northern South China Sea." *Continental Shelf Research*, 24(12): 1301-1319.

Calbet, A. (2008). "The trophic roles of microzooplankton in marine systems." *ICES Journal of Marine Science*: *Journal Du Conseil* 65 (3): 325-331.

Calbet, A. and M. R. Landry. (2004). "Phytoplankton growth, microzooplankton grazing,

and carbon cycling in marine systems." *Limnology and Oceanography*, 49(1): 51-57.

Calbet, A., I. Trepat, R. Almeda, V. Salo, E. Sais, J. I. Movilla, M. Alcaraz, L. Yebra, R. Simo. (2008). “Impact of mico- and nanograzers on phytoplankton assessed by standard and size-fractionated dilution grazing experiments.” *Aquatic Microbial Ecology*, 50: 145-156.

Calbet, A. and E. Saiz.(2013). "Effects of trophic cascades in dilution grazing experiments: from artificial saturated feeding responses to positive slopes." *Journal of Plankton Research*, 35(6): 1183-1191.

Calijuri, Md. C., A. Dos Santos, A. Jati. (2002). “Temporal changes in the phytoplankton community structure in a tropical and eutrophic reservoir (Barra Bonita, SP—Brazil).” *Journal of Plankton* Research, 24:617-634.

Cambazoglu, M. K., I. M. Soto, S. D. Howden, B. Dzwonkowski, P. J. Fitzpatrick, R. A. Arnone, G. A. Jacobs, and Y. Lau. (2017). “Inflow of shelf waters into the Mississippi Sound and Mobile Bay estuaries in October 2015.” *Journal of Applied Remote Sensing*, 11 (3): 032410. doi:http://dx.doi.org/10.1117/1.JRS.11.032410.

Cermeño, P. E. Marañon, J. Rodriguez, E. Fernandez. (2005). “Large-sized phytoplankton sustain higher carbon-specific photosynthesis than smaller cells in a coastal eutrophic ecosystem.” *Marine Ecology Progress Series*, 297: 51-60.

Chakraborty, S and S. L. Lohrenz. (2015). “Phytoplankton community structure in the river-influenced continental margin of the northern Gulf of Mexico.” *Marine Ecology Progress Series* 521:31-47.

Chen, X., S. E. Lohrenz, and D. A. Wiesenburg. (2000). “Distribution and controlling

mechanisms of primary production on the Louisiana–Texas continental shelf." *Journal of Marine Systems*, 25 (2): 179-207.

Chen, Y. L., H. Y. Chen, G. C. Gong, Y. H. Lin, S. Jan, M. Takahashi. (2004). "Phytoplankton production during a summer coastal upwelling in the East China Sea." *Continental Shelf Research*, 24: 1321-1338.

Chisholm, S. W. (1992). "Phytoplankton size," In: Falkowski, P.G., Woodhead, A. D., Vivirito K. (eds), *Primary Productivity and Biogeochemical Cycles in the Sea*. Environmental Science Research 43. Springer, Boston, MA.

Christaki, U., C. Courties, F. Joux, W. H. Jeffrey, J. Neveux, J. Naudin. (2009). Community structure and trophic role of ciliates and heterotrophic nanoplankton in Rhone River diluted mesoscale structures (NW Mediterranean Sea)." *Aquatic Microbial Ecology*, 57:263-277

Cifuentes, L., R. Coffin, J. Morin, T. Bianchi, P. Eldrigde. (1999). "Particulate organic matter in the Gulf of Mexico estuaries – implications for net heterotrophy." In: Bianchi, T., J. Pennock, R. Twilley (eds) *Biogeochemistry of Gulf of Mexico Estuaries*. John Wiley and Sons.

Cloern, J. (1996). "Phytoplankton bloom dynamics in coastal ecosystems: a review with some general lessons from sustained investigation of San Francisco Bay, California." *Reviews of Geophysics*, 34(2): 127-168.

Cloern, J. (2018). "Why large cells dominate estuarine phytoplankton." *Limnology and Oceanography*, 63: 392-409.

Cloern, J. E. and A. D. Jassby. (2010). "Patterns and scales of phytoplankton variability in estuarine–coastal ecosystems." *Estuaries and Coasts*, 33:230-241.

Cloern, J., S. Q. Foster, A. E. Kleckner. (2014). “Phytoplankton primary production in the world’s estuarine-coastal ecosystems.” *Biogeosciences,* 11: 2477-2501.

Conroy, B. J., J. Brandon, D. K. Steinberg, M. R. Stukel, J. I. Goes, V. J. Coles. (2016). “Meso- and microzooplankton grazing in the Amazon River plume and western tropical North Atlantic.” *Limnology and Oceanography*, 61(3): 825-840.

Côté, B. and T. Platt. (1984). “Utility of the light-saturation curve as an operation model for quantifying the effects of environmental conditions on phytoplankton photosynthesis.” *Marine Ecology Progress Series*, 18: 57-66.

Cowlishaw, R. J. (2002). “Microzooplankton trophic interactions and their impact on phytoplankton production and community structure in the South Slough Arm of Coos Bay, Oregon. *Dissertation, University of Oregon.*

Cullen, J. J., X. Yang. H. L. MacIntyre. (1992). “Nutrient Limitation of Marine Photosynthesis.” In: Falkowski, P.G., Woodhead, A. D., Vivirito K. (eds) *Primary Productivity and Biogeochemical Cycles in the Sea. Environmental Science Research* 43. Springer, Boston, MA.

Dagg, M. J. (1995). "Copepod Grazing and the Fate of Phytoplankton in the Northern Gulf of Mexico." *Continental Shelf Research,* 15 (11-12): 1303-1317.

Dagg, M. and G. Breed. (2003). “Biological effects of Mississippi River nitrogen on the northern Gulf of Mexico-a review and synthesis.” *Journal of Marine Systems*, 43: 133-152.

Dagg, M. R. Benner, S. Lohrenz, D. Lawrence. (2004). “Transformations of dissolved and particulate materials on continental shelves influenced by large rivers: plume processes.” *Continental Shelf Research*, 24(7-8): 833-858.

Dolan, J. R and K. McKeon. (2005). "The reliability of grazing rate estimates from dilution experiments: have we over-estimated rates of organic carbon consumption by microzooplankton?" *Ocean Science,* 1 (1): 1-7.

Dolan, J. (1991). “Guilds of ciliate microzooplankton in the Chesapeake Bay.” *Estuarine, Coastal and Shelf Science,* 33(2): 137-152.

Dolan, J., C. Gallegos, A. Moigis. (2000). “Dilution effects on microzooplankton in dilution grazing experiments.” *Marine Ecology Progress Series,* 200: 127-139.

Dorado, S., T. Booe, J. Steichen, A. S. McInnes, R. Windham, A. Shepard, A. E. Lucchese, H. Preischel, J. L. Pinckney, S. E. Davis. (2015). “Towards an understanding of the interactions between freshwater inflows and phytoplankton communities in a subtropical estuary in the Gulf of Mexico.” *PLoS One* 10:e0130931

Dortch, Q. and T. E. Whitledge. (1992). “Does nitrogen or silicon limit phytoplankton production in the Mississippi River plume and nearby regions?” *Continental Shelf Research,* 12:1293-1309.

Du, J., K. Park, J. Shen, B. Dzwonkowski. (2018). “Role of baroclinic processes on flushing characteristics in a highly stratified estuarine system, Mobile Bay, Alabama.” *Journal of Geophysical Research: Oceans,* 123(7): 4518-4537.

Dugdale, R. C., F. P. Wilkdeson, F. Chai, R. Feely. (2007). “Size-fractionated nitrogen uptake measurements in the equatorial Pacific and confirmation of the low Si-high-nitrate low-chlorophyll condition.” *Global Biogeochemical Cycles,* 21:1-10.

Dzwonkowski, B., K. Park, R. Collini. (2015). “The coupled estuarine-shelf response of a

river-dominated system during the transition from low to high discharge." *Journal of Geophysical Research: Oceans*, 120: 6145-6163.

Dzwonkowski, B., K. Park, L. Jiang. (2011). "Subtidal across-shelf velocity structure and surface transport effectiveness on the Alabama shelf of the northeastern Gulf of Mexico." *Journal of Geophysical Research*: *Oceans*, 116 (C10).

Dzwonkowski, B., A. T. Greer, C. Briseno-Avena, J. W. Krause, I. M. Soto, F. J. Hernandez, A.L. Deary, J. D.Wiggert, D. Joung, P. J. Fitzpatrick, S. J., O'Brien, S. L. Dykstra, Y. Lau, M. K. Cambazoglu, G. Lockridge, S. D. Howden, A. M. Shiller, W. M. Graham. (2017). "Estuarine influence on biogeochemical properties of the Alabama shelf during the fall season." *Continental Shelf Research*, 140. 96-109. DOI: 10.7266/N79Z930H UDI: R4.x260.000:0042; DOI: 10.7266/N7668B83 UDI: R4.x260.000:0043).

Eppley, R. W. (1972). "Temperature and phytoplankton growth in the sea." *Fisheries Bulletin*, 70:1063-1085.

Fahnenstiel, G. L., M. J. McCormick, G. A. Lang, D. G. Redalje, S. E. Lohrenz, M. Markowitz, B. Wagoner, and H. J. Carrick. (1995). "Taxon-specific growth and loss rates for dominant phytoplankton populations from the northern Gulf of Mexico." *Marine Ecology Progress Series*, 117 (1-3): 229.

Falkowski, P. G. and J. A. Raven. (2013). *Aquatic Photosynthesis* Princeton University Press.

Felip, M. and J. Catalan. (2000). "The relationship between phytoplankton biovolume and chlorophyll in a deep oligotrophic lake: decoupling in their spatial and temporal maxima." *Journal of Plankton Research*, 22(1): 91-106.

Finkel. Z. V., J. Beardall, K. J. Flynn, A. Quigg, T. A. V. Rees, J. A. Raven. (2010). "Phytoplankton in a changing world." *Journal of Plankton Research*, 32(1): 119-137.

First, M. R., H. L. Miller III, P. J. Lavrentyev, J. L. Pinckney, A. B. Burd. (2009). Effects of microzooplankton growth and trophic interactions on herbivory in coastal and offshore environments." *Aquatic Microbial Ecology,* 54: 255-267.

Fitzwater, S. E., G. A. Knauer, J. H. Martin. (1982). "Metal contamination and its effect on primary production measurements." *Limnology and Oceanography*, 27:544-551.

Frame, E. R. and E. J. Lessard. (2009). "Does the Columbia River plume influence phytoplankton community structure along the Washington and Oregon coasts?" *Journal of Geophysical Research: Oceans,* 114 (C2).

Fuhrman, J. (1992). "Bacterioplankton roles in cycling of organic matter: the microbial food web." In *Primary Productivity and Biogeochemical Cycles in the Sea*. Springer, Boston, MA: 361-383.

Gallegos, C. L. (1989). "Microzooplankton Grazing on Phytoplankton in the Rhode River, Maryland: Nonlinear Feeding Kinetics." *Marine Ecology Progress Series*.Oldendorf, 57 (1): 23-33.

Gallegos, C. L. (1992.) "Phytoplankton photosynthesis, productivity, and species composition in a eutrophic estuary: comparison of bloom and non-bloom assemblages." *Marine Ecology Progress Series,* 81: 257-267.

Gaulke, A. K., M. S. Wetz, H. W. Paerl. (2010). "Picophytoplankton: A major

contributor to planktonic biomass and primary production in a eutrophic, river-dominated estuary." *Estuarine, Coastal and Shelf Science*, 90:45-54.

Geider, R. J., H. L. MacIntyre, T. M. Kana. (1997). "Dynamic model of phytoplankton growth and acclimation: responses of the balanced growth rate and the chlorophyll *a*:carbon ratio to light, nutrient-limitation and temperature." *Marine Ecology Progress Series*, 148: 187-200.

Gifford, D. J. (1988). "Impact of Grazing by Microzooplankton in the Northwest Arm of Halifax Harbour, Nova Scotia." *Marine Ecology Progress Series*, 47 (3): 249-258.

Gilbert, P. M., and J. M. Burkholder. (2006). "The complex relationships between increases in fertilization of the Earth, coastal eutrophication and proliferation of harmful algal blooms." In: *Ecological Studies, Ecology of Harmful Algae*. Eds. E. Graneli and J. T. Turner. 189: 341-354.

Gilpin, L. C., K. Davidson, and E. Roberts. (2004). "The influence of changes in nitrogen:silicon ratios on diatom growth dynamics." *Journal of Sea Research*, 51(1): 21-35.

Gin, K. Y., S. Zhang, Y. K. Lee. (2003). "Phytoplankton community structure in Singapore's coastal waters using HPLC pigment analysis and flow cytometry." *Journal of Plankton Research*, 25(12). 1507-1519.

Gin, K. Y., X. Lin, S. Zhang. (2000). "Dynamics and size structure of phytoplankton in the coastal waters of Singapore." *Journal of Plankton Research*, 22(8): 1465-1484.

Greer, A. T., C. B. Woodson, C. E. Smith, C. M. Guigand, R. K. Cowen. (2016).

"Examining mesozooplankton patch structure and its implications for trophic interactions in the northern Gulf of Mexico." *Journal of Plankton Research*, 38(4): 1115-1134.

Greer, A. T., A. M. Shiller, E. E. Hofmann, J. D. Wiggert, S. J. Warner, S. M. Parra, C. Pan, J. W. Book, D. Joung, S. Dykstra, J. W. Krause, B. Dzwonkowski, I. M. Soto, M. K. Cambazoglu, A. L. Deary, C. Briseno-Avena, A. D. Boyette, J. A. Kastler, V. Sanial, L. Hode, U. Nwankwo, L. M. Chiaverano, S. J. O'Brien, P. J. Fizpatrick, Y. H. Lau, M. S. Dinniman, K. M. Marin, P. Ho, A. K. Mojzis, S. D. Howden, F. J. Hernandez, I. Church, T. N. Miles, S. Spoanaugle, J. N. Moum, R. K. Cowen, G. A. Jacobs, O. Schofield, and W. M. Graham. (2018). "Functioning of coastal river-dominated ecosystems and implications for oil spill response: from observations to mechanisms and models." *Oceanography*, 31(3): 91-103.

Greer, A. T., A. D. Boyette, V. J. Cruz, M. K. Cambazoglu, B. Dzwonkowski, L. M. Chiaverano, S. L. Dykstra, C. Briseño-Avena, R. K. Cowen, J. D. Wiggert. (2020). "Contrasting fine-scale distributional patterns of zooplankton driven by the formation of a diatom-dominated thin layer." *Limnology and Oceanography*, in press.

Grimes, C. B. (2000). "Fishery production and the Mississippi River discharge." *Marine Fisheries*, 26(8): 17-26.

Gunter, G. (1979). "The annual flows of the Mississippi River." *Gulf Research Reports*, 6: 283-290.

Hahn, M. W. and M. G. Höfle. (2001). "Grazing of protozoa and its effect on populations of aquatic bacteria." *FEMS Microbiology Ecology*, 35:113-121

Hansen, P. J., P. K. Bjørnsen, B. W. Hansen. (1997). “Zooplankton grazing and growth: scaling within the 2-2000 μm body size range. *Limnology and Oceanography,* 42(4): 687-704.

Haraguchi, L., H. H. Jakobsen, N. Lundholm, J. Carstensen. (2018). “Phytoplankton community dynamic: a driver for ciliate trophic strategies.” *Frontiers in Marine Science,* 5(272):1-15.

Harding, L. W, B. W. Meeson, T. R. Fisher, Jr. (1986). “Phytoplankton production in two east coast estuaries: photosynthesis-light functions and patterns of carbon assimilation in Chesapeake and Delaware Bays.” *Estuarine, Coastal and Shelf Science,* 23(6): 773-806.

Hardy, A. C. and E. R. Gunther. (1935). “The plankton of the South Georgia whaling grounds and adjacent waters, 1926-1927.” *Discovery Rep.,* 11 (1935): 1-456.

Harrison, W. G. and T. Platt. (1980). “Variations in assimilation number of coastal marine phytoplankton: effects of environmental co-variates.” *Journal of Plankton Research,* 2(4): 249-260.

Hillebrand, H., C. Dürselen, D. Kirschtel, U. Pollingher, T. Zohary. (1999). “Biovolume calculation for pelagic and benthic microalgae.” *Journal of Phycology*, 35:403-424.

Holiday, D., G. Carter, R. Gould, and H. McIntyre. (2007). “Harmful algal blooms in the Mississippi Sound and Mobile Bay: using MODIS Aqua and *in situ* data for HABs in the northern Gulf of Mexico. *Conference Proceeding, Ocean Sciences Meeting,* Orlando, FL March 2-7.

Howell-Kübler, A. N., E. J. Lessard, J. M. Napp. (1996). “Springtime microprotozoan

abundance and biomass in the southeastern Bering Sea and Shelik of Strait, Alaska." *Journal of Plankton Research,* 18:731-745.

Iriarte, A. (1993). "Size-fractionated chlorophyll a biomass and picophytoplankton cell density along a longitudinal axis of a temperate estuary (Southampton Water)." *Journal of Plankton Research*, 15: 485-500.

Iriarte, A. and D. A. Purdie. (1994). "Size distribution of chlorophyll a biomass and primary production in a temperate estuary (Southampton Water): the contribution of photosynthetic picoplankton." *Marine Ecology Progress Series*, 115: 283-297.

Iriarte, J. L., C. A. Vargas, F. J. Tapia, R. Bermúdez, R. E. Urrutia. (2012). "Primary production and plankton carbon biomass in a river-influenced upwelling area off Concepción, Chile." *Progress in Oceanography,* 92:97-109

Jakobsen, H. H. and J. Carstensen. (2011). "FlowCAM: Sizing cells and understanding the impact of size distributions on biovolume of planktonic community structure." *Aquatic Microbial Ecology,* 65:75-87.

Jeon, J. J., J. S. Kim, J. H. Kim, S. T. Kim, K. A. Seong, T. . Kim, J. Y. Song, S. K. Kim. (2005). "Feeding and grazing impact of the newly described dinoflagellate *Stoeckeria algicida* on the harmful algal *Heterosigma akashiwo*." *Marine Ecology Progress Series*. 295: 69-78.

Jett, C. (2004). *Estimation of Microzooplankton Grazing in the Suwannee River Estuary, Florida, USA.* Doctoral dissertation, University of Florida, 2004.

Jochem, F. J. (2003). Photo- and heterotrophic pic- and nanoplankton in the Mississippi River plume: distribution and grazing activity. *Journal of Plankton Research*, 25(10): 1201-1214.

Johnson, M. D. (2011). “Acquired phototrophy in ciliates: a review of cellular interactions and structural adaptations.” *Journal of Eukaryotic Microbiology,* 58: 185-195.

Joint, I. R, and A. J. Pomeroy. (1981). “Primary production in a turbid estuary.” *Estuarine and Coastal Shelf Science,* 13: 303-316.

Juhl, A. R., M. C. Murell. (2005). “Interactions between nutrients, phytoplankton growth, and microzooplankton grazing in a Gulf of Mexico estuary.” *Aquatic Microbial Ecology*, 38(2): 147-156.

Justić D, N. N. Rabalais, R. E. Turner, Q. Dortch. (1995). “Changes in nutrient structure of river-dominated coastal waters: stoichiometric nutrient balance and its consequences.” *Estuarine, Coastal and Shelf Science,* 40:339-356.

Karnan, C. R. Jyothibabu, T. M. Manojkumar, L. Jagadeesan, N. Arunpandi. (2017). “On the accuracy of assessing copepod size and biovolume using FlowCAM and traditional microscopy.” *Indian Journal of Marine Science*, 46(7): 1261-1264.

Kemp, W. M. and W. R. Boynton. (1984). “Spatial and temporal coupling of nutrient inputs to estuarine primary production: the role of particulate transport and decomposition.” *Bulletin of Marine Science,* 35: 522-535.

Kiørboe, T. (1993). “Turbulence, phytoplankton cell size, and the structure of pelagic food webs.” *Advances in Marine Biology,* 29: 1-72.

Kiørbe, T. (2001). “Formation and fate of marine snow: small-scale processes with large-scale implications.” *Scientia Marina*. 65: 57-71.

Kirk, J. T. O. (1996). *Light and photosynthesis in aquatic ecosystems*. Cambridge University Press. 509 pp.

Kudela, R. M. A. R. Horner-Devine, N. S. Banas, B. M. Hickey, T. D. Peterson, R. M McCabe, E. J. Lessard, E. Frame, K. W. Bruland, D. A. Jay, J. O. Peterson, W. T. Peterson, P. M. Kosro, S. L. Placios, M.C. Lohan, E. P. Dever. (2010). "Multiple trophic levels fueled by recirculation in the Columbia River plume." *Geophysical Research Letters*, 37: 18607-18614.

Kremp, A., T. Tamminen, and K. Spilling. (2008). "Dinoflagellate bloom formation in natural assemblages with diatoms: nutrient competition and growth strategies in Baltic spring phytoplankton." *Aquatic Microbial Ecology*, 50: 181-196.

Kruk, C., M. Devercelli, V L. Huszar, E. Hernández, G. Beamud, M. Diaz, L. H. Silva, A. M. Segura. (2017). "Classification of Reynolds' phytoplankton functional groups using individual traits and machine learning techniques." *Freshwater Biology,* 62:1681-1692.

Kruk, C., E. Peeters, E. H. Van Nes, V. L. M. Huszar, L S. Costa, M. Scheffer. (2011). "Phytoplankton community composition can be predicted best in terms of morphological groups." *Limnology and Oceanography,* 56:110-118.

Kruk, C., V. L. M. Huszar, E. Peeters, S. Bonilla, L. Costa, M. Lurling, C. S. Reynolds, M. Scheffer (2010). "A morphological classification capturing functional variation in phytoplankton." *Freshwater Biology,* 55:614-627.

Landry, M. R., S. L. Brown, L. Campbell, J. Constantinou, and H. Liu. 1998. "Spatial Patterns in Phytoplankton Growth and Microzooplankton Grazing in the Arabian Sea during Monsoon Forcing." *Deep Sea Research Part II: Topical Studies in Oceanography,* 45 (10): 2353-2368.

Landry, M. R. and A. Calbet. 2004. "Microzooplankton Production in the Oceans." *ICES*

Journal of Marine Science: Journal Du Conseil, 61 (4): 501-507.

Landry, M. R., J. Constantinou, and J. Kirshtein. (1995). "Microzooplankton Grazing in the Central Equatorial Pacific during February and August, 1992." *Deep Sea Research Part II: Topical Studies in Oceanography*, 42 (2-3): 657-671.

Landry, M. R., J. Constantinou, M. Latasa, S. L. Brown R. R. Bidigare, M. E. Ondrusek. (2000). “Biological response to iron fertilization in the eastern equatorial Pacific (IronEx II). III. Dynamics of phytoplankton growth and microzooplankton grazing. *Marine Ecology Progress Series*, 201: 57-72.

Landry, M. R., B. C. Monger, and K. E. Selph. (1993). "Time-Dependency of Microzooplankton Grazing and Phytoplankton Growth in the Subarctic Pacific." *Progress in Oceanography*, 32 (1): 205-222.

Landry, M. R., K. E. Selph, S. L. Brown, M. R. Abbott, C. I. Measures, S. Vink, C. B. Allen, A. Calbet, S. Christensen, H. Nolla. (2002). "Seasonal Dynamics of Phytoplankton in the Antarctic Polar Front Region at 170° W." *Deep Sea Research Part II: Topical Studies in Oceanography*, 49 (9): 1843-1865.

Landry, M. R, J. Kirshtein, and J. Constantinou. (1995). "A refined dilution technique for measuring the community grazing impact of microzooplankton, with experimental tests in the central Equatorial Pacific." *Marine Ecology Progress Series.Oldendorf*, 120 (1): 53-63.

Lehrter, J. C., J. R. Pennock, and G. B. McManus. (1999). "Microzooplankton Grazing and Nitrogen Excretion Across a Surface Estuarine-Coastal Interface." *Estuaries and Coasts*, 22 (1): 113-125.

Leising, A. W., R. Horner, J. J. Pierson, J. Postel, C. Halsband-Lenk. (2005). “The

balance between microzooplankton grazing and phytoplankton growth in a highly productive estuarine fjord." *Progress in Oceanography*, 67(3-4): 366-383.

Lenz, J. (1992). "Microbial loop, microbial food web and classical food chain: Their significance in pelagic marine ecosystems." *Ergebnisse der Limnologie=Advances in Limnology/Internationale Vereinigung fur Theoretische und Angewandete Limnologie.* 37:265-279.

Lessard, E. J. and M. C. Murrell. (1998). "Microzooplankton Herbivory and Phytoplankton Growth in the Northwestern Sargasso Sea." *Aquatic Microbial Ecology*, 16 (2): 173-188.

Levinsen, H., J. T. Turner, T. G. Nielsen, B. W. Hansen. (2000). "On the trophic coupling between protists and copepods in arctic marine ecosystems." *Marine Ecology Progress Series*, 204:65-77

Leys, C. C. Ley, O. Klein, P. Bernard, L. Licata. (2013). "Detecting outliers: do not use standard deviation around the mean, use absolute deviation around the median." *Journal of Experimental Social Psychology*, 49(4): 764-766.

Liefer, J. D., A. Robertson, H. L. MacIntyre, W. L. Smith, C. P. Dorsey. (2013). "Characterization of a toxic *Pseudo-nitzschia* spp. bloom in the northern Gulf of Mexico associated with domoic acid accumulation in fish." *Harmful Algae*, 26:20-32.

Liefer J. D., H. L. MacIntyre, L. Novoveská, W. L. Smith, C. P. Dorsey. (2009a). "Temporal and spatial variability in *Pseudo-nitzschia* spp. in Alabama coastal waters: A "hot spot" linked to submarine groundwater discharge?" *Harmful Algae*, 8:706-714.

Liu, H. and M. Dagg. (2003). "Interactions between nutrients, phytoplankton growth, and micro-and mesozooplankton grazing in the plume of the Mississippi River." *Marine Ecology Progress Series,* 258: 31-42.

Lohrenz, S. E., M. J. Dagg, and T. E. Whitledge. (1990). “Enhanced primary production at the plume/oceanic interface of the Mississippi River.” *Continental Shelf Research,* 10(7): 639-664.

Lohrenz, S. E., G. L. Fahnenstiel, and D. G. Redalje. (1994). “Spatial and temporal variations of photosynthetic parameters in relation to environmental conditions in coastal waters of the northern Gulf of Mexico.” *Estuaries and Coasts*, 17 (4): 779-795.

Lohrenz, S. E., G. L. Fahnenstiel, D. G. Redalje, G. A. Lang, M. J. Dagg, T. E. Whitledge, and Q. Dortch. (1999). “Nutrients, irradiance, and mixing as factors regulating primary production in coastal waters impacted by the Mississippi River plume.” *Continental Shelf Research,* 19 (9): 1113-1141.

Lohrenz, S. E., G. L. Fahnenstiel, D. G. Redalje, G. A. Lang, X. Chen, and M. J. Dagg. (1997). “Variations in Primary Production of Northern Gulf of Mexico continental shelf saters Linked to Nutrient Inputs from the Mississippi River.” *Marine Ecology Progress Series* 155: 45-54.

Lohrenz, S. E., D. G. Redalje, G. L. Fahnenstiel, and G. A. Lang. (1992). “Regulation and distribution of primary production in the northern Gulf of Mexico.” *Nutrient Enhanced Coastal Ocean Productivity. Publication Number TAMU-SG-92-109, Sea Grant Program,* Texas A & M University, Galveston, Texas (1992): 95-104.

Lohrenz, S. E., S. Chakraborty, M. Huettel, J. Herrera Silveira, K. Gundersen, D. Redalje, J. Wiggert, B. E. Denton, J. Lehrter (2014). "Primary production." In: Benway, H. M., Coble, P. G. (eds), 2014. *Report of the U.S. Gulf of Mexico Carbon Cycle Synthesis Workshop, March 27-28, 2013. Ocean Carbon and Biogeochemistry Program and North American Carbon Program.* 28-38.

Lui, H. and M. Dagg. (2003). "Interactions between nutrients, phytoplankton growth, and micro- and mesozooplantkon grazing in the plume of the Mississippi River." *Marine Ecology Progress Series*, 258: 31-42.

Mackey, M. D. D. J. Mackey, H.W. Higgins, S. W. Wright. (1996). "CHEMTAX-a program fro estimating class abundances from chemical markers: applications to HPLC measurements of phytoplankton." *Marine Ecology Progress Series* 144: 265-283.

MacIntyre, H.L. and J. J. Cullen. (1996). "Primary production by suspended and benthic microalgae in a turbid estuary: time-scales of variability in San Antonio Bay, Texas. *Marine Ecology Progress Series* 145: 245-268.

MacIntyre, H. L., A. L. Stutes, W. L. Smith, C. P. Dorsey, A. Abraham, R. W. Dickey RW. (2011). "Environmental correlates of community composition and toxicity during a bloom of pseudo-nitzschia spp. in the northern Gulf of Mexico." *Journal of Plankton Research,* 33:273-295.

Maguer, J.F., S. L'Helguen, M. Waeles, P. Morin, R. Riso, J. Caradec. (2009). "Size-fractionated phytoplankton biomass and nitrogen uptake in response to high nutrient load in the North Biscay Bay in spring". *Continental Shelf Research*, 29(8): 1103-1110.

Mallin, M. A., H. W. Paerl, J. Rudek. (1991). “Seasonal phytoplankton composition, productivity, and biomass in the Neuse River estuary, North Carolina.” *Estuarine, Coastal, and Shelf Science*, 32 609-623.

Mallin, M. A., H. W. Paerl, J. Rudek, P. W. Bates. (1993). “Regulation of estuarine primary production by watershed rainfall and river flow.” *Marine Ecology Progress Series*, 93:199-203.

Malone, T. C., M. B. Chervin. (1979). “The production and fate of phytoplankton size fractions in the plume of the Hudson River, New York Bight.” *Limnology and Oceanography*, 24(4): 683-696.

Malone. T. C. (1980). “Size-fractionated primary productivity of marine phytoplankton.” In Falkowski P. G. (eds) *Primary Productivity in the Sea.* Environmental Science Research 19. Springer, Boston, MA.

Malone, T. C., H. W. Ducklow, E. R. Peele, and S. E. Pike. (1991). “Picoplankton carbon flux in Chesapeake Bay.” *Marine Ecology Progress Series*, 78: 11-22.

Margalef, R. (1978). “Life-forms of phytoplankton as survival alternatives in an unstable environment.” *Oceanologica acta*, 1(4): 493-509.

McGehee, A.M. and D. G. Redalje. 2016. Phytoplankton pigment specific growth and losses due to microzooplankton grazing in a northern Gulf of Mexico estuary during winter/fall. Gulf and Caribbean Research 27(1): 1-10.

McManus, G. B. and L. F. Santoferrara. (2013). “Tintinnids in microzooplankton communities,” in *The Biology and Ecology of Tintinnid Ciliates: Models for Marine Plankton.* Eds. J. R. Dolan, D. J. S. Montagnes, S. Agatha, D. W. Coats, and D. K. Stoecker. John Wiley and Sons, Ltd. 2013.

McNair, H. M., M. A. Brzezinski, and J. W. Krause. (2018). “Diatom populations in an upwelling environment decrease silica content to avoid growth limitation.” *Environmental Microbiology,* 20:4184-4193

Menden-Deuer, S. and E. J. Lessard. (2000). “Carbon to volume relationships for dinoflagellates, diatoms, and other protist plankton.” *Limnology and Oceanography,* 45:569-579

Montagnes, D. J. S. (2013). “Ecophysiology and behavior of tintinnids,” in *The Biology and Ecology of Tintinnid Ciliates: Models for Marine Plankton.* Eds. J. R. Dolan, D. J. S. Montagnes, S. Agatha, D. W. Coats, and D. K. Stoecker. John Wiley and Sons, Ltd. 2013.

Morey, S., W. W. Schroeder, J. J. O’Brien, J. Zavala-Hidalgo. (2003). “The annual cycle of riverine influence in the eastern Gulf of Mexico basin.” *Geophysical Research Letters,* 30(16).

Mortazavi, B., R. L. Iverson, W. M. Landing, F. G. Lewis, W. Huang. (2000). “Control of phytoplankton production and biomass in a river0dominated estuary: Apalachicola Bay, Florida, USA.” *Marine Ecology Progress Series,* 198: 19-31.

Murrell, M. C. and E. M. Lores. (2004). "Phytoplankton and Zooplankton Seasonal Dynamics in a Subtropical Estuary: Importance of Cyanobacteria." *Journal of Plankton Research,* 26 (3): 371-382.

Murrell, M. C., R. S. Stanley, E. M. Lores, G. T. DiDonato, and D. A. Flemer. (2002). “Linkage between microzooplankton grazing and phytoplankton growth in a Gulf of Mexico estuary.” *Estuaries,* 25 (1): 19-29.

National Marine Fisheries Service. (2017). “Fisheries of the United States, 2016.” *U. S.*

Department of Commerce, NOAA Current Fishery Statistics No. 2016.

Neuer S. and T. J. Cowles. (1994). “Protist herbivory in the oregon upwelling system.” *Marine Ecology Progress Series.* Oldendorf, 113:147-162

Nixon, S. (1995). “Coastal marine eutrophication: A definition, social causes, and future concerns.” *Ophelia,* 41: 199-219.

Nixon, S., C. Oviat, J. Frithsen, B Sullivan. (1986). “Nutrients and the productivity of estuarine and coastal marine ecosystems.” *Journal of the Limnological Society of Southern Africa,* 12(1-2): 43-71.

Novoveská, L. and H. MacIntyre. (2019). “Study of the seasonality and hydrology as drivers of phytoplankton abundance and composition in a shallow estuary, Weeks Bay, Alabama (USA).” *Journal of Aquatic Marine Biology,* 8:69-80

Olli, K. (1999). "Diel vertical migration of phytoplankton and heterotrophic flagellates in the Gulf of Riga." *Journal of Marine Systems* 23 (1–3): 145-163. doi:http://dx.doi.org/10.1016/S0924-7963(99)00055-X.

Ortell, N. and A. C. Ortmann. (2014). "Interactions among members of the microbial loop in an estuary dominated by microzooplankton grazing." *Aquatic Microbial Ecology,* 72 (1): 63-71.

Ortmann, A. C., R. Courtney Metzger, J. D. Liefer, and L. Novoveska. (2011). "Grazing and viral lysis vary for different components of the microbial community across an estuarine gradient." *Aquatic Microbial Ecology,* 65 (2): 143-157.

Palomares-García, R. R., J. J. Bustillos-Guzmán, and D. López-Cortés. (2006). "Pigment-Specific Rates of Phytoplankton Growth and Microzooplankton Grazing in a Subtropical Lagoon." *Journal of Plankton Research,* 28 (12): 1217-1232.

Paranjape, M. A. (1990). "Microzooplankton Herbivory on the Grand Bank (Newfoundland, Canada): A Seasonal Study." *Marine Biology*, 107 (2): 321-328.

Parra, S. M., V. Sanial, A. D. Boyette, M. K. Cambazoglu, I. M. Soto, A. T. Greer, L. M. Chiaverano, A. Hoover, and M. S. Dinniman. (2020). "Bonnet Carre Spillway freshwater transport and corresponding biogeochemical properties in the Mississippi Bight." *Continental Shelf Research*, 104114.

Parsons, M. L. and Q. Dortch. (2002). "Sedimentological evidence of an increase in *Pseudo-nitzschia* (bacillariophyceae) abundance in response to coastal eutrophication." *Limnology and Oceanography*, 47:551-558.

Parsons, T.R., M. Takahashi, B. Hargrave (2013). "Biological oceanographic processes." Pergamon.

Peltomaa, E. and M. Johnson. (2017). "*Mesodinium rubrum* exhibits genus-level but not species-level cryptophyte prey selection." *Aquatic Microbial Ecology*, 78: 147-159.

Peters, R. H. (1983). "The Ecological Implications of Body Size." Cambridge University Press, Cambridge.

Pierce, R. H., M. S. Henry, P. C. Blum, J. Lyons, Y. S. Cheng, D. Yazzie, and Y. Zhou. (2003). "Brevetoxin concentrations in marine aerosol: human exposure levels during a *Karenia brevis* harmful algal bloom." *Bulletin of Envrionmental Contamination and Toxicology*. 70(1): 161-165.

Putt, M. and D. Stoecker. (1989). "An experimentally determined carbon:volume ratio for marine oligotrichous ciliates from estuarine and coastal waters." *Limnology and Oceanography*, 34(6):1097-1103.

Qian, Y., A. E. Jochens, M. C. Kennicutt II, D. C. Biggs DC. (2003). "Spatial and temporal variability of phytoplankton biomass and community structure over the continental margin of the northeast Gulf of Mexico based on pigment analysis." *Continental Shelf Research,* 23:1-17.

Qui, D. L. Huang, J. Zhang, S. Lin. (2010). "Phytoplankton dynamics in and near the highly eutrophic Pearl River Estuary, South China Sea." *Continental Shelf Research*, 30: 177-186.

Rabalais, N. N., and R. E. Turner. 2019. "Gulf of Mexico hypoxia: past, present, and future." *Limnology and Oceanography Bulletin* 28(4): 117-124.

Raimbault, P., M. Rodier, I. Taupier-Letage. (1988). "Size fraction of phytoplankton in the Ligurian Sea and the Algerian Basin (Mediterranean Sea): size distribution versus total concentration." *Marine Microbial Food Webs,* 3(1). 1-7.

Rabalais, N. N., R. E. Turner, W. J. Wiseman. (2001). "Hypoxia in the Gulf of Mexico." *Journal of Environmental Quality,* 30:320-329

Rakocinski, C. F., J. Lyczkowski-Shultz, S. L. Richardson. (1996). "Ichthyoplankton assemblage structure in Mississippi Sound as revealed by canonical correspondence analysis." *Estuarine, Coastal and Shelf Science,* 43:237-257

Reckermann, M., and M. J. W. Veldhuis. (1997). "Trophic interactions between picophytoplankton and micro- and nanozooplankton in the western Arabian Sea during the NE monsoon 1993." *Aquatic Microbial Ecology,* 12: 263-273.

Redalje, D. G., S. E. Lohrenz, G. L. Fahnenstiel. (1994). "The relationship between primary production and the vertical export of particulate organic matter in a river-impacted coastal ecosystem. *Estuaries*, 17(4): 829-838.

Reynolds, C.S. (1988). “Functional morphology and the adaptive strategies of freshwater phytoplankton.” In: *Growth and Reproductive Strategies of Freshwater Phytoplankton* (Eds C. D. Sandgren). Cambridge.

Reynolds, C. S. (2006). *The Ecology of Phytoplankton*. Cambridge.

Reynolds, C.S., M. Dokulil, J. Padisák. (2000). “Understanding the assembly of phytoplankton in relation to the trophic spectrum: where are we now?” *Hydrobiologia*, 424: 147-152.

Rossi, V., V. Garcon, J. Tassel, J. Romagnan, L. Stemmann, F. Jourdin, P. Morin, Y. Morel. (2013). “Cross-shelf variability in the Iberian Peninsula upwelling system: impact of a mesoscale filament.” *Continental Shelf Research,* 59(15): 97-114.

Salmaso, N., L. Naselli-Flores, J. Padisák. (2015). “Functional classifications and their application in phytoplankton ecology.” *Freshwater Biology*, 60:603-619

Schiller, R. V., V. H. Kourafalou, P. Hogan, and N. D. Walker. (2011). “The dynamics of the Mississippi River plume: impact of topography, wind and offshore forcing on the fate of plume waters.” *Journal of Geophysical Research: Oceans,* 116(C6).

Schoener, D. and G. McManus. (2012). “Plastid retention, use, and replacement in a kleptoplastic cliate.” *Aquatic Microbial Ecology*, 67: 177-187.

Sherr, E. B and B. F. Sherr. (1994). "Bacterivory and herbivory: key roles of phagotrophic protists in pelagic food webs." *Microbial Ecology,* 28 (2): 223-235.

Sherr, E.B. and B.F. Sherr. (2002). “Significance of predation by protists in aquatic microbial food webs.” *Antonie Van Leeuwenhoek*, 81:293-308

Sherr, E. B., and B. F. Sherr. (2007). “Heterotrophic dinoflagellates: a significant

component of microzooplankton biomass and major grazers of diatoms in the sea." *Marine Ecology Progress Series,* 352:187-197.

Sherr, E. B., B.F. Sherr, L. Fessenden. (1997). "Heterotrophic protists in the central arctic ocean." *Deep Sea Research Part II: Topical Studies in Oceanography,* 44:1665-1682.

Sherr, E. B., B. F. Sherr, A. J. Hatz. (2009). "Microzooplankton grazing impact in the western Arctic Ocean." *Deep Sea Research Part II: Topical Studies in Oceanography*, 56(17): 1264-1273.

Sin, Y., R. L. Wetzel, I. C. Anderson. (1999). "Spatial and temporal characteristics of nutrient and phytoplankton dynamics in the York River estuary, Virginia: analyses of long-term data." *Estuaries,* 28: 260-275.

Smayda, T. J. (1980). "Phytoplankton species succession." *The Physiological Ecology of Phytoplankton*, 493-570.

Smayda, T. J. and C. S. Reynolds. (2003). "Strategies of marine dinoflagellate survival and some rules of assembly." *Journal of Sea Research,* 49:95-106

Smetacek, V. (1981). "The Annual Cycle of Protozooplankton in the Kiel Bight." *Marine Biology,* 63 (1): 1-11.

Smith, W. O., D. J. Demaster. (1996). "Phytoplankton biomass and productivity in the Amazon River plume: correlation with seasonal discharge." *Continental Shelf Research,* 16(3): 291-319.

Smith, M. and P. Hansen. (2007). "Interaction between *Mesodinium rubrum* and its prey: importance of prey concentration, irradiance and pH." *Marine Ecology Progress Series,* 338: 61-70.

Spillane, T. (2016). “Diatom frustules as a mechanical defense against predation by heterotrophic dinoflagellates.” Master’s Thesis. Washington State University.

Steidinger, K. A., G. A. Vargo, P. A. Tester, and C. R. Tomas. (1998). “Bloom dynamics and physiology of *Gymnodinium breve* with emphasis on the Gulf of Mexico.” In: Anderson, D., A. Cembella, G. Hallegraeff (Eds.), *Physiological Ecology of Harmful Algal Blooms.* Springer-Verlag, Berlin, pp. 133-153.

Stoecker, D. K., P. J. Hansen, D. A. Caron, A. Mitra. (2017). “Mixotrophy in the marine plankton.” *Review of Marine Science,* 9: 311-335.

Strom, S. L. and Michael W. Strom. (1996). "Microplankton Growth, Grazing, and Community Structure in the Northern Gulf of Mexico." *Marine Ecology Progress Series,* 130: 229-240.

Strom, S. L. M. A. Brainard, J. L. Holmes, M. B.Olson. (2001). “Phytoplankton blooms are strongly impacted by microzooplankton in coastal North Pacific Waters.” *Marine Biology,* 138: 355-368.

Strom, S. L., E. L. Macri, and M. Brady Olson. (2007). “Microzooplankton grazing in the coastal Gulf of Alaska: Variations in top-down control of phytoplankton.” *Limnology and Oceanography,* 52(4): 1480-1494.

Stukel, M., V. Coles, M. Brroks, R. Hood. (2014). “Top-down, bottom-up and physical controls on diatom-diazotroph assemblage growth in the Amazon River plume.” *Biogeosciences,*. 11: 3259-3278.

ter Braak, C. J.F., and P.F.M. Verdonschot. (1995). “Canonical correspondence analysis and related multivariate methods in aquatic ecology.” *Aquatic Sciences* 57(3): 255-289.

Thingstad, A. K. and E. Sakshaug. (1990). “Control of phytoplankton growth in nutrient recycling ecosystems. Theory and terminology.” *Marine Ecology Progress Series,* 63: 261-272.

Tilstone, G. H., F. G. Figueiras, E. G. Fermin, B. Arbones. (1999). “Significance of nanophytoplankton photosynthesis and primary production in a coastal upwelling system (Ria de Vigo, NW Spain).” *Marine Ecology Progress Series,* 183: 13-27.

Tilstone, G., T. Smyth, A. Poulton, R. Hutson. (2009). “Measured and remotely sensed estimates of primary production in the Atlantic Ocean from 1998 to 2005.” *Deep Sea Research Part II: Topical Studies in Oceanography,* 56(15): 918-930.

Tomas, C. R., ed. (1997). *Identifying marine phytoplankton*. Elsevier.

Turner, R.E. and N. N. Rabalais (1991). “Changes in mississippi river water quality this century.” *Bioscience,* 41:140-147

Vandermeulen, R. (2012). “Factors influencing the spatial and temporal distribution of primary productivity respiration in the Mississippi coastal estuarine region.” Masters Thesis. The University of Southern Mississippi, Hattiesburg, MS. 151 pp.

Vargas C., P. Contrera, J. Iriarte. (2011). “Relative importance of phototrophic, heterotrophic, and mixotrophic nanoplankton in the microbial food web of a river-influenced coastal upwelling area.” *Aquatic Microbial Ecology,* 65:233-248.

Vargas, C.A., P.Y. Contreras, J. L. Iriarte. (2012). Relative importance of phototrophic, heterotrophic, and mixotrophic nanoplankton in the microbial food web of a river-influenced coastal upwelling area *Aquatic Microbial Ecology,* 65:233-248

Vargas, C. A., R. A. Martínez, L. A. Cuevas, M.A. Pavez, C Cartes, H.E. González, R.

Escribano, G. Daneri. (2007). “The relative importance of microbial and classical food webs in a highly productive coastal upwelling area.” *Limnology and Oceanography*, 52:1495-1510

Verity, P. G., D. K. Stoecker, M. E. Sieracki, and J. R. Nelson. (1993). "Grazing, Growth and Mortality of Microzooplankton during the 1989 North Atlantic Spring Bloom at 47 N, 18 W." *Deep Sea Research Part I: Oceanographic Research Papers*, 40 (9): 1793-1814.

Verity, P. G. (1996). "Microzooplankton Grazing of Primary Production at 140 W in the Equatorial Pacific." *Deep Sea Research Part II: Topical Studies in Oceanography*, 43 (4-6): 1227-1255.

Verity, P. G. and C. Langdon. (1984). “Relationships between lorcia volume, carbon, nitrogen, and ATP content of tintinnids in Narragansett Bay.” *Journal of Plankton Research*, 6(5): 859-868.

Verity, Peter G., Diane K. Stoecker, Michael E. Sieracki, and James R. Nelson. (1993). “Grazing, Growth and Mortality of microzooplankton during the 1989 North Atlantic Spring Bloom at 47 N, 18 W.” *Deep Sea Research Part I: Oceanographic Research Papers*, 40 (9): 1793-1814.

Walsh, J. J. (1976). “Herbivory as a factor in patterns of nutrient utilization in the sea.” *Limnology and Oceanography*, 21: 659-683.

Ward, B. A., S. Dutkiewicz, O. Jahn, M. J. Follows. (2012). “A size-structured food-web model for the global ocean.” *Limnology and Oceanography*, 57(6): 1877-1891.

Watkins, S. M., A. Reich, L. E. Fleming, R. Hammond. (2008). “Neurotoxic shellfish poisoning.” *Marine Drugs*. 6(3): 431-455.

Wawrik, B. and J. H. Paul (2004). “Phytoplankton community structure and productivity along the axis of the Mississippi River plume in oligotrophic Gulf of Mexico waters.” *Aquatic Microbial Ecology,* 35:185-196.

Welschmeyer, N. A. 1994. "Fluorometric Analysis of Chlorophyll a in the Presence of Chlorophyll b and Pheopigments." *Limnology and Oceanography,* 39 (8): 1985-1992.

Willen, E. (1991). “Planktonic diatoms-an ecological review.” *Algological Studies* 62:69-106.

Zhang, S., H. Liu, Y. Ke, B. Li. (2017). “Effect of silica content of diatoms on protozoan grazing.” *Frontiers in Marine Science* 4: 202-209.